UNIVERSITÀ
DEGLI STUDI
FIRENZE

DOTTORATO DI RICERCA IN
AREA DEL FARMACO E TRATTAMENTI INNOVATIVI
Curriculum Scienze Farmaceutiche

CICLO XXXIII

COORDINATORE Prof.ssa Ghelardini Carla

Design and optimization of drug delivery systems based on natural products for dermal and mucosal applications

Settore Scientifico Disciplinare CHIM/09

Dottoranda
Dott.ssa Vanti Giulia

Tutore
Prof.ssa Bilia Anna Rita

Coordinatore
Prof.ssa Ghelardini Carla

Anni 2017/2020

Alla mia famiglia

e alle persone che hanno sempre creduto in me

Index

INTRODUCTION

AIMS OF THE PHD THESIS

Aim of the thesis was the design and optimization of nanodrug delivery systems based on natural products for dermal and mucosal application.

Particularly, the described researches deal with the formulation of different lipid-nanocarriers: oil-in-water microemulsions, conventional liposomes, modified vesicles, like glycerosomes and propylene glycol-nanovesicles, and innovative vesicular systems called escinosomes and ascosomes. All these systems are very versatile and were in some cases loaded in hydrogels to increase their viscosity and/or mucoadhesion, as well as to provide semi-solid dosage forms which combine innovative and conventional technological approaches.

Vesicles and microemulsions were prepared and optimized by different techniques and were physically and chemically characterized by dynamic/electrophoretic light scattering analyses, scanning/transmission electron microscopy and high performance liquid chromatography, in order to determine various technological parameters such as average hydrodynamic diameter, polydispersity index, ζ-potential, deformability, shape and encapsulation efficiency of loaded drugs, as well as to monitor the chemical and physical stability.

In vitro release kinetics of the formulated drugs were evaluated by dialysis bag method and vertical diffusion Franz cells, using cellulose nitrate artificial membranes and suitable mathematical models. *In vitro* permeation performances were investigated by parallel artificial membrane permeation assay (PAMPA) and vertical diffusion Franz cells, using fresh excised rabbit ear skin , BALB/c nude mice skin and porcine buccal mucosa.

Different cell lines were selected for *in vitro* activity or cytotoxicity studies. African Green Monkey kidney cells (Vero) infected with the herpes simplex virus type 1 were employed to evaluate the *in vitro* anti-herpetic activity of formulated substances, whereas different bacteria and fungi strains were used to test the *in vitro* antimicrobial activity. Cytotoxicity tests were done on immortalized human skin keratinocytes cell line (HaCaT). Uptake studies of drugs formulated in parenteral and oral dosage forms were carried out using parental and

doxorubicin-resistant human erythroleukemia cells (K562, K562/DOXO), and Caco-2 cell line, respectively.

In addition, *in vivo* experiments of acute dermal irritation/corrosion and acute dermal toxicity were carried out on Sprague Dawley rats, according to the OECD guidelines.

In detail, a commercial saw palmetto carbon dioxide (CO_2) extract was formulated in conventional liposomes, for the topical delivery of the active constituents and the potential usage in hair loss treatment.

Glycerosomes, nanovesicles based on glycerol, were developed for loading three different Lamiaceae essential oils, i.e. *Melissa officinalis* L., *Origanum onites* L. and *Satureja thymbra* L., in order to protect the sensitive and volatile compounds from the direct exposure to environmental agents, as well as to provide a dosage form for dermal delivery of the essential oil avoiding skin irritancy.

Since, vesicle bilayer can be made of a variety of amphiphilic molecules, innovative nanovesicular systems were explored in this thesis using bioactive molecules as vesicle bilayer forming components. In particular, escinosomes are escin-based vesicles, whereas ascosomes are ascorbyl derivatives-based vesicles. Both nanocarriers were developed for the skin delivery of the active bilayer constituents, as well as for loading and carrying further selected model drugs (berberine chloride and khellin, respectively).

This thesis also aimed to develop two different microemulsion-based hydrogel (microemulgel) loaded with clobetasol propionate for the treatment of mucus membrane pemphigoid, a chronic vesicobullous dermatosis with autoimmune pathogenesis, and cannabidiol for the treatment of atopic dermatitis, a chronic relapsing condition characterized by itching and redness of the skin, widely spread among infants and children. Moreover, a novel microemulsion was designed for the dermatological application of khellin, selected as model natural drug because of its lipophilicity and anti-inflammatory properties.

Both liposomes and microemulsions are very versatile systems, suitable for all the administration routes and also investigated in food-industry. Accordingly, a further study were focused on developing nanoliposomes loaded with berberine chloride and tariquidar, to enhance the intracellular uptake of the antitumoral drug in doxorubicin resistant human leukemia cells (K562/DOXO), thanks to the activity of the Pg-p inhibitor. Another investigation was focused on

formulating essential oils of *Origanum onites* and *Satureja thymbra* in propylene glycol-nanovesicles, proposed as safe and effective delivery systems of alternative food preservatives. Lastly, a microemulsion for the oral delivery of an extract enriched of polyphenols from unripe olives (*Olea europaea* L.) was developed and *in vitro* fully characterized.

THE ROLE OF NATURAL PRODUCTS IN THERAPY

It is uncertain where or when natural products first began to be used, but the association between plants and health have occurred since the beginning of the humankind *(Khan IA, 2012; Mehta P, 2015).*

Natural products (isolated compounds or extracts), mainly derived from plants, bacteria and fungi, play a key role in drug discovery and still represent a versatile approach to develop successful medications for treating and preventing many complex diseases. Thanks to their wide structure variability and interaction with multiple biological targets, natural product represent in fact the main source of bioactive molecules and innovative drugs, to which synthetic libraries cannot compare *(Cheng YC, 2020; Cameron A, 2011).*

Currently, the global market of natural products, mainly derived from the plant kingdom, is estimated at more than $ 80 billion in US and it is continuously growing up. Herbal drugs and extracts, sold as dietary supplements, food, or herbal drugs are the principal products, while single isolated constituents represent a smaller proportion. In addition, according to the WHO, between 65 and 80% of population in developing countries presently use medicinal plants as therapeutic remedies *(Khan IA, 2012; Cameron A, 2011; Bhattaram VA, 2002).*

Over centuries, natural products found application in the treatment of skin disorders and local pain, as well as in skin care, and they are currently widely used in dermatology and cosmetics. First medical books, from the ancient Greece and ancient China, recorded the application of topical plasters to treat rheumatism and in recent decades the cutaneous administration of natural products found increased application both in the treatment of skin pathologies and systemic diseases, by dermal and transdermal delivery *(Mehta P, 2015; Cheng YC, 2020)*.

The tangible importance of natural products in the drug discovery process and their role in therapy, specifically in the treatment of skin pathologies, is unquestionable, but in many cases they do not possess drug-like characteristics

and their efficacy and clinical use are limited because of physical and/or chemical instability, unsuitable partition coefficient (log P), unfavourable intrinsic dissolution rate or inappropriate molecular size. These unfavourable properties often cause low aqueous solubility, poor permeation and absorption through biological membranes and barriers, low biodistribution, rapid metabolism and clearance, resulting in drug plasma levels below the therapeutic concentration, and reduced or annulled efficacy. A reduced bioavailability can be also related to distribution/accumulation of drugs in non-targeted tissues and organs, which also increases the side effects. Furthermore, incompatibility of some constituents with other components of the formulation, can severely limit their clinical practice *(Kesarwani K, 2013; Jain H & Chella N, 2020).*

THE SKIN: A VALUABLE ROUTE FOR ADMINISTRATION OF DRUGS

The skin has become recognized as an important drug delivery route which can be reached directly. It is an ideal site for the application of drugs for achieving local (topical/dermal) and systemic (transdermal) therapeutic effects. Local or topical drug delivery assumes treating various skin diseases, while transdermal delivery aims to achieve systemically active drug levels in order to treat systemic diseases *(Heather AB, 2012; Dragicevic N & Maibach HI, 2016)*.

Topical and transdermal drug delivery are attractive alternative to conventional routes of administration, principally oral and parenteral, because they offer numerous advantages, among them the usage of smaller doses to achieve localized therapeutic effects, or first pass metabolism bypass to reach systemic effects. In addition, dermal and transdermal delivery provide convenient and pain-free self-administration, improving the patient compliance. This is also evident from the increasing market for dermal and transdermal delivery products and explains the increasing interest of skin, as a site of drug application, to pharmaceutical research *(Paudel KS, 2010).*

On the other end, skin represents a formidable barrier for percutaneous drug absorption. Only those drugs having particular physicochemical properties with adequate lipophilicity (log Po/w ≅ 1-3), solubility, molecular weight or size and hydrogen bonding can be delivered passively via skin. These drugs topically applied can reach the different skin layers in optimum concentration to provide their therapeutic efficacy or even can reach the blood stream providing a regional

or systemic effect *(Katz M, 1971; Kováčik A, 2020).* In addition, many skin inflammatory diseases are characterized by leucocyte invasion leading to a proliferation and abnormal differentiation of keratinocytes with a consequent increase in skin thickness and alterations of skin barrier properties *(Korting HC, 2010)*. Significant efforts have been devoted to developing strategies to overcome the impermeability of intact or impaired human skin. There are many ways for circumventing the *stratum corneum*, which represents the uppermost layer of the skin and it is responsible for its protection, but at the same time provides the main barrier to drug penetration. These methods can be divided into chemical and physical penetration enhancement methods *(Dragicevic N & Maibach HI 2016; Jain H & Chella N, 2020).*

The chemical methods often focused on the design of synthetic or semisynthetic compounds *(Ita KB, 2016; Fang JY, 2006)*, but different kinds of nanocarriers increasingly represent a suitable strategy, as they have numerous advantages in comparison to conventional drug formulations *(Ramanunny AK, 2021; Bilia AR, 2014; Bilia AR, 2017; Bilia AR 2018b; Bilia AR 2019b; Puglia C, 2017)*. The recent researches focus on developing various types of nanodelivery systems, typically lipid-based, which allow controlled and targeted drug delivery (dermal or transdermal), improved therapeutic effectiveness and reduced side effects of drugs. As carriers they can be classified in polymeric-based and lipid-based nanovectors (*Sala M, 2018)*. Polymeric nanoparticles include nanospheres and nanocapsules, polymeric micelles and dendrimers. Lipid nanocarriers include solid lipid nanoparticles *(Souto EB, 2020)*, nanostructured lipid carriers *(Sharma G, 2017)*, liposomes and flexible vesicles *(Chacko IA, 2020; Pierre MBR, 2011)*, nanocochleates and nanoscale emulsions, namely nanoemulsions and microemulsions *(Shakeel F, 2012; Rai VK, 2018; Ita K, 2017).*

Structure and function of healthy human skin

Knowing skin structure (Figure 1), function, and especially its penetration pathways is fundamental to understanding how topical and transdermal dosage forms work and how different methods may be employed to enhance percutaneous drug penetration *(Heather AB, 2012; Lane ME, 2013; Bouwstra JA, 2002; Manikkath J, 2018).*

The skin is the largest organ of the body, covering about 1.7 m^2 and comprising approximately 10% of the total body mass of an average person. The

primary function of the skin is to provide a barrier between the body and the external environment. In addition, the skin has a role in homeostasis, regulating body temperature and blood pressure. The skin also functions as an important sensory organ in touch with the environment, sensing stimulation in the form of temperature, pressure, and pain. While the skin provides an ideal site for administration of therapeutic compounds for local and systemic effects, it presents a formidable barrier to the permeation of most compounds. Human skin is composed of four main regions: *stratum corneum*, viable epidermis, dermis, and subcutaneous tissues. A number of appendages are associated with the skin: hair follicles and eccrine and apocrine sweat glands. From a skin permeation viewpoint, the *stratum corneum* provides the main barrier, together with the skin tight junctions *(Bäsler K, 2016),* whereas the other layers and appendages are important target sites for drug delivery. The epidermis is a multilayered region that varies in thickness from about 0.06 mm on the eyelids to about 0.8 mm on the palms of the hands and soles of the feet. There are no blood vessels in the epidermis, therefore epidermal cells must source nutrients and remove waste by diffusion across the epidermal–dermal layer to the cutaneous circulation in the dermis. The *stratum corneum* provides an efficient physical barrier, but, when it is damaged, environmental contaminants can access the epidermis to initiate an immunological response. An understanding of these systems is important as they can be involved in skin diseases and may also be therapeutic targets for the management of these skin disorders. The outermost layer, the *stratum corneum* (or horny layer), consists of 10–20 μm of high density (1.4 g/cm3 in the dry state) and low hydration (10%–20% compared with about 70% in other body tissues) cell layers. Although this layer is only 10–15 cells in depth, it serves as the primary barrier of the skin, regulating water loss from the body and preventing permeation of potentially harmful substances and microorganisms from the skin surface. The corneocytes lack a nucleus and are composed of about 70%–80% keratin and 20% lipid within a cornified cell envelope (~10 nm thick). The cornified cell envelope is a protein/lipid polymer structure formed just below the cytoplasmic membrane that subsequently resides on the exterior of the corneocytes. The dermis is about 2–5 mm in thickness and consists of collagen fibrils that provide support, and elastic connective tissue that provides elasticity and flexibility, embedded within a mucopolysaccharide matrix. Within this matrix is a sparse cell population, including fibroblasts that produce the components of the connective tissue, mast cells involved in immune and

inflammatory response, and melanocytes responsible for pigment production. Due to this structure, the dermis provides little barrier to the permeation of most drugs, but may reduce the permeation to deeper tissues of very lipophilic drugs. A number of structures and appendages are contained or originate within the dermis, including blood and lymph vessels, nerve endings, hair follicles, sebaceous glands, and sweat glands. Contained within the dermis is an extensive vascular network that acts to regulate body temperature, provides oxygen and nutrients to and removes toxins and waste products from tissues, and facilitates immune response and wound repair. This extensive blood supply ensures that most permeating molecules are removed from the dermo–epidermal junction to the systemic blood supply, thus establishing a concentration gradient between the applied chemical on the skin surface and the dermis. Lymph vessels within the dermis play important roles in regulating interstitial pressure, mobilizing immune response and waste removal. As they also extend to the dermo–epidermal junction, they can also remove permeated molecules from the skin. While small molecule permeants such as water are primarily removed via the blood flow, it has been shown that clearance by the lymph vessels is important for large molecules such as interferon. Finally, there are three appendages that originate in the dermis: the hair follicles and associated sebaceous glands, eccrine, and apocrine sweat glands, involved the absorption of the molecules in the blood system *(Heather AB, 2012; Lane ME, 2013; Bouwstra JA, 2002; Manikkath J, 2018)*.

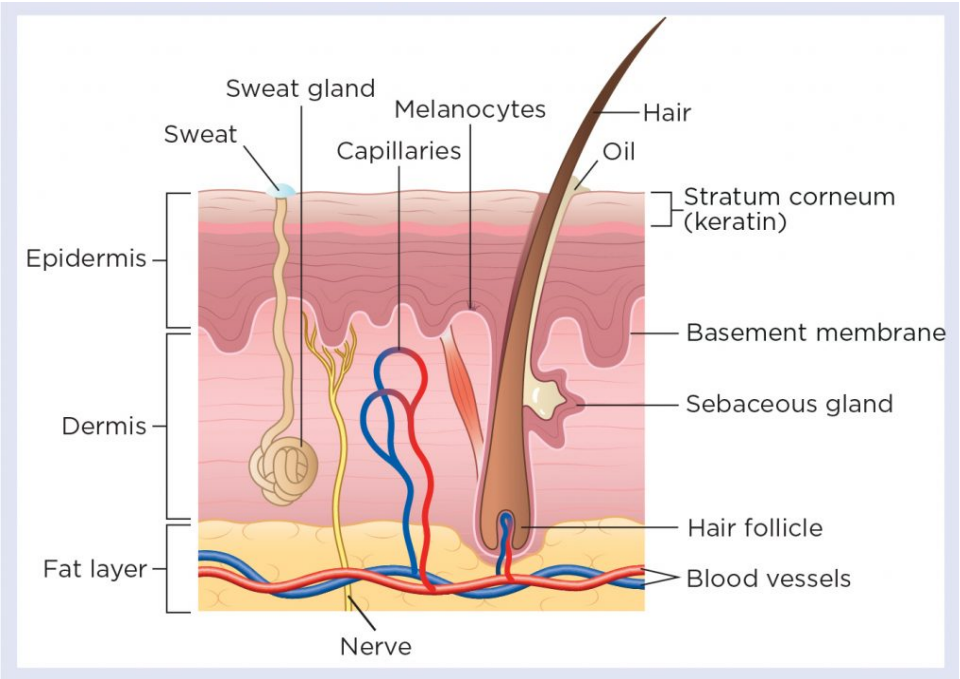

Figure 1. Cross-section of human skin.

Skin permeation pathways

While for most applications this will involve permeation to the deeper skin tissues (e.g., antihistamines, anesthetics, anti-inflammatories, antimitotics) or systemic uptake, other applications may necessitate targeting the skin surface (e.g., sunscreens, cosmetics, barrier products) or appendages (e.g., antiperspirants, hair growth promoters, anti-acne products). The passive absorption of drugs through the skin occurs via diffusion through intact epidermis (transepidermal route) (Figures 2a-2b) and/or skin appendages (transappendageal route) (Figure 2c). Two pathways through the bulk of the *stratum corneum* (SC) may exist: the intercellular lipid route between the corneocytes (intercellular) (Figure 2b) and the transcellular route through the corneocytes and interleaving lipids (transcellular) (Figure 2a), (*Heather AB, 2012; Manikkath J, 2018).* The appendageal route dominates during the lag phase of the diffusional process. In addition, the appendages represent only 0.1%–1% of the total skin surface area. Transcellular route is often regarded as a polar route through the *stratum corneum*, as the predominantly highly hydrated keratin provides an aqueous environment for the diffusion of hydrophilic drugs. Corneocytes in fact contain an intracellular keratin matrix that is relatively hydrated and thus polar in nature; permeation hence requires repeated

partitioning between this polar environment and the lipophilic domains surrounding the corneocytes. Based on the large body of permeation data, the view of most skin scientists is that transport through the *stratum corneum* is predominantly by the intercellular route. Intercellular route involves drug permeation only via repeated partitioning between the internal polar environment of corneocytes and the lipophilic domains surrounding the lipid bilayers. Although the intercellular environments occupies only a small area of the *stratum corneum*, it provide the only continuous route through the *stratum corneum*. Evidence of the importance of the intercellular route has been generated over many years. Within the intercellular lipid domains, transport can take place via both lipid (diffusion via the lipid core) and polar (diffusion via the polar head groups) pathways. The diffusional rate-limiting region of very polar permeants is the polar pathway of the *stratum corneum*, which is fairly independent of their partition coefficient, while less polar permeants probably diffuse via the lipid pathway, and their permeation increases with increase in lipophilicity. Clearly the relative contribution of these three pathways to skin permeation will depend on the physicochemical characteristics of the permeants. The permeation process from a transdermal drug delivery system into the systemic circulation involves a series of processes starting with release of the drug from the formulation, followed by diffusion into and through the *stratum corneum*, then partitioning to the more aqueous epidermal environment, diffusion to deeper tissues and possible uptake into the capillaries located in the dermis. The permeation of an infinite dose of a molecule applied to the skin surface in an *in vitro* experiment can be measured over time and plotted as cumulative amount permeating (Q) versus time. Steady-state permeation or flux (J) can be viewed fairly simplistically based on Fick's laws of diffusion:

$$J = \frac{dQ}{dt} = \frac{DPCv}{h}$$

where Q is the amount permeating a unit area of skin, D is the diffusion coefficient of the permeant in the skin, P is the partition coefficient between the *stratum corneum* and the vehicle, Cv is the applied concentration of permeant, and h is the diffusional path length. As *the stratum corneum* is the main barrier for most permeants, diffusion coefficient within and the path length of the intercellular route through the *stratum corneum* are most relevant. More complex mathematical approaches have been developed in order to describe and/or

predict skin permeation under a range of conditions, such as partition coefficient, molecular size and aqueous solubility, and other factors such as ionization and permeant binding within the *stratum corneum (Heather AB, 2012; Lane ME, 2013; Bouwstra JA, 2002; Manikkath J, 2018)*.

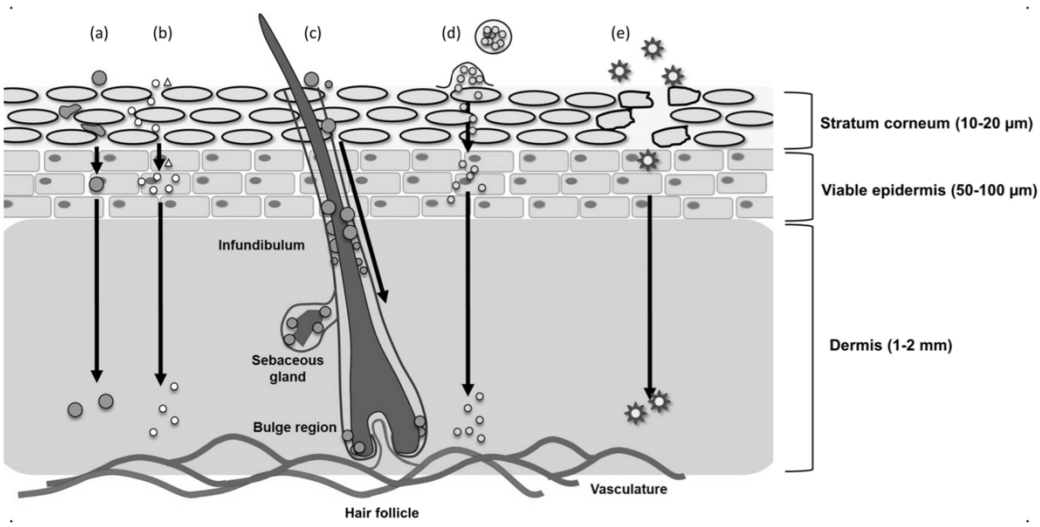

Figure 2. Pathways of intra- and transdermal transport of drug from nanoparticles. **(a)** Flexible particles (size>intercorneocyte diameter) undergoing deformation between corneocytes; **(b)** Rigid particles (size<intercorneocyte diameter) traversing through intercellular route; **(c)** Particles infiltrating hair follicle (transappendageal route)- bulge region (size ~600 nm), infundibulum (~120 nm, ~800 nm), sebaceous gland (200-300 nm); **(d)** Particle fusing/ degrading on SC and releasing drug, which can cross skin through transcellular, intercellular or transappendageal routes; **(e)** Disrupted SC with particles traversing transcellularly through viable epidermis.

(From*: Delving deeper into dermal and transdermal drug delivery: factors and mechanisms associated with nanocarrier-mediated strategies (2018).*
DOI: 10.2174/1381612824666180924122640)

NANO-SIZED DRUG DELIVERY SYSTEMS

Diverse strategies have been used to optimize the skin bioavailability of natural products (*Cheng YC, 2020; Jain H & Chella N, 2020)*. They are mainly chemical strategies producing semisynthetic compounds or synthetic analogues, but recently there is an increasing interest in developing appropriate formulations *(Münch S, 2017)*, including nanodelivery systems having optimal drug loading, ideal release kinetics and extended shelf-life, with a consequent considerable greater clinic effectiveness and less side-effects *(Bilia AR, 2017; Bilia AR 2019b; Puglia C, 2017)*. Nanomedicine represents an excellent tool to increase

bioavailability and activities of natural products, and to overcome anatomic barriers, such as the skin. Nano-delivery systems can therefore represent proper carriers for skin delivery of suitable therapeutic drug concentrations within the deeper skin layers and provide a sustained and/or controlled release *(Ramanunny AK, 2021)*.

Liposomes

Liposomes were first developed for drug delivery purposes as early as the 1970s *(Gregoriadis G, 1976a; Gregoriadis G, 1976b)*. In the last twenty years, liposomes and derived modified nanovesicles have represented the most studied and diffused colloidal delivery system, principally because they are smart approaches to increase stability and/or solubility and, as a consequence, bioavailability of drugs, thanks to their extreme versatility in loading both hydrophilic and hydrophobic molecules, to the high biocompatibility and the easy surface modification and preparation *(Bilia AR, 2019b)*. Accordingly, liposomes has been successfully developed, over the years, for dermal, transdermal and mucosal administration, as well as for other routes.

The name liposome derives from the two Greek words "lipo", meaning fat, and "soma", meaning body, which perfectly describes these spherical objects that are made mainly of natural or synthetic phospholipids (mostly phosphatidylcholine) and cholesterol, which acts as a fluidity buffer *(Riaz MK, 2018)*. Liposomes can be one bilayer forming unilamellar vesicles (ULV), several concentric bilayers forming oligolamellar or multilamellar vesicles (OLV, MLV) or nonconcentric bilayers forming multivesicular vesicles (MVV). Generally, ULV are, in turn, classified as Small Unilamellar Vesicles (SUV), Medium Unilamellar Vesicles (MUV), Large Unilamellar Vesicles (LUV), Giant Unilamellar Vesicles (GUV). The size of these vesicular structures can be rather small (in the range of 20 nm) or rather large (exceeding 1 μm), *(Bozzuto G & Molinari A, 2015)*.

Conventional liposomes generally accumulate in the upper layers of the *stratum corneum* with minimal permeation to deeper tissues or systemic circulation and are mainly suitable for local delivery of drugs *(Chen J, 2013)*. The characteristics of the formulation profoundly influence the permeation. In order to facilitate the passage of the drugs across the *stratum corneum*, a new type of liposome, elastic liposome, was first introduced by Cevc in 1992 *(Cevc G, 1992)*. Elastic vesicles were obtained by incorporation of edge activators into the lipid

bilayer. Unlike the conventional liposomes, vesicles with increased elasticity were able to squeeze through channels one-tenth their diameter, spontaneously penetrating across the *stratum corneum* by the intercellular route *(Chen J, 2013)*.

Numerous research groups have been worked with elastic liposomes, calling them with various names, such as flexible liposomes, deformable liposomes, ultradeformable or ultraflexible liposomes. Typically, elastic liposomes are composed of phospholipids, such as phosphatidylcholine, plus surfactant, and consist of at least one inner aqueous compartment surrounded by a lipid bilayer (Figure 3). The surfactant acts as edge activators that destabilize the lipid bilayer and increase the elasticity of the vesicle *(Chen J, 2013)*.

Moreover, other materials, working as penetration enhancers, such as propylene glycol, ethanol, transcutol, charged lipids, PEG-lipids and others are also reported to be included in the vesicle bilayer, obtaining different type of elastic vesicles (transferosomes, etosomes, penetration enhancer-containing vesicles (PEV), niosomes, cubosomes, invasomes *etc.*) *(Sala M, 2018; Chacko IA, 2020; Pierre MBR, 2011)* with increased skin permeability, because they interact and alter the complex structure of skin and thus enhance the partition of drug into different layers, beside modifying the vesicle bilayer fluidity (*Dragicevic N & Maibach HI 2016; Kováčik A, 2020).*

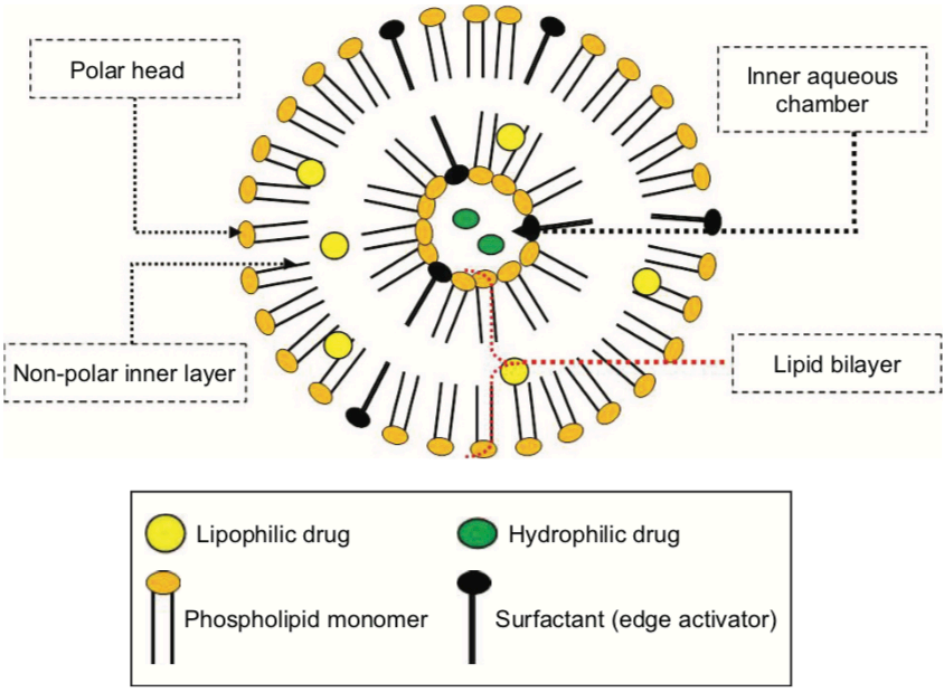

Figure 3. Schematic illustration of bilayer elastic liposomes displaying various components and structural morphology.

(From: *Elastic liposomes as novel carriers: recent advances in drug delivery (2017). DOI: 10.2147/IJN.S138267*)

Depending on their composition, elastic liposomes may penetrate through the *stratum corneum* with intact structure, or fuse and mix with skin lipids to lose their structure (Figure 4), (*Chacko IA, 2020)*. Therefore, different permeation behaviors of the elastic liposomes are mostly due to the difference in formulation ingredients. Currently, the skin permeation enhancing ability of elastic liposomes is generally considered to be due to the synergistic effect of elastic liposomes acting as drug carriers, as well as, permeation enhancers. However, based on the results of the most recent literature, the former mechanism may be more important than the latter *(Chen J, 2013)*.

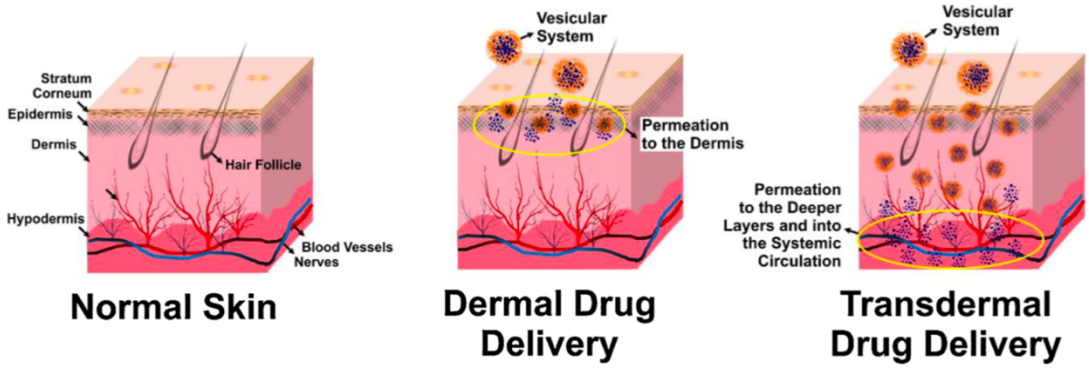

Figure 4. Representation of the healthy skin, the application, and the release from vesicular systems during dermal and transdermal drug delivery.

(From: *Lipid vesicles: A versatile drug delivery platform for dermal and transdermal applications (2020). DOI: 10.1016/j.colsurfb.2020.111262*)

Microemulsions

Recently, there has been considerable interest in the formulation of micro and nanoemulsion, for delivery hydrophilic and lipophilic drugs. Microemulsions are nanosized emulsions, which represent a versatile drug delivery system, as they can be used through all the administration routes (*Santos P, 2008)*. Microemulsions are very successful formulations because can improve solubility and, as a consequence, bioavailability of numerous drugs and extracts, due to their high solubilizing power (*Kreilgaard M, 2002)*. They are also easy to prepare, have great stability, as the oily and aqueous phases do not simply separate over

time, and long shelf life *(Ita K, 2017; Shukla T, 2018; Heuschkel S, 2008)*. In 1959, Schulman and co-workers visualized the existence of small emulsion-like structures by electron microscopy and subsequently coined the term "microemulsions". They are currently defined as optical isotropic, homogeneous and thermodynamically stable transparent dispersions of two immiscible liquids stabilized by an interfacial film of surfactants. Structurally, there are three different type of microemulsions: oil-in-water (o/w), water in oil (w/o) and bicontinuous systems (Figure 5). They have droplet size between 10 and 100 nm and require very low energy to be formulated, since they form spontaneously when aqueous, oil and amphiphilic components are brought into contact, besides having a lower production cost compared to nanoemulsions *(Talegaonkar et al., 2008; He et al., 2010)*. By contrast, nanoemulsions are non-equilibrium systems prepared using lower surfactant concentrations than microemulsions and with a spontaneous tendency to separate into the constituent phases. Nanoemulsions are, in fact, obtained by application of high energy, generally using a microfluidic or ultrasonic approach, to reduce droplet size to the nanoscale. Nevertheless, nanoemulsions may possess a relatively high kinetic stability, even for several years, due to their very small size, essentially the consequence of significant steric stabilization between droplets. They have droplets covering the size range of 20–500 nm and referred to as mini-emulsions, ultrafine emulsions and submicrometer emulsions *(Odriozola-Serrano et al., 2014; Ali et al., 2017)*.

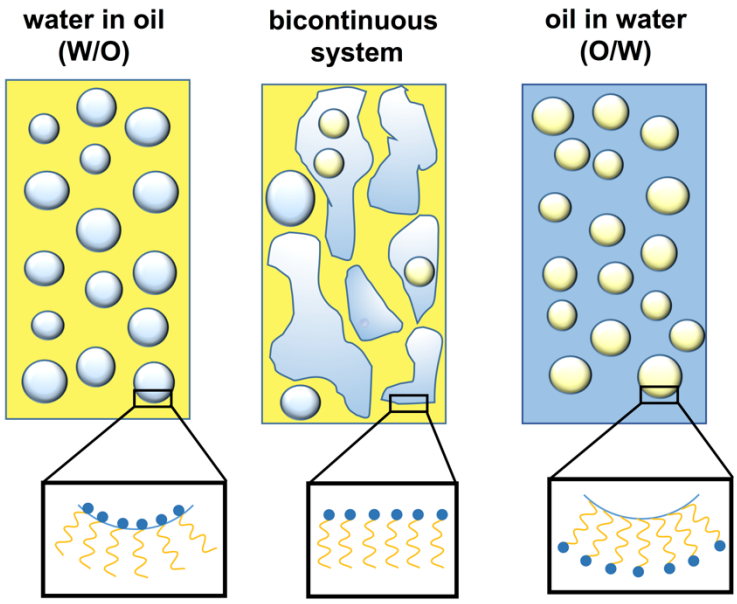

Figure 5. The different types of microemulsion.

Microemulsions are mainly used for their dermal/transdermal delivery potential owing to the presence of surfactants and co-surfactants, which act, together with the oil phase, as penetration enhancers *(Ita K, 2017)*. Thereby, the microemulsions, besides solubilizing drugs, reduce the interfacial tension at the skin surface. The permeation enhancer, sometime surfactant or lipid, used in the formulation may dissolve or perturbates the lipid bilayer structure of the *stratum corneum*. By this way, it minimizes the barrier function of the *stratum corneum* and opens a pore or passage for drug transfer across skin. The penetration enhancer alters the arrangements of the lipid bilayer and keratinized cells of *stratum corneum* and allows the drug penetration at a specific rate. The interaction between the *stratum corneum* (skin barrier) and penetration enhancer was best explained by Lipid-protein-partitioning theory. As per this theory, the drug permeation across skin, mainly depends on 1) drug interaction with intercellular lipid bilayer, 2) interaction with the keratinized cells and 3) the interaction of excess of co-solvent or penetration enhancer with the lipid bilayer of the *stratum corneum*; this may result in reversible dissolution of skin barrier and promotes the drug transfer across the skin. Once the barrier get minimized, the drug diffusion may take place via three significant pathways 1) intercellular: passage in between the cells, suitable for hydrophilic substances, 2) intracellular: drug transfer across the cells, ideal for lipophilic substances, and 3) follicular/transappendageal: drug transfer via hair follicle or other skin appendages (Figure 2), *(Shukla T, 2018; Heather AB, 2012; Manikkath J, 2018;).*

Furthermore, when choosing components for microemulsions, it is important to balance solubility/permeation properties with toxicological considerations. Sometimes, a substance with a great solubilizing potential may also cause irritation or have other deleterious effects on the skin *(Ita K, 2017).*

Nanocarrier-gel combination

Conversely, nanovesicles are aqueous colloidal dispersions with unsuitable viscosity properties especially for dermal, transdermal, and mucosal applications because of the low residence time on the skin and mucosa, in addition to drug leakage upon application and during storage. Accordingly, the double encapsulation of the drug into the vesicles and the encapsulation of the vesicles into semisolid formulations such as hydrogels (Figure 6) represent a substantial strategy to circumvent the drawbacks of nanovesicles and an opportunity to

optimize the drug release kinetics, providing a further level of control over the spatial and temporal release of the drug *(Elnaggar YS; 2014)*.

Indeed, vesicles are compatible with different polymeric gelling agents, in particular with ester and ether derivatives of cellulose, which is the world's most abundant, natural, renewable, non-toxic and biodegradable biological macromolecule *(Rincón-Iglesias M, 2019)*. Hence, cellulose-based polymers represent a structurally diverse class of biological macromolecule with a wide range of physicochemical properties, extensively used to prepare hydrogels for various pharmaceutical applications *(Arca HC, 2018)*.

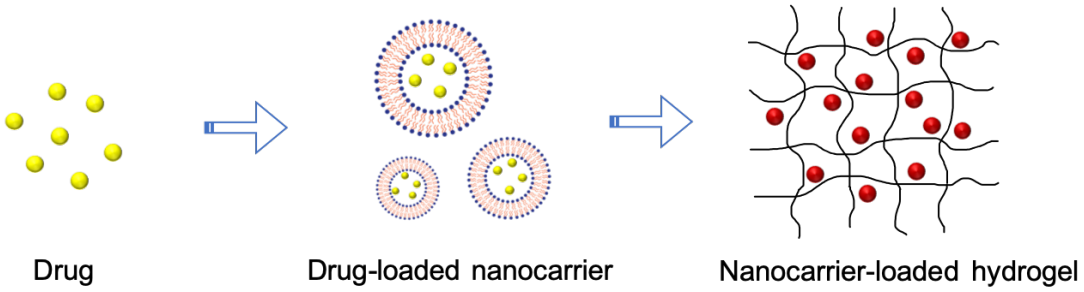

Figure 6. Drug-nanocarrier-hydrogel composite.

Accordingly, when emulsion and gel are used in a combined form, the dosage form prepared is named emulgel. This innovative system has been recently used as vehicle to deliver various drugs to the skin, for topical as well as systemic actions. In fact, the presence of a gelling agent in water phase converts the emulsion into emulgel. The obtained oil-in-water system is used to entrap lipophilic drugs, while hydrophilic drugs are encapsulated in the reverse (water-in-oil) system. Emulsions have high ability to penetrate the skin and topically used emulgels have several desirable properties, like being thixotropic, greaseless, easily spreadable as well as removable, emollient, non-staining, water soluble, bio-friendly, transparent, and having longer shelf-life, pleasant appearance *etc*. Similarly, when microemulsion and gel are used in combination, the prepared dosage form is called microemulgel, having the advantages of both emulgel and microemulsion. Both hydrophilic and hydrophobic drugs can be incorporated into microemulgels, which also provide a large surface area for drug absorption, while oil portion increases the bioavailability by improving

permeability of drugs. Also the stability of microemulsion is increased when it is incorporated in gel *(Ashara KC, 2016).*

ORAL MUCOSA DRUG DELIVERY

The oral mucosa has many properties which make it an attractive site for drug delivery but also provides several challenges for researchers investigating novel delivery techniques to overcome. Many different formulations including sprays, tablets, mouthwashes, gels, pastes, patches and innovative nanocarriers are presently used or studied for delivery into and/or across the oral mucosa. The delivery system used depends on the application for which the drug has been developed. Systems designed for local delivery to mucosal diseases require different pharmacokinetic behaviours compared to topical delivery for systemic applications. Currently there are a small number of drugs which are routinely delivered via the oral mucosa e.g. systemic delivery of glyceryl trinitrate for angina relief and topical corticosteroid administration for inflammatory diseases of the oral mucosa including lichen planus *(Hearnden V, 2012)*.

Structure of human oral mucosa

The oral mucosa is composed of an outermost layer of stratified squamous epithelium below this lies a basement membrane, a lamina propria followed by the submucosa as the innermost layer. The epithelium is similar to stratified squamous epithelia found in the rest of the body in that it has a mitotically active basal cell layer, advancing through a number of differentiating intermediate layers to the superficial layers, where cells are shed from the surface of the epithelium. The epithelium of the buccal mucosa is about 40–50 cell layers thick, while that of the sublingual epithelium contains somewhat fewer. The epithelial cells increase in size and become flatter as they travel from the basal layers to the superficial layers (Figure 7), *(Madhav NS, 2009; Sattar M, 2014; Sankar V, 2011).*

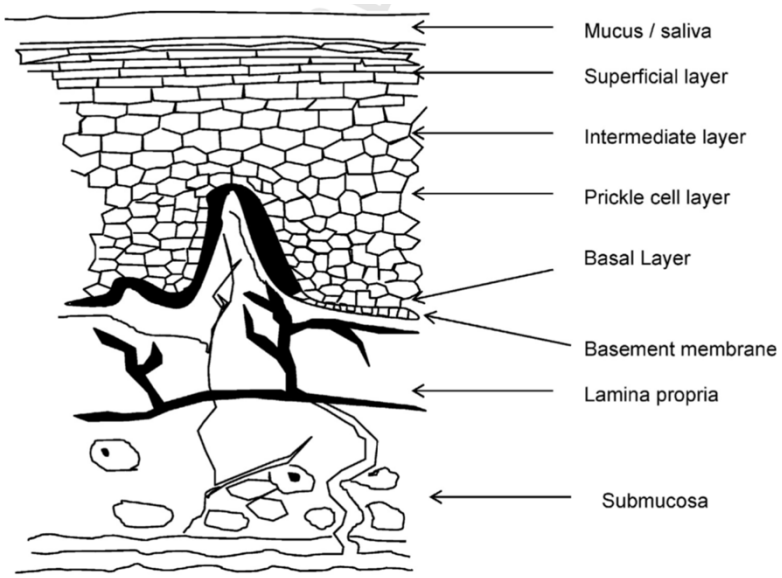

Figure 7. Structure of buccal mucosa.

(From: *Oral transmucosal drug delivery–current status and future prospects (2014). DOI: 10.1016/j.ijpharm.2014.05.043*)

Permeability

The permeability barrier is responsible for preventing exogenous and endogenous materials from entering the body across the oral mucosa and prevents loss of fluid from the underlying tissues to the environment *(Hearnden V, 2012; Madhav NS, 2009)*. The permeability barrier, which depends on the of level of keratinisation in buccal mucous membranes, is not as extensive as the skin's *stratum corneum*. It is estimated that the permeability of the buccal mucosa is 4–4000 times greater than that of the skin *(Hearnden V, 2012; Madhav NS, 2009; Sattar M, 2014; Sankar V, 2011)*.

As indicative by the wide range in this reported value, there are considerable differences in permeability between different regions of the oral cavity because of the diverse structures and functions of the different oral mucosae. In general, the permeability of the oral mucosae decrease in the order of, sublingual greater than buccal, and buccal greater than palatal. This ranking is based on the relative thickness and degree of keratinization of these tissues, with the sublingual mucosa being relatively thin and non-keratinized, the buccal thicker and non-keratinized, and the palatal intermediate in thickness but keratinized. Intercellular spaces at the upper one-third of the epithelium. This barrier exists in the outermost 200 μm of the superficial layer. According to permeation studies

performed using a number of very large molecular weight tracers, it seems apparent that flattened surface cell layers present are the main barrier to permeation, while the more isodiametric cell layers are relatively permeable. In both keratinized and non-keratinized epithelia, the limit of penetration coincided with the level where the membrane coating granules could be seen adjacent to the superficial plasma membranes of the epithelial cells. Since the same result was obtained in both keratinized and non-keratinized epithelia, keratinization by itself is not expected to play a significant role in the barrier function. The components of the membrane coating granules in keratinized and non-keratinized epithelia are however different. The membrane coating granules of keratinized epithelium are composed of lamellar lipid stacks, whereas the non-keratinized epithelium contains membrane coating granules that are non-lamellar. The membrane coating granule lipids of keratinized epithelia include sphingomyelin, glucosylceramides, ceramides, and other non-polar lipids, however for non-keratinized epithelia, the major membrane coating granule lipid components are cholesterol esters, cholesterol, and glycosphingolipids. Aside from the membrane coating granules the basement membrane may present some resistance to permeation as well, however the outer epithelium is still considered to be the rate-limiting step to mucosal penetration. The structure of the basement membrane is not dense enough to exclude even relatively large molecules *(Madhav NS, 2009; Sattar M, 2014).*

Not surprisingly, the loss of the permeability barrier in ulcerated or eroded areas of oral mucosa means that drugs diffuse more freely into the tissue than in intact areas of mucosa. However, the reduced barrier function can also lead to faster loss of drug from ulcer sites *(Sankar V, 2011).*

Oral mucosa: drug delivery site for local and systemic diseases

Oral mucosal delivery has the potential to treat many different conditions and diseases. Each therapy requires distinct penetration and drug retention profiles in order to optimize treatment and minimize side effects . Superficial infections, such as candidiasis, affect only the most superficial epithelial cells and drugs used to treat these infections do not need to cross the permeability barrier but should be delivered to the surface of the epithelium. Level of drug penetration required depends on the condition requiring therapy. Superficial infections such as candidiasis do not need to cross the permeability barrier. Mucosal diseases such as dysplastic lesions require retained delivery to the

affected epithelium. Oral lichen planus affects basal cells and the adjacent connective tissue and requires delivery to these cells. For systemic delivery, the therapeutic agent needs to cross the permeability barrier and should not be retained in the epithelium. Thereby, the oral cavity has been proposed as a potential topical delivery site for the local and systemic delivery of therapeutic agents *(Sankar V, 2011).*

Furthermore, drug delivery via the oral mucosa has several advantages: drugs are self-administrable and well accepted by patients. The oral mucosa is easily accessible, self-repair after damage or trauma and provides a more hydrated environment for solubilisation of drugs. In addition, there are fewer Langerhans cells in the oral mucosa than the skin reducing the risk of an allergic response, a drawback commonly experienced in transdermal delivery *(Sankar V, 2011; Hearnden V, 2012)*.

Specifically, local drug delivery can provide a more targeted and efficient drug-delivery option than systemic delivery for diseases of the oral mucosa. The main advantages of local drug delivery include (i) reduced systemic side effects, (ii) more efficient delivery as a smaller amount of drug is wasted or lost elsewhere in the body, (iii) targeted delivery as drugs can be targeted to the diseased site more easily when delivered locally, thereby reducing side effects *(Sankar V, 2011).*

At the same time, mucosal delivery sites have the advantage of delivering drugs also directly into the systemic circulation, avoiding first pass drug metabolism in the liver and pre-systemic elimination of the drug in the gastrointestinal tract. The high vascularity and good permeability of the oral mucosa, also makes it an ideal site for transmucosal absorption and systemic delivery of drugs which are required rapidly, for example, in the management of pain, seizures and angina pectoris. In particular, the absorption through the sublingual mucosa allows high bioavailability and almost immediate onset of action *(Hearnden V, 2012; Sattar M, 2014)*

Formulative approaches for oral mucosa delivery

The transmucosal absorption (systemic) represents the main challenge for the oral mucosa drug delivery. However, the local delivery still remain important for many oral mucosa conditions and an appropriate drug absorption is recommended to reach the desired therapeutic effect.

Some drugs can pass across the oral mucosa's permeability barrier without the need for a delivery device. *(Hearnden V, 2012)*. The amount of drug absorbed depends on the drug concentration, vehicle of drug delivery, mucosal contact time, venous drainage of the mucosal tissues, degree of the drug's ionization and the pH of the absorption site, size of the drug molecule, and relative lipid solubility (partition coefficient). Drug absorption via the oral mucosa is a passive diffusion process. By simplifying the oral mucosa into a hydrophobic membrane, Fick's first law can be used to describe the drug absorption process across epithelial membranes, which occurs by two different mechanisms: transcellular and paracellular *(Madhav NS, 2009).*

The unique properties of the oral mucosa have also imposed unique drug delivery challenges in formulation research. Currently used formulations are tablets, sprays, mouthwashes, gels, patches, wafers/films. However, some of the delivery challenges have led to research into technologies such as mucoadhesives, permeability enhancers and enzyme inhibitors, as well as nanosized drug delivery vectors such as liposomes, nanoparticles, micro/nanoemulsions *(Gavin A, 2015)*, SMEDDS, nanoemulgels *(Srivastava M, 2016)*, that could enhance both topical and systemic transmucosal delivery of drugs *(Hearnden V, 2012; Madhav NS, 2009)*.

Designers of drug delivery systems must consider many different factors including the acceptability to the patient, drug release profile and the practicality of using them. Disturbances to taste, speech and eating must all be considered for patient acceptability. If the aim is to produce a self-administrable device this should be easy to administer, should have good shelf life and should be easy to withdraw in the case of adverse effects. The drug release profile and penetration across the oral mucosa's epithelium are crucial in developing a therapeutically effective treatment. Sustained delivery may be beneficial compared to repeated administration for some applications however the exact release profile will depend on the condition being treated. Lastly, ingredients of the formulation are crucial to reach an appropriate permeation for the specific disease: e.g. most easily diffusible materials are lipid soluble substances, non-ionised species, and those with low molecular weights *(Hearnden V, 2012)*.

THEMATICS ADDRESSED IN THE THESIS

Among the nanocarriers with possible application in nanomedicine, conventional liposomes, modified nanovesicles, innovative vesicular systems and the correspondent hydrogels, as well as microemulsions and microemulgels were developed, optimized and characterized in this thesis work.

Conventional liposomes

Conventional liposomes are first-generation drug delivery systems but still represent extremely versatile carriers in terms of route of administration, encapsulation efficiency of both hydrophilic and lipophilic molecules and size range (from 50 nm to a few microns), which has a primary role in affecting their biodistribution and pharmacokinetics *(Bilia AR, 2016; Bilia AR, 2017; Bilia AR, 2019b)*. Their usefulness is also related to their great biocompatibility and biodegradability and a wide-ranging use because of their flexibility in being formulated in a broad range of pharmaceutical dosage forms, including (colloidal) solutions, aerosol, semi-solid or solid forms *(Naeem S, 2018)*. Liposomes, due to their ability to modulate drug transfer and serve as nontoxic penetration enhancers, represent useful nanocarriers for a variety of dermally active compounds. Their differences, in composition, charge and size, strongly influence their performance in topical drug delivery systems, accumulating the drug in upper layers of skin and/or in the hair follicles, acting as drug-depot, reducing the systemic absorption of the drug, or increasing transdermal drug penetration *(Bilia AR, 2017; Bilia AR, 2019b)*. Accordingly, many approaches of formulations have been applied both to isolated natural products and extracts *(Bilia AR, 2016; Bilia AR, 2017; Bilia AR, 2018b)*.

Development of nanoliposomes loaded with carbon dioxide Serenoa repens L. (saw palmetto) extract

Nanoliposomes based on saw palmetto (*Serenoa repens* (W. Bartram) Small) carbon dioxide (CO_2) extract were developed and characterised in these studies for the topical delivery. The CO_2 extract is a complex mixture constituted mainly of free fatty acids, sterols, phosphoglycerides, glycerides and carotenoids *(Marti G, 2019)*. Extraction by supercritical CO_2 is a suitable technique to avoid thermolability of the active natural products and represent an emergent technique especially used for the recovery of lipophilic phytocomplexes from

plants. Furthermore, supercritical CO_2 is not toxic, no-flammable, not expensive and eco-friendly *(De Monte C, 2014)*. Accordingly, there is an increasing interest in the use of saw palmetto CO_2 extract because it represents a good alternative to the widely used ethanol and hexane extracts. In addition, this CO_2 extract has a qualitative and quantitative composition similar to those of the traditional extracts *(Marti G, 2019)* and preserves the biological properties of the active constituents *(Zhu H, 2018)*. The saw palmetto CO_2 extract has many biological activities, including anti-inflammation, anti-androgen and anti-proliferation effects (*Guccione C, 2018)*, and it has been recently investigated for the treatment of hair loss because of the inhibition of 5α-reductase enzyme, responsible of the conversion of testosterone to the most potent androgen, the 5α-dihydrotestosterone *(Zhu H, 2018)*. The study clearly evidenced that the extract significantly increased human keratinocyte cell viability compared to dihydrotestosterone-only treated cells ($p<0.05$) and it also increased hair density, weight and thickness compared to dihydrotestosterone-only treated mice ($p<0.05$). In addition, the extract treatment significantly triggered follicle growth and decreased inflammatory response, as well as it significantly decreased TGF-β2 and cleaved the caspase 3 expression in hair loss mouse models compared to the treatment with dihydrotestosterone ($p<0.05$). Finally, the saw palmetto significantly enhanced Bcl-2 expression and reduced Bax expression compared to dihydrotestosterone ($p<0.05$) [9]. Due to the promotion of hair regeneration in hair loss mouse models, by activating TGF-β signaling and mitochondrial signaling pathway, nanoliposomes based on the saw palmetto CO_2 extract were developed and fully characterized as regards physical and chemical properties of the nanocarrier.

Modified nanovesicles

Liposomes mostly consist of mixtures of phospholipids and cholesterol, which generally accumulate in the *stratum corneum* and in the skin appendages, with negligible permeation through deeper skin layers, because of their low flexibility, as reported by most of the literature *(Sinico C, 2008; Iqbal B, 2018; Gillet A, 2011)*. By contrast, some molecules can impart deformability or elasticity to the bilayer membrane of liposomes, resulting in considerable improved drug permeability through the skin by several orders of magnitude *(Matos C, 2019; Fernández-García R, 2019; Carita AC, 2018)*. However, this enhanced permeation is sometimes limited to overcome the main skin barrier, the *stratum corneum*, in

order to achieve the deeper skin layers without having systemic absorption, and, thus, treat local skin diseases, avoiding side effects of the loaded drug. By contrast, in some other cases nanovesicles improve drug absorption through the skin until the blood stream to provide a systemic effect. Hence, modified nanovesicles can allow both dermal (local/topical) and transdermal (systemic) drug delivery, based on their composition and flexibility. Moreover, these nanocarries can also effectively protect the drug against the degradation from endogenous enzymes and from environmental conditions *(Cevc G, 2008)*.

Glycerosomes of Melissa officinalis L. essential oil for effective anti-HSV type 1

Glycerosomes are modified nanovesicles developed by Manca at al. *(Manca ML, 2013)*, based on glycerol, a polyalcohol largely used as humectant in semisolid preparations, which can also increase the fluidity and deformability of the vesicle bilayer, improving the permeation of the active ingredients through the skin. Glycerosomes were used in this thesis as lipid nanocarriers for loading *Melissa officinalis* L. (Lamiaceae).

Lamiaceae is a well-known family of aromatic herbs, diffused in many regions of the world. Numerous plants belonging to this family are largely used for medicinal purposes and in perfumery, as well as they are extensively applied to impart flavor and aroma to foods. Most of them are rich in essential oils (EOs) *(Nieto G, 2017; Karpiński TM, 2020)* which consist of complex mixtures of volatile, liquid, odorous, flavor and strongly active compounds. Due to their various biological properties, principally antioxidant and antimicrobial, they have been widely used since the Middle Ages and currently, they also may have several applications in different fields, from medicine and cosmetics to food. However, their high volatility and low stability to direct exposure to light, oxygen, heat, and humidity can limit their potential. Also, in folk medicine, EOs were widely used and applied on the skin after dilution to avoid local irritations.

Nanocarriers, such as liposomes, micelles, lipid and polymeric nanoparticles, micro/nanoemulsion and cyclodextrin complexes, which can definitely load the essential oils, represent an innovative challenge to optimise the essential oil formulation, overcoming these main limitations *(Bilia AR, 2014; Isacchi B, 2011b; Guccione C, 2017; Isacchi B, 2012)*. The resulting nanocarriers are stable and efficient, easily and safely produced, capable of stabilizing the essential oil, modulating its release and optimising its activity *(Bilia AR, 2019b)*. Recently, Risaliti and coworkers (2019) demonstrated enhanced antioxidant,

anti-inflammatory and antimicrobial activities of the essential oils of *Rosmarinus officinalis* L. and *Salvia triloba* L. plants, when formulated in liposomes *(Risaliti L, 2019)*. The same authors further improved antifungal properties against 10 different drug-resistant *Candida* strains of *Artemia annua* L. EO loaded in nanoliposomes *(Risaliti L, 2020b)*.

The lemon balm essential oil obtained from hydro-distillation of *Melissa officinalis* L. (Lamiaceae) is one of the most known antiviral essential oils *(ESCOP, 2013)*, active against the herpes labialis. This is the most frequent clinical manifestation of reactivated herpes simplex virus type 1 (HSV-1) infections. About 80 percent of the global population carries HSV-1. After establishing latency, HSV can reactivate causing frequent infections in some patients. Since 1970, several efficient antiviral drugs have been developed, and in particular, acyclovir, the most commonly used drug in HSV treatment, is able to specifically inhibit the viral DNA polymerase when new viral DNA is synthesized during the replication cycle. Although antiviral therapy by acyclovir and other related nucleoside analogues has allowed continual and substantial progress in the treatment of both primary and recurrent infections, some limitations of these drugs have been reported in recent years, mainly represented by viral resistance and long-term toxicity *(Whitley R, 2018)*. Consequently, new antiviral agents are urgently needed to obtain effective antiviral therapies. In particular, essential oils are widely used in folk medicine and many of them can directly inactivate herpes virus and interfere with virion envelope structures or mask viral structures that are necessary for adsorption or entry into host cells, also inhibiting acyclovir-resistant HSV-1 isolates, as demonstrated by the assays with isolated constituents or some essential oils *(Schnitzler P, 2019; Astani A, 2010; Astani A, 2011)*. Previously, some studies have focused on the anti-HSV-1 activity of aqueous or hydro-alcoholic extracts of *Melissa officinalis* and their principal phenolic compounds, namely caffeic acid, *p*-coumaric acid and rosmarinic acid *(Astani A, 2012; Astani A, 2014; Mazzanti G, 2008; Nolkemper S, 2006)*. Other studies were focused on the essential oil and/or isolated main constituents citral and β-caryophyllene against HSV-1 and/or HSV-2, but none of them were given using a formulated essential oil *(Schnitzler P, 2008; Allahverdiyev A, 2004)*.

Innovative nanovesicular systems

The majority of pathological skin conditions are treated with topical formulations delivering therapeutically effective concentration of drugs in skin

layers and exerting a local effect. By contrast, many potent drugs display scarce ability to penetrate the skin, in particular the *stratum corneum*, which represents the main obstacle that limit their absorption after topical application and hence inherent potency. Particularly, many skin inflammatory diseases are characterized by leucocyte invasion leading to a proliferation and abnormal differentiation of keratinocytes with a subsequent increase in skin thickness and alterations of skin barrier properties *(Korting HC, 2010)*. Nano-delivery systems can represent proper carriers for skin delivery of suitable therapeutic drug concentrations within the deeper skin layers and provide a sustained and/or controlled release *(Patzelt A, 2017)*. Phospholipid-based nanovesicles are particularly suitable for topical formulations because of their high biocompatibility with skin lipids and negligible toxicity. Modified nanovesicles, based on glycerol and propylene glycol can impart flexibility to the liposomal bilayer, allowing to reach the deeper skin layers, but a further modification was investigated in this thesis.

Innovative nanovesicular systems, escinosomes and ascosomes, were developed using bioactive molecules as vesicle bilayer components. Escinosomes are escin-based vesicles, whereas ascosomes are ascorbyl derivatives-based vesicles. Both nanocarriers were developed for the skin delivery of selected model drugs.

Development and percutaneous permeation study of escinosomes, escin-based vesicles loaded with berberine chloride

The first study was designed to explore the conversion of the bioactive amphiphilic saponin escin (ESN), into a vesicle bilayer-forming component. Escinosomes, the obtained nanovesicles made of phosphatidylcholine plus ESN, were loaded with berberine chloride, selected as model drug for dermal delivery.

Saponins are natural non-ionic surfactants with useful pharmacological and biological properties, mainly distributed in plants, lower marine animals, and some bacteria. Saponins contain an aglycone with a steroid (C27) structure or a triterpene (C30) moiety, represented by a four-ringed steroid nucleus or a five-ringed structure. The amphiphilic properties of saponins are due to sugar moieties attached with one (monodesmosidic saponins , usually glycosylated at C-3 position) or two (bidesmosidic) hydroxyl or carboxyl moieties. When dissolved in water, saponins produce foam, which is related to their name from the Latin word *sapo (Vincken JP, 2007)*.

ESN is the major active saponin isolated from the seed of *Aesculus hippocastanum*. It is a triterpenoid glycoside with three sugar units linked at C-3 of the aglycone moiety, and consisted of a mixture of α-escin and β-escin. ESN is clinically used to increase venous wall tone and to achieve anti-oedema and anti-inflammatory effects, accounting for its efficacy in the treatment of chronic venous insufficiency, haemorrhoids and post-operative oedema *(Gallelli L, 2019)*. It has been shown that, after application on dorsal and ventral skin in mice and rats, 25% and 50%, respectively of the topical dose was absorbed by the skin. Following topical administration in pigs, high ESN concentrations were found under the site of application, even in deeper muscle structures *(Gallelli L, 2019)*. Previously, a study using 1,2-dimyristoyl-sn-glycero-phosphocholine (DMPC, 15 mg/ml) vesicles evaluated the effects of ESN addition. Vesicles were stable below 1 mol % of ESN. Between 1 and 6–7 mol % of ESN, the formation of vesicles was also observed, but large aggregates that precipitate over time occurred. Micelle-sized structures were formed at ESN contents above 6–7 mol % *(Sreij R, 2017)*. In a further study, the interaction of ESN with cholesterol and/or natural dipalmitoylphosphatidylcholine (DPPC) monolayers was investigated using Langmuir isotherms *(De Groot C, 2018)*. Intercalation of ESN in a monolayer made of pure cholesterol was low, whereas in a pure DPPC monolayer, no intercalation of ESN was detectable. By contrast, in aqueous pseudo-ternary systems (ESN, DPPC, cholesterol) and in pseudo-binary systems (ESN, cholesterol), colloidal microstructures built up from ring-like and worm-like subunits were observed *(De Groot C, 2018)*.

BRB is a natural quaternary isoquinoline alkaloid isolated from several medicinal plants of the genera *Berberis*, *Hydrastis*, *Coptis*, *Coscinium*, *Mahonia*, which are traditionally used for various skin conditions. BRB is a representative natural constituent having a variety of biological effects through different mechanisms of actions *(Hou Q, 2019)*. Despite the evidenced potentiality of BRB in the treatment of skin diseases, its topical application is limited because of low penetration into skin and scarce dermal availability due to its high hydrophilicity, the aqueous solubility of 1–2 mg/mL at 25 °C and the approximate logP value of −1.5 hinder its delivery across the skin layers *(Spinozzi S, 2014).* Recently, BRB-oleate complex was made by the hydrophobic ion pairing approach to enhance BRB dermal penetration. The proposed complex resulted in enhanced lipid solubility of BRB, compared with the free drug *(Vincken JP, 2007).* A further study on BRB-oleate complex loaded in hydrogels significantly

alleviated psoriasis symptoms and reduced the inflammatory cytokines levels *(Gallelli L, 2019)*.

In order to assess that ESN potential activity remained after the formulation in the vesicles, the hyaluronidase inhibition activity of these escinosomes was evaluated. Developed escinosomes were characterized by high stability and high deformability, working as vector through the different skin layers *(Carita AC, 2018)*. Nanovesicle deformability after BRB loading was also examined, in order to evaluate their passage through the skin and BRB transport in the different skin layers. A further aim of the present work was to investigate the anatomical similarities of rabbit ear skin with human abdominal skin with respect to the *stratum corneum* and epidermal thickness as well as the hair follicular density, in order to evaluate permeation properties of the different formulations using vertical diffusion Franz cells.

Hydroxypropyl methylcellulose hydrogel of berberine chloride-loaded escinosomes: dermal absorption and biocompatibility

In this study, hydroxypropyl methylcellulose (HPMC) was selected to prepare an escinosome-based hydrogel, because it is a water-soluble, inert, tasteless, odorless, and stable between pH 3 and 11, non-toxic and non- irritating material, biocompatible and viscoelastic biological macromolecule used as an excipient and controlled-delivery component in the dermal and transdermal drug delivery systems. Due to the presence of polar (hydroxypropyl) and non-polar (methyl) groups in HPMC, it can make intermolecular, intramolecular and hydrophobic interactions, based on the degree of substitution of polar and non-polar groups *(Ghadermazi R, 2019)*.

The resulting escinosome-based hydrogel was investigated to enhance the skin permeability of BRB, selected as model drug. The formulation, designed for topical application, combined the advantages of a modified release and increased permeability across the skin (escinosome components), with optimal viscosity properties and higher residence time on the skin (polysaccharide matrix).

The penetration and permeation properties of BRB loaded in escinosomes and formulated as HPMC-hydrogel were evaluated with nude mouse skin, using the Franz cell system. In addition, the acute dermal irritation/corrosion was tested *in vivo* using Sprague-Dawley rats.

Hydroxyethyl cellulose hydrogel for skin delivery of khellin in ascosomes: characterization, in vitro/in vivo performance and acute toxicity

Ascosomes represent a further innovative nanocarrier developed in this thesis, able to maintain the antioxidant properties of L-ascorbic acid and to enhance its skin penetration. Ascosomes were prepared using phosphatidylcholine plus alkanoyl-6-O-ascorbic acid esters, namely ascorbyl octanoate (ASC8) and ascorbyl decanoate (ASC10).

L-ascorbic acid (vitamin C) is widespread in vegetables and plays an important role in the prevention and treatment of a large number of chronic diseases, including skin disorders. In particular, L-ascorbic acid has an important biological role because it is involved in the collagen synthesis, helping to prevent and treat ultraviolet (UV)-induced photodamage *(Pullar JM, 2017)*. However, after topical application, vitamin C can hardly penetrate the hydrophobic *stratum corneum* of the skin due to its high solubility in water (33 g/100 mL). Moreover, upon light irradiation or exposure to either high pH (greater than 6) or heat, vitamin C is easily degraded by radical species, certain enzymes and/or transition metal ions *(Pinnel SR, 2001)*. In order to overcome these severe drawbacks, amphiphilic derivatives, such as alkanoyl-6-O-ascorbic acid esters (ASCn, where n indicates the number of carbons in the alkyl side chain), were synthetized.

Because of their amphiphilic nature, ASCn form supramolecular assemblies in aqueous dispersions, and have been investigated as potential platforms for drug delivery systems. Specifically, the study focused on the evaluation of the potential use of ascosomes as carriers for the skin delivery of khellin (2-methyl-5,8-dimethoxy-furanochromone), selected as a model lipophilic drug.

Khellin is the major constituent of *Ammi visnaga* (L.) Lam. (Apiaceae), whose fruits have been described in diverse Pharmacopoeias because of the numerous pharmacological properties, including those related to skin pathologies, for instance vitiligo and psoriasis *(World Health Organization, 2007)*. The chemical structure is related to psoralen constituents, but khellin has a greater therapeutic interest because of the lower phototoxic and mutagenic effects when compared to these derivatives. Besides the high therapeutic potential, khellin has a very low solubility in water (25 mg/100 mL), *(Hassan MA, 1998)*, which can limit the therapeutic efficacy.

A hydrogel formulation based on khellin-loaded ascosomes was developed in order to facilitate the application of the formulations on the skin and evaluate the *in vitro* permeation through nude mouse skin, as well the *in vivo* performance

after skin application to observe the acute toxicity for skin and liver. The selected biopolymer was hydroxyethyl cellulose, due to the peculiar characteristics. It is, indeed, a water soluble non-ionic cellulose derivative, very suitable for dermatological use, because of the high biocompatibility, biodegradability, nontoxicity and hydrophilicity *(Harika K, 2012)*. The hydrogel of khellin-loaded ascosomes was developed in order to overcome the short residence time of the liquid formulation upon application on the skin, and to enhance the stability of the vesicles preventing their aggregation. Permeation properties were *in vitro* evaluated using nude mouse skin and the safety profile of most the promising formulation was *in vivo* investigated by acute dermal irritation/corrosion test, observing also acute toxicity on skin and liver by histological and pathological analyses.

Microemulsions

This thesis also deal with the development of three different oil-in-water microemulsions for the oral mucosa delivery of clobetasol propionate and for the dermal administration of cannabidiol and khellin.

The wide interest for microemulsions as drug delivery systems, in particular for topical application and dermal/transdermal delivery, is principally due to the enhanced absorption of drug across biological membranes. Specifically, enhanced skin delivery has been demonstrated in comparison to conventional emulsions and gels, attributed both to the interaction of their components on the skin and their phase structure and globule size, which can easly cross the *stratum corneum*. However, while coarse emulsions are creamy in appearance and tend to adhere well to the skin, microemulsions are generally very fluid and not appropriate for topical application. Accordingly, a suitable consistency could be obtained by the use of proper gelling constituents (*Santos P, 2008).*

Mucoadhesive microemulgel for topical delivery of clobetasol propionate in the treatment of mucus membrane pemphigoid of the oral cavity

A microemulsion of cloebetasol propionate (CP-ME) was developed for the treatment of mucus membrane pemphigoid (MMP), a chronic vesicobullous dermatosis with autoimmune pathogenesis and main involvement of the mucous membranes. It is defined by the presence of autoantibodies (IgG and/or IgA), which target basement membrane antigens. MMP shows a predominant involvement of the oral mucosa (90%), and the vesicobullous lesions frequently

develop in erosions difficult to heal. Erosions are painful and make feeding and phonation difficult, with a considerable reduction in the patient's quality of life. This is a rare autoimmune disease, with an incidence of 2/million/year and it generally affects middle-aged and elderly people *(Carey B, 2019; Leuci S, 2000)*. Due to the rarity of pathology, there are not specific pharmaceutical products. However, the topical treatment of pemphigoid forms localized in the oral cavity was mainly based on clobetasol propionate solutions, directly applied on the buccal mucosa, whereas the systemic treatment of severe or not-localized MMP was mainly based on prednisone. CP solution (Clobetasolo ISDIN) is actually used as off-label drug, thanks to its anti-inflammatory, anti-pruritic and vasoconstrictive properties. CP is in fact a synthetic corticosteroid with high specificity for the glucocorticoid receptors *(Carey B, 2019; Leuci S, 2000)*. However, the CP solution has low residence time on the oral mucosa and the purpose of this work was to formulate CP in a microemulsion-based hydrogel (microemulgel, CP-MEgel) with mucoadhesive properties. In fact, microemulsions, defined as transparent, monophasic, optically isotropic and thermodynamically stable colloidal dispersions with small droplet sizes, offer significant advantages. Meanwhile the hydrogel increases the viscosity and the mucoadhesion of the formulation, and, as a consequence, the residence time on the application site, in order to increase CP concentration in the epidermal-dermal layers and the cutaneous bioavailability. Compatible excipients with the injured buccal mucosa, with high safety profile upon ingestion and with good flavour were selected among various vehicles, by a preliminary screening. Different microemulsions were prepared by the titration method, in order to select the most homogenous one, which was loaded with CP. A pseudo-ternary diagram was constructed in order to define the microemulsion existence range and chemical and physical stability studies were carried out storing the microemulsion at 25 °C and 4 °C for 3 months. Subsequently, different gelling agents were added to the microemulsion in different percentages and carboxymethyl cellulose (CMC) and carboxymethyl chitosan (CMChit) were selected as optimal thickening agents because of their many physical and chemical properties and their ability to rapidly and uniformly jellifying the system, as well as for their mucoadhesive property *(Hu D, 2016)*. CMChit is a cationic polysaccharide (at pH<4.1) with antimicrobial activity and permeation enhancing property; it also induces the cell growth and works as emulsion stabilizer. CMC is an anionic polysaccharide, abundant in nature and with low

cost. In addition, both these compounds are water soluble (hence suitable for dispersion in the aqueous external phase of the microemulsion) and mucoadhesive. They are biocompatible and biodegradable, and they have gelling activity and skin regeneration/wound healing properties, in addition to moisture absorbtion/retention *(Shariatinia Z, 2018, Fonseca Santos B, 2017; Kanikireddy V, 2020)*. The viscosity of the obtained microemulgel (CP-MEgel) was measured by the Brookfield rotational viscometer and the chemical and physical stability was monitored for three months, storing the sample at 25 °C, away from the light. Dynamic light scattering analysis and scanning/transmission electron microscope observation were performed to physically characterize the developed microemulsion and microemulgel. Finally, *in vitro* release and permeation studies were carried out by vertical diffusion Franz cells and porcine buccal mucosa.

Development and optimization of biopharmaceutical properties of a new microemulgel of cannabidiol for locally-acting dermatological delivery

Furthermore, a cannabidiol-loaded microemulsion (CBD-ME) was developed for the treatment of the atopic dermatitis, a chronic relapsing condition that is characterized by itching and redness of the skin. Atopic dermatitis is primarily a disease of infancy and early childhood. Common symptoms are dry skin, itching, redness and lichenification of the skin, associated to sleep disturbance and emotional distress *(Schneider L . 2012)*. Nowadays, there are not therapies able to induce the remission of atopic dermatitis, and two kind of approaches are used. The no pharmacological one consists in using of emollients and bath oils, and avoiding of clinically relevant allergens. The pharmacological approach, employed as first-line therapy, consists in the topical application of creams, gels or foams based on corticosteroids, whereas severe refractory diseases are treated by oral administration of steroids and systemic immunomodulators such as cyclosporine A *(Ring J. 2012, Wollenberg A. 2018)*. Recently, the usage of cannabinoids in treating various dermatological conditions is gaining increasing interest. Cannabinoids exert in fact anti-inflammatory and anti-pruritic activities, due to their interaction with the CBD2 endocannabinoid receptors localized in the skin cells *(Sheriff T. 2019)*. Cannabidiol (CBD) is a non-psychotropic phytocannabinoid, which demonstrated a role in modulating skin inflammatory response. In this study CBD was formulated in a microemulgel, in order to control its cutaneous

absorption and retention. The microemulsion was prepared by the aqueous titration method and a pseudo-ternary diagram was constructed in order to define the microemulsion existence range. Microemulsion components were carefully selected for their biopharmaceuticals properties and their safety profile in cutaneous applications. Isopropyl myristate, selected as microemulsion oily phase, is an emollient and a well-known skin penetration enhancer, widely used in cosmetics and pharmaceutical preparations. Solutol HS 15 (polyoxyl 15 hydroxystearate) is a potent emulsifying and solubilizing agent, selected as non-ionic surfactant, whereas Transcutol P, largely investigated for the skin penetration enhancing property, was chosen as cosolvent. CBD-ME was then incorporated in Sepigel 305 by manual stirring, well known as excellent rheology modifier. Viscosity and pH of the obtained microemulgel (CBD-MEgel) were measured and the physical and chemical stability was monitored. Microemulsion and microemulgel were both physically characterized by dynamic light scattering techniques and scanning/transmission electron microscopy, whereas the final content of cannabidiol was evaluated by HPLC-DAD. I*n vitro* release and permeation properties of CBD were investigated by vertical diffusion Franz cells, using nitrate cellulose membranes and rabbit ear skin, respectively.

Microemulsion-hydrogel composite as a promising vehicle for dermal delivery of lipophilic molecules: the case of khellin

Another study of thesis was focused on developing a novel ME loaded with khellin (2-methyl-5,8-dimethoxy-furanochromone), selected as model natural drug and largely used for the anti-inflammatory properties *(Risaliti L, 2020)*. The ME was then loaded in a tridimensional gel matrix using different cellulose derivatives and the release and viscosity properties of the final formulations were investigated.

An oil in water (O/W) ME was prepared using glycerol (2.25%), Labrasol® (20.25%) and vitamin E acetate (2.50%), and a pseudo-ternary diagram was constructed to determine the optimal component ratios. Naturally occurring vitamin E plays key roles in protecting cell membranes from lipid peroxidation by free radicals, reducing the age-dependent increase of collagenase expression by inhibiting protein kinase C activity *(Nachbar F, 1995; Ricciarelli R, 1999)*. Rather than vitamin E itself, esters are often used in topical products, because there are stable and easily bio-converted to its biologically active form, vitamin E. Accordingly, in the present study vitamin E acetate was selected as lipophilic

phase due to the dermatological properties *(Gehring W, 1998)*. Among the surfactants the non-ionic category is very often used in ME formation and represent a valid alternative to natural surfactants as they are of low toxicity, low irritancy and high biodegradability. Labrasol®, a mixture of mono-, di- and tri-glycerides of C8 and C10 fatty acids, was selected as surfactant because its non-ionic nature results less irritating to human skin *(McCartney F, 2019)*. ME formulations need also of cosurfactants, typically polyols or alkanols, which help to reduce the interfacial tension, and in turn to reduce the size of the dispersed droplets. The presence of the cosurfactant also reduces the rigidity of the interfacial film, leading to the formation of a bicontinuous structure typical of ME. In the present study glycerol was selected because of its diverse actions on the epidermis including protection against irritating stimuli, improvement of skin barrier function and mechanical properties, hydration, and acceleration of wound-healing processes *(Fluhr JW, 2008)*.

Generally, O/W ME viscosity can be increased and optimized for topical use by the use of hydrophilic polymers, which do not affect ME stability because they do not interact with the component of the ME, in particular surfactants or cosurfactants *(Jaiswal M, 2016)*. Among the hydrophilic polymers, carboxymethylcellulose (CMC) was chosen because it is the most used viscosity modifiers (thickeners) to stabilize emulsions. The viscosity is both concentration and temperature dependent: increasing temperatures give decreasing viscosities, while increasing concentrations give increased viscosities *(Chen H, 2007)*.

Other nanodrug delivery systems for different administration routes or purposes

Both liposomes and microemulsions are very versatile systems, suitable for all the administration routes and also investigated in food industry, besides in the pharmaceutical and cosmetic ones. Part of the PhD thesis deals with the development of nanoliposomes loaded with berberine chloride plus tariquidar, to enhance the intracellular uptake of the antitumoral drug in human leukemia cells with overespression of Pg-p, thanks to the efflux pump inhibitor. Moreover, glycerosomes and propylene glycol nanovesicles loaded with *Origanum onites* L. and *Satureja thymbra* L. essential oils were explored as food-grade delivery systems of alternative preservatives and sanitizers. Lastly, a microemulsion for the oral delivery of an olive extract (*Olea europaea* L.) was developed and *in vitro* fully characterized.

Co-delivery of berberine chloride and tariquidar in nanoliposomes enhanced intracellular berberine chloride in a doxorubicin-resistant K562 cell line due to P-gp overexpression

In the present paper, the co-encapsulation of berberine chloride (BRB) and tariquidar (TAR) in nanoliposomes was investigated with the aim of enhancing solubility and improving desired effects of both the antineoplastic drug and the P-gp inhibitor.

Drug resistance is a well-known phenomenon and represents the cause of the non-responsiveness of some diseases to drug treatments. The occurrence was firstly described in bacteria resistant to antimicrobial drugs *(Du D, 2018)*, but similar mechanisms have been found to take place in other diseases, including cancer. Nowadays, it is widely known the multidrug resistance (MDR), a cross-resistance to a broad variety of anticancer drugs unrelated in structure and activity, which produces chemotherapy failure and tumor progression. One of the most studied mechanisms of MDR is the overexpression of drug efflux pumps belonging to the adenosine triphosphate (ATP) binding cassette (ABC) transporters family, characterized by a broad and overlapping spectrum of substrates. The main ABC transporters clinically associated with the development of MDR are P-glycoprotein (P-gp/ABCB1), MDR related proteins (MRPs/ABCCs), and breast cancer resistance protein (BCRP/ABCG2), *(Wu Q, 2014)*. Nowadays, the MDR phenomenon represents a major obstacle in the treatment of cancer diseases, and among the strategies to reverse the MDR phenotype, the inhibition of P-gp function and expression is essential to discover fruitful anticancer drugs *(Yang X, 2016)*. This hindrance can be overcome by the co-administration of antitumor drugs with substances able to inhibit MDR transporters such as P-gp. Such agents are known as chemosensitizers, as they can resensitize cancer cells to antineoplastic drugs, increasing the drug intracellular concentration by the P-gp efflux pump inhibition *(Zhang H, 2021)*. However, although several compounds show an inhibitor effect on the function of P-gp, clinical trials have revealed that most of these chemosensitizers are toxic, with limited benefits to cancer patients. Therefore, new strategic approaches are needed to increase the efficacy of these inhibitors and decrease their toxicity *(Zinzi L, 2014)*. The co-encapsulation within delivery systems has been experimented to improve pharmacokinetic and pharmacodynamic features of P-gp inhibitors *(Hu CMJ, 2012)*. Among the nanocarriers, liposomes represent the most versatile drug delivery systems in terms of drug loading, biocompatibility, nontoxic, and non-immuno-genic properties, and with an excellent

biodegradability *(Temidayo OB, 2018)*. Hence, liposomes can enhance drug solubility, giving a sustained release system, providing targeted drug delivery, reducing the toxic effect of drugs, protecting against drug degradation, and the surrounding environment *(Bilia AR, 2019b; Bilia AR, 2017)*. In clinical practice, liposomal formulations of important and effective drugs against both neoplastic and other diseases have been employed for many years, e.g., Doxil®, Ambisome®, DepoDur, Myocet, DaunoXome, DepoCyte, and Lipo-platin, are the most representative among others *(Bulbake U, 2017)*.

BRB is the most commonly available salt form of a natural quaternary ammonium isoquinoline alkaloid. It was originally used as a broad-spectrum antibacterial drug and it has a wide range of pharmacological activities, including inhibitory effects on a variety of tumors. BRB affects the molecular mechanisms that cause tumors through various signaling pathways, and it diminishes the expression of genes encoding cytokines involved in inflammatory path-ways (e.g., tumor necrosis factor-α (TNF-α), interleukins), prostaglandins, cyclooxygenase−2 (COX−2), and inducible nitric oxide synthase (iNOS) via interfering with AMP-activated protein kinase *(Liu D, 2019; Refaat A, 2015; Jeong HW, 2009)*. Despite these interesting antineoplastic activities, BRB is a substrate of P-gp *(Godugu C, 2014)*, and it is eliminated from the cells, resulting in reduced antitumor efficacy. Furthermore, due to its poor aqueous solubility, BRB shows a very low oral bioavailability (<1%), *(Godugu C, 2014; Kumar A, 2015)*. Studies in humans showed that BRB efflux is due to multidrug resistance protein 1 and multidrug resistance-associated protein 1, reducing accumulation of BRB in cells, but it is also well-known BRB can also bind strongly to human serum albumin, which makes it difficult to achieve effective concentrations. Metabolic studies of BRB in animals suggest that BRB is metabolized rapidly and that the liver is the main metabolic site. It was shown that only 4.93% and 0.5% of an i.v. dose of 2 mg/kg BRB was eliminated from the urine and bile, respectively *(Liu YT, 2010; Ye M, 2009)*. Hence the need for an adequate drug delivery system to increase BRB bioavailability. TAR (XR9576) is a third-generation synthetic potent P-gp inhibitor, whose potential to overcome P-gp mediated MDR of tumors has been investigated in human phase I/II clinical trials. However, further clinical development of TAR as a MDR reversal agent halted due to the scarce efficacy and side effects when used in combination with cytotoxic anticancer drugs *(Matzneller P, 2018)*. In addition, in the present study D-α-Tocopheryl polyethylene glycol 1000 succinate (TPGS) was also investigated as a possible P-

gp inhibitor and compared with TAR to select the best MDR reversal agent *(Tan S, 2017)*. The first step of the study was characterized by the optimization of composition of the nanoliposome bilayer, based on the key properties such as particle size, polydispersity, ζ-potential, and morphology. Encapsulation efficiency (EE%) and recovery (R%) of drugs were also evaluated. Transmission electron microscopy analysis (TEM) in both the parental human leukemia cell line K562 and the doxorubicin (DOXO) resistant counterpart for P-gp overexpression, K562/DOXO, was used to investigate the endocytosis properties of the developed nanoliposomes loaded with horseradish peroxidase (an electron-dense enzyme). Possible changes in the potency of TAR loaded in nanoliposomes was evaluated using DOXO cytotoxicity in both cell lines study. Finally, BRB plus TAR-loaded nanoliposomes were investigated for the ability to enhance BRB uptake in K562/DOXO cell lines. Due to its fluorescent properties, the BRB is a suitable probe for evaluating directly the uptake by flow cytometry *(Zhang Y, 2019)*.

Nanovesicles loaded with Origanum onites L. and Satureja thymbra L. essential oils and their activity against food-borne pathogens and spoilage microorganisms

In another study of this thesis, *O. onites* and *S. thymbra* EOs (Lamiaceae) were isolated and analysed by GC-MS, and for the first time, they were formulated in propylene glycol-nanovesicles, proposed as safe and food-grade delivery systems.

EOs obtained from aromatic and medicinal plants, as well as their components have largely demonstrated antibacterial and antifungal properties against a wide range of microbial pathogens, including numerous food-borne pathogens and key spoilage bacteria *(Kerekes EB, 2015; Vergis J, 2015)*. Food poisoning is considered as one of the most common causes of illness and death in developing countries, which are associated with bacterial contamination especially from Gram negative bacteria, mainly represented by *Salmonella typhi*, *Escherichia coli* and *Pseudomonas aeruginosa (Zhou Y, 2019)*. Among Gram positive bacteria, *Staphylococcus aureus* and *Bacillus cereus* are the most causative agents of food-borne illnesses or food spoilage *(Wei S, 2019)*. Over the last years, synthetic preservatives are largely used to successfully prevent and control bacterial contamination of food, but their use can result in unwanted chemical residues in food and feed chains. In addition, there is an increasing resistance of these pathogens to the synthetic preservatives *(King M, 2009)*. Hence, the discovery of

alternative preservatives, mainly originated by natural sources have been increased during the last years. EOs are reported as potentially effective and safe natural food preservatives by many publications *(Kerekes EB, 2015)*.

Plants of genus *Origanum* L. and *Satureja* L. are well-known aromatic herbs, widely used in traditional and modern medicine, as well as in food and cosmetics. Many of them are referred with the common name "oregano" *(Lombrea A, 2020)*. Among the oregano plants, *O. vulgare* L. is one of the most popular aromatic species, including six subspecies; *O. vulgare* subsp. *glandulosum* (Desf.) Ietsw., *O. vulgare* subsp. g*racile* (K. Koch) Ietsw., *O. vulgare* subsp. *hirtum* (Link) Ietsw., *O. vulgare* subsp. *virens* (Hoffmanns. & Link) Ietsw., *O. vulgare* subsp. *viridulum* (Martrin-Donos) Nyman, and *O. vulgare* subsp. *vulgare (Euro+Med PlantBase, 2011)*. Strikingly, the two most commercially important oregano herbs are considered the *O. vulgare* subsp. *hirtum* (known as "Greek oregano") and *O. onites* L. (known as "Turkish oregano", "Island oregano" or "Cretan oregano") *(Drabova L, 2019; Stefanaki A, 2016)*. The latter herb is a narrowly distributed East Mediterranean species, occurring mainly in Turkey and Greece. The interest for this species is due to the high essential oil yield and carvacrol content (69.0–92.6%), *(Stefanaki, A, 2016; Tasdemir K, 2019)*. *S thymbra* L. is distributed in the Mediterranean region and its smell is close to that of oregano *(Skoula M, 2005)*. Essential oil of *S. thymbra* is rich in monoterpene derivatives such as γ-terpinene, *p*-cymene and carvacrol *(Tepe B, 2015)*. Both EOs exert a broad range of pharmacological properties, especially antimicrobial activity, which are attributed to their chemical constituents (i.e. carvacrol, γ-terpinene and *p*-cymene), *(Glamočlija J, 2006; Tepe B, 2016)*.

Although EOs possess good antimicrobial properties, they have potential limitations for commercial applications due to their physical and organoleptic properties such as strong flavour, volatility and chemical instability. Consequently, different types of food-grade delivery systems, mainly nanoemulsions *(Amaral DMF, 2015)*, but also innovative nanocochleates *(Asprea M, 2017)* have now been evaluated for improving their performance as antimicrobials.

In this thesis, two different types of modified vesicles, obtained by mixing membrane components with water-soluble, non-volatile organic solvents, such as polyols, were approached to formulate *O. onites* and *S. thymbra* EOs. In particular, both glycerol and propylene glycol are among the most widely used raw materials in food, cosmetic and pharmaceutical industries. Glycerol shows

excellent solubility in water, and, due to its GRAS status, it is very safe to use *(Becker LC, 2019)*. Propylene glycol is a colorless, odorless and completely water-soluble solvent very similar to glycerol, also having the GRAS status and high safety.

O. onites and *S. thymbra* EOs were isolated and analysed by GC-MS, and they were formulated in vesicles based on glycerol and propylene glycol, proposed as safe and food-grade delivery systems. Obtained nanovesicles were optimized in terms of size and essential oil loading, and they were fully characterized as regards physical and chemical parameters. Successively, they were investigated for the antimicrobial activity against a panel of different bacteria and fungi, comparing the activity with that of pure essential oils. Moreover, the safety profile was assessed by *in vitro* test on HaCaT cell line.

Formulation of a phenol-rich extract from unripe olives (Olea europaea L.) in microemulsion to improve its solubility and intestinal permeability

A further research project aimed to prepare a suitable and cheap drug-delivery-system to improve the bioavailability of phenolic compounds present in extracts from Tuscan unripe olives (cv Moraiolo) harvested before any stone lignification. A phenol-rich extract (OE) was prepared from freeze-dried olives using a hydroalcoholic solvent, was characterized by HPLC-DAD and formulated in a microemulsion for the oral delivery.

The beneficial health properties associated to a regular consumption of extra virgin olive oil (EVOO) and other food products derived from the olive tree (*Olea europaea* L.) are well-known, mainly thanks to the presence of specific phenolic compounds *(De Bock M, 2014; Giovannelli L, 2013; Carpi S, 2019; Romani A, 2019)*.

The main phenolic compound present in the olive fruits is the secoiridoid oleuropein, followed by other secoiridoids, namely ligstroside, nuzhenide (only present in seeds) and demethyloleuropein (which appears in late ripening stages), and by the phenylpropanoid derivative verbascoside *(Cecchi L, 2015; Zanoni B, 2014; Morello JR, 2005; Ryan D, 2002)*. Their concentration is affected by ripening stage and the part of the fruit *(Cecchi L, 2015*; *Ghanbari R, 2012; Omar SH, 2010; Ryan D, 1999)*. Oleuropein reaches the maximum concentration (up to 14% *w/w* dm) in young fruits *(Omar SH, 2010)*. Then, during the green maturation, its level, as well as those of verbascoside and ligstroside, constantly decreases *(Cecchi L, 2015*; *Amiot MJ, 1986; Amiot MJ, 1989)*.

Several beneficial properties have been described for the main phenolic compounds present in unripe olive. Oleuropein showed potential antioxidant, anti-inflammatory, anti-atherogenic, anti-cancer, anti-viral, anti-aging, and neuroprotective properties *(Omar SH, 2010*; *(Perrinjacquet-Moccetti T, 2008; Garcia-Villalba R, 2014; Hornedo-Ortega R, 2018)*. Verbascoside, also known as acteoside or kusaginin *(Alipieva K, 2014)*, is a bio-active molecule well-known for its antioxidant, anti-inflammatory, antibacterial, antifungal, potential anticancer, and anti-tuberculosis properties *(Alipieva K, 2014; Funes L, 2009; Attia YM, 2018; Zhang Y, 2018; Garro HA, 2020; Reid AM, 2019)*. In a recent study, ligstroside showed beneficial effects against Alzheimer's disease and the capability in expanding the lifespan and enhancing the cognitive function of aged mice *in vivo (Grewal R, 2020)*.

The phytocomplex, that is a whole or partially purified extract of a plant constituent, offers greater efficacy and more advantages than a single isolated ingredient, thanks to synergistic interactions *(Williamson EM, 2001; Lee OH, 2010)*, and this is also true for the biological effects exerted by phenolic compounds from *Olea europaea* L. *(Lee OH, 2010)*. All this evidence makes dried unripe olives, very rich in verbascoside, ligstroside and, particularly, oleuropein (up to 10% *w*/*w*) and total phenolic content (up to 18% *w*/*w*), a very interesting raw material for preparing a new ingredient for food supplement greatly rich in phenols from *Olea europaea* L. *(Cecchi L, 2020a)*. This is especially true if olives are harvested at a very early stage, before any stone lignification, with this fact making the fruit easy to mince in order to obtain the ingredient.

Oleuropein and ligstroside are absorbed and subjected to phase-II metabolism in humans and then they are extensively metabolized to yield many other metabolites whose specific role in the biological properties attributed to oleuropein and ligstroside are yet to be clarified *(Garcia-Villalba R, 2014)*. A study on rats supplemented by a phenolic extract of olive cake, suggests that these molecules and their metabolites are widely distributed in multiple organs or further metabolized *(Serra A, 2012)*. The high correlation found in plasma among the metabolites of hydroxytyrosol (glucuronide and sulfate) and of oleuropein aglycon glucuronide was suggested as indicative of a variable efficiency of gastric hydrolysis in each individual *(Garcia-Villalba R, 2014)*. The exposure to hydroxytyrosol resulted in a significant degree from ingested oleuropein aglycone contained in EVOO *(Hornedo-Ortega R, 2018)*. In terms of gender

research, it has been pointed out that hydroxytyrosol metabolism is more efficient in female than in males *(Domínguez-Perles R, 2017)*.

Novel nanoformulations based on drug delivery systems are designed with the aim of enhancing bioavailability, solubility, physicochemical stability, intestinal permeation, resident time in the gastrointestinal tract, and controlled release of natural products *(Ali A, 2019; Bilia AR, 2017; Bilia AR, 2019b)*.

Amongst the various drug delivery systems, the microemulsion (ME) is considered an ideal alternative for the oral delivery of olive extract. ME is able to transform the dried extract into an oral dosage form to overcome the limited oral bioavailability, thereby increasing the therapeutic efficacy of the extract. Oil in water microemulsions have been formulated with food acceptable components to increase the solubility, stability, and ameliorate the intestinal permeability of the extract's constituents *(Porter CJH, 2007; Porter CJH, 2008; Yin YM, 2009)*. Additionally, several excipients used in these systems, including Cremophor, Tween 80, Labrasol, and Transcutol, could inhibit the function of P-gp *(Rege BD, 2002; Takahashi Y, 2002; Lin YL, 2007)*.

The more suitable ingredients of ME were selected after the solubility study in different vehicles. ME was chemically and physically characterized with DLS and HPLC-DAD analyses to evaluate the size, homogeneity, morphology, and encapsulation efficiency. Parallel Artificial Membrane Permeability Assay (PAMPA) and Caco-2 cells were used as *in vitro* models to evaluate the ability of the formulation to ameliorate the intestinal permeability of OE *(Kansy M, 1998; Piazzini V, 2019d)*.

Caco-2 cells are the most widely used *in vitro* model to assess the intestinal permeability of pure compounds, extracts and formulations *(Lea T, 2015; Piazzini V, 2017b; Piazzini V, 2019b)*. However, the long cell growth cycle and the high costs limit its use as a high throughput tool. For this reason, other *in vitro* models, aimed to simulate gastrointestinal permeability, maintaining a good correlation with the *in vivo* permeability but with lower costs, have been developed, such as the Parallel Artificial Membrane Permeability Assay (PAMPA), *(Piazzini V, 2017a; Kansy M, 1998; Bergonzi MC, 2014; Piazzini V, 2017b)*. Recently, the PAMPA model has also been successfully used and validated for testing the permeability of bioactive compounds from extracts of several species and their formulations (e.g., *Vitex agnus-castus*, *Silybum marianum*, *Chenopodium quinoa*, *Trigonella foenum-graecum*, and *Posidonia oceanica*), *(Piazzini V, 2017a; Piazzini V, 2017b; Piazzini V, 2019d; Navarro del Hierro J, 2020)*.

MATERIALS AND METHODS

DEVELOPMENT AND PERCUTANEOUS PERMEATION STUDY OF ESCINOSOMES, ESCIN-BASED NANOVESICLES LOADED WITH BERBERINE CHLORIDE

1. Materials

Phospolipon 90G (P90G) was purchased from Lipoid AG (Cologne, Germany) with the support of its Italian agent AVG srl. Cholesterol (CHOL), ESN, BRB and hydroxypropyl methylcellulose (HPMC) were provided by Sigma-Aldrich (Milan, Italy). Methanol (MeOH), methanol HPLC grade, acetonitrile (ACN), formic acid, dichloromethane (CH_2Cl_2), dimethylsulphoxide (DMSO) and formaldehyde solution, phosphate saline buffer (PBS), acetate buffer, NaOH, potassium borate, hyaluronidase from bovine testes Type IV-S, powder (mouse embryo tested, 750-3000 units/mg solid), compound 48/80 (condensation product of N-methyl-p-methoxyphenethylamine with formaldehyde, hyaluronic acid potassium salt from human umbilical cord, p-dimethylaminobenzaldehyde (98%, Ehrlich's reagent) were purchased from Sigma-Aldrich (Milan, Italy). Piroxicam, progesteron, Prisma Buffer (P/N 110151), Hydration Solution (P/N: 120706) and Skin-PAMPA™ system were purchased from pION Inc. (Massachusets, USA). Ultrapure water was produced by a synergy UV Simplicity water purification system provided by Merck KGaA (Molsheim, France). Phosphotungstic acid (PTA) was purchased from Electron Microscopy Sciences (Hatfield, USA).

2. Methods

2.1. HPLC-DAD analytical method

Quantitative determination of active constituents was carried out by the 1200 High Performance Liquid Chromatograph (HPLC) equipped with a Diode Array Detector (DAD) from Agilent Technologies Italia Spa (Rome, Italy). DAD was set up at the two wavelengths of 210 nm for ESN and 346 nm for BRB. Chromatographic analysis were performed using a reverse-phase column Luna-C18, 250 mm x 4.6 mm, 5 μm particle size, maintained at 27 C. A gradient elution method with 1 mL/min flow rate for 32 min was applied, using (A) acetonitrile

and (B) water at pH 3.2 (by formic acid) like mobile phases. Acetonitrile was selected because of its low UV cut off, which avoids interference with the ESN signal. The analytical method was: 0–3 min 85% (B), 3–9 min 85%–70% (B), 9–10 min 70% (B), 10–17 min 70%–50% (B), 17–19 min 50% (B), 19–26 min 50%–45% (B), 26–30 min 45%–40% (B), 30–35 min 40%–1% (B), 35–40 min 1%, 40–47 min 1%–85% (B). R^2 was calculated both for BRB and ESN and resulted respectively 0.99925 and 0.99979. Limit of detection (LOD) and limit of quantification (LOQ) were calculated both for BRB and ESN by determination of signal-to-noise ratio, in accordance to the ICH guidelines. LOD was 0.60 ng for BRB and 400.00 ng for ESN, while LOQ was 1.51 ng for BRB and 988.00 ng for ESN.

2.2. Development and optimisation of nanovesicles

Nanovesicles were prepared using the thin layer evaporation method at specific conditions *(Leto I, 2016; Asprea M, 2019)*. Different liposomes were developed by varying the lipid constituents and loading BRB. In particular, 330 mg of P90G, 100 mg of CHOL and 50 mg of ESN were used as lipophilic components and they were dissolved in CH_2Cl_2/MeOH, while 13 mg of BRB were solubilized in water (10 mL). The organic solvent was removed by rotary evaporator for 20 min and the dried lipid film was then hydrated with the aqueous phase (with or without BRB) for 30 min at 35 °C *(Isacchi B, 2017)*. First, conventional liposomes with P90G and CHOL were prepared; then, the same liposomes were prepared by adding ESN; finally, in the third formulation, P90G plus ESN were used to prepare the vesicles. The same three types of vesicles, loaded with BRB, were prepared in parallel. Finally, the Sonopuls Ultrasonic Homogenizer HD 2200 by Bandelin electronic GmbH & Co. KG (Berlin, German), was used in order to reduce vesicle size and improve sample homogeneity.

2.3. Physical characterization of nanovesicles

Nanovesicle characterization during the development and the optimization steps was made by measuring size, homogeneity and possible aggregation state by Dynamic and Electrophoretic Light Scattering (DLS and ELS, Zetasizer Nanoseries ZS90) by Malvern instrument (Worcestershire, UK), with a scattering angle of 90° at 25 °C *(Bhattacharjee S, 2016; Isacchi B, 2011)*. Average Hydrodynamic Diameter (AHD, nm), size distribution expressed as Polydispersity Index (PdI, dimensionless measurement) and ζ-Potential (mV), were obtained using the software provided by Malvern. Scattering was measured

on samples diluted 50/100-fold in ultrapure water and every measurement was performed in triplicate. Nanovesicle morphological characterization was performed by transmission electron microscope (CM12 TEM, PHILIPS, The Netherlands) equipped with an OLYMPUS Megaview G2 camera with an accelerating voltage of 80 kV. TEM allowed to visualize vesicle dispersion and dimensions. A drop of the diluted sample was applied and dried by desiccation on a carbon film copper grid. This was then counterstained with 1% *w/v* of phosphotungstic acid solution and examined at different magnifications *(Isacchi B, 2011)*. The deformability of vesicles was measured by extrusion *(Nava G, 2011)*. It was performed by 21 passages through polycarbonate extrusion membranes with 50 nm cut-off, using the LiposoFast-Basic extruder by Avestin Europe GmbH (Mannheim, Germany) joined to a 7 atm pressure source. Before the extrusion, each formulation was properly diluted in water. Deformability was expressed as the ratio among vesicles diameter before and after extrusion (equation 1). Values around the unit are index of good deformability.

$$\mathrm{D} = \frac{\text{average size (nm) before extrusion}}{\text{average size (nm) after extrusion}} \quad (1)$$

2.4. Technological characterization of nanovesicles

In order to characterize the liposomal dispersions, the encapsulation efficiency (EE%) and the total recovery (R%) were calculated for each formulation. EE% is defined as the percentage of entrapped drug in relation to the weighed drug (equation 2):

$$\mathrm{EE\%} = \frac{\text{encapsulated drug}}{\text{weighted drug}} \times 100 \quad (2)$$

In order to determine the amount of entrapped drug, vesicles were purified from free BRB and free ESN, by dialysis bag method *(Righeschi C, 2014; Isacchi B, 2012)*, using Spectra/Por® regenerated cellulose membranes with 3.5 KDa molecular weight cut-off (MWCO), by Repligen Europe B.V. (Breda, The Netherlands). The dialysis bag was stirred in ultrapure water (1 L), at room temperature for 1 h. After the purification, the samples were diluted in methanol, in order to dissolve and break the vesicles and release the encapsulated substances. Finally, a centrifugation at 14,000 rpm for 10 min was applied and the amounts of BRB and ESN were determined by HPLC-DAD. Rather, R% is defined as the percentage

of total drug recovered after the preparation procedure in relation to the weighed drug (equation 3):

$$R\% = \frac{\text{total recovered drug}}{\text{weighted drug}} \times 100 \quad (3)$$

and it was measured using the same procedure without the purification step by dialysis. Moreover, the pH-meter (Basic 20+) by Crison Instrument (Barcelona, Spain) was used to measure the pH of each formulation.

2.5. Stability studies

The stability studies were carried out storing the samples for 1 month at 4 °C in the dark. Every ten days, physical (size, PdI, ζ-potential) and chemical (EE% and R%) parameters of the vesicles were investigated by DLS/ELS and HPLC-DAD.

2.6. Release of active constituents from the vesicles

The dialysis bag method, with Spectra/Por® regenerated cellulose membranes of 3.5 KDa MWCO (molecular weight cut-off) by Repligen Europe B.V. (Breda, The Netherlands), was applied to study the release kinetic of ESN and BRB from liposomes *(Moreno-Bautista G, 2011; Asprea M, 2017)* and from aqueous solution (BRB aqueous solution, B-SOL) or dispersion (ESN water dispersion, E-W), at the same concentrations used in liposomes, 1.3 mg/mL and 5 mg/mL respectively. 250 mL of PBS (pH 7.4) was used as release medium and the experiment was carried out in sink conditions at 37 °C under magnetic stirring, until 24 h. Therefore, 0.5 mL withdrawals were done at specified time points (30, 60, 120, 240, 360, and 1440) min and replaced by equal volumes of fresh buffer. Finally, all samples were centrifuged at 14,000 rpm for 10 min and analysed by HPLC-DAD.

2.7. Hyaluronidase inhibition assay

The hyaluronidase inhibition activity was investigated using a colorimetric assay reported by Murata and coworkers *(Murata T, 2012)*. Samples were dissolved in 0.1 M acetate buffer (pH 4.0, 0.2 mL) and were mixed with 0.1 mL hyaluronidase (400 unit/mL buffer) and incubated for 20 min at 37 °C. Next, compound 48/80 in buffer (0.3 mg/mL, 0.2 mL) was added as activator and allowed to react for 20 min at 37 °C. Then, hyaluronic acid potassium salt in

buffer (0.4 mg/mL, 0.5 mL) was added and the mixture was incubated for 40 min at 37 °C. NaOH (0.4 M, 0.2 mL) was added to the mixture and cooling with ice stopping the reaction. Then, potassium borate solution (0.4 M, 0.2 mL) was added, vortexed and the mixture boiled for three minutes. The mixture was cooled using ice and 6 mL of a solution of p-dimethylaminobenzaldehyde (1% *w*/*v* in acetate buffer) was then added and the sample was placed for 20 min at 37 °C. The hyaluronidase inhibitory activities (HIA%) were measured at 600 nm, mean ± SD (n = 3), and calculated as follows:

$$\text{HIA\%} = \frac{[(\text{control} - \text{control blank}) - (\text{sample} - \text{sample blank})]}{(\text{control} - \text{control blank})} \times 100 \quad (4)$$

where control was acetate buffer and blank was the hyaluronidase enzyme in acetate buffer. 2.9.

2.8. Skin-PAMPA™: in itro simulation of stratum corneum permeation by vesicles

The Skin-PAMPA™ model from pION was employed as *in vitro* permeation assay, in order to evaluate and compare the permeability of the three formulations with BRB and predict BRB skin absorption *(Sinkó B, 2012)*. B-SOL, was used as reference of free-BRB permeability. The skin-PAMPA membranes were used after an overnight hydration by the Hydration Solution, until all wells turned into translucent. After that, the wells in the bottom plate (donor) were filled with 200 μL of samples, while the wells in skin-PAMPA™ top plate (P/N: 120656, pION) (acceptor) were filled with 200 μL of fresh acceptor solution, Prisma Buffer, at pH 7.4. A lid was used to cover the top plate, once the sandwich was assembled and a Parafilm layer was applied around the perimeter to seal the two compartments. Then, the 96-well STIRWELL™ PAMPA sandwiches (P/N: 110243, pION) were incubated into a chamber with a wet filter paper under the lid, to maintain a high relative humidity and minimize evaporation. The assay was carried out at room temperature (25 °C ± 2 °C) for 5 h, according to the protocol. After the permeation time had elapsed, samples from acceptor and donor plate were collected and analysed by HPLC-DAD. The Effective Permeability (P_e) expressed as cm/s was calculated according to the following approximate equation *(Avdeef A, 2012)*:

$$P_e \approx (-2.303 \cdot V_D) / (A \cdot t) \cdot \log_{10} (1 / (1 - R) \cdot C_{D(t)} / C_{D(0)}) \quad (5)$$

where A is the filter area [0.3 cm^2], multiplied by a nominal porosity of 70% according to the manufacturer, V_D is the donor volume [0.2 cm^3], t is the incubation time, $C_{D(o)}$ is the concentration [mol x cm^3] of the compound in the donor phase at time t, $C_{D(o)}$ is the initial concentration [mol x cm^3] of the compound in the donor phase at time 0, and R is the membrane retention factor (equation 6):

$$R = 1 - C_{D(t)} / C_{D(0)} - V_A / V_D \cdot C_{A(t)} / C_{D(0)} \quad (6)$$

and r_a is the sink asymmetry ratio (gradient-pH-induced), defined according to the following equation:

$$r_a = V_D / V_A \cdot P_{e\,(A \rightarrow D)} / P_{e\,(D \rightarrow A)} \quad (7)$$

2.9. Histological evaluation of rabbit ear skin and human abdominal skin

Cross-sections of rabbit ear skin were prepared at the Department of Experimental and Clinical Medicine, of the University of Florence, Florence, Italy. Human skin samples were kindly provided by operators from the Surgical Clinic, Careggi General Hospital, Florence, Italy, taken from surgical specimens removed for reductive abdominoplasty and intended for disposal. Both the rabbit and human skin samples were taken from discarded specimens intended for disposal, which exempted us from the need for a preliminary ethical permission. In the present study, the histological comparison between human abdominal skin and rabbit ear skin was investigated by conventional light microscopical analysis, in order to confirm the suitability of this animal model in the percutaneous studies *(Nicoli S, 2007)*. Whole-thickness rabbit skin tissue was peeled off the inner part of the ear, close to the acoustic meatus, since preliminary studies showed little or no permeation through the skin from the ear apex. In particular, skin layers were manually stripped from the underlying cartilage within a rectangular incision made with a sharp blade and cut into discs 2 cm in diameter, paying attention not to damage the skin surface. Skin integrity was verified by light microscopy.

2.10. Percutaneous penetration studies using rabbit ear skin

The skin discs thus prepared were used for the permeation study by the Franz cell system *(Patel P, 2016)*, in order to compare the permeation characteristics of the three formulations with BRB and BRB aqueous solution; all

of them having the same BRB concentration (1.3 mg/mL). In order to avoid dehydration, the freshly cut skin was kept moisten between sheets of filter paper wet with PBS and the skin outer surface was gently dried by dabbing with filter paper, before placement on the vertical diffusion Franz cells (3.14 cm^2 diffusion area). The donor chamber was filled with 1 mL of sample and the acceptor chamber was filled with 7 mL of PBS under magnetic stirring. During the experiment, the apparatus was maintained at 37 °C by a thermostatic bath circulation. The skin was placed between the two compartments, with the external layer facing the donor chamber and with dermis touching the buffer solution in the acceptor chamber. A suitable O-ring seal was used between the donor chamber and the skin, in order to prevent leakage of the sample and its spreading out over the entire skin surface *(Desmedt B, 2015)*. Finally, the cells were clamped together and the donor chamber was sealed by Parafilm to avoid evaporation during the assay. The system was incubated for 6 h and 24 h. After 24 h, the acceptor solutions were analysed by HPLC-DAD after 14,000 rpm centrifugation for 10 min, while the donor samples were first diluted with MeOH in order to allow vesicle break and fully dissolution of ESN/BRB. The amounts of BRB and ESN retained in the skin were also determined. Each skin lamina was washed 3 times with 3 mL PBS and dried with filter paper. The inner part of the skin specimen, in contact with the sample, was cut and divided into equal pieces. These were soaked in 1 mL of methanol, exposed to 3 h of ultrasonication bath and then shaken in a water bath for 3 h, in order to extract all the accumulated drugs *(Lai F, 2007)*. Finally, the samples were centrifuged 10 min at 14,000 rpm and analysed by the liquid chromatograph. The permeation parameters were calculated as following: absorbed dose (A_{24}), expressed as percentage of the applied dose absorbed through the skin and that recovered in the receptor compartment; absorbable dose retained inside the skin (S_{24}), expressed as percentage of the applied dose recovered inside the skin; total absorbed dose (TA_{24}), expressed as sum of the two percentages A_{24} and S_{24}.

2.11. Histological studies of rabbit ear skin after percutaneous penetration studies

After the permeation experiments, 6 h and 24 h respectively, fragments of cutaneous tissue were resected from the central part of each skin disc exposed to the different BRB samples, fixed in cold 4% formaldehyde in 0.1 M PBS, pH 7.4, at 4 °C for 4 h, cryoprotected by 5 min incubation in cold saccharose 10% in PBS, washed in PBS, embedded in KillikTM medium by Bio-Optica (Milan, Italy),

quickly frozen by immersion in isopenthane and stored at 80 °C until needed. Sections, 7 μm thick, were cut with a Reichert/Leica 2800 Frigocut cryostat (Wetzlar, Germany). Part of specimens were stained with hematoxylin and eosin (HE) for conventional light microscopical analysis, others were observed directly under a Zeiss Axioskop fluorescence microscope (Oberkochen, Germany) equipped with a 350 filter, close to the absorption peak of BRB, which emits in the yellow-green region of the visible spectrum (550). The fluorescence of BRB was assumed as an index of drug penetration into different skin tissues.

HYDROXYPROPYL METHYLCELLULOSE HYDROGEL OF BERBERINE CHLORIDE-LOADED ESCINOSOMES: DERMAL ABSORPTION AND BIOCOMPATIBILITY

3. Materials

Phospholipon 90G (P90G) was purchased from Lipoid AG (Cologne, Germany) with the support of its Italian agent AVG srl. Cholesterol, ESN, BRB, hydroxypropyl methylcellulose (HPMC) and hydroxyethyl cellulose (medium viscosity according to the monograph of Pharm. Eur., HEC) were provided by Sigma-Aldrich (Milan, Italy). HMPC characteristics: average MW was 86 kDa, methoxyl content was 28–30%, hydroxylpropyl content of 7–12%. HEC characteristics: average MW was 720 kDa, viscosity of 2% colloidal dispersions was 4500–6500 mPa·s. Carbomer was from Galeno Srl (Prato, Italy). Ethanol 75% *v*/*v* (EtOH), methanol analytical/HPLC grade, acetonitrile, formic acid, dichloromethane, dimethylsulphoxide, formaldehyde solution and phosphate saline buffer (PBS) were purchased from Sigma- Aldrich (Milan, Italy). Ultrapure water was produced by a synergy UV Simplicity water purification system provided by Merck KGaA (Molsheim, France). Phosphotungstic acid was purchased from Electron Microscopy Sciences (Hatfield, PA, USA).

4. Methods

4.1. HPLC-DAD analysis

The LC 20 Shimadzu High Performance Liquid Chromatograph (HPLC) equipped with a Diode Array Detector (DAD) was used to per- form the quantitative analysis of BRB and ESN. The chromatographic analysis were carried out by using a reverse-phase Dikma Diamonsil C-18 column, 200 mm × 4.5 mm, 5 μm particle size, by a gradient mode at flow rate of 1.0 mL/min. The mobile phases were (A) formic acid/water pH 3.2, (B) acetonitrile. The multi-step linear gradient was: 0–3 min 15% B; 3–9 min 15–30% B; −10 min 30% B; 10–17 min 30–50% B; 17–19 min 50% B; 19–26 min 50–55% B; 26–30 min 55–60% B; 30–32 min 60–15% B; 32–40 min 15% B. The column temperature was set at 27 °C and the chromatograms were acquired at 210 nm for ESN and 346 nm for BRB.

4.2. Nanovesicle preparation

Nanovesicles were prepared using the thin layer evaporation method as previously reported *(Isacchi B, 2012)*. Briefly, 330 mg of P90G and 50 mg of ESN were dissolved in a dichloromethane/methanol mixture. After that, the organic solvent was removed by rotary evaporator under vacuum for 20 min and the obtained lipid film was hydrated with 10 mL of water in order to obtain escinosomes (EL), or 10 mL of 1.3 mg/mL BRB aqueous solution in order to obtain escinosomes loaded with BRB (B-EL). The hydration was carried out for 30 min at 35 °C by mechanic stirrer. The blank liposome (L) was also prepared using only P90G as component and hydrating the lipid film with 10 mL of water. Finally, the Sonopuls Ultrasonic Homogenizer HD 2200 by Bandelin electronic GmbH & Co. KG (Berlin, German), was used in order to reduce vesicle size and improve sample homogeneity.

4.3. Nanovesicle physical and chemical characterization

Physical and chemical characterization of the developed formulations was performed as previously described by Righeschi and coworkers *(Righeschi C, 2014)*. Physical characterization was carried out evaluating size, homogeneity and aggregation state of nanovesicles, using the Dynamic and Electrophoretic Light Scattering (DLS and ELS, Zetasizer Nano ZS90) by Malvern instrument (Worcestershire, UK). Thus, Average Hydrodynamic Diameter (AHD, nm), Polydispersity Index (PdI, dimensionless measurement) and ζ-Potential (mV), were determined using the soft- ware provided by Malvern. Chemical characterization was evaluated calculating encapsulation efficiency (EE%) and total recovery (R%) of BRB and ESN. In order to determine EE%, the not encapsulated drug was re- moved by the dialysis method. The dialysis was performed using Spectra/Por® regenerated cellulose membranes, with 3.5 kDa molecular weight cut-off (MWCO), by Repligen Europe B.V. (Breda, The Netherlands). The dialysis bag was stirred in 1 L of ultrapure water for 1 h, at 21±3 °C; the purified samples were diluted in methanol and centrifuged at 14,000 rpm for 10 min. Thus, BRB and ESN amounts were determined by HPLC-DAD. In parallel, R% was determined using the same method without dialysis and analysing samples by HPLC- DAD. R% and EE% were calculated using the equations previously reported *(Isacchi B, 2011b)*.

4.4. Preparation of the HPMC-hydrogels

The two formulations (EL, B-EL) and the blank liposome (L) were gelled by adding 3% *w/v* HPMC in the vesicle dispersion and stirring the sample manually at 21±3 °C until a complete homogeneity. The obtained HPMC-hydrogels, G-EL (hydrogel of escinosomes), G-B-EL (hydrogel of BRB-loaded escinosomes) and G-L (hydrogel of blank lipo- some) were left to stand at 4 °C for two days before use, in order to remove air bubbles. HPMC-hydrogels of ESN water dispersion (G-ESN$_W$) and hydrogel of ESN plus BRB water dispersion (G-BE$_W$) were also prepared following the same procedure. The concentrations of ESN and BRB were the same in both hydrogels of vesicles and hydrogels of water dispersions (5 mg/mL and 1.3 mg/mL, respectively). Moreover, the pH of G-EL and G-B-EL was measured by the Basic 20+ pH-meter (Crison Instrument).

4.5. HMPC-hydrogel viscosity measurement

HPMC-hydrogel viscosity (mPa·s) was measured at 21 ± 3 °C by Brookfield DVE-RV Digital Viscometer (Ametek Brookfield; Milan, Italy), using a 06 spindle without the spindle guard lag and all data were fitted to a mathematical model, which involved the plotting of data on a graph. Measurements were performed with 47 mL of sample in a 50 mL beaker, selecting 2 min (time required for the viscosity reading to reach a constant value) as time of spindle rotation for each spindle rotational speed, namely 2.5, 4, 5, 10, 20, 50 and 100 rpm. Every 2 min, the rotational speed was increased (up rotational speed) from 2.5 rpm to 100 rpm and the hydrogel viscosity measurements were recorded. Then, every 2 min, the rotational speed was decreased (down rotational speed) from 100 rpm to 2.5 rpm and the hydrogel viscosity measurements were evaluated again. The spindle was selected by the "trial and error" method *(Ametek B, 2017)*. Therefore, it was selected the spindle able to produces on-scale readings with the highest number of the possible speeds. On-scale readings were those having % Torque between 10 and 100. The viscometer was recalibrated according to the manual *(Ametek B, 2017)* using glycerol as Newtonian fluid and calculating the new range of viscosity measurements based on the new experimental conditions, namely 50 mL beaker and absence of guard lag. The new range was determined working with the selected spindle (06) at one of the seven selected speeds (S_1) and it was calculated using the equation 8:

$$R_1 = 100\eta / T \quad (8)$$

where R_1 is the full-scale range of measurement under the new conditions, η is the viscosity (mPa·s) of the Newtonian fluid and T is the obtained % Torque.
For all the other six selected speeds the new ranges were calculated using the equation 9:

$$R_1 / R_2 = S_2 / S_1 \quad (9)$$

where S_2 is one of the six remaining speeds for which R_2 has to be deter- mined. The new ranges were determined for all the tested speeds, namely 2.5, 4, 5, 10, 20, 50 and 100 rpm. Temperature uniformity of the sample and the spindle was ensured by spindle rotation inside the sample for 30 min, before starting measurement. The hydrogels were maintained at 4 °C for two days before viscosity measurements, in order to remove the entrapped air.

4.6. Release of BRB and ESN from HPMC-hydrogels

The *in vitro* release of ESN and BRB from the HPMC-hydrogels (G-B-EL and G-EL) was investigated using cellulose nitrate filters (Sartorius Stedim Biotech GmbH, Germany), with 0.45 μm pore sizes and 130 μm thickness, as synthetic membranes *(Ng SF, 2012)* and adopting the TK-20B transdermal diffusion tester (Shanghai Kai Kai Technology Co., Ltd., China) by the vertical diffusion Franz cells. The receptor compartment was filled with 7 mL solution of 75% (*v*/*v*) EtOH and PBS, with a volume ratio of 40:60 *(Lai F, 2007)*, and it was maintained at 37 °C during the whole experiment, stirring continuously at 500 rpm by magnetic stirrer. The cell diffusion area of 3.14 cm^2 was covered by the synthetic membrane, previously hydrated by the acceptor solution, and the donor compartment was filled with 1 g of hydrogel. All cells were gripped by suitable clamps, while donor chambers and sampling ports were covered with parafilm in order to avoid evaporation. 0.1 mL of release medium was withdrawn from the receptor compartment at specific time points (1, 2, 4, 6, 8, 24 h) and it was replaced with the same volume of fresh EtOH/PBS solution *(Isacchi B, 2011a)*. All samples were analysed by the HPLC-DAD after 14,000 rpm centrifugation for 10 min. ESN and BRB released from hydrogels during 24 h were calculated as percentage of the applied dose absorbed through the membrane and recovered in the receptor compartment.

4.7. HPMC-hydrogel stability

B-EL hydrogel (G-B-EL) and EL hydrogel (G-EL) were stored up to 45 days at 4 °C in the dark, in order to be tested for the pH and viscosity stability, by pH-meter and viscometer as described in the experimental part.

4.8. In vitro skin absorption studies on nude mouse skin

Healthy male BALB/c nude mice, 6–8 weeks, weight 20 ± 2 g, were purchased from Beijing Vital River Laboratory Animal Technology Co., Ltd. All experimental procedures and animal care were performed in accordance with the protocol of animal experiments handling issued by the Animal Research Center of Tianjin University of Traditional Chinese Medicine. The experimental procedure was approved by the Animal Ethics Committee of Tianjin University of Traditional Chinese Medicine (Document Number: TCM-LAEC2018024). The skin of nude mice was excised freshly from euthanized animals. Fat and other tissues attached to the skin were removed carefully. The excised skin was kept wet in a physiological saline and stored in freezer at −20 °C before experiments. The *in vitro* skin absorption study was conducted by the TK-20B trans- dermal diffusion tester (Shanghai Kai Kai Technology Co., Ltd., China), using the vertical diffusion Franz cells with an effective diffusion area of 3.14 cm^2 and a receptor volume of 7.0 mL. The cells were gripped by suitable clamps, the receptor compartment was filled with a solution of 75% (*v*/*v*) EtOH and PBS, with a volume ratio of 40:60 *(Lai F, 2007; Dragicevic N, 2017)*, and it was maintained at 37 °C during the experiment, stirring continuously at 200 rpm by magnetic stirrer. 1 mL of each vesicular or aqueous formulation and 500 mg of each hydrogel formulation were loaded on the *stratum corneum* side, applying the infinite dose technique, according to the OECD guidelines *(OECD, 2004)*. The donor chambers and the sampling ports were covered with parafilm in order to avoid the evaporation. The test lasted 24 h. 0.5 mL of sample was taken from the receptor compartment at predetermined time points (1, 2, 4, 6, 8, 10, 12, 24 h) and replaced with the same volume of fresh acceptor solution. At the end of the experiment, the acceptor solutions were analysed by the HPLC- DAD after 14,000 rpm centrifugation for 10 min, while the donor samples were first diluted with methanol in order to ensure the fully dissolution of ESN/BRB by breaking vesicles. Then, the amounts of BRB and ESN retained in the skin at the end of the experiment were also deter- mined. Each skin section was washed tree times with

3 mL of PBS and dried gently with filter paper. The internal part of the skin specimen, in contact with the sample, was cut and divided into equal pieces. Been soaked in 1 mL of methanol, the samples were exposed to 3 h of ultra-sonication bath and then gently shaken on the platform of an orbital incubator until 24 h for extracting the residual drugs. Finally, the samples were centrifuged 10 min at 14,000 rpm and analysed by HPLC-DAD. The skin absorption parameters were calculated as following *(Vanti G, 2019)*: absorbed dose (A_{24}), expressed as percentage of the applied dose absorbed through the skin and recovered in the receptor compartment; absorbable dose retained inside the skin (S_{24}), expressed as percentage of the applied dose recovered inside the skin; total absorbed dose (TA_{24}), expressed as sum of A_{24} and S_{24}. ESN flux (μg/cm^2 h) across the skin was calculated as the slope of the regression line after achieving steady state conditions (sampling interval 8–24 h) and ESN permeability coefficient (K_p, cm/h) was calculated by dividing the flux per ESN concentration in the donor compartment. By contrast, BRB flux was plotted as a function of time and it was compared between the formulations.

4.9. In vivo test: acute dermal irritation/corrosion

The *in vivo* irritation test was carried out according to the OECD guidelines *(OECD, 2015)* for skin irritation testing of chemicals and the experiment was approved by the Institutional Animal Care and Use Committee of Tianjin International Joint Academy of Biotechnology and Medicine (document number: TJAB-TJU20180041). Animal care and operation procedures were in strict accordance with the China Laboratory Animal Use Regulations and the animals were used in accordance with the institutional ethical guideline. Sprague-Dawley rats (male, 190 ± 10 g) were housed in stainless steel wire bottom cages with a control environment (25 ± 1 °C, 50–60% humidity, 12 h light/dark cycle), free diet. All the animals were acclimated to pre-adaptation for at least one day. Two sides of the spinal (about 3 cm × 2 cm) were shaved 24 h before the experiment. Subsequently, rats were randomly divided into four groups of six: control group (C), G-L group (blank), G-EL group and G-B-EL group according to the three types of escinosome HPMC-hydrogels (Table 1). Then, 0.5 mL of gel were administered on the skin of rat's back, and the animals were examined after 1 h, 4 h and 24 h, in order to observe appearance changes.

Table 1. Body weight of rats belonging to the three treated groups: G-L group (hydrogel of blank liposome), G-EL group (hydrogel of escinosomes) and G-B-EL group (hydrogel of BRB-loaded escinosomes).

Group	1(g)	2(g)	3(g)	4(g)	5(g)	6(g)
G-L	204.3	196.0	197.5	208.6	230.3	218.7
G-EL	242.4	196.2	230.6	190.4	198.2	223.1
G-B-EL	214.5	215.8	214.6	217.9	202.6	197.6

HYDROXYETHYL CELLULOSE HYDROGEL FOR SKIN DELIVERY OF KHELLIN LOADED IN ASCOSOMES: CHARACTERIZATION, *IN VITRO*/*IN VIVO* PERFORMANCE AND ACUTE TOXICITY

5. Materials

Ammi visnaga dried extract, containing 95% khellin, was purchased from Galeno srl (Comeana, Italy). Phospholipon® 90G (P90G) was purchased from Lipoid GmbH (Ludwigshafen, Germany). Hydroxyethyl cellulose (Natrosol® 250 MR) and Phosphate Buffered Saline (PBS 0.01 M, 29 mM NaCl, 2.5 mM KCl, 7.4 mM Na2HPO4·7H2O, 1.3 mM KH2PO4) pH 7.4 were purchased from Sigma Aldrich (Milan, Italy). All the sol- vents (Sigma Aldrich, Milan, Italy) were HPLC grade. Ultrapure water was produced by a synergy UV Simplicity water purification system provided by Merck KGaA (Molsheim, France). TK-20B transdermal diffusion tester (Shanghai Kai Kai Technology Co., Ltd., China); Formic acid (purity by HPLC-MS > 98.0%, Tokyo Chemical Industry, Japan); Acetonitrile (HPLC grade, Fisher Scientific, Belgium). TG, T-CHO, LDL-C, HDL-C, AST, ALT, AKP activity assay kits and MDA, T-SOD, CAT, GSH-Px activity assay kits were obtained from Jiancheng Bio-Engineering Institute Co., Ltd. (Nanjing, China).

6. Animals

Healthy male BALB/c nude mice (6–8 weeks, weight 20 ± 2 g) and Sprague-Dawley rats (male, female, 190 ± 10 g) were purchased from Beijing Vital River Laboratory Animal Technology Co., Ltd. and housed in stainless steel wire bottom cages with a control environment (25 ± 1 °C, 50–60% humidity, with a 12 h light/dark cycle). All experimental procedures and animals care were approved by the Animal Ethics Committee of Tianjin University of Traditional Chinese Medicine (Ethic approval number: TJAB-TJU20160039); all studies were per-formed in accordance with the protocol of animal experiments handling issued by the Animal Research Center of Tianjin University of Traditional Chinese Medicine.

7. Methods

7.1. Vesicle preparation

Different vesicles were prepared and loaded with khellin. Conven- tional liposomes were prepared using phospholipon 90G (P90G, 0.084 M, conventional liposomes, L), while ascosomes were developed using ascorbyl derivatives (0.04 M) plus P90G (0.044 M). Ascosomes made with ascorbyl octanoate (ASC8), and ascorbyl decanoate (ASC10) were named LA8 and LA10, respectively. All the vesicles were loaded with 2 mg/mL of khellin, obtaining liposomes loaded with khellin (KL), ascosomes based on ASC8 loaded with khellin (KA8), and ascosomes based on ASC10 loaded with khellin (KA10). The vesicles were obtained by the lipid film hydration method *(Asprea M, 2019)* dissolving the proper amount of P90G/ASC8 or P90G/ASC10 and khellin in dichloro- methane, followed by evaporation of the solvent under vacuum (Rotavapor R200, Büchi, Switzerland) for 30 min keeping the flask in a water bath (37 ± 0.5 °C). The resulting dried film was hydrated by adding 10 mL of distilled water or PBS solution (phosphate buffer saline, pH 7.4) and the dispersion was stirred at 850 rpm for 30 min in a water bath at 38 ± 0.5 °C steady temperature *(Vanti G, 2019)*. The vesicle dispersion was then kept in an ice bath and sonicated in order to obtain SUV (small unilamellar vesicles) and minimize the content of polydispersed MLV (large multilamellar liposomes). The ultrasound treatment was per- formed using a Sonopuls HD 2200 ultrasound device (Bandelin Electronic GmbH, Berlin, Germany) coupled to a MS 72 probe, applying a sonication time of 1 min with pulsed duty cycles of 1/5 sec on and 1/5 sec off, and 50% amplitude. These conditions were selected to avoid the thermal damage threshold and to prevent the degradation of the dispersed solutes. The colloidal dispersions were stored in a refrigerator at 4 ± 0.5 °C.

7.2. Vesicle characterization

Dynamic light scattering and electrophoretic light scattering were used to measure average diameter, polydispersity index (PDI) and ζ- potential of the vesicles *(Vanti G, 2020b)*. Specifically, a Zetasizer Nano ZS90 apparatus (Malvern Instruments, Malvern, UK), equipped with a 633 nm red laser, was used at 25 ± 0.5 °C, with a scattering angle at 90°. The liposomes dispersions, 20 µL of each, were diluted with 980 µL of distilled water, and the average out of three measurements was taken. Particle sizes were calculated from the signal intensity

of the scattered light, autocorrelation functions were analysed by the cumulants method to obtain the hydrodynamic diameter of the scattering objects (Figure 1S), and the PdI, using the Zetasizer software provided by Malvern. The ζ-potential (mV) of the vesicles was measured by electrophoretic light scattering, using the same operating conditions. The electrophoretic mobility was calculated through the Henry correction to the Smoluchowski's equation. The encapsulation efficiency (EE%), defined as the percentage of entrapped drug in relation to the weighed drug was calculated using the following equation:

$$\mathrm{EE\%} = \left(\frac{\text{encapsulated drug}}{\text{weighted drug}}\right) 100 \quad (2)$$

The dialysis bag method *(Righeschi C, 2014; Isacchi B, 2012)* and the Spectra/Por® regenerated cellulose membranes, with a cut-off of 3.5 kDa (Repligen Europe B.V., Breda, The Netherlands), were used to purify the vesicles from the not entrapped khellin. Vesicles were introduced in the dialysis bag and stirred in 1 L of ultrapure water, at 25 ± 0.5 °C for 1 h. After the purification, the amount of khellin was determined by HPLC-DAD analysis. In addition, the recovery (R%), defined as the percentage of total drug recovered after the preparation procedure in relation to the weighed drug:

$$\mathrm{R\%} = \left(\frac{\text{total recovered drug}}{\text{weighted drug}}\right) 100 \quad (3)$$

R% was measured using the same procedure of EE% by disruption of the vesicles with MeOH and evaluation by HPLC analysis, but without the dialysis purification step.

7.3. HPLC-DAD analytical method

Quantification of khellin was carried out using a Shimadzu liquid chromatograph equipped with an SPD-20A UV detector and managed by a LabSolutions workstation (Shimadzu Corporation, Japan). A 200 mm, 4.6 mm i.d., 5 μm Dikma Diamonsil C18 column was used. Chromatographic analysis was carried out in gradient mode using a flow rate of 1.0 mL/min. The mobile phases were (A) formic acid/ water (pH 3.2) and (B) Acetonitrile. The multi-step linear solvent gradient used was: 0–6 min 50–60% B; 6–8 min 60–90% B; 8–10 min 90–50% B. The column temperature was set to 30 °C and the chromatograms were acquired at 247 nm, as reported in the supplementary (Figure 1S).

Before HPLC analysis 200 µL of khellin-loaded vesicles were treated with methanol (dilution factor = 5), placed in the ultrasonic bath for 20 min at room temperature, and subsequently ultra-centrifuged for 10 min at 10,000 rpm, using the supernatant for the HPLC. The method was validated for Limit of detection (LoD), Limit of quantitation (LoQ), specificity, linearity, precision, accuracy, stability.

7.4. LoD and LoQ

LoD, also called detection limit, represented the smallest amount or concentration of the analyte in the test sample that can be reliably distinguished from zero. LoQ, the lowest concentration of the analyte that can be determined with an acceptable repeatability and trueness were calculated. The found values of LoD and LoQ were 0.0043 µg/mL and 0.085 µg/mL, respectively.

7.5. Specificity

The specificity was evaluated by comparing the representative chromatograms obtained from blank methanol, PBS containing mouse skin, khellin reference solution and transdermal receiving solution.

7.6. Linearity

The linearity was obtained by calculating a regression line from the plot of peak area vs. concentration for the six khellin reference solutions in methanol (i.e., 1, 10, 20, 60, 80, and 120 µg/mL). The regression equation is y = 187,164.4503x + 138,101.9943, R^2 = 0.9999, which indicates the HPLC method has good linearity as reported in the supplementary (Figure 2S).

7.7. Precision

The intraday precision is reported in the supplementary (Table 2) was established by analysing the khellin reference solutions (1, 40 and 100 µg/mL) for five times on the same day. The inter-day precision is reported in the supplementary (Table 3) of the method was determined by repeating the analysis for three consecutive days. The RSD (%) values were calculated to determine the intra-day and inter-day precision. The RSD of the intra-day precision and the inter-day precision were less than 3%, which proving that precision meets requirements.

Table 2. Intra-day precision of khellin at three level of concentration.

Group	1 (μg/mL)	2 (μg/mL)	3 (μg/mL)	4 (μg/mL)	5 (μg/mL)	Average (μg/mL)	RSD (%)
Low dose	4.98	5.21	5.03	5.04	5.21	4.98	2.0
Middle dose	39.97	39.99	39.93	40.31	39.98	40.04	0.4
High dose	96.64	96.5	96.38	96.25	96.32	96.42	0.2

Table 3. Inter-day precision of khellin at three level of concentration.

Group	Day 1 (μg/mL)	Day 2 (μg/mL)	Day 3 (μg/mL)	Average (μg/mL)	RSD (%)
Low dose	4.90	4.86	4.85	4.87	0.5
Middle dose	40.04	40.16	40.21	40.14	0.2
High dose	99.91	100.96	101.34	100.74	0.7

7.8. Accuracy

Intra-day and inter-day accuracy of khellin was established at three levels of added concentrations using the same scheme of the analysis of precision. Results are reported in the supplementary.

7.9. Stability

The stability of the khellin samples were determined as follows: 5.03 mg of khellin was dissolved in 10 mL of methanol and 1 mL of the methanolic solution of khellin was added to the PBS containing 2.5 g of small pieces of mouse skin and stirred at 100 rpm at 37 ± 0.5 °C. Then, 0.5 mL of the sample was taken at predetermined time intervals (0, 1, 2, 4, 6, 8, 10, and 24 h) and analysed by the HPLC method after centrifugation. The RSD of stability of the khellin was 2.0%.

7.10. In vitro release of khellin from vesicles

The *in vitro* release study was performed using 2 mL of ascosomes loaded with khellin (2 mg/mL), introduced in a dialysis membrane having a cut-off of 3–5 kDa *(Vanti G, 2019)*. The experiment was carried out in 200 mL of PBS pH 7.4, selected as release medium, under continuous stirring at 37 ± 0.5 °C. An aliquot of 1 mL of release medium was removed at pre- determined time intervals (0.5, 1, 2, 4, 6, 8, 12 and 24 h) and replaced with 1 mL of fresh PBS maintained at 37 ± 0.5 °C. The quantification of khellin was performed by HPLC-DAD.

7.11. Ex vivo skin permeation study of khellin loaded in ascosomes

Ex vivo skin permeation study was conducted to test the differences of permeability between three vesicular formulations loaded with khellin, namely

KL, KA8, KA10, and compared with the saturated solution of khellin in PBS. To perform the test, the skin of nude mice (healthy male BALB/c nude mice 6–8 weeks, weight 20 ± 2 g) was excised. Adipose tissue attached to the skin was removed carefully. The skin was stored in a freezer at −20 ± 1 °C before experiments. *Ex vivo* skin permeation tests were conducted with Franz-type diffusion cells with an effective diffusion area of 3.14 cm^2 and receptor volume of 7.8 mL. The receptor compartment, containing PBS (pH 7.4), was maintained at 37 ± 0.5 °C and stirred continuously with a magnetic stirrer at 200 rpm. 1 mL of each formulation was placed on the *stratum corneum* side and covered with parafilm. The permeability experiments were conducted until 24 h and 0.5 mL of the receiving solution was taken from the receptor compartment at predetermined intervals (1, 2, 3, 4, 6, 8, 10, 21 and 24 h) and replaced with the same volume of fresh phosphate buffer at same temperature. The withdrawn samples were centrifuged at 10,000 rpm for 10 min, then the supernatant was analysed by HPLC to determine the content of khellin. For each group, the permeation study was performed in triplicate.

7.12. Hydroxyethyl cellulose hydrogel formulations of ascosomes loaded with khellin

Four different hydrogel formulations were prepared: a blank hydro- gel using PBS and three hydrogels loaded with KL, KA8 and KA10 by adding 3% *w/v* of hydroxyethyl cellulose (Natrosol® 250 MR) under gently stirring until the hydroxyethyl cellulose was completely moisturized. A glass rod and a vortex were used to stir the formulations. Additionally, two hydroxyethyl cellulose hydrogels containing free khellin were prepared: the khellin high-dose hydrogel (HK hydrogel), having a concentration of 200 mg/kg b.w., and the khellin low-dose hydrogel (LK hydrogel), having a concentration of 4 mg/kg b.w. The hydrogels were kept at room temperature for 48 h before performing any tests.

7.13. Characterization of the hydroxyethyl cellulose hydrogel formulations

A pH-meter (pH-Meter BASIC 20+, Crison, Milan, Italy) was used in order to evaluate the pH of all the semisolid formulations and, consequently, the stability and the suitability for application in damaged skin of the preparations *(El-Ridy MS, 2018)*. The samples were analysed as such without any dilution.

The rheological characterization of fresh hydroxyethyl cellulose hydrogels (48 h after preparation) was carried out both at 25 ± 0.5 °C and 32 ± 0.5 °C using the Brookfield DVE Digital Viscometer (Ametek Brookfield, United States)

equipped with three different disc spindles (04-05-06). Viscosity measurements (Pa·s) were carried out at constant time variations of 2 min, both increasing and decreasing the rotational speed. Moreover, to predict the physical stability of these hydroxyethyl cellulose hydrogels, the flow properties were determined after have kept the formulations at room temperature (20 ± 0.5 °C) for one month *(Zhang Y, 2018a)*. Three measurements were performed for each sample and the mean value was determined.

7.14. Skin irritation test of hydroxyethyl cellulose hydrogel formulations in rats

Hydrogel formulations based on ASC10 ascosome loaded with khellin were selected for the *in vivo* studies. Acute irritation test was performed with rats according to OECD guidelines *(OECD, 2015)* to verify the safety of the developed preparations. Forty Specific Pathogen Free Sprague-Dawley rats (SPF SD rats, half males and half females) were randomly divided into 8 groups. Groups were labelled as follows: normal skin control group (C); damaged skin control group (DC); normal skin group treated with hydrogel of khellin-loaded ASC10 ascosomes (LKP); damaged skin group treated with hydrogel of khellin-loaded ASC10 ascosomes (DLKP); normal skin group treated with hydrogel containing low dose khellin (LK); damaged skin group treated with hydrogel containing low dose khellin (DLK); normal skin group treated with hydrogel containing high dose khellin (HK) and damaged skin group treated with hydrogel containing low dose khellin (DHK). The dose of khellin for the groups LKP, DLKP, LK, DLK was 4 mg/kg, while the group with "high dose" of khellin (HK, DHK) was treated with 200 mg/kg.

Formulations given to C and DC groups were prepared using pH 7.4 PBS by adding 3% *w/v* of hydroxyethyl cellulose; formulations given to LKP and DLKP groups were prepared using khellin ascosomes by adding 3% *w/v* of hydroxyethyl cellulose. Finally, formulations given to LK and DLK groups were prepared using 50% ethanol solution of 2 mg/mL khellin gelled with 3% *w/v* of hydroxyethyl cellulose; while formulations given to HK and DHK groups were prepared using 50% ethanol containing 10 mg/mL khellin gelled with 3% *w/v* of hydroxyethyl cellulose.

Rats were let to adapt to the environment for 1 day under laboratory conditions, normal diet and free access to food and water. Twenty-four hours before the test, rats were shaved on the back, obtaining a bare skin of about 3 × 3 cm (about 10% of the body surface area), *(OECD, 2015)*. After 24 h of hair

removal, the damaged skin groups (namely DC, DLKP, DLK, DHK) were obtained by abrasions in the depilatory site by using spun paper. Each formulation was applied twice per day for 10 days. Body weight changes were recorded and behaviour observation was taken. Any variations on skin and mucous membranes, hair luster, respiration and nervous system, limb movement and other poisoning performance were recorded minutely.

7.15. Acute toxicity study of hydroxyethyl cellulose hydrogel formulations

To avoid the potential effects of khellin on liver *(Vrzal R, 2013)*, an acute toxicity study on Sprague-Dawley rats (male and female, 190 ± 10 g), having free access to food and water, acclimatized to the environment one day before test, was carried out. Rats were randomly divided into 8 groups by following the same grouping and modelling method as reported for the irritation test.

Biochemical analysis on rats' serum and hepatic tissue was designed to evaluate the influence of khellin and its preparations on liver function, indicating a possible metabolic damage. After 10 days of administration, blood was taken from the femoral artery of the rats (the syringe was rinsed with blood anticoagulant in advance). 7–8 mL blood were collected and put into a 15 mL centrifuge tube. After centrifugation at 3000 rpm for 10 min, the supernatant was tested according to the kit instructions. Serum levels of glutamic-pyruvic transaminase (ALT), glutamic oxalacetic transaminase (AST), alkaline phosphatase (AKP), triglyceride (TG), total cholesterol (T-CHO), low density lipoprotein (LDL-C), and high density lipoprotein (HDL-C) were measured. The rat liver tissue was excised, washed with PBS and weighed. The liver index (liver weight/body weight × 100) was calculated. Liver tissue (1 g) was taken according to the ratio of weight (g): volume (mL) = 1:9. Nine volumes of physiological saline was added, mechanically homogenized under ice water bath conditions and centrifuged at 3000 r/min for 10 min; the final supernatant was taken and analysed. The level of malondialdehyde (MDA), total superoxide dismutase (T-SOD), catalase (CAT), glutathione peroxidase (GSH-Px) in the liver tissue was measured. Moreover, the liver tissue and the ex- posed skin tissue were fixed in 10% formaldehyde solution and embedded in paraffin. After HE staining, pathologic observation was carried out under an optical microscope *(OECD, 2017)*.

7.16. Statistical analysis

The values are expressed as the mean ± standard error. Statistical analyses were performed using one-way ANOVA along with Bonferroni's post hoc test. The Student's test has been used for the analysis of paired data. $p \leq 0.05$ was considered to be a statistically significant difference.

GLYCEROSOMES OF *MELISSA OFFICINALIS* L. ESSENTIAL OIL FOR EFFECTIVE ANTI-HSV TYPE 1

8. Materials

Phosphatidylcholine (Phospholipon 90G, P90G) was purchased from Lipoid AG (Cologne, Germany) with the support of its Italian agent AVG srl. Cholesterol 95%, dichloromethane, methanol and acetonitrile were purchased from Sigma-Aldrich (Milan, Italy), vegetable glycerol Eur Ph. was purchased by Galeno srl (Prato, Italy). *Melissa officinalis* (lemon balm) essential oil was from Chiron Kentauros (Pelion, Greece). Ultrapure water was produced by a synergy UV Simplicity water purification system provided by Merck KGaA (Molsheim, France). Phosphotungstic acid (PTA) was purchased from Electron Microscopy Sciences (Hatfield, USA).

9. Methods

9.1. Chemical analysis of MEO by Gas Chromatography–Mass Spectrometry (GC–MS)

Melissa officinalis essential oil was analysed by GC-MS, in order to identify the qualitative and quantitative composition. The analysis were performed by Shimadzu GC-2010-GCMS-QP2010 system, operating at 70 eV. This was equipped with a split/splitless injector (230 °C) and a fused silica HP-5 MS capillary column (30 m x 0.25 mm i.d., film thickness 0.25 μm). The temperature program was from 50 °C to 290 °C, at a rate of 4 °C/min. Helium was used as a carrier gas at a flow rate of 1.0 mL/min. The injection volume of each sample was 1.0 μL. Arithmetic indices for all compounds were determined according to Van den Dool and Kratz *(Van den Dool H, 1963)*, using n alkanes as standards. The identification of the components was based on comparison of their mass spectra with those of NIST21 and NIST107 *(Masada Y, 1976)*, by comparison of their retention indices with literature data *(Adams RP, 2007)* and by co-chromatography with authentic constituents of MEO (Fluka, Sigma).

9.2. HPLC-DAD analysis

Quantitative determination of MEO, in terms of citral and β-caryophyllene, the two main components of the essential oil, was carried out using the 1200 high performance liquid chromatograph (HPLC) equipped with a diode array detector (DAD), by Agilent Technologies Italia Spa (Rome, Italy).

Chromatograms were acquired at 210 nm for β-caryophyllene and 233 nm for citral *(De Almeida Borges VR, 2013; Gaonkar R, 2016)*. Chromatographic analysis were performed using a reverse-phase column Eclipse XDB C-18 (150x4.6) mm, 3.5 μm particle size, maintained at 27°C. A gradient elution method, with 0.8 mL/min flow rate, was applied, using (A) acetonitrile and (B) formic acid/water (pH 3.2) as mobile phases. The analytical method was: 0-3 min 80% (B), 3-20 min 80-1% (B), 20-30 min 1% (B), 30-40 min 1-80% (B). The coefficient of determination (R^2) was 0.9998 for citral calibration curve, and 0.9999 for β-caryophyllene calibration curve.

9.3. Preparation of vesicles

MEO was loaded inside glycerosomes (MEO-GS), by the thin layer evaporation method in two steps *(Manca ML, 2013)*, using a 10% *v/v* glycerol/water solution as medium. Different amounts of phosphatidylcholine (330 or 600 mg) and cholesterol (10 mg) were used the experimental conditions of preparation were optimized varying the hydration time, hydration volume and the optional use of an ultrasonication bath, as reported in Table 4. The selected formulation was prepared with 600 mg of phosphatidylcholine and 10 mg of cholesterol dissolved in dichloromethane, using the ultrasonication bath for 1 min, in order to improve their dissolution. Subsequently, evaporation of dichloromethane was carried out using rotavapor for 20 min at 30 °C, in order to obtain a homogenous lipid film on the internal surface of the flask. At this point, 100 μL of MEO were added inside the flask and the lipid film was hydrated with 5 mL of 10% glycerol/water solution, by using the mechanic stirrer *(Van Hoogevest P, 2017)* and the ultrasonication bath *(Zhang K, 2017)*, for 30 min at 25 °C. Then, a further 5 mL of 10% *v/v* glycerol/water solution was added and the dispersion was mechanically shaken for 30 min more, at 25 °C, using an ultrasonication bath.

Table 4. Preparation of MEO-loaded glycerosomes (MEO-GS).

P90G:chol ratio(mg/mL)	MEO conc (mg/mL)	Hydration time (min)	Hydration volume (mL)	Ultrasonication bath
33:1	10	30	10	no
60:1	10	30	10	yes
60:1	10	30	10	no
60:1	10	30+30	5+5	yes
60:1	10	30+30	5+5	no
60:1	10	60	10	no
60:1	10	60+60	5+5	no

9.4. Physical characterization of MEO-GS

Average hydrodynamic diameter (nm), polydispersity index (PdI) and ζ-potential (mV) of glycerosomes were measured by Dynamic and Electrophoretic Light Scattering, DLS-ELS (Zetasizer Nanoseries ZS90) by Malvern instrument (Worcestershire, UK) at 25 °C, with a scattering angle of 90 °C *(Bhattacharjee S, 2016)*. Glycerosomes were diluted using ultrapure water before measurements, in order to achieve a suitable scattering intensity. Successively, glycerosomes were observed by Transmission Electron Microscope, TEM (CM12 TEM, PHILIPS, The Netherlands) equipped with an OLYMPUS Megaview G2 camera and with an accelerating voltage of 80 kV. A drop of sample, 5-folds diluted in water, was applied and dried by desiccation on a carbon film copper grid and it was counterstained with 1% *w/v* of phosphotungstic acid solution for 3 minutes. Then, the sample was examined at different amplifications.

9.5. Deformability

Deformability of glycerosomes was measured by extrusion, using the LipoFast-Basic extruder (Avestin Europe GmbH; Mannheim, Germany). The samples were extruded through a 19 mm polycarbonate membrane with 50 nm pore size (Avestin Europe GmbH; Mannheim, Germany), at a constant pressure of 7 bar, for 5 min. The extruded sample was collected in a syringe, meanwhile vesicle size and PdI were monitored by DLS analysis, before and after extrusion. Finally, deformability of vesicles was calculated according to the equation 1, *(Vanti G, 2019)*:

$$D = \frac{\text{average size (nm) before extrusion}}{\text{average size (nm) after extrusion}} \quad (1)$$

9.6. Chemical characterization of MEO-GS

Encapsulation efficiency (EE%) and total recovery (R%), of MEO inside glycersomes, were evaluated in terms of citral and β-caryophyllene, the two main components of the essential oil. EE% was calculated according to the equation 2:

$$\mathrm{EE\%} = \left(\frac{\text{encapsulated citral or } \beta\text{–caryophyllene}}{\text{initial citral or } \beta\text{–caryophyllene}}\right) 100 \qquad (2)$$

where *encapsulated citral or β-caryophyllene* is the concentration of the single components after the purification step. In fact, MEO-GS were purified from free MEO by the dialysis bag method *(Bilia AR, 2019a)*, using Spectra/Por® regenerated cellulose membranes with 3.5 KDa molecular weight cut-off (MWCO), by Repligen Europe B.V. (Breda, The Netherlands). The dialysis bag was stirred in 1 L of ultrapure water, at room temperature for 1 h. After that, the purified glycerosomes were diluted in methanol, in order to break vesicles and release the encapsulated MEO. Samples were centrifuged at 14,000 rpm for 10 min and they were analysed by HPLC-DAD. MEO total recovery was determined using the same procedure without the purification step by dialysis, and it was calculated according to the equation 3:

$$\mathrm{R\%} = \left(\frac{\text{total recovered citral or } \beta - \text{caryophyllene}}{\text{initial citral or } \beta\text{–caryophyllene}}\right) 100 \qquad (3)$$

where *total recovered citral or β-caryophyllene* is the concentration of the single components after the preparation procedure of MEO-GS.

9.7 In vitro release

The release of MEO from MEO-GS was evaluated by the dialysis bag method *(Moreno-Bautista G, 2011; Risaliti L, 2019)*, using Spectra/Por® regenerated cellulose membranes with 3.5 KDa MWCO), by Repligen Europe B.V. (Breda, The Netherlands), and it was compared to the release from a DMSO solution of MEO, at the same concentration of essential oil as used to prepared glycerosomes (10 mg/mL). The experiment was carried out with 1 mL of sample, magnetically stirred in 200 mL of PBS, used as release medium. The temperature was set at 37 °C; 0.5 mL of medium were collected at specified time points (30, 60, 120, 240, 360, 1440 min) and they were replaced by equal volumes of fresh medium, thus maintaining the sink conditions *(Asprea M, 2019)*. The collected release medium was analysed by HPLC-DAD. The amount of released MEO was expressed as

percentage of citral amount recovered in the release medium, as against citral amount contained inside the cellulose bag.

9.8. Stability studies

Physical and chemical stability of MEO-GS were investigated after storing the samples 4 months at 4 °C away from light. Once every month, size, PdI and ζ-potential were measured by DLS-ELS, whereas R% and EE% of citral and β-caryophyllene were evaluated by HPLC-DAD. At the same storage conditions, MEO chemical stability was also monitored in terms of citral and β-caryophyllene concentration.

9.9. Cells, viruses and growth conditions

In vitro assays were performed using African Green Monkey kidney cells (Vero), maintained in Dulbecco's modified Eagle's medium (DMEM), containing 10% foetal bovine calf serum (FCS), by Gibco BRL, Invitrogen, as described by Matta and coworkers *(Matta MK, 2008)*. The media were supplemented with 100 U/mL penicillin and 100 μg/mL streptomycin, provided by Sigma-Aldrich. The viruses were grown and titrated as previously described *(Nishioka Y, 1977)* and the virus titers were expressed in plaque-forming units (pfu) per mL. The HSV-1 strain vCLIDA61, used throughout the study, was generated at the Laboratory of Pharmacology of the Department of Pharmacognosy/Pharmacology, School of Pharmacy, Aristotle University of Thessaloniki, Greece. The virus was generated by substituting the thymidine kinase gene (TK, UL23) of the HSV ORF61 *(Kyratsous CA, 2009)* with sequences encoding the firefly luciferase gene by homologous recombination. Upon infecting cells, vCLIDA61 expresses firefly luciferase under the control of the TK gene promoter/regulatory elements. Therefore, by measuring the luciferase activity it is possible to measure the virus growth and the progress of the HSV-1 infection. To measure the effects of MEO (free or glycerosome-formulated) on the subsequent steps of HSV-1 infection, i.e. post-entry, the Vero cell cultures were first infected with HSV-1 and then MEO or MEO-GS were added in the cell growth medium (DMEM supplemented with 10% FCS and antibiotics) at various concentrations.

9.10. Antiviral assays

Vero cells were seeded into 12-well culture plates (Corning) at a density of 0.5 X 10^6 cells/well and incubated at 37 °C with 5% CO_2 until they reached 95%

confluence. HSV-1 preparations (1,500 plaque forming units (pfus) in 500 μl DMEM supplemented with 1% FCS) were pre-incubated for 60 min at 30 °C, either in the absence or presence of various concentrations of MEO (unformulated, dissolved in DMSO) or MEO-GS (glycerosome-formulated, as a diluted aqueous suspension), prior to being used to infect the Vero cell monolayers (100 μL virus preparation/ well). After a 60-min infection of the cells at 37 °C the virus preparations were aspirated and DMEM, supplemented with 10% FCS and antibiotics, was added. The infection was allowed to proceed for 24 h prior to lysing the cells and assaying for luciferase activity. The above-described assays measure the effects of the essential oil both on the virus itself (virucidal activity) and on the early stages of virus infection (virus adsorption to and penetration of the target cells).

9.11. Luciferase assays

The HSV-1-infected Vero cell monolayers, in the 12-well plates, were first washed with PBS before subsequently being lysed with 250 μL. Luciferase lysis buffer (1% Triton X-100, 25 mM glycylglycine pH 7.8, 15 mM $MgSO_4$, 4 mM EGTA, 1 mM dithiothreitol) for 7 min at room temperature. The luciferase activities were determined from triplicate infections, as previously described *(Panagiotidis CA, 1999)*, using a Berthold Sirius luminometer. In short, luciferase assays were performed as follows: 100 μL from each lysate was placed in a reaction tube compatible with the luminometer (Sarstedt No 55.476, 75 x 12 mm) containing 500 μL luciferase (LUC) reaction buffer (25 mM glycylglycine pH 7.8, 15 mM $MgSO_4$, 4 mM EGTA, 15 mM potassium phosphate, 1 mM dithiothreitol, 2 mM ATP). Each tube was then inserted into the luminometer, which had been programmed to inject 100 μL luciferin reagent (0.4 mM luciferin, 2 mM dithiothreitol, 25 mM glycylglycine pH 7.8, 15 mM $MgSO_4$, 4 mM EGTA), and, after a 10^{-s} delay, record light production (luciferase activity, in relative light units (rlu)) for 10 seconds at room temperature.

9.12. MTT assay

The cytotoxicity assays were adapted from Armaka, et al. *(Armaka M, 1999)*. Specifically, Vero cells were seeded into 96-well plates at a density of 1×10^4 cells/well in 100 μl DMEM supplemented with 5% FCS. Following an 1 h exposure to various MEO or MEO-GS concentrations, the cells were incubated for 48 h in fresh media before adding 10 μl of 5 mg/mL MTT and incubating for

another 2.5 h at 37 °C. Following media removal, the blue formazan crystals formed by metabolically active live cells, were solubilized by shaking the plates for 1 h at 37 °C after the addition of 100 µl of solubilization solution (1 vol. 20% SDS, 1 vol. N,N dimethylformamide, 5 vol. isopropanol) to each well, and the optical density was measured at 570 nm (test absorbance) and 630 nm (reference absorbance). The final value was obtained by subtracting the value obtained at 630 nm (nonspecific absorbance) from that obtained at 570 nm.

NANOVESICLES LOADED WITH *ORIGANUM ONITES* AND *SATUREJA THYMBRA* ESSENTIAL OILS L. AND THEIR ACTIVITY AGAINST FOOD-BORNE PATHOGENS AND SPOILAGE MICROORGANISMS

10. Materials

Phosphatidylcholine (Phospholipon 90G, P90G) was purchased from Lipoid AG (Cologne, Germany) with the support of the Italian agency AVG srl. Cholesterol 95%, dichloromethane, methanol and acetonitrile were purchased from Sigma-Aldrich (Milan, Italy); vegetable glycerol Eur Ph. and propylene glycol Eur Ph. were purchased from Galeno srl (Prato, Italy). Ultrapure water was produced by a synergy UV Simplicity water purification system provided by Merck KGaA (Molsheim, France). Phosphotungstic acid (PTA) was purchased from Electron Microscopy Sciences (Hatfield, USA).

11. Plant Materials

The fresh aerial parts of the wild plants *Origanum onites* L. and *Satureja thymbra* L. were collected from Symi island (SE Aegean, Greece) in summer 2018. The plant materials were authenticated by Associate Prof. Th. Constantinidis; Voucher specimens were deposited to a personal Herbarium of the Department of Pharmacognosy and Chemistry of Natural Products, School of Pharmacy, NKUA (Voucher Specimen Numbers: Tomou & Skaltsa 004/005)

12. Methods

12.1. Hydrodistillation and identification of OOEO and STEO by Gas Chromatography–Mass Spectrometry (GC-MS)

Air-dried parts (40.0 g) of each plant were cut into small pieces and subjected separately to hydrodistillation for 2 h, using a modified Clevenger type apparatus with a water-cooled oil receiver to reduce artifacts produced during distillation by over-heating according to Hellenic Pharmacopoeia *(National organization for medicines, 2002)*. The EOs were obtained by Gas Chromatography (GC) grade *n*-pentane and dried over anhydrous sodium sulfate and stored at -20°C. The compositions of the volatile constituents were established by GC/MS analyses, performed on a Hewlett-Packard 7820A-5977B MSD system operating in EI mode (70eV) equipped with a split/splitless injector, using a fused silica HP-

5 MS capillary column (30 m x 0.25 mm I.D., film thickness: 0.25 μm). Helium was used as a carrier gas at a flow rate of 2.0 mL/min. The oven temperature was increased from 60°C to 300°C at a rate of 3°C/min, and subsequently held at 300°C for 10 min. Injection was at 220°C in a split ratio 1:5. Injection volumes of each sample were 2 μL. Retention indices for all compounds were determined according to the Van den Dool approach *(Van den Dool H, 1963)*, using *n*-alkanes as standards. The identification of the components was based on comparison of their mass spectra with those of Wiley and NBS/NIST Libraries and those described by Adams *(Adams RP, 2017)*, as well as by comparison of their retention indices with literature data. In many cases, the essential oils were subjected to co-chromatography with authentic compounds (Fluka, Sigma). Semi-quantification through peak area integration from GC peaks was applied to obtain the component percentages. The analyses were carried out twice for each sample.

12.2. HPLC-DAD analysis

Quantitative analyses of OOEO and STEO in nanovesicles was based on the determination of carvacrol, the most abundant and marker constituent of both essential oils. Analyses were carried out using a 1100 High Performance Liquid Chromatograph (HPLC) equipped with a diode array detector (DAD), by Agilent Technologies Italia Spa (Rome, Italy). The chromatographic analyses were performed using a reverse-phase column Luna C-18 100 Å (250x4.6) mm, 5 μm particle size, maintained at 25°C; and the chromatograms were acquired at 276 nm *(Hajimehdipoor H, 2010)*. A gradient elution method, with 1 mL/min flow rate, was applied, using (A) acetonitrile and (B) formic acid/water (pH 3.2) as mobile phases. The analytical method was: 0-3 min 30-30% (B), 3-10 min 30-80% (B), 10-15 min 80-80% (B), 15-20 min 80-95% (B), 20-22 min 95-95% (B), 22-27 min 95-30%. The calibration curve was prepared using a 0.001 μL/μL standard solution of carvacrol in methanol and successive dilutions. The coefficient of determination (R^2) of carvacrol calibration curve was 0.9999.

12.3. Preparation of vesicles loaded with OOEO and STEO

O. onites and *S. thymbra* essential oils (OOEO and STEO) were formulated in lipid nanovesicles by the lipid film hydration method *(Risaliti L, 2021)*, in two steps *(Vanti G, 2020a; Manca ML, 2013)*. Different amounts of phosphatidylcholine (P90G) and cholesterol were tested for the development of the formulation, and the experimental conditions of the preparation were optimized varying media

and time of hydration, as well as the use of ultrasonic bath and/or mechanic stirrer, as reported in Table 5. The selected formulations were prepared with 600 mg of phosphatidylcholine and 10 mg of cholesterol dissolved in dichloromethane, using the ultrasonic bath for 1 min in order to improve the dissolution. Subsequently, evaporation of dichloromethane was carried out using the rotavapor for 20 min at 30°C, in order to obtain a homogenous lipid film on the internal surface of the flask. At this stage, OOEO (100 μL) or STEO (100 μL) or OOEO plus STEO (50 μL + 50 μL) were added to the flask and the lipid film was hydrated with 5 mL of 5% *v/v* glycerol/water solution (glycerosomes, GS) or 1% *v/v* propylene glycol/water solution (propylene glycol-nanovesicles, PG-nanovesicles, PGV), by using the mechanic stirrer for 30 min at 25°C and immersing the flask in the ultrasonic bath, as shown in Tables 5-6-7. Then, a further 5 mL of the selected dispersant medium was added, and the dispersion was mechanically shaken for additional 30 min, at 25°C, in the ultrasonic bath.

Table 5. Preparation of OOEO-loaded vesicles.

P90G:chol ratio (mg/mL)	OOEO (mg/mL)	Hydration time (min)	Hydration volume (mL)	Ultrasonic bath	Mechanic stirrer
15:0.5	10	30	5 (PBS)	no	yes
30:1	10	30	5 (PBS)	no	yes
30:6	10	30/60	5 (PBS)	no	yes
60:1	10	30+30	2.5+2.5 (1%G/W)	yes	yes
60:1	10	30+30	2.5+2.5 (5%G/W)	yes	yes
60:1	10	30+30	2.5+2.5 (10%G/W)	yes	yes
60:1	10	60+60	2.5+2.5 (5%G/W)	yes	yes
10:1	10	30+30	2.5+2.5 (5%G/W)	yes	yes
60:1	10	30+30	2.5+2.5 (1%PG/W)	yes	yes
60:1	10	30+30	2.5+2.5 (5%PG/W)	yes	yes

G/W=glycerol/water solution; PG/W=propylene glycol/water solution

Table 6. Preparation of STEO-loaded vesicles.

P90G:chol ratio (mg/mL)	STEO (mg/mL)	Hydration time (min)	Hydration volume (mL)	Ultrasonication bath	Mechanic stirrer
60:1	10	30+30	2.5+2.5 (5%G/W)	yes	yes
60:1	10	30+30	2.5+2.5 (1%PG/W)	yes	yes

G/W=glycerol/water solution; PG/W=propylene glycol/water solution

Table 7. Preparation of OOEO plus STEO-loaded vesicles.

P90G:chol ratio (mg/mL)	OOEO+STEO (mg/mL)	Hydration time (min)	Hydration volume (mL)	Ultrasonication bath	Mechanic stirrer
60:1	5+5	30+30	2.5+2.5 (5%G/W)	yes	yes
60:1	5+5	30+30	2.5+2.5 (1%PG/W)	yes	yes

G/W=glycerol/water solution; PG/W=propylene glycol/water solution

12.4. Physical characterization of nanovesicles loaded with OOEO and STEO

Average hydrodynamic diameter (nm), polydispersity index (PdI) and ζ-potential (mV) of the developed nanovesicles were measured by Dynamic and Electrophoretic Light Scattering, DLS/ELS (Zetasizer Nanoseries ZS90) by Malvern instrument (Worcestershire, UK), at 25°C, with a scattering angle of 90°C *(Vanti G, 2020b; Manaia EB, 2017)*. Glycerosomes and PG-nanovesicles loaded with the essential oils were diluted with ultrapure water before measurements, in order to achieve a suitable scattering intensity. Successively, the two systems loaded with OOEO plus STEO were observed by Transmission Electron Microscope, TEM (CM12 TEM, PHILIPS, The Netherlands) equipped with an OLYMPUS Megaview G2 camera, with an accelerating voltage of 80 kV. A drop of sample, 5-folds diluted in water, was applied and dried by desiccation on a carbon film copper grid and it was counterstained with 1% *w/v* of phosphotungstic acid solution for 3 minutes *(Vanti G, 2019)*. Then, the sample was examined at different amplifications.

12.5. Chemical characterization of nanovesicles loaded with OOEO and STEO

Encapsulation efficiency (EE) and total recovery (R) of OOEO and STEO loaded inside nanovesicles were evaluated in terms of carvacrol content, the marker constituent of both the essential oils. EE was calculated according to the following equation:

$$\mathrm{EE} = \left(\frac{\text{encapsulated carvacrol}}{\text{initial carvacrol}}\right) \times 100, \qquad (2)$$

where *encapsulated carvacrol* is the concentration of the single component after the purification step. In fact, vesicles were purified from free EOs by the dialysis bag method *(Vanti G, 2021)*, using Spectra/Por® regenerated cellulose membranes with 3.5 KDa molecular weight cut-off, by Repligen Europe B.V. (Breda, The Netherlands). The dialysis bag was stirred in 1 L of ultrapure water, at room temperature for 1 h. After that, the purified formulations were diluted in

methanol, in order to break vesicles and release the encapsulated EOs. Samples were centrifuged at 14,000 rpm for 10 min and supernatants were analysed by HPLC-DAD. OOEO and STEO total recovery (R) was determined using the same procedure without the purification step by dialysis, and it was calculated according to the following equation:

$$R = \left(\frac{\text{total recovered carvacrol}}{\text{initial carvacrol}}\right) \times 100, \quad (3)$$

where *total recovered carvacrol* is the concentration of the single component after the preparation of the formulation, determined by chromatographic analysis.

12.6. Determination of antibacterial and antifungal activity

The Gram-positive bacteria *Bacillus cereus* (food isolate), *Staphylococcus aureus* ATCC 11632 and *Listeria monocytogenes* NCTC 7973, and the Gram-negative bacteria *Escherichia coli* ATCC 35210, *Pseudomonas aeruginosa* ATCC 27853 and *Salmonella enterica* subsp. *enterica* serovar Typhimurium ATCC 13311 were used in order to determine the potential antibacterial activity. For determination antifungal activity 6 strains of fungi were used: *Aspergillus fumigatus* ATCC 1022, *Aspergillus niger* ATCC 6275, *Trichoderma viride* IAM 5061, *Penicillium verrucosum* var. *cyclopium* (food isolate), *Candida albicans* (oral isolate) and *Candida krusei* (oral isolate) were tested for their susceptibility. The bacterial strains were cultured on solid Tryptic Soy agar (TSA), while micromycetes were cultured on solid malt agar (MA) and yeast were sustained on Sabouraud dextrose agar (SDA) medium. The cultures were sub-cultured once a month and stored at 4°C for further utilization. All the tested microorganisms are deposited at the Mycological Laboratory, Department of Plant Physiology, Institute for Biological Research "Siniša Stankovic" - National Institute of Republic of Serbia, University of Belgrade, Serbia. The antimicrobial activity of samples was determined by the modified microdilution method *(CLC-Pred web-service, 2021; Clinical and Laboratory Standards Institute, 2009).* The results were presented as minimum inhibitory concentrations (MICs) and minimum bactericidal/fungicidal concentrations (MBCs/MFCs). Streptomycin (Sigma-Aldrich S6501, St Louis, MO, USA) and ketoconazole (Zorkapharma, Šabac, Serbia) were used as positive controls, and blank-glycerosome (Blank-GS) and blank-propylene glycol-nanovesicles (Blank-PGV) were used as negative control. All the experiments on antimicrobial activity were repeated in triplicate.

12.7. Evaluation of cytotoxicity in HaCaT cell line

Crystal violet assay was used for determination of the antiproliferative effect, according to the previous protocol *(Stojković D, 2020)* with modifications. Antiproliferative effect of pure and formulated OOEO/STEO was analyzed on spontaneously immortalized human skin keratinocytes (HaCaT) cell line. Cell line was grown in high-glucose Dulbecco's Modified Eagle Medium (DMEM) supplemented with 10% fetal bovine serum (FBS), 2 mM L-glutamine and 1% penicillin and streptomycin (Invitrogen) at 37°C in 5% CO_2. Twenty-four hours before treatment with the extract 1×10^4 cells/well were seeded in a 96-well plate. After, the medium was removed, fresh medium supplemented with different concentrations of the extract and compound (6.25-400 μg/mL) dissolved in phosphate buffered saline was added to the cells. Control cells were grown in medium. Potassium dichromate ($K_2Cr_2O_7$) was used as a positive control and PBS as negative control. The experiment was performed in triplicate for each condition and cells were incubated with the extract for 24 h. After that period, the medium was removed and the cells were washed twice with phosphate buffered saline (PBS), stained with 0.5% crystal violet staining solution and incubated for 15 min at room temperature. Afterwards, crystal violet was removed, the cells were washed in a stream of tap water and left to air-dry at room temperature for 24 h. The absorbance of dye dissolved in methanol was measured in a microplate reader at 590 nm (OD590). The results were expressed as IC_{50} (%) value in μg/mL. The criterion used to categorize the cytotoxic activity of pure and formulated OOEO/STEO to cancer cell lines was as follows: $IC_{50} \leq 20$ μg/mL = highly cytotoxic, IC_{50} ranged between 21 and 250 μg/mL = moderately cytotoxic, IC_{50} ranged between 201 and 500 μg/mL = weakly cytotoxic, and $IC_{50} >$ 501 μg/mL = no cytotoxicity. All analyses were performed in triplicate; each replicate was quantified also three times. Data were expressed as mean standard deviation, where applicable. In the cases where statistical significance differences were identified, the dependent variables were compared using Tukey's honestly significant difference (HSD) test.

DEVELOPMENT OF NANOLIPOSOMES LOADED WITH CARBON DIOXIDE *SERENOA REPENS* L. (SAW PALMETTO) EXTRACT

13. Materials and Methods

13.1. Preparation and characterization of saw palmetto nanoliposomes

Nanoliposomes were prepared by the lipid film hydration method as previously reported *(Risaliti L, 2019; Asprea M, 2019; Leto I, 2016)*. A mixture of 330 mg of phospholipon 90G (P90G) and increasing amounts (1, 2.5, 5 and 10 mg) of saw palmetto extract were tested to verify the vesicle formation. The samples were prepared by dissolving proper amount of P90G and the extract in CH_2Cl_2, followed by evaporation of the solvent under vacuum, in a water bath at 35 °C, to obtain a thin lipid film (*Isacchi B, 2017; Vanti G, 2019)*. After the hydration with 10 ml of ultrapure water (600 rpm for 30 min in a water bath at 35 °C), multilamellar structures were formed *(Risaliti L, 2019)*. Ultrasonication produced homogeneous small unilamellar vesicles, without damaging the structure of the vesicles *(Bilia AR, 2019a*). The best conditions to optimize the formulation in terms of size and polydispersity were 5 min of sonication with cycles of 1 sec on and 1 sec off. The optimized nanoliposomes loaded with 0.1 % *w/v* of *Serenoa repens* CO_2 extract were analysed by Dynamic and Electrophoretic Light Scattering (DLS and ELS) in order to characterize them in terms of Average Hydrodynamic Diameter (AHD, nm), Polydispersity Index (PdI, dimensionless measurement) and ζ-Potential (mV), (*Isacchi B, 2011a; Isacchi B, 2011b)*. Morphological characteristics of the developed nanoliposomes were observed by transmission electron microscope (TEM), using the negative staining technique (1% *w/v* of phosphotungstic acid solution), and were examined at different magnifications, as previously reported *(Vanti G, 2019; Bilia AR, 2019a; Isacchi B, 2011a; Isacchi B, 2011b*).

CO-DELIVERY OF BERBERINE CHLORIDE AND TARIQUIDAR IN NANOLIPOSOMES ENHANCED INTRACELLULAR BERBERINE CHLORIDE IN A DOXORUBICIN-RESISTANT K562 CELL LINE DUE TO P-gp OVEREXPRESSION

14. Materials

Phosphotungstic acid (PTA) was purchased from Electron Microscopy Sciences (Hatfield, USA). Berberine chloride (BRB, $C_{20}H_{18}ClNO_4$, PM: 371,81 g/mol), sodium chloride, cholesterol ($C_{27}H_{46}O$, 95%, PM: 386,65 g/mol), sodium hydroxide (NaOH, PM: 40 g/mol), Phosphate buffer (PBS 0,01 M, pH 7.4 (NaCl 29 mM, KCl 2,5 mM, $Na_2HPO_4 \cdot 7H_2O$ 7,4 mM, KH_2PO_4 1,3 mM), D-α-Tocopherol polyethylene glycol 1000 succinate (TPGS), acetonitrile and methanol HPLC grade, dichloromethane, dimethyl sulfoxide (DMSO), ethanol, aqueous glutaraldehyde aqueous solution (25% *v*/*v*), trypan blue, 3-(4,5-dimethylthiazol−2-yl)−2,5-diphenyltetrazolium bromide were from Sigma-Aldrich (Milan, Italy). Phospholipon 90G (P90G: phosphatidylcholine 90%, PM: 775 g/mol), and Phospholipon 100H (P100H: hydrogenated phosphatidylcholine 100%), were purchased from Lipoid AG (Cologne, Germany) with the support of its Italian agent AVG srl. Tariquidar (TAR, C38H38N4O6, 98.57%, PM: 646.73g/mol) was from MedChemExpress, Europe; bidistilled water purified by MILLIQ-plus from Millipore (Milford, MA, USA); doxorubicin (DOXO) was from TEVA Pharmaceutical industries (Milan, Italy); FITC Annexin/Dead cell Apoptosis Kit with FITC annexin V and propidium iodide (PI) for Flow Cytometry; culture medium RPMI 1640, fetal bovine serum (FBS), l-glutamine, penicillin G and Streptomycin were from Gibco®, European Division (San Giuliano Milanese, Italy); Peroxidase Type VI was from *Armoracia rusticana* L. (horseradish, PM 44,000 g/mol, Sigma-Aldrich, Milan, Italy).

15. Cell Cultures

K562 human erythroleukemia parental cell line (ATCC, Rockville, MD, USA) were used *(Teodori E, 2020)*. Cells grew in RPMI 1640 culture medium added with penicillin G 100 U/mL, streptomycin 100 mg/mL, L-glutamine 2 mM and 10% Foetal Bovine Serum (FBS), at 37° C in a humidified atmosphere at 5% of CO_2. The culture was maintained by two weekly passages in complete fresh medium.

The DOXO-resistant K562 clone (K562/DOXO), was obtained by exposure of the parental K562 cells to increasing drug concentrations up to 400 nM DOXO, using the same culture medium of the parental line, and characterized by expression of a unique membrane P-gp (180 kD molecular weight). To restore drug resistance by P-gp activity, the K562/DOXO cells were monthly exposed to 400 nM DOXO for 72 h, and to maintain the P-gp overexpression, the same procedure was used and the cells monthly exposed to the 400nM drug doxorubicin for 72 h. After DOXO treatment, the cultures were washed by centrifugation (5 min at 1200 rpm), resuspended and incubated in the drug-free growth medium, at 37 °C in a humidified atmosphere at 5% of CO_2. This maintenance method represents the maintenance routine of the doxo-resistant cell line; these cells are used after 3 weeks of culture in drug-free medium.

16. Methods

16.1. HPLC-DAD analytical method for the evaluation of BRB, TPGS and TAR

Evaluation of BRB, TAR and TPGS was obtained by the 1200 High Performance Liquid Chromatography apparatus (HPLC) equipped with a Diode Array Detector (DAD), (Agilent Technologies Italia Spa, Rome, Italy). The DAD wavelengths for TAR, TPGS and BRB were 240, 284 and 346 nm, respectively. Chromatography was performed at 27 °C, using a gradient elution method with (A) acetonitrile and (B) water at pH 3.2 (by formic acid), as mobile phases and a reverse-phase column Luna-C18 (250 mm × 4.6 mm, 5 μm particle size). The flow rate was 1 mL/min for 35 min. The analytical method was 0.1–3 min 85% (B), 3–9 min 85–70% (B), 9–10 min 70% (B), 10–17 min 70–50% (B), 17–25 min 50–1% (B), 25–35 min 1–85% (B). Acetonitrile was selected as the low UV cut off-mobile phase, in order to avoid the interference with the TAR signal. The external standard method was used for the quantitative determination of the investigated drugs during the whole set of experiments. BRB calibration curve was prepared using a stock solution of BRB in HPLC grade MeOH at a concentration of 0.54 mg/mL, which was subsequently diluted 2, 5, 10, 20, 50 and 100 times with HPLC grade MeOH. The linearity of the calibration curve obtained, expressed by the R^2 value, resulted 0.99998. TAR calibration curve was set using a stock solution of TAR at a concentration of 0.253 mg/mL in a mixture of CH_2Cl_2 and MeOH with a 25:75 ratio. Subsequently, appropriate dilutions, namely 2, 5, 10 and 100 times with HPLC grade MeOH, were prepared. R^2 value resulted in 0.99972. A stock

solution of TPGS in HPLC grade MeOH had a concentration of 0.320 mg/mL, subsequently diluted 2, 5, 20, 50 and 100 times with HPLC grade MeOH. R^2 value resulted in 0.99981.

16.2. Preparation and optimisation of nanoliposomes

The nanoliposomes were prepared according to the thin layer evaporation method as previously reported *(Vanti G, 2019)*. Two phospholipids, namely natural P90G and P100H, and cholesterol were used for the preparation of the vesicles, testing different combinations and gravimetric ratios, as reported in Table 8. Briefly, the lipid components were weighed, solubilized in a 250 mL glass flask with CH_2Cl_2, and then, for the complete solubilization of the components, were sonicated for 1–2 min in the ultrasonic bath. The organic solvent was removed by a rotary evaporator for 30 min at 35 °C, and the obtained dried lipid film was hydrated with 10 mL of PBS, by stirring at 650 rpm for 30 min, at 35 °C (P90G) and 55 °C (P100H), temperatures higher than the phospholipid transition temperature. In order to optimize polydispersity index (PdI) and sizes of nanoliposome suspension, ultrasonication by Sonopuls Ultrasonic Homogenizer HD 2200 (Bandelin electronic GmbH & Co. KG; Berlin, German) and MS72 or KE76 probes was carried out for 5 min at 5 cycles and 50% power, in an ice bath. Subsequently, to remove possible metal particles released by the probe, the samples were centrifuged at 25 °C for 1 min at 2000 rpm.

Table 8. Developed nanoliposomes.

P90G (mg)	P100H (mg)	Chol (mg)	PBS (mL)
330	/	10	10
330	/	20	10
330	/	100	10
660	/	100	10
660	/	200	10
650	/	300	10
/	330	10	10
/	330	20	10
/	330	100	10
/	500	10	10
/	500	20	10
/	500	100	10

16.3. Preparation and optimization of nanoliposomes loaded with BRB

The nanoliposomes were prepared as reported in the paragraph, adding 0.7 mg/mL of BRB to the liposomal suspension. Briefly, P90G, cholesterol and BRB were weighed in different gravimetric ratios (Table 9) and they were solubilized in a 250 mL glass flask with a mixture of CH_2Cl_2/MeOH, using the ultrasonic bath. Then the organic solvents were evaporated using a rotavapor combined with a membrane pump for 30 minutes at 35 °C, until a homogeneous lipid film was obtained, then hydrated with 10 mL of PBS using a mechanical stirrer at 650 rpm for 30 minutes and keeping the flask in a thermostatic bath at 35 °C. Finally, the ultrasonication was applied using the homogenizer with MS72 probe for 5 minutes, at 5 cycles and 50% power.

Table 9. Developed nanoliposomes loaded with berberine chloride.

P90G (mg)	Chol (mg)	BRB (mg)	PBS (mL)
330	10	7	10
330	20	7	10
330	100	7	10
660	100	7	10
660	200	7	10
650	300	7	10

16.3.1. Formulation of nanoliposomes loaded with BRB (BRB-L)

The nanoliposomes loaded with BRB were prepared according to the previous method, by adding 0.7 mg/mL of BRB to the final liposomal suspension. Briefly, P90G, cholesterol, and BRB were weighed in different gravimetric ratios (Table 9) and they were solubilized in a 250 mL glass flask with a mixture of CH_2Cl_2 and MeOH, using the ultrasonic bath. Successively, the preparation method continued as previously reported, until the ultrasonication of lipid suspension in 10 mL PBS.

16.3.2. Formulation of nanoliposomes loaded with P-gp inhibitors (TAR-L and TPGS-L)

The liposomal formulations made of 660 mg of P90G plus 100 mg of Chol, and loaded with TAR or TPGS, were developed using the method reported in Section 16.3. Briefly, TAR or TPGS were added to the organic phase of CH_2Cl_2/MeOH at the final concentration of 0.647 mg/mL (1mM) and 7.6 mg/mL (13 mM), namely 10% *w*/*w* of the lipid component weight, respectively. The

obtained formulations were optimized by performing 10 or 5-min sonication for TAR-L and TPGS-L, respectively, at 5 cycles and 50% power, using the homogenizer with MS72 probe.

16.3.3. Formulation of nanoliposomes loaded with BRB plus TAR (BRB/TAR-L)

The procedure of this formulation was the same reported previously for nanoliposomes loaded with BRB (Section 16.3.1) using the following lipid ratio: 660 mg of P90G and 100 mg of Chol. BRB plus TAR were added in the organic solvent to reach a final concentration of 0.7 mg/mL and 0.647 mg/mL, respectively. The optimization was carried out using a 5 min sonication at 5 cycles (50% power, MS72 probe).

16.4. Physical characterization and morphological study of nanoliposomes by Transmission Electron Microscope (TEM)

During the entire optimization procedures, nanoliposome characterization has been performed by evaluating size, homogeneity and possible aggregation state, with the aid of Dynamic and Electrophoretic Light Scattering (DLS and ELS, Zetasizer Nanoseries ZS90) by Malvern instrument (Worcestershire, UK), by using a scattering angle of 90 °C at 25 °C *(Vanti G, 2020a)*. Autocorrelation functions were analysed by the cumulant method in order to obtain the Average Hydrodynamic Diameter (AHD, nm), the size distribution expressed as PdI (Polydispersity Index, dimensionless measurement) and ζ-potential (mV), using the software provided by Malvern. Scattering measurements, in triplicate, were performed on samples, diluted 50/100-fold in ultrapure water. Nanoliposome morphology was investigated for vesicle dispersion, dimension and deformability by TEM (CM12 TEM, Philips, The Netherlands) equipped with an Olympus Megaview G2 camera, applying an 80 kV accelerating voltage. For this purpose, a drop of the diluted sample, released on a carbon film copper grid, was dried by desiccation, counterstained with 1% (*w*/*v*) of phosphotungstic acid solution and examined at different magnifications *(Vanti G, 2020b)*.

16.5. Chemical characterization of nanoliposomes: encapsulation efficiency (EE%) and total recovery (R%)

For each liposomal formulation, the encapsulation efficiency (EE%) and the total recovery (R%) of BRB and TAR were calculated. EE% is expressed as the percentage of the ratio of entrapped and weighted drug (equation 2):

$$EE\% = \left(\frac{\text{encapsulated drug}}{\text{weighet drug}}\right) 100 \quad (2)$$

In order to evaluate the entrapped drug, nanoliposomes were purified from free BRB and free TAR or TPGS, by dialysis bag method *(Bilia AR, 2019a)*, using Spectra/Por® regenerated cellulose membranes (12–14 KDa molecular weight cut-off) (MWCO) (Repligen Europe B.V., Breda, The Netherlands). Briefly, the dialysis bag was stirred at 100 rpm, for 30 min, in ultrapure water (1 L), at 25 °C. Then, to dissolve and disrupt the nanoliposome membranes, the purified samples were diluted in methanol and the encapsulated substances were released. The process was enhanced by immersing the diluted samples in ultrasonication bath for 30 min. All samples were centrifuged two times at 14,000 rpm for 10 min and analysed by HPLC-DAD. Recovery (R%), defined as the percentage of total recovered drug after the preparation procedure in relation to the weighed drug, was measured using the same procedure described for the EE% without the dialysis purification step, and applying the equation 3:

$$R\% = \left(\frac{\text{total recovered drug}}{\text{weighet drug}}\right) 100 \quad (3)$$

16.6. TEM analysis of K562 and K562/DOXO cells incubated with peroxidase-loaded nanoliposomes

In order to better understand the mechanism of interaction of the nanoliposomes with the K562 cell membrane, nanoliposomes loaded with horseradish peroxidase were prepared, fully characterized and incubated with K562 or K562/DOXO cells. Since nanoliposome horseradish peroxidase works as a probe, the fine morphological interactions of nanoliposomes may be followed by TEM evaluation and analysed with DLS. Briefly, a nanoliposomal formulation loaded with a solution of peroxidase in PBS (1 mg/mL) was prepared using TLE method as reported previously. 10 mL of this solution was used to hydrate the lipid film by a mechanical stirring at 37 °C for 30 min at 1300 rpm. The optimization of formulation was carried out by 5 min ultrasonication with 0.5 **s** intervals, without cycles, at a maximum intensity of 50%. K562 or K562/DOXO cells were incubated with peroxidase-loaded nanoliposomes, for 15 and 120 min, respectively. Peroxidase-loaded nanoliposomes, K562 or K562/DOXO cells, submitted at the same protocol, were centrifuged, fixed in Karnovsky liquid (2%

paraformaldehyde and 4% glutaraldehyde in 0.2 M cacodylate buffer, pH 7.4), post-fixed in 1% OsO_4 in 0.1 M phosphate buffer, pH 7.4, dehydrated in a series of acetone with increasing title, passed briefly in propylene oxide and finally included in epoxy resin (Epon812). The analysis was conducted on ultra-fine sections with a thickness of about 80 nm, obtained with an Ultrotome III ultramicrotome, contrasted with uranyl acetate and alkaline bismuth sub-nitrate. The observation was made at TEM at an accelerated voltage of 80 kV. The micrographs were taken with a digital camera connected to the microscope.

16.7. In vitro BRB release from BRB-L or BRB/TAR-L

The release of BRB from BRB-L and BRB/TAR-L was investigated over a period of 2 h, in presence of the culture medium (RPMI medium 1640 with 10% FBS, fetal bovine serum), to mimic the cell incubation conditions. A comparison of the release properties of the formulation with an aqueous BRB solution at the same concentrations was carried out. The experiment was performed on dialyzed nanoliposomes (according to the procedure described in Section 16.7), using the dialysis bag method and the Spectra/Por® regenerated cellulose membranes of 12–14 KDa MWCO by Repligen Europe B.V. (Breda, The Netherlands), *(Guccione C, 2017)*. BRB-loaded nanoliposomes and BRB aqueous solution were diluted (DF = 10) in the culture medium, and an exact volume (3 mL) of the suspension/solution was transferred into the dialysis bag. The experiment was carried out in 100 mL of PBS (pH 7.4), selected as medium and maintained at the constant temperature of 37 °C by a magnetic stirrer (100 rpm) with a heating plate. At specified time points (15, 30, 45, 60, 75, 90, 105, 120, 180, 240 and 300) min the medium was taken for the analysis and replaced by equal volumes of fresh buffer, in order to maintain the sink conditions. Finally, all samples were centrifuged at 14,000 rpm for 10 min and analysed by HPLC-DAD. The amount of released BRB was expressed as the percentage of the drug released in the medium divided by the drug present inside the bag. The amount of BRB released during the study was expressed by the following formula (equation 10):

$$\%\ \text{release} = (\text{released drug})/(\text{drug inside the bag}) \times 100 \quad (10)$$

16.8. Stability studies of BRB-L and BRB/TAR-L in cell culture medium

The stability of developed BRB-L and BRB/TAR-L within the culture medium (RPMI medium 1640 with 10% FBS) was evaluated. Aliquots of the dialyzed

formulations were diluted 10 times in the culture medium (as in the *in vitro* tests) and incubated for 2 h at 37 °C, using the PST−60HL−4 Thermo-Shaker (Biosan). After the incubation time, physical (size, PdI, ζ-potential) and chemical (EE% and R%) parameters of nanoliposomes were determined by DLS/ELS and HPLC-DAD.

16.9. Cytotoxicity of DOXO in the absence and in the presence of free or liposomal TAR or TPGS

Cell death by apoptosis was determined after treatment of the K562/DOXO cell line with DOXO in the absence and in the presence of free or liposomal TAR and TPGS. The test was also carried out using empty liposomes. The solution of TAR or TPGS in DMSO was prepared at a concentration 10 times higher than that present in the nanoliposome formulations, and diluted in the cell suspension with an DF=100, in order to reduce the percentage of DMSO to 1% *v*/*v*, avoiding cell toxicity. Similarly, TAR-loaded liposomes were diluted in the cell suspension with a DF=10. DOXO in DMSO was added in order to obtain a final concentration equal to 10 μM. The final concentrations of TAR and TPGS in the cell wells were 10 μM and 13.2 μM, respectively. The samples were incubated for 1 h at 37 °C in a humidified atmosphere with 5% CO_2. An aliquot of samples (3 mL) from each well were collected after 15, 30, 45 and 60 min, and washed twice with PBS, and resuspended in complete medium and incubated for 24 h at 37 °C in a humidified atmosphere with 5% CO_2. At the end of the incubation, the cell samples were counted and prepared for the detection of apoptotic and/or necrotic cell percentage, using a cytometer. A kit containing Annexin V conjugated with fluorescein isothiocyanate (FITC) and a solution of propidium iodide (PI) was used. The cells are centrifuged at 1200 rpm for 5 min, and the cell pellets (approximately 1×10^6 cells) were resuspended in 100μL of buffer A (solution of Annexin-binding in deionized water) and 5 μL of FITC-Annexin plus 1 μL of the PI 1X (100 μg/mL buffer A) solution added to the 100 μL of cell suspension. Cells were incubated at room temperature for 15 min. After 400 μL of buffer A were added and samples were shaken gently, leaving them in ice and in the dark until the time of analysis on the cytometer. With this kit the viable cells do not acquire any fluorescence, the necrotic cells stain red as they have the damaged membrane, the cells in the early phase of apoptosis are colored green and the cells in the late phase of apoptosis stain both red and green. The different cell populations can then be distinguished using a flow cytometer with an excitation

wavelength of 488 nm and accessorized with filters with an emission wavelength of 530 nm for the acquisition of apoptotic cells stained green with FITC and of a 620 nm emission filter for the acquisition of necrotic cells stained red with the PI. Cells stained in both green and red represent cells in late apoptosis.

16.10. Uptake studies by flow cytometry

BRB, being a fluorescent molecule, is a suitable probe to measure cell uptake and the functionality of the P-gp pump in K562/DOXO cells, due to overexpression of this pump. Flow cytometry was used to evaluate cellular uptake of fluorescent BRB in human parental and DOXO-resistant K562 cell line. A cell density of approximately 8×10^5 cells/mL, in the exponential growth phase, was used. Samples were prepared by diluting the formulations in the cell suspension with DF=10. The solution of BRB and TAR in DMSO were prepared at a concentration 10 times higher than the concentration present in the formulations, and diluted in the cell suspension with an DF=100 in order to reduce the percentage of DMSO to 1% *v/v* and to avoid cell toxicity. The final concentration of TAR in the cell wells was 10 μM. The P-gp inhibitor was added 15 min before BRB. Preliminarily, two incubation times with the nanoliposomes were used, namely 2 and 4 h (data not shown). Since the results showed a similar uptake, therefore a single exposure time was chosen for the subsequent experiments, i.e., 2 h at 37 °C in a humidified atmosphere with 5% CO_2. Aliquots of each sample suspension were used to establish uptake of the BRB. Therefore, in order to evaluate the uptake, 1 mL of each sample was washed twice with cold PBS, by centrifugation at 1200 rpm for 5 min at 4 °C to remove non-internalized BRB. The pellet of each sample was then resuspended in 1 mL of cold PBS and kept on ice, in the dark, until read at the cytometer. The fluorescence of BRB (λ_{ex} 488nm/λ_{em} nm, 530 ± 30 nm) was explored to measure the degree of cell accumulation. All samples were acquired by a FACS Canto flow cytometer (Becton Dickinson) and for each sample 20,000 events were acquired, analysed by FCS 6 Express software (De Novo Software, Glendale, CA), and transformed into fluorescence histograms. The fluorescence ratio (RF) of treated samples and the control sample (empty liposomes) is evaluated.

16.11. Statistical analysis

All experiments were independently carried out at least three times. All results represented as means ± SD and statistical analysis was performed using

the one-way Anova test and Bonferroni's multiple comparison test (GraphPad Prism software, Inc., San Diego, CA, USA). $p < 0.05$ was considered significant.

MUCOADHESIVE MICROEMULGEL FOR THE TOPICAL DELIVERY OF CLOBETASOL PROPIONATE IN THE TREATMENT OF MUCUS MEMBRANE PEMPHIGOID OF THE ORAL CAVITY

17. Materials

Cremophor RH 40 was purchased from Caelo Caesar & Loretz GmbH (Hilden, Germany), while Vitamin E acetate and 50% benzalkonium chloride aqueous solution were purchased from ACEF Spa (Piacenza, Italy). Clobetasol propionate, vegetable glycerol Eur Ph., propylene glycol Eur Ph., polyethylene glycol 400, carboxymethyl cellulose, xanthan gum and hydroxyethyl cellulose were bought from Galeno Srl (Prato, Italy), whereas carboxymethyl chitosan was from Kraeber & Co GmbH (Ellerbek, Germany). Phosphate buffered saline (PBS), Tween 20, Tween 80 and dimethyl sulfoxide, as well as the organic solvents methanol HPLC grade, acetonitrile HPLC grade, formic acid HPLC grade and ethanol were purchased from Sigma Aldrich (Milano, Italy). Ultrapure water was produced using the Milli-Q-system (Millipore SA, Molsheim, France).

18. Methods

18.1. HPLC-DAD analysis

Quantitative analyses of CP, during the various studies of pre-formulation and formulation of microemulsion, were carried out using a High Performance Liquid Chromatograph (HPLC) coupled to an UV-visible detector (DAD), by Agilent Technologies Italia Spa (Rome, Italy), and the Kinetex EVO C18 column (150x4.6 mm, 5 μm), maintained at 25 °C. The analytical method involves the use of (A) acetonitrile and (B) formic acid/water (pH 3.4) as mobile phase, at the flow rate of 1 mL/min, with the following gradient: 0-20 min 70-1% (B), 20-30 min 1-70% (B). Chromatograms were acquired at 238 nm. The calibration curve, with a coefficient of determination R^2 of 0.9998, was prepared using a standard solution of CP in methanol (0.5 mg/mL) and successive dilutions. Limit of quantification (LOQ) and limit of detention (LOD) were determined according to the ICH guidelines as signal-to-noise ratio. LOQ was 2.216 ng and LOD was 0.554 ng.

18.2. Preparation of microemulsion and pseudo-ternary phase diagram construction

The microemulsion was prepared using the aqueous titration method. The oily phase (Vitamin E acetate) was combined, under magnetic stirring at 50 °C for 5 min, with the S_{mix} mixture of surfactant plus cosolvent, using a 1:9 gravimetric ratio. S_{mix} was made of Cremophor RH 40 (surfactant) and glycerol (cosolvent) in 1:1 gravimetric ratio. The obtained final mixture was, thus, titrated adding ultrapure water dropwise and keeping the sample on the heating magnetic stirrer, set at the constant temperature of 35 °C, and 700 rpm. Finally, the obtained microemulsion was left 1 h at 21 °C, under magnetic stirring, to stabilize. The existing region of the developed microemulsion was determined by the pseudo-ternary phase diagram construction. Thereby, vitamin E acetate and S_{mix} were mixed at various ratios (1:9, 2:8, 3:7, 4:6, 5:5, 6:4, 7:3, 8:2, 9:1) and were titrated with water. During water addition, changes in sample appearance were visually monitored to determine if transparent microemulsion, emulsion, gel or turbidity had formed.

18.3. Preparation of CP-ME

The clobetasol propionate-loaded microemulsion (CP-ME) was obtained adding 0.054% *w/w* of CP to the ME prepared as described in paragraph 18.2, in order to get a 0.05% *w/w* final concentration of CP in the microemulgel. The system was left under magnetic stirring for 24 h at 21 °C, until CP was completely solubilized. After that, 0.5% *w/w* of 1 g/mL aqueous solution of anhydrous citric acid and 0.0002% *w/w* of methylene blue were added to the microemulsion as pH regulator and dye, respectively.

18.4. Preparation of CP-MEgel

CP-ME was gelled by adding different kind of thickening agents (carboxymethyl cellulose, hydroxypropyl methylcellulose, carboxymethyl chitosan, xanthan gum), at increasing concentrations (0.1, 0.5, 1, 1.5, 2, 2.5, 3, 3.5, 4, 4.5, 5 and 6)% *w/w*. The incorporation of the powder into CP-ME was obtained by magnetic or manual stirring. Subsequently, 0.1% *w/w* of 50% benzalkonium chloride aqueous solution was added to CP-MEgel as preservative against microorganism growth. The obtained microemulgel was allowed to stabilize for 2 days at room temperature (21 °C) far from the light, until the gelling process was complete and the air bubbles removed. An hydrogel of CP aqueous dispersion (CP-gel) was also prepared using the same percentage of CP (0.05%

w/*w*) and gelling agents, carboxymethyl cellulose (5% *w*/*w*) and carboxymethyl chitosan (2% *w*/*w*), used for the final formulation of gelled microemulsion.

18.5. Physical characterization of CP-ME and CP-MEgel

Dynamic light scattering techniques were used for the characterization and the stability studies of both CP-ME and CP-MEgel. Average hydrodynamic diameter (Size, nm) and polydispersity index (PdI, dimensionless measurement) of microemulsion droplets were measured by the Zetasizer Nanoseries ZS90 (Malvern instrument; Worcestershire, UK), with a scattering angle of 90° at 25 °C. Light scattering analysis on CP-MEgel was performed at 25 °C, applying a 20-fold dilution in ultrapure water.

CP-ME, CP-MEgel and CP-MEgel aqueous dispersion, obtained by a 20-fold dilution in ultrapure water, were also analyzed by the Scanning Electron Microscope (SEM) Gaia 3 (Tescan s.r.o, Brno, Czech Republic), a FIB-SEM (Focused Ion Beam-Scanning Electron Microscope), operating in high-vacuum mode with electron beam voltage of 20 kV and Bright-field Transmission Electron Microscope (TEM) detector. Gaia 3 was equipped with an EDS-X-ray microanalysis system (EDAX, AMETEK, USA) TEAM EDS Basic Software Suite TEAM™. The Gaia 3 microscope is delivered with a STEM (Scanning Transmission Electron Microscopy) detector, which provides a complementary method for image acquisition of transmitted electrons. The detector consists of several semi-conductor sensors for bright field and dark field imaging. By placing the detection system below the specimen, the transmitted electron signal can be collected.

18.6. Chemical characterization of CP-ME and CP-MEgel

The amount of CP present in the final formulation (microemulsion or microemulgel) was expressed as total recovery, calculated as percentage of the total drug recovered after the preparation procedure in relation to the weighed drug. CP-ME was diluted in methanol (FD=10) in order to dissolve the dispersed phase of the microemulsion and solubilize CP. The process was enhanced by 10 min of ultrasonication bath, after that the samples were centrifuged for 10 min at 14,000 rpm and the supernatant was analyzed by HPLC-DAD. CP-MEgel (100 mg) was instead dispersed in water (2 mL) and stirred for 10 min first, then it was 10-fold diluted in methanol to extract CP and the methanolic samples were

treated and analysed as described for CP-ME. Moreover, the pH of CP-MEgel was measured by the Basic 20+ pH-meter (Crison Instrument; Barcelona, Spain).

18.7. Viscosity measurements

Viscosity (mPa·s) of CP-ME and CP-MEgel was measured at 25 °C and 37 °C, by a Brookfield DVE-RV digital viscometer (Ametek Brookfield; Milan, Italy). The 06 spindle was selected for the measurements, by the "trial and error" method [19], because it was able to produce on-scale readings (% Torque between 10 and 100) with the highest number of the possible speeds. The viscosity analyses were performed without spindle guard lag, using 50 g of sample in a 50 mL beaker, according to the previous instrument recalibration *(Vanti G, 2020b)*, selecting 2 min as spindle rotation time (time required for the viscosity reading to reach a constant value) for each rotation speed, specifically: 0.5, 0.6, 1, 1.5, 2, 3, 5, 10, 20, 30, 50 and 100 rpm. Every 2 minutes, the rotational speed was increased (up viscosity ramp) from 0.5 to 100 rpm and the viscosity measurements were recorded. Then, every 2 min, the rotational speed was reduced (down viscosity ramp) from 100 rpm to 0.5 rpm and the viscosity measurements were recorded. Temperature uniformity of sample and spindle was monitored by a temperature sensor and keeping the beaker in a water bath during the test. Additionally, the spindle was left to rotate inside the sample for 30 min before starting measurement. Viscosity measurements were carried out after two days from the preparation of CP-MEgel, in order to remove the entrapped air bubbles.

18.8. Physical and chemical stability of CP-ME

CP-ME was stored either at room temperature (25 °C) or in fridge (4 °C), away from light, for 3 months, in order to evaluate the chemical and physical stability. Every week for the first 35 days and, subsequently, every 10 days, average dimensions of the microemulsion droplets (size) and homogeneity of the sample (PdI) were monitored by DLS, whereas CP concentration in the microemulsion (recovery) was determined by HPLC-DAD, as described in paragraph 18.6.

18.9. Physical and chemical stability of CP-MEgel

The physical stability of CP-MEgel was evaluated storing the formulation at 25 °C for 3 months. Specifically, the viscosity was measured by the rotational viscometer at both 25 °C and 37 °C, while the droplet sizes of the gelled CP-ME

were checked by light scattering analysis. In parallel, the chemical stability of CP-MEgel stored at the same conditions was evaluated by measuring the pH and determining the CP content (recovery) by HPLC-DAD analysis, as described in paragraph 18.6.

18.10. Release study of CP-MEgel by vertical diffusion Franz cells

In vitro CP release from CP-MEgel and CP-gel was investigated by vertical diffusion Franz cells, using cellulose nitrate filters (Sartorius Stedim Biotech GmbH, Germany), with 0.45 μm pore sizes and 130 μm thickness, as synthetic membranes *(Vanti G, 2020b).* The receptor compartment was filled with 7 mL of 1% *v/v* Tween 20/PBS solution, while the cell diffusion area of 3.14 cm^2 was covered by the synthetic membranes, previously hydrated by the acceptor solution, and the donor compartment was filled with an exact amount of formulation (1 g) by a syringe. During the experiment, the system was maintained at 37 °C by a thermostatic circulation bath, under constant magnetic stirring (500 rpm). All cells were gripped by suitable clamps, while donor chambers were closed with suited caps and sampling ports sealed with parafilm, in order to reduce the evaporation. The release medium (0.2 mL) was collected from the receptor compartment at established time points (1, 2, 3, 4, 5, 6, 7 h) and it was replaced with the same volume of fresh 1% *v/v* Tween 20/PBS solution. All samples were analysed by the HPLC-DAD. CP released from the formulations during 7 h was calculated as $\mu g/cm^2$ of the applied dose absorbed through the membrane and recovered in the receptor compartment.

18.11. Preparation of porcine buccal mucosa

Full thickness samples of porcine vestibular mucosa from the inner cheek aspect, comprising the surface epithelium and the underlying connective tissue, were dissected using the muscular capsule as cleavage surface. The samples were enveloped in a gauze soaked with isotonic PBS and kept at 4°C until further use.

18.12. Permeation study of CP throught porcine buccal mucosa

Cross-sections of porcine buccal mucosa, taken from a local slaughterhouse, were prepared at the Department of Experimental and Clinical Medicine, of the University of Florence, Florence, Italy.

The disk sections of porcine buccal mucosa, prepared as described, were used for the permeation study by the Franz cell apparatus. Vertical diffusion cells

had a 3.14 cm^2 diffusion area. The donor compartment was filled with 1 mL of sample, while the acceptor compartment was filled with 7 mL of 1% *v*/*v* Tween 20/PBS solution and it was kept under continuous magnetic stirring. The mucosa was placed between the two compartments with the external layer facing the donor compartment and with dermis touching the buffer solution in the acceptor compartment. The system was incubated for 7 h and during the experiment, the apparatus was maintained at 37 °C by a thermostatic circulation bath. 0.2 mL of the acceptor medium were withdrawn at determined time points (1, 2, 3, 4, 5, 6, 7 h) and were replaced by the same volume of fresh buffer. After that all samples were analysed by HPLC-DAD. The amounts of CP retained in the mucosa were also determined. Each mucosa section was washed 5 times with 3 mL of PBS and it was dried with filter paper. The inner section of the mucosa slice, which was in contact with the two chambers, was cut and divided into equal pieces. These ones were soaked in 0.5 mL of methanol and exposed to 3 h of ultrasonication bath, in order to extract all the accumulated drug. Finally, the samples were centrifuged 10 min at 14,000 rpm and analysed by HPLC-DAD. The permeation parameters were calculated as following: absorbed dose (A_7), expressed as micrograms of CP absorbed through the mucosa and recovered in the acceptor compartment ($\mu g/cm^2$); absorbable dose retained inside the mucosa (M_7), expressed as $\mu g/cm^2$ of the applied dose recovered inside the mucosa; total absorbed dose (TA_7), expressed as sum of the two values A_7 and M_7.

DEVELOPMENT AND OPTIMIZATION OF BIOPHARMACEUTICAL PROPERTIES OF A NEW MICROEMULGEL OF CANNABIDIOL FOR LOCALLY-ACTING DERMATOLOGICAL USE

19. Materials

Cannabidiol was purchased from A.C.E.F Spa (Piacenza, Italy); isopropyl myristate, Sepigel 305, carbomer and xanthan gum were from Galeno Srl (Prato, Italy), while methyl parahydroxybenzoate and propyl parahydroxybenzoate were purchased from Caelo Caesar & Loretz GmbH (Hilden, Germany). Solutol HS 15 was a gift of BASF (Ludwigshafen, Germany) with the support of BASF Italia, BTC Chemical Distribution Unit (Cesano Maderno, Monza e Brianza, Italy), whereas Transcutol P was generously gifted by Gattefossé (Saint Priest, France). Methanol, acetonitrile and formic acid of HPLC grade were purchased from Sigma Aldrich (Milano, Italia). Ultrapure water was produced using a synergy UV Simplicity water purification system provided by Merck KGaA (Molsheim, France).

20. Methods

20.1. HPLC-DAD analysis

Qualitative and quantitative determination of CBD during pre-formulation and formulation studies was carried out using a 1100 High Performance Liquid Chromatograph (HPLC) equipped with a Diode Array Detector (DAD) from Agilent Technologies Italia Spa (Rome, Italy). Chromatographic analyses were performed at 26 °C, using an Eclipse XDB-C18 column (150 mm × 4.6 mm, i.d. 3.5 μm) from Agilent Technologies Italia Spa (Rome, Italy) A gradient analytical method with 0.8 mL/min flow rate for 35 min was applied, using (A) acetonitrile and (B) water at pH 3.2 (by formic acid), as mobile phases, and the following timetable: 0-20 min 70-1% (B), 20-35 min 1-70% (B). Chromatograms were acquired at 210 nm. The calibration curve, with a coefficient of determination R^2 of 0.99997, was prepared using a standard solution of CBD in methanol (0.01 mg/mL) and successive dilutions of 2, 5, 10, 20, 50, 100-fold. Limit of detection (LOD) and limit of quantification (LOQ) were calculated by determination of signal-to-noise ratio, in accordance to the ICH guidelines LOQ was 2.00 ng, while LOD was 0.45 ng.

20.2. Preparation of microemulsion and pseudo-ternary phase diagram construction

The ME was prepared using the aqueous titration method *(Cecchi L, 2020b)*. The oily phase (isopropyl myristate) was combined with S_{mix} (surfactant plus cosolvent) in 1:9 gravimetric ratio, under magnetic stirring at *ca.* 50 °C for 5 min (temperature of the sample was monitored by a temperature sensor). S_{mix} consisted of Solutol HS 15 (surfactant) and Transcutol P (cosolvent), in 20:9 gravimetric ratio. Successively, the lipophilic mixture was cooled to 35 °C and titrated with ultrapure water dropwise, keeping the sample on the heating magnetic stirrer, set at the constant temperature of 35 °C and 700 rpm. Thus, the obtained ME was allowed to stabilize at 35 °C for 10 min; then it was let cool to room temperature (21±2 °C), under gentle magnetic stirring. The existing region of the developed microemulsion was determined by the pseudo-ternary phase diagram construction using the ProSim Ternary Diagram 1.0 software. Thereby, isopropyl myristate and S_{mix} were mixed at various ratios (1:9, 2:8, 3:7, 4:6, 5:5, 6:4, 7:3, 8:2, 9:1) and the obtained mixtures were titrated with water. During water addition, changes in sample appearance were visually monitored to determine if clear ME, emulsion, gel or turbidity had constituted.

20.3. Preparation of CBD-ME

The cannabidiol-loaded ME (CBD-ME) was prepared as described in paragraph 20.2, adding CBD to the lipophilic mixture of isopropyl myristate, Solutol HS 15 and Transcutol P. CBD concentration in CBD-ME was 1.03% *w/w*, in order to obtain a final concentration in the MEgel of 1% *w/w*. Subsequently, 0.2% *w/w* of a paraben mixtures ($PABA_{mix}$), consisting in methyl parahydroxybenzoate plus propyl parahydroxybenzoate in 75:25 gravimetric ratio, was added to CBD-ME as preservative against the microorganism growth.

20.4. Formulation of CBD-MEgel

CBD-ME was gelled by adding different thickening agents (Sepigel 305, Carbomer and xanthan gum), at increasing concentrations, i.e. 1.5, 2, 2.5% *w/w*. The gelation was obtained by magnetic and manual stirring. The final obtained MEgel loaded with CBD (CBD-MEgel) was left to stabilize at room temperature (21±2 °C) for 1 day, far from the light, in order to remove the entrapped air bubbles before subsequent tests. A gel, loaded with unformulated CBD (CBD-gel), was also prepared following the same procedure used for CBD-MEgel and the same concentration of CBD (1% *w/w*) and Sepigel 305 (2.5% *w/w*).

20.5. Physical characterization of CBD-ME and CBD-MEgel

20.5.1. Droplet size

The physical characterization of the developed ME and the correspondent MEgel was carried out by dynamic/electrophoretic light scattering (DLS/ELS) techniques, using the Zetasizer Nanoseries ZS90, equipped with a 4 mW He-Ne laser, operating at 632.8 nm, and an APD detector (Malvern instrument; Worcestershire, UK). Time correlation functions were analysed using the Zetasizer software version 7.02, provided by Malvern and all data were analysed by the Cumulants method. Average hydrodynamic diameter (Size, nm) and polydispersity index (PdI, dimensionless measurement) were measured both during formulation development and stability studies. All measurements were carried out at 25 °C using 10x10x45 mm polystyrol/polystyrene cuvettes and a scattering angle of 90°. CBD-MEgel was analysed at both 25 °C and 35 °C, applying a 20-fold dilution in ultrapure water.

20.5.2. Scanning and Transmission Electron Microscope analysis

CBD-ME, CBD-MEgel and CBD-MEgel diluted dispersion (obtained by 20-fold dilution in ultrapure water), were analyzed by the Scanning Electron Microscope (SEM) Gaia 3 (Tescan s.r.o, Brno, Czech Republic), a FIB-SEM (Focused Ion Beam-Scanning Electron Microscope), operating in high-vacuum mode with electron beam voltage of 20 kV and Bright-field Transmission Electron Microscope (TEM) detector. Gaia 3 was equipped with an EDS-X-ray microanalysis system (EDAX, AMETEK, USA) TEAM EDS Basic Software Suite TEAM™. The Gaia 3 microscope is delivered with a STEM (Scanning Transmission Electron Microscopy) detector, which provides a complementary method for image acquisition of transmitted electrons. The detector consists of several semi-conductor sensors for bright field and dark field imaging. By placing the detection system below the specimen, the transmitted electron signal can be collected.

20.6. Chemical characterization of CBD-ME and CBD-MEgel

20.6.1. Determination of CBD recovery

Recovery (R%) expresses the amount of CBD present in CBD-ME and CBD-MEgel and it was calculated as percentage of the total drug recovered after the preparation in relation to the initial weighed drug. CBD-ME was diluted in

methanol (FD=100) to induce the rupture of the microemulsion and solubilize CBD, whereas CBD-MEgel (100 mg) was dispersed in water (2 mL) and left under magnetic stirring at 400 rpm for 10 min. An aliquot of this dispersion was then taken and diluted in methanol with a dilution factor of 10. All methanolic samples were briefly vortexed, sonicated 5 min (CBD-ME samples) or 10 min (CBD-MEgel samples), by an ultrasonication bath set at 25±2°C, and were centrifuged 10 min at 14,000 rpm. The obtained supernatants were analyzed by HPLC-DAD.

20.6.2. Determination of pH

pH of CBD-ME and CBD-MEgel was measured by a Basic 20+ pH-meter (Crison Instrument; Barcelona, Spain). The pH meter was calibrated with buffer solutions at pH 4.0, 7.0 and 9.0, before each use.

20.7. Rheological properties of CBD-MEgel

Viscosity (mPa·s) of CBD-MEgel was measured at 25±1 °C and 35±1 °C, by a Brookfield DVE-RV digital viscometer (Ametek Brookfield; Milan, Italy), using a 06 spindle, selected by the "trial and error" method, because able to provide on-scale readings (% Torque between 10 and 100) with the highest number of the possible speeds. The measurements were performed without spindle guard lag, using 50 g of sample in a 50 mL beaker, according to the previous instrument recalibration *(Vanti G, 2020b)* and selecting 2 min as spindle rotation time (time required for the viscosity reading to reach a constant value) for each rotational speed (0.5, 1, 2, 3, 5, 10, 20, 30, 50 and 60 rpm). Every 2 minutes, the rotational speed was increased (up viscosity ramp) from 0.5 to 60 rpm; then, every 2 min, the rotational speed was reduced (down viscosity ramp) from 60 rpm to 0.5 rpm All the viscosity measurements were recorded and plotted on a graph as a function of the spindle rotational speed. Temperature uniformity of sample and spindle was ensured by immersing the beaker in water bath with a temperature sensor and by rotating the spindle inside the sample for 30 min before starting each measurement. Viscosity analyses were carried out after 1 day from the preparation of CBD-MEgel, in order to remove the entrapped air bubbles.

20.8. Acceptor medium selection

Solubility studies of CBD in different buffer solutions were carried out in order to select an acceptor medium for the release and permeation tests. Tween

20, Tween 80, propylene glycol (PG) and polyethylene glycol 400 (PEG 400) were mixed at 5% *v/v* in PBS and were evaluated as acceptor mediums solubilizing an excess of CBD in an exact volume of solution. The suspension was kept under continuous magnetic stirring for 24 h at room temperature. Subsequently, all samples were centrifuged 10 minutes at 14,000 rpm and they were analyzed by HPLC-DAD after proper dilutions in ethanol.

20.9. In vitro release by vertical diffusion Franz cells

In vitro CBD release from CBD-MEgel and CBD-gel was investigated by the Franz cells apparatus, using cellulose nitrate filters (Sartorius Stedim Biotech GmbH, Germany), with 0.45 μm pore sizes and 130 μm thickness, as synthetic membranes *(Vanti G, 2020b).* The system consists of two compartments, donor and acceptor, separated by a horizontally oriented membrane. The receptor compartment was filled with 7 mL of 5% *v/v* Tween 20/PBS solution, selected as release medium, and was kept under constant magnetic stirring (500 rpm), while the donor compartment was loaded with an exact amount of gel (1 g), by 1 mL syringe. Cell diffusion area of 3.14 cm^2 was covered by the synthetic membranes, previously hydrated by the acceptor solution. Finally, the cells were clamped together. Donor chambers were closed with suited caps and sampling ports were sealed with parafilm, in order to avoid evaporation. During the experiment, the system was maintained at 35 °C by a thermostatic circulation bath and a water jacket around cells. The release medium (0.2 mL) was collected from the sampling port of the receptor compartment at established time points (0.5, 1, 2, 3, 5, 7, 24 h) and it was replaced with the same volume of fresh 5% *v/v* Tween 20/PBS solution. All samples were analysed by the HPLC-DAD. CBD released from the gels during 24 h was calculated as μg/cm^2 of the applied dose absorbed through the membrane and recovered in the receptor compartment.

20.10. Permeation study through rabbit ear skin and skin accumulation

Permeation experiments of CBD-MEgel and CBD-gel were carried out using rabbit skin excised from the inside of rabbit's ear. In particular, the skin was manually removed from the underlying cartilage within a rectangular incision made with a sharp blade and cut into discs of 2 cm in diameter, taking care not to damage the skin surface, as previously described by Vanti and coworkers *(Vanti G, 2019)*. The integrity of the skin was carefully checked by visual inspection. In order to avoid dehydration, the freshly cut skin was kept moisten

between sheets of filter paper wet with PBS and the skin outer surface was gently dried by dabbing with filter paper, before placement on the vertical diffusion Franz cells (3.14 cm^2 diffusion area). The skin was placed between the two compartments, upon cell diffusion area (3.14 cm^2), with the *stratum corneum* facing the donor chamber and with dermis touching the buffer solution in the acceptor chamber. 1 g of sample was collected by 1 mL syringe and put in the donor compartment above the skin, while 7 mL of 5% *v/v* Tween 20/PBS solution were posed in the acceptor compartment, kept under continuous magnetic stirring at 500 rpm. The system was closed and incubated for 24 h, at the constant temperature of 35 °C, maintained by a thermostatic circulation bath. The release medium (0.2 mL) was collected from the receptor compartment at fixed time points (0.5, 1, 2, 3, 5, 7, 24 h) and it was replaced with the same volume of fresh buffer solution. All the samples were analysed by HPLC-DAD. The amount of CBD retained in the skin was also determined. Each skin lamina was washed 3 times with 3 mL PBS and dried with filter paper. The inner section of the skin specimen, in contact with the sample, was cut and divided into equal pieces. These were soaked in 0.3 mL of methanol, exposed to 3h of ultrasonication bath and then shaken in a water bath for further 3h in a PST−60HL−4 Thermo-Shaker (Biosan), in order to extract all the accumulated drug. Finally, the samples were centrifuged 10 min at 14,000 rpm and analysed by liquid chromatography. The permeation parameters were calculated as following: absorbed dose (A), expressed as micrograms of CBD absorbed through the skin and recovered in the acceptor compartment (μg/cm^2); absorbable dose retained inside the skin (S), expressed as μg/cm^2 of the applied dose recovered inside the skin; total absorbed dose (TA), expressed as sum of the two values A and S.

20.11. CBD-ME stability study

Chemical and physical stability of CBD-ME, stored at 25 °C and 4 °C away from the light, was monitored for 3 months. Average sizes and PdI of the dispersed phase droplets were measured by DLS/ELS, whereas CBD concentration, expressed as total R%, and pH were determined by HPLC-DAD and pH-meter, respectively, as described in paragraphs 20.6.1 and 20.6.2. Stability was assessed every week for the first month, every two weeks thereafter.

20.12. CBD-MEgel stability study

In parallel, chemical and physical stability studies on CBD-MEgel were carried out storing the sample at 25 °C, far from the light, for 3 months. The viscosity properties of the sample were evaluated by the rotational viscometer, at both 25 °C and 37 °C, whereas droplet average sizes of the MEgel were monitored by DLS analysis, as described in paragraph 20.5.1. At the meantime, CBD content in the MEgel, expressed as total R%, was measured by HPLC-DAD analysis, as reported in paragraphs 20.6.1, and the pH was checked by the pH-meter. Stability was evaluated once a month for three months.

MICROEMULSION-HYDROGEL COMPOSITE AS A PROMISING VEHICLE FOR DERMAL DELIVERY OF LIPOPHILIC MOLECULES: THE CASE OF KHELLIN

21. Materials

Ammi visnaga dried extract containing 95% khellin, vegetable glycerol Eur Ph., carboxymethyl cellulose and hydroxyethyl cellulose were purchased from Galeno Srl (Prato, Italy). Labrasol ALF was a generous gift from Gattefossé (Saint Priest, France), whereas vitamin E acetate was bought from A.C.E.F. spa (Piacenza, Italy). All the organic solvents, ethanol, acetonitrile and formic acid of analytical grade were from Sigma-Aldrich (Steinheim, Germany). Ultrapure water was produced using a synergy UV Simplicity water purification system provided by Merck KGaA (Molsheim, France). Phosphotungstic acid (PTA) was purchased from Electron Microscopy Sciences (Hatfield, USA).

22. Methods

22.1. HPLC-DAD Analysis

For the chromatographic analysis, an HP1100 liquid chromatograph coupled with an UV-visible detector (DAD) was used (Agilent Technologies, Palo Alto, CA, USA) as previously described *(Risaliti L, 2020)*. The analysis were carried out by an Eclipse XBD-C18 column (150×4.6 mm, 3.5 μm; Agilent Technologies Spa, Rome, Italy), working at 25 °C. Elution was performed at a flow rate of 0.4 mL/min, using (A) acetonitrile and (B) H2O (pH 3.2 by formic acid) as solvents for the mobile phase, with the following multistep linear gradient: 0.1-13 min 50-80% (A), 13-15 min 80-50% (A), 15-18 min 50-50% (A). Chromatograms were recorded at 246 nm. The calibration curve was prepared by solubilizing khellin in ethanol, in order to obtain a concentration of 0.1 mg/ml, and diluting the stock solution 2, 5, 10, 20, 50, 100, 200 times. A linear relationship was obtained, with a coefficient of determination (R^2) of 0.99998.

22.2. Pseudo-ternary phase diagram construction

The pseudo-ternary phase diagram was constructed following the water titration method and plotting all spreadsheet data on a triangular diagram, in order to define the existence area of the ME. The selected surfactant and co-surfactant were mixed at various ratios (Smix), for each of which the pseudo-

ternary phase diagram was built using different weight ratios oil-phase/Smix: 5:95, 10:90, 20:80, 30:70, 40:60, 50:50, 60:40, 70:30, 80:20, 90:10 and 95:5. Each of the mixtures obtained using these different oil-phase/Smix ratios were tested adding water dropwise to the blend, under vigorous stirring at 35 °C. During water addition, the change in sample appearance was monitored to determine if transparent ME, bulk emulsion, gel, turbidity or two separated phases had formed.

22.3. Solubility of khellin into the ME

After the elaboration of a pseudo-ternary phase diagram, the maximum loading content of khellin into the formulation was evaluated adding increasing amounts of the active ingredient khellin to the ME under stirring. The samples were gently stirred for 24 h at room temperature, protected from the light. Afterwards, the excess of khellin was removed by centrifugation at 13,148×g for 10 min and the supernatant was analysed by HPLC after dilution with ethanol. The analyses were performed in triplicate.

22.4. Development of K-ME-GEL formulation

After the preparation of the ME formulation, khellin was added, and maintained at 35±2 °C for 4 h under magnetic stirring at 700 rpm. Exactly weighed quantities of CMC and HEC at increasing concentrations in the range between 1 and 6% *w/v*. The formulations were subjected to manual mechanical stirring until complete dispersion of the viscosifiers. Finally, after the preparation, the pH measurement of the hydrogel was performed using the BASIC 20+ pH-meter (Crison Instrument; Barcelona, Spain). The pH meter was calibrated before each use with buffer solutions of pH 4.0, 7.0, and 9.0. The measurement of pH of formulation was done in triplicate and mean values were calculated.

22.5. K-ME-GEL viscosity measurments

The viscosity (mPas·s) of the K-ME-GEL was measured at 21±2 °C and 35±2 °C, by a digital DVE-RV Brookfield viscometer (Ametek Brookfield; Milan, Italy), using a 06 spindle, selected by the "trial and error" method, because able to produce readings on scale with the greatest possible number of speeds (%Torque between 10 and 100). Measurements were performed with 50 g of sample in a 50 mL beaker, without the spindle guard lag, according to the previous instrument

recalibration *(Vanti G, 2020b)*, and selecting 2 min as spindle rotation time (time required for the viscosity reading to reach a constant value) for each rotational speed, i.e. , 20, 30, 50, 60 and 100 rpm for tests carried out at 21±2 °C and 12, 20, 30, 50, 60 and 100 rpm for tests carried out at 35±2 °C. Every 2 minutes, the rotational speed was increased (up rotational speed) from 5 (from 12 for the tests at 35 °C) to 100 rpm and the hydrogel viscosity measurements were recorded. Then, every 2 minutes, the rotational speed was reduced (down rotational speed) from 100 rpm to 5 rpm (12 for the tests at 35 °C) rpm and the hydrogel viscosity measurements were re-evaluated. The temperature uniformity of the sample and the spindle was guaranteed by the rotation of the spindle inside the sample for 30 minutes, before starting the measurement. The hydrogel was kept at 21±2 °C for one day before the viscosity measurements, in order to remove any trapped air. Each measurement was made in duplicate.

22.6. Characterization of K-ME and K-ME-GEL

Droplet sizes of the developed ME and ME-GEL were measured by DLS, Zetasizer Nano series ZS90 (Malvern Instruments, Worcestershire, UK) equipped with a 4 mW He-Ne laser operating at 632.8 nm and an APD detector. Time correlation functions were analysed to obtain the hydrodynamic diameter of the droplets (Size, nm) and the droplet size distribution (polydispersity index, PdI) using the Zetasizer software version 7.02, provided by Malvern *(Vanti G, 2020a)*. All data were analysed by the Cumulants method, fitting with a single exponential to the correlation function to obtain globule size distribution. Scattering was measured in an optical quality 10x10x45 mm polystyrol/polystyrene cuvettes cell at a 90° angle. K-ME was analysed as such, whereas K-ME-GEL was first diluted in distilled water, applying a 20-fold dilution factor. ζ-potential was measured using the same instrument; for all samples, an average of three measurements at stationary level was taken. The temperature was kept constant at 25 °C by a Peltier temperature controller. ζ-potential was calculated from the electrophoretic mobility, using the Henry correction to Smoluchowski's equation.

Successively, K-ME and K-ME-GEL were observed by Transmission Electron Microscope, TEM (CM12 TEM, PHILIPS, The Netherlands) equipped with an OLYMPUS Megaview G2 camera and with an accelerating voltage of 80 kV. A drop of sample, was applied and dried by desiccation on a carbon film copper

grid and it was counterstained with 1% (*w/v*) of phosphotungstic acid solution for 3 minutes. Then, the sample was examined at different amplifications.

The amount of khellin in both ME and ME-GEL was expressed as total recovery and it was calculated as percentage of the total drug recovered after the preparation in relation to the weighed drug. The microemulsion was diluted in ethanol (FD=100) in order to solubilize khellin. The process was enhanced by 10 min of ultrasonication bath, after that the samples were centrifuged for 10 min at 14,000 rpm and the supernatant was analyzed by HPLC-DAD. The hydrogel (100 mg) was diluted in ultrapure water (2 mL) and stirred for 10 min first, and then it was 5-fold diluted in ethanol to solubilize khellin. Thus, the samples were sonicated, centrifuged and analysed as described for K-ME.

22.7. In vitro release study

The *in vitro* release test was conducted by the dialysis bag method, using Spectra/Por® regenerated cellulose membranes with 3.5 KDa molecular weight cut-off (Repligen Europe B.V.; Breda, The Netherlands), to evaluate the release of khellin through the obtained K-ME-GEL *(Bilia AR, 2019a)*. The dialysis bag was filled with 2 mL of the formulation and it was placed in a beaker containing 200 mL of 5% Tween 20/PBS. Given the lipophilic characteristics of khellin, the mixture of 5% Tween 20 and PBS was used to maintain the sink conditions, since the volume of dissolution media must to be at least 5–10 times greater than the volume at the saturation point of the drug. The system was maintained at a controlled temperature of 35±2°C, under magnetic stirring at 100 rpm. Withdrawals of 0.5 mL volume from the dialysis medium were made in duplicate at 30 minutes, 1, 2, 3, 4, 5, 7 and 24 hours. The volume of the withdrawn dispersing medium was replenished after each collection. The quantity of khellin in the acceptor solution was determined by HPL-DAD analysis. The study was performed in duplicate.

In order to assess the mechanism of the khellin release from the K-ME-GEL the data were fitted on different kinetic models, namely Korsmeyer-Peppas model ($Mt/M\infty = k \cdot tn$, where $Mt/M\infty$ is the fraction of khellin released at the time t, k is the release rate constant and n is the release exponent); Higuchi model ($Qt = kH \cdot t1/2$, where Qt is the amount of khellin released in the time t and kH is the Higuchi dissolution constant), Hixson-Crowell model ($Wo1/3\text{-}Wt1/3 = k \cdot t$, where W0 is the initial amount of khellin in formulations, Wt is the remaining amount of khellin in formulation at time t and k is a constant).

22.8. Stability studies

The stability of developed K-ME-GEL was evaluated after storing the samples 4 weeks at 4 °C away from light *(Vanti G, 2019)*. Once every week, the chemical parameters of the hydrogel were evaluated measuring pH, viscosity properties and recovery of khellin.

FORMULATION OF A PHENOL-RICH EXTRACT FROM UNRIPE OLIVES (*OLEA EUROPAEA* L.) IN MICROEMULSION TO IMPROVE ITS SOLUBILITY AND INTESTINAL PERMEABILITY

23. Materials

Ultrapure water was produced using the Milli-Q-system (Millipore SA, Molsheim, France). Acetonitrile of HPLC and HPLC-MS grades were from Panreac (Barcelona, Spain). Formic acid, hexane and ethanol of analytical reagent grade were from Sigma-Aldrich (Steinheim, Germany). Standards of tyrosol (> 99.5%, Sigma-Aldrich, Steinheim, Germany) and rutin (> 99%), luteolin-7-*O*-glucoside (> 98%), verbascoside (> 99%) and oleuropein (> 98%) from Extrasynthese (Genay, France) were used for quantitative analysis.

Cremophor EL, Tween 80, and Phosphate buffered saline BioPerformance Certified pH 7.4 (PBS), were obtained from Sigma Aldrich (Saint Louis, MO, USA) with the support of Sigma Aldrich Italia (Milan, Italy). Soluplus® was a gift from BASF (Ludwigshafen, Germany) with the support of BASF Italia, BTC Chemical Distribution Unit (Cesano Maderno, Monza e Brianza, Italy). Captex 300, Captex 355, Labrasol ALF, Capryol 90, Transcutol HP, Labrafac, Labrafil 1944, Labrafil 2125, Lauroglycol 90 were from Gattefossé (Saint Priest, France).

24. Methods

24.1. Olive samples and preparation of the phenolic extract

Samples of olive fruits (*Olea europaea* L.) from the Moraiolo cultivar were collected during the 2017 Summer before any stone lignification, particularly on the July 18th. Unripe olives were carry-on harvested from 10 selected plants in a farm located in Fiesole (Florence, Italy), which applied regular irrigation of orchards. About 1 Kg of olives were picked along the whole circumference of the selected plants at a height of about 170 cm. As soon as arrived in the laboratory, olives were deep-frozen in liquid N_2 and immediately freeze-dried. The mean weight of olives was 0.493 grams per olive, while the moisture content, evaluated as the water lost during the lyophilization process, was 57%. After lyophilization, the dried olives were minced in a laboratory miller (Zautec, Germany), thus obtaining about 430 grams of a homogeneous olive powder.

Starting from this powdered material, a phenolic extract was prepared at laboratory scale as follow. Ten aliquots of 2.5 grams of powder were weighted in plastic tubes and cold extracted twice with 40 mL of EtOH:H_2O 80:20 *v/v*, homogenizing the mixture with ULTRA-TURRAX at 8117 x g for 4 minutes. The obtained mixture was cold centrifuged for 10 min at 1167 x g, and the recovered solution was defatted twice with 60 mL of hexane and then evaporated under vacuum. The dried extract was recovered with three aliquots of 16 mL, 8 mL and 4 mL of water and with the aid of ultrasounds. The obtained solution was then freeze-dried, thus obtaining a dried phenolic extract. The yield of the extract was 40% on the initial powder base, thus we obtained a total of approx. 10 grams of the extract.

The extract was characterized by HPLC-DAD: 50 mg of dried extract were dissolved in 1 mL of MeOH:H_2O 50:50 *v/v*, and the obtained solution was used for the chromatographic analysis.

24.2. HPLC-DAD analysis

For the chromatographic analysis, an HP1100 liquid chromatograph coupled with DAD detector was used (Agilent Technologies, Palo Alto, CA, USA) as previously described *(Cecchi L, 2018b)*. A Poroshell 120, EC-C18 (150 mm × 3.0 mm id, 2.7 μm; Agilent Technologies, Palo Alto, CA, USA) column coupled with a pre-column of the same phase, working at 26°C, was used for separation of phenolic compounds. Elution was performed at a flow rate of 0.4 ml/min, using (A) acetonitrile and (B) H_2O (pH 3.2 by formic acid) as solvents for the mobile phase, with the following multistep linear gradient: solvent A was increased from 5% to 40% in 40 min, then remained at 40% for 5 min, increased to 100% in 5 min, and stayed at 100% for 3 min, then returned to 5% in 2 min. Total elution time of 55 min, equilibration time 10 min, injection volume, 2 μL. Chromatograms were recorded at 240, 280 and 330 nm.

Quantification of phenolic compounds was carried out using 5 six-points calibration lines, built using hydroalcoholic solutions of tyrosol (linearity range 0-1.21 μg, R^2=0.9999), oleuropein (linearity range 0-3.16 μg, R^2=0.9986), luteolin-7-*O*-glucoside (linearity range 0-1.57 μg, R^2=0.9956), rutin (linearity range 0-1.25 μg, R^2=0.9975) and verbascoside (linearity range 0-1.96 μg, R^2=0.9996). Limit of quantifications (LOQ) were evaluated according to a previous study *(Cecchi L, 2019)*, using the above standards, and all the obtained values were lower than 0.1 mg/kg. Tyrosol and hydroxytyrosol were expressed as mg_{tyr} kg^{-1}, rutin as mg_{rut} kg^{-}

[1], luteolin-7-*O*-glucoside as mg_{lut} kg^{-1}, verbascoside as mg_{ver} kg^{-1}, and oleuropein, comselogoside and ligstroside as mg_{ole} kg^{-1}. Finally, the total phenolic content was calculated as sum of the content of the previous phenolic compounds.

24.3. Solubility study

The solubility of the powdered OE in different vehicles was evaluated by adding an excess of OE to 5 mL of each of the tested solvent/tenside: Water, Capryol 90, Captex 300, Captex 355, Labrafac, Labrafilm 1944, Labrafilm 2125, Labrasol ALF, Lauroglycol 90, Transcutol and Cremophor EL. Each mixture of solvent and OE was stirred for 24 h at 25°C, then it was centrifuged at 13148 x g for 10 minutes. After removing the precipitate, the supernatant was diluted with EtOH and analyzed by HPLC-DAD to determine the concentration of the phenolic compounds from the OE. The analyses were performed in triplicate.

24.4. Pseudo-ternary phase diagram construction

The Chemix School (version 3.60, Arne Standnes, Norway) was used for constructing the pseudo-ternary phase diagram following the water titration method, in order to define the area of existence of the ME *(Lawrence, MJ, 2000).* The selected surfactant and co-surfactant were mixed at various ratios (S_{mix}), for each of which the pseudo-ternary phase diagram was built using different weight ratios oil-phase/S_{mix}: 0:100, 5:95, 10:90, 20:80, 30:70, 40:60, 50:50, 60:40, 70:30, 80:20, 90:10. Each of the mixtures obtained using these different oil-phase/S_{mix} ratios was tested adding water dropwise to each blend, under vigorous stirring at room temperature; during water addition, the change in samples appearance was monitored to determinate if transparent ME, emulsion or gel was present.

24.5. Solubility of the olive extract into the microemulsion

After the elaboration of pseudo-ternary phase diagram, the maximum loading content of olive extract into the formulation was evaluated adding increasing amount of extract powder to the ME under stirring. The sample was gently stirred for 24 h at room temperature, protected from the light. Afterwards, excess extract was removed by centrifugation at 13148 x g for 10 min and the supernatant was analysed by HPLC after dilution with ethanol. The analyses were performed in triplicate.

24.6. Characterization of microemulsion

24.6.1. Particle size and ζ-potential measurements

Droplet sizes of the developed ME were measured by a Dynamic Light Scattering (DLS), Zsizer Nano series ZS90 (Malvern Instruments, Malvern, UK) equipped with a JDS Uniphase 22 mW He-Ne laser operating at 632.8 nm, an optical fiber-based detector, a digital LV/LSE-5003 correlator and a temperature controller (Julabo water-bath) set at 25°C. Time correlation functions were analysed to obtain the hydrodynamic diameter of the particles (Size) and the particle size distribution (polydispersity index, PdI) using the ALV-60X0 software V.3.X provided by Malvern. Autocorrelation functions were analysed by the Cumulants method, fitting a single exponential to the correlation function to obtain particle size distribution. Scattering was measured in an optical quality 4 ml borosilicate cell at a 90° angle, diluting the samples in distilled water. ζ-potential was measured using the same instrument; for all samples, an average of three measurements at stationary level was taken. The temperature was kept constant at 25°C by a Haake temperature controller. ζ-potential was calculated from the electrophoretic mobility, using the Henry correction to Smoluchowski's equation.

24.6.2. In vitro release study

The release studies of OE from ME in comparison to OE hydroalcoholic solution (EtOH:H_2O 70:30) were carried out with the dialysis bag method (regenerated cellulose dialysis membranes, Spectrum Laboratories, Inc., Breda, The Netherlands, MWCO 12-14 kD). Two mL of the ME or the solution were placed into dialysis membranes, sealed and then immersed into 200 mL of the release medium at 37°C under magnetic stirring. Simulated gastric fluid (SGF, pH 1.2), simulated intestinal fluid (SIF pH 6.8), and PBS were used as release media. The composition of the gastric fluid was 2 g of NaCl and 7 mL of HCl per liter of deionized water. The intestinal fluid was composed of 6.805 g of KH_2PO_4 and 0.896 g of NaOH per liter of deionized water *(United States Pharmacopeial Convention Inc., 2002).*

At predetermined time intervals, 1 mL of each release medium was withdrawn and replaced with equal volume of fresh solution. The total phenolic concentration in samples was finally determined by HPLC. All studies were performed in triplicate.

24.7. Chemical and physical stability during storage

To estimate the shelf life, the OE-ME was stored in sealed glass containers at 4°C for one month. Chemical and physical stabilities were checked periodically by monitoring transparency, phase separation, colour variation as the changes in particle size, homogeneity, ζ-potential and extract concentration by DLS and HPLC/DAD analyses.

24.8. In vitro Parallel Artificial Membrane Permeability Assay (PAMPA)

The test was carried out in a 96-well, MultiScreen-IP PAMPA (Millipore corporation) filter plate. The ability of compounds to diffuse from a donor compartment into an acceptor compartment was evaluated, by placing a polyvinylidene difluoride (PVDF) membrane filter pretreated with a lipid-containing organic solvent between the two compartments. DMSO/PBS (0.05 mL/mL, pH 7.4) mixture was used as receptor buffer. The artificial membrane added to each filter consisted in a combination of lecithin and cholesterol 10 g/L and 8 g/L, respectively, in 1,7-octadiene. Immediately after the deposition of the lipid solution (5 µL), 250 µL of extract solution and OE-ME were added to each well of the donor plate. Each receptor plate was filled with 250 µL of EtOH/PBS buffer. Afterwards, the donor plate was placed into the receptor plate, ensuring that the underside of the membrane was in contact with the buffer. The plate assembly was covered and incubated at room temperature for 2 h.

Then, the samples were withdrawn, diluted with ethanol, centrifuged for 10 min at 13148 x g and the OE concentration was determined by HPLC. The P_e (cm/s) was calculated according to the following equation:

$$P_e = \frac{-\ln\left[1 - \frac{C_{At}}{C_{eq}}\right]}{A\left(\frac{1}{V_D} + \frac{1}{V_A}\right)t} \quad (11)$$

where A is the active surface area (0.3 cm^2 × apparent porosity of the filter), V_D and V_A the well volume of the donor and acceptor plate (mL), respectively, t the incubation time (s), C_{At} and C_{Dt} the concentration of APP in the acceptor and donor plate at time t, respectively. C_{eq} was calculated according to the equation:

$$C_{eq} = \frac{[C_{Dt} \times V_D + C_{At} \times V_A]}{V_A + V_D} \quad (12)$$

The experiments were performed in quadruplicate.

24.9. MTS assay for cell viability

Viability analyses were performed using Cell Titer 96 Aqueous One solution cell proliferation (3-(4,5-dimethylthiazol-2-yl)-5-(3-carboxymethoxyphenyl)-2-(4-sulfophenyl)-2H- tetrazolium) (MTS) assay kit (Promega Madison, WI, USA). Briefly, Caco-2 cells were transferred to flat bottom 96-well tissue culture plates (Corning, USA) at a seeding density of 5×10^3 cells/well and allowed growing for 24 h under the conditions detailed above. For MTS assay, the culture medium was removed and replaced with fresh medium containing OE-ME and the cells were incubated for 2 and 24 h. Then the cells were exposed to MTS solution and allowed incubating for 2 and 24 h at 37°C. The product of the reaction was measured at 490 nm using a spectrophotometer (Multilabel Counter 1240 Victor 3, Perkin Elmer). The cell death was expressed as a percentage of values obtained from control, untreated cells, calculated from three replicates of each ME dilution.

24.10. Cell culture for transport studies

For transport studies, cells were seeded at 50000 cells/well in cell, culture inserts with polyethylene terephthalate (PET) membranes (BRAND, Italy). Culture medium (DMEM) was added to apical (AP) and basolateral (BL) side and was replaced every day for the first week and daily, thereafter. Cells were let to differentiate for 18-21 days.

24.10.1. Monolayer integrity

The integrity of the layer was evaluated with the Lucifer Yellow (LY) permeability assay. LY was diluted in the transport buffer (Hank's Balanced Salt Solution, HBSS, with Ca^{2+}, Mg^{2+}, 25m M HEPES, pH 7.4) and added to the AP compartment at a final concentration of 100 μM. After incubation at 37°C for 1h, the HBSS in the BL chamber was collected, and the concentration of LY determined by using 485nm excitation and 530 nm emission, on a fluorescence plate reader (Multilabel Counter 1240 Victor 3, Perkin Elmer). The percentage of AP to BL permeability was calculated, according to the following equation:

$$\%\text{Permeability} = \frac{(\text{Fluorescence in the BL} - \text{blank})}{(\text{Fluorescence LY} - \text{blank})} \times 100 \qquad (13)$$

The critical maximum flux of LY to identify leaky monolayers was fixed to be less than 3% of starting concentration.

24.10.2. Transport experiments

Transport studies were performed according to Hubatsch et al., (2007), *(Hubatsch I, 2007; Piazzini V, 2018)*. Briefly, the culture medium (DMEM) was replaced with preheated (37°C) transport HBSS medium supplemented with 25 mM HEPES (pH 7.4). After that, the cell monolayer was equilibrated for 30 min at 37°C; Caco-2 cells were then exposed for 2 h with OE-ME 1:100 or OE not formulated, in the apical (AP) chamber, while the basolateral (BL) chamber contained only HBSS.

At predetermined time intervals, 0.3 mL of medium in the BL side was taken for HPLC analyses and replaced with the same volume of fresh HBSS. At the end of the experiment, the integrity of the layer was re-evaluated with the LY permeability assay as described above.

The apparent permeability coefficient (P_{app}, cm/s) was calculated according to the following equation:

$$P_{app} = V_D / (A \times M_D) \times (\Delta M_R / \Delta t) \quad (14)$$

where: V_D = apical (donor) volume (mL), M_D = apical (donor) amount, $\Delta M_R/\Delta t$ = change in amount of compound in receiver compartment over time.

24.11. Statistical analysis

The experiments were performed at least in triplicate. The results of the quantitative analysis of OE, the physicochemical characterization of ME and the *in vitro* tests were expressed as means ± SD and analyzed by Mann Whitney test. All analyses were carried out using GraphPad Prism 7.0 (GraphPad Software, San Diego, CA, USA). *p* value of 0.05 was considered significant.

RESULTS AND DISCUSSION

DEVELOPMENT AND PERCUTANEOUS PERMEATION STUDY OF ESCINOSOMES, ESCIN-BASED NANOVESICLES LOADED WITH BERBERINE CHLORIDE

25. Results

25.1. Development and optimisation of nanovesicles

Three different nanovesicles were developed using the thin layer evaporation method. Firstly, CL were formulated using P90G and CHOL using, respectively, 33 and 10 mg/mL of formulation. Subsequently, ESN (5 mg/mL) was added to form conventional liposomes loaded with ESN (ECL). Finally, a third type of vesicle was formulated using only ESN and P90G (escinosomes, EL). Optimisation of formulations in terms of vesicle size and sample homogeneity was obtained by the Ultrasonic Homogenizer HD 2200, using the different conditions displayed in Table 10. CL, ECL, and EL showed the best PdI in the following conditions: 150 s of sonication, 10 min of sonication for 5 cycles and 60 s of sonication for 5 cycles, respectively. Thereby, these formulations were selected and loaded with BRB. The formulations with BRB were similarly optimized by the Ultrasonic Homogenizer HD 2200 using different sonication times, as reported in Table 11. B-CL, B-ECL, and B-EL formulations showed the lowest PdI after 10 min of sonication for 5 cycles and they were selected for the following studies.

Table 10. Optimization of CL (conventional liposome), ECL (conventional liposome loaded with ESN) and EL (escinosome) in terms of AHD and PdI, by sonication. Data are shown as mean ± SD (n = 3).

Formulation	Composition (ratio *w*/*w*)	Sonication time (s) / Sonication cycles	AHD (nm)	PdI
CL	P90G-CHOL (33:10)	150 s	106.2 ± 8.1	0.24 ± 0.01
ECL	ESN-P90G-CHOL (5:33:10)	60 s	180.7 ± 3.2	0.40 ± 0.01
ECL	ESN-P90G-CHOL (5:33:10)	150 s	152.6 ± 9.1	0.39 ± 0.03
ECL	ESN-P90G-CHOL (5:33:10)	300 s / 5 cycles	142.9 ± 3.1	0.38 ± 0.02
ECL	ESN-P90G-CHOL (5:33:10)	300 s	132.4 ± 0.5	0.36 ± 0.01
ECL	ESN-P90G-CHOL (5:33:10)	600 s / 5 cycles	127.3 ± 6.2	0.38 ± 0.03
EL	ESN-P90G (5:33)	30 s	139.1 ± 1.2	0.27 ± 0.01
EL	ESN-P90G (5:33)	60 s / 5 cycles	137.4 ± 6.9	0.26 ± 0.01
EL	ESN-P90G (5:33)	60 s	103.2 ± 2.3	0.34 ± 0.04
EL	ESN-P90G (5:33)	150 s	104.1 ± 11.5	0.41 ± 0.03
EL	ESN-P90G (5:33)	180 s	107.9 ± 2.9	0.43 ± 0.01
EL	ESN-P90G (5:33)	300 s	117.9 ± 12.1	0.40 ± 0.02
EL	ESN-P90G (5:33)	600 s / 5 cycles	70.0 ± 1.4	0.40 ± 0.01

Table 11. Optimization of B-CL (conventional liposome loaded with BRB), B-ECL (conventional liposome loaded with ESN and BRB) and B-EL (BRB loaded escinosome) in terms of AHD (Average Hydrodynamic diameter) and PdI (Polydispersity Index), by sonication. Data are shown as Mean ± SD (n = 3).

Formulation	Composition (ratio *w*/*w*)	Sonication time (s) / Sonication cycles	AHD (nm)	PdI
B-CL	BRB+P90G-CHOL (1.3:33:10)	150 s	164.0 ± 25.7	0.28 ± 0.04
B-CL	BRB+P90G-CHOL (1.3:33:10)	300 s / 5cycles	124.4 ± 7.6	0.31 ± 0.06
B-CL	BRB+P90G-CHOL (1.3:33:10)	600 s / 5 cycles	106.5 ± 18.1	0.26 ± 0.02
B-ECL	BRB+ESN-P90G-CHOL (1.3:5:33:10)	150 s	178.5 ± 9.6	0.25 ± 0.02
B-ECL	BRB+ESN-P90G-CHOL (1.3:5:33:10)	180 s	187.8 ± 1.9	0.23 ± 0.03
B-ECL	BRB+ESN-P90G-CHOL (1.3:5:33:10)	300 s / 5 cycles	178.0 ± 6.3	0.23 ± 0.00
B-ECL	BRB+ESN-P90G-CHOL (1.3:5:33:10)	300 s	191.7 ± 1.6	0.22 ± 0.02
B-ECL	BRB+ESN-P90G-CHOL (1.3:5:33:10)	600 s / 5 cycles	166.1 ± 23.2	0.20 ± 0.02
B-EL	BRB+ESN-P90G (1.3:5:33)	150 s	238.9 ± 79.7	0.26 ± 0.05
B-EL	BRB+ESN-P90G (1.3:5:33)	180 s	195.9 ± 2.8	0.22 ± 0.02
B-EL	BRB+ESN-P90G (1.3:5:33)	300s / 5 cycles	227.0 ± 76.7	0.23 ± 0.05
B-EL	BRB+ESN-P90G (1.3:5:33)	300 s	275.6 ± 20.9	0.26 ± 0.04
B-EL	BRB+ESN-P90G (1.3:5:33)	600s / 5 cycles	150.1 ± 5.2	0.17 ± 0.02

25.2. Physical characterization of nanovesicles

Physical data of the developed nanovesicles are reported in Table 12. All the formulations analysed by DLS/ELS had sizes ranging from 100 to 140 nm, being CLs the smallest ones. All the nanovesicles had negative ζ-potential values with the highest found for EL. Both CL and EL formulations had low PdI and good

deformability, since the ratio of vesicle diameter before and after extrusion was close to the unit (Table 12). ECL did not display deformability. Then, the three different formulations loaded with BRB were also characterized in terms of average diameter, PdI, ζ-potential, and deformability (Table 12). The best homogeneity and deformability parameters were found for EL loaded with BRB (B-EL) and conventional liposomes loaded with BRB (B-CL). The high flexibility of the membrane allow vesicles to pass through skin pores, even smaller than the vesicle diameter, and control the transport of ESN and BRB through the different skin layers. A slight increase in size was observed for B-EL when compared with the unloaded vesicles (Table 12), but this was not expected to affect skin permeability.

Table 12. Physical characterization of all liposomes. Data are shown as Mean±SD (*n*=3).

Formulation	Composition (ratio *w*/*w*)	AHD (nm)	PdI	ζ-potential (mV)	Deformability
CL	P90G-CHOL (33:10)	106.2 ± 8.1	0.24 ± 0.01	-26.9 ± 1.3	1.05 ± 0.04
ECL	ESN-P90G-CHOL (5:33:10)	127.3 ± 6.2	0.38 ± 0.03	-31.4 ± 2.5	*
EL	ESN-P90G (5:33)	137.4 ± 6.9	0.26 ± 0.01	-40.5 ± 3.1	0.89 ± 0.01
B-CL	BRB + P90G-CHOL (1.3:33:10)	106.5 ± 18.1	0.26 ± 0.02	-29.5 ± 0.2	1.02 ± 0.01
B-ECL	BRB + ESN-P90G-CHOL (1.3:5:33:10)	166.1 ± 23.2	0.22 ± 0.02	-30.1 ± 0.4	*
B-EL	BRB + ESN-P90G (1.3:5:33)	150.1 ± 5.2	0.17 ± 0.02	-34.8 ± 5.1	1.09 ± 0.01

AHD = Average Hydrodynamic Diameter; PdI = Polydispersity Index; * = not deformable. CL = conventional liposome; ECL = conventional liposome loaded with ESN; EL = escinosome; B-CL = conventional liposome loaded with BRB; B-ECL = conventional liposome loaded with ESN and BRB; B-EL = BRB loaded escinosome.

TEM analysis with the negative staining technique was performed to evaluate the morphology and architecture of the nanovesicles, in particular escinosomes (EL, composed only by P90G and ESN, Figure 8). By this procedure, the whole liposomes appeared clearly outlined on an electron-dense background. The vesicles had spherical shape, a membrane-like envelope and often showed an inner lamellar structure (Figure 8). Similarly, after loading escinosomes with BRB, the B-EL formulation (Figure 9b) still maintained the spherical shape and the lamellar structure of empty escinosomes (Figure 9a).

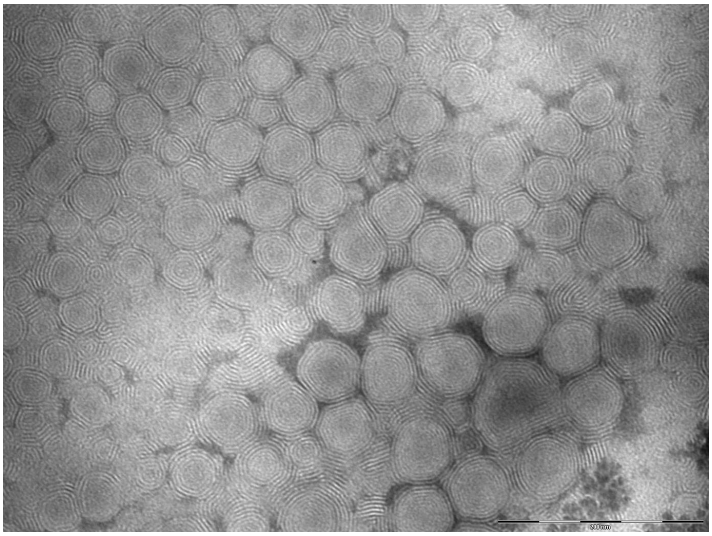

Figure 8. TEM image of empty escinosomes (EL).

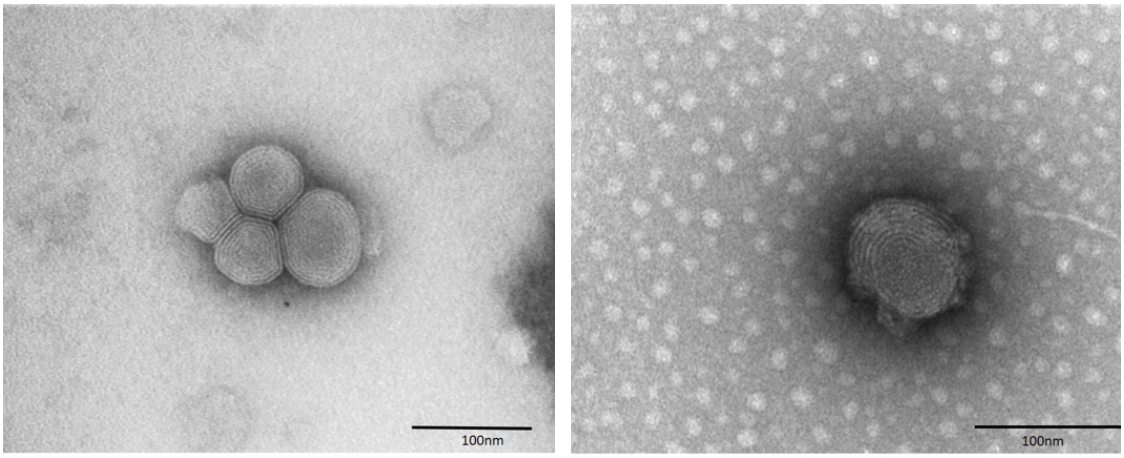

Figure 9. Morphological comparison by TEM between **(a)** empty escinosomes (EL) and **(b)** BRB loaded escinosome (B-EL).

25.3. Technological characterization of nanovesicles

In Table 13 the chemical characterization of all liposomes is reported and expressed as drug concentration, recovery and encapsulation efficiency. When 0.5% ESN was added to the vesicles both R% and EE% were more than 95% for both ECL and escinosome (EL) formulations (Table 13). Interestingly, the loading of 0.13% BRB to obtain B-CL, BRB loaded escinosome (B-EL) and B-ECL resulted in a similar R%, but the resulting EE% were quite different (Table 13). EE% of B-CL and B-ECL were quite similar (*ca.* 44 and 47% respectively), while EE% of BRB

in B-EL was more than 66.7%. The pH was about 5 in all the developed liposome dispersions.

Table 13. Chemical characterization of all liposomes. R% = Recovery; EE% = Encapsulation Efficiency. CL = conventional liposome; ECL = conventional liposome loaded with ESN; EL = escinosome; B-CL = conventional liposome loaded with BRB; B-ECL = conventional liposome loaded with ESN and BRB; B-EL = BRB loaded escinosome. Data are shown as mean ± sd (n=3).

Formulation	**ESN**			**BRB**		
	ESN %*w/v*	**R%**	**EE%**	**BRB %*w/v***	**R%**	**EE%**
CL	/	/	/	/	/	/
E-CL	0.5%	98.04 ± 0.12	97.14 ± 0.72	/	/	/
EL	0.5%	97.34 ± 3.40	95.46 ± 0.93	/	/	/
B-CL	/	/	/	0.13%	95.76 ± 2.58	44.10 ± 0.71
B-ECL	0.5%	98.02 ± 0.23	94.80 ± 0.11	0.13%	96.21 ± 0.32	47.60 ± 0.56
B-EL	0.5%	96.50 ± 3.90	93.16 ± 9.68	0.13%	97.06 ± 7.10	66.70 ± 5.33

25.4. Stability studies of the developed nanocarriers

Escinosomes (EL) and BRB loaded escinosomes (B-EL), selected as the two formulations with the most promising chemical and physical characteristics, were tested for stability. Both formulations were kept protected from light at 4°C and their physical and chemical parameters were monitored every 10 days. EE%, average size, PdI and ζ-potential were rather stable during the test. Overall, both samples remained stable for up to 1 month under proper storage conditions (Figures 10-11). EL physical stability in terms of size, PdI and ζ-potential is reported in Figure 10a. After 30 days of storage, the ζ-potential value ranged from -40 mV to *ca.* -35 mV. PdI was very stable during the storage period, while sizes of vesicles increased slightly. EL chemical stability in terms of R% and EE% of ESN was displayed in Figure 10b.

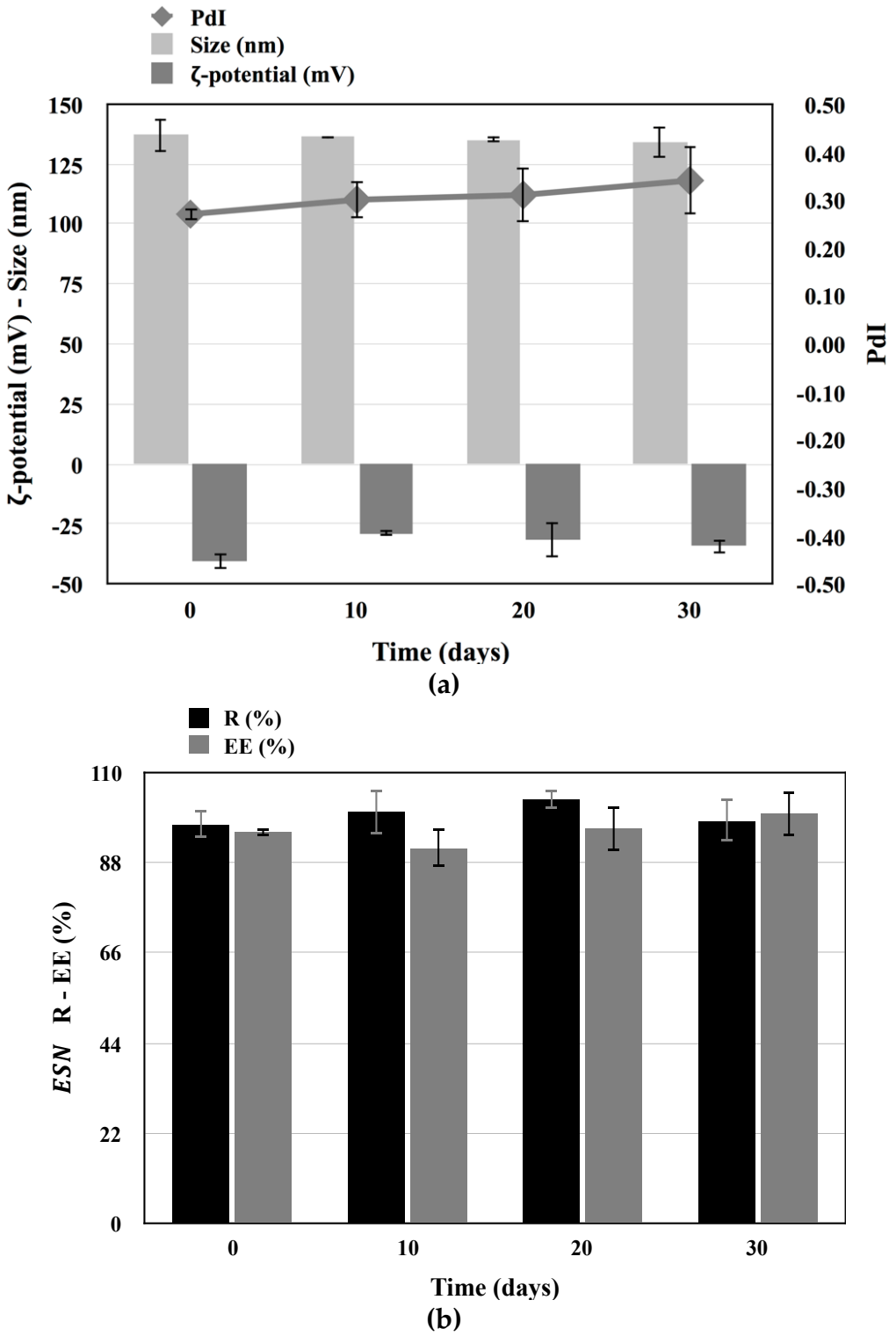

Figure 10. Graphs of the physical and chemical stability studies of EL (escinosome): (**a**) size, ζ-potential and PdI (Polydispersity Index); (**b**) R% (Recovery) and EE% (Encapsulation Efficiency) of ESN. Data are shown as mean ± sd (n=3).

B-EL physical stability in terms of size, PdI and ζ-potential is reported in Figure 11a, which shows that all values remained constant during the storage period. Figure 11b and 11c reported the B-EL chemical stability in terms of R% and EE% of loaded BRB and B-EL chemical stability in terms of R% and EE% of loaded ESN respectively. A slight decrease in both R% and EE% of BRB was found after 30 days storage, while ESN remained highly loaded in the vesicles.

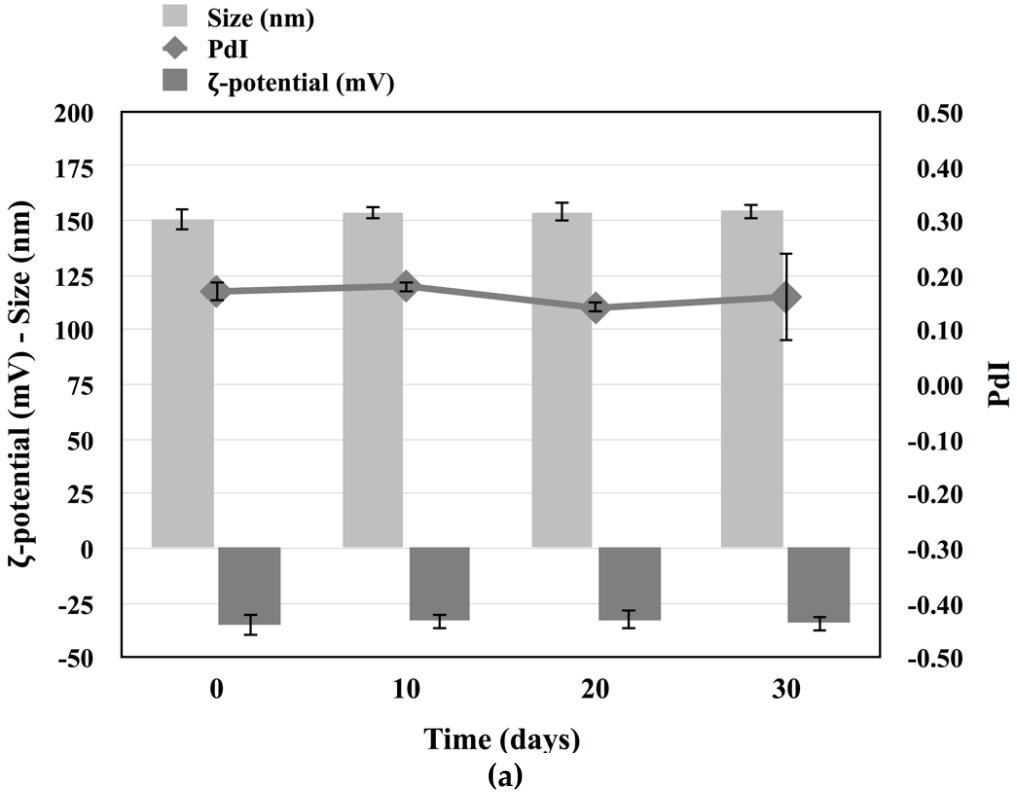

(a)

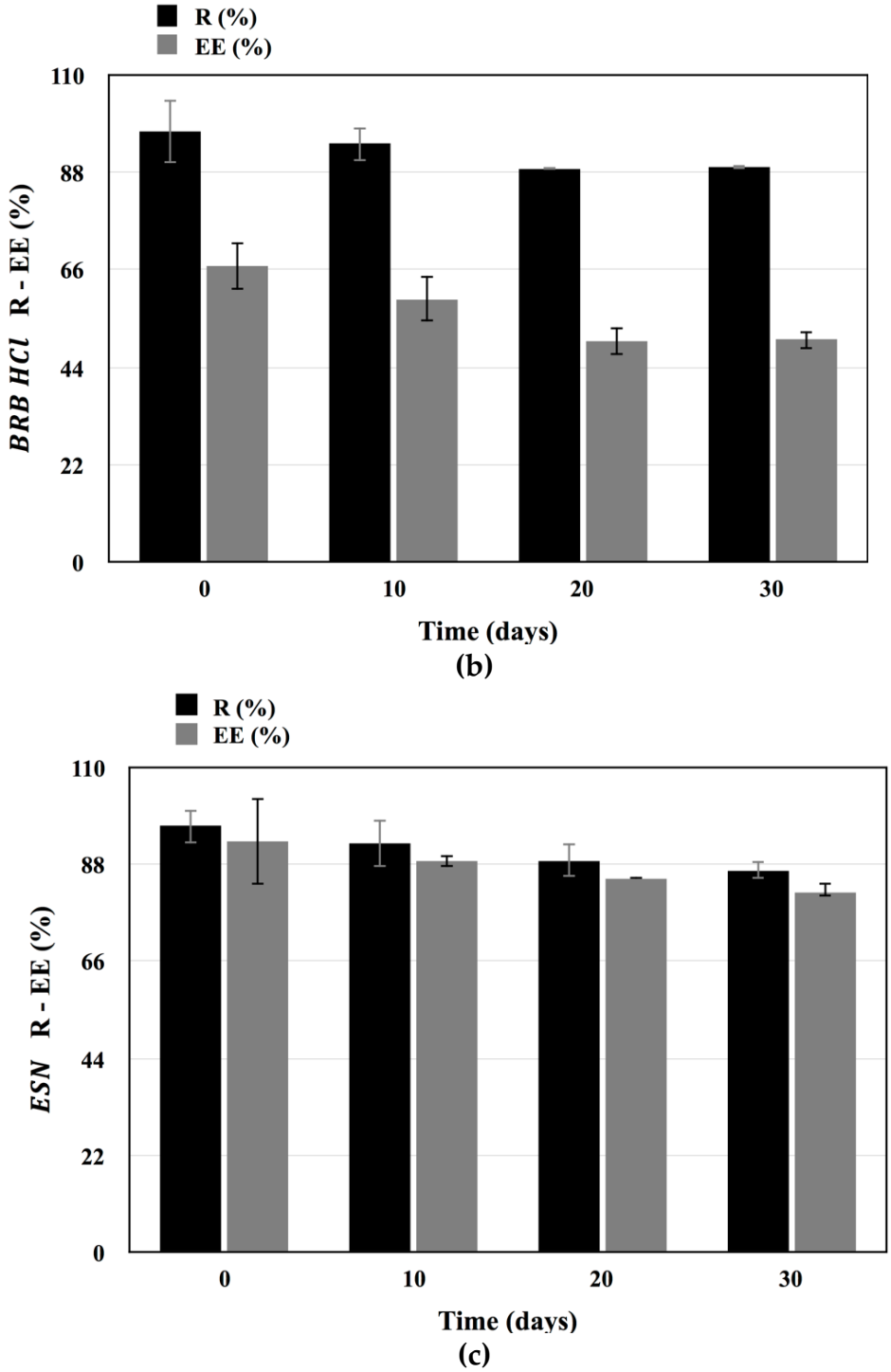

Figure 11. Graphs of the physical and chemical stability studies of B-EL (BRB loaded Escinosome): (**a**) size, ζ-potential and PdI (Polydispersity Index); (**b**) R% (Recovery) and EE% (Encapsulation Efficiency) of BRB; (**c**) R% (Recovery) and EE% (Encapsulation Efficiency) of ESN. Data are shown as mean ± sd (n=3).

25.5. Release studies of ESN and BRB from vesicles

Many methods are reported in the literature to evaluate the release kinetics of vesicles, useful to predict the *in vivo* performance. No standard methods and guidelines are established so far. In this study, BRB and ESN release from the different vesicles was investigated by adopting the dialysis bag method, under constant temperature (37°C) and sink conditions. The release of both BRB and ESN were investigated using the HPLC method reported in the experimental part. B-EL showed the most interesting kinetics (Figure 12). In the first 30 min, only 40% of BRB was released, followed by a prolonged release in the following hours attaining 75% after 24 h. This release kinetic suggests that this formulation could provide a persistent delivery of BRB over time if administered *in vivo*. B-CL showed a similar release rate, but attaining about 100% of BRB released after 24 h, while B-ECL showed the fastest release kinetic, very close to B-SOL one, with almost 95% of BRB released after 2 h. By contrast, ESN was only detectable after 24 h because of its low UV-visible absorption and low detectability by HPLC-DAD, but also because of its very slow release. In fact, despite a faster release from the aqueous dispersion ESNW (22.18 ± 3.66%), ESN reached not more than 18% after 24 h in all formulations. This behaviour can be explained by the fact that ESN was strongly retained in the vesicles possibly conferring them a high physical stability. ESN could therefore really represent a vesicle bilayer forming material.

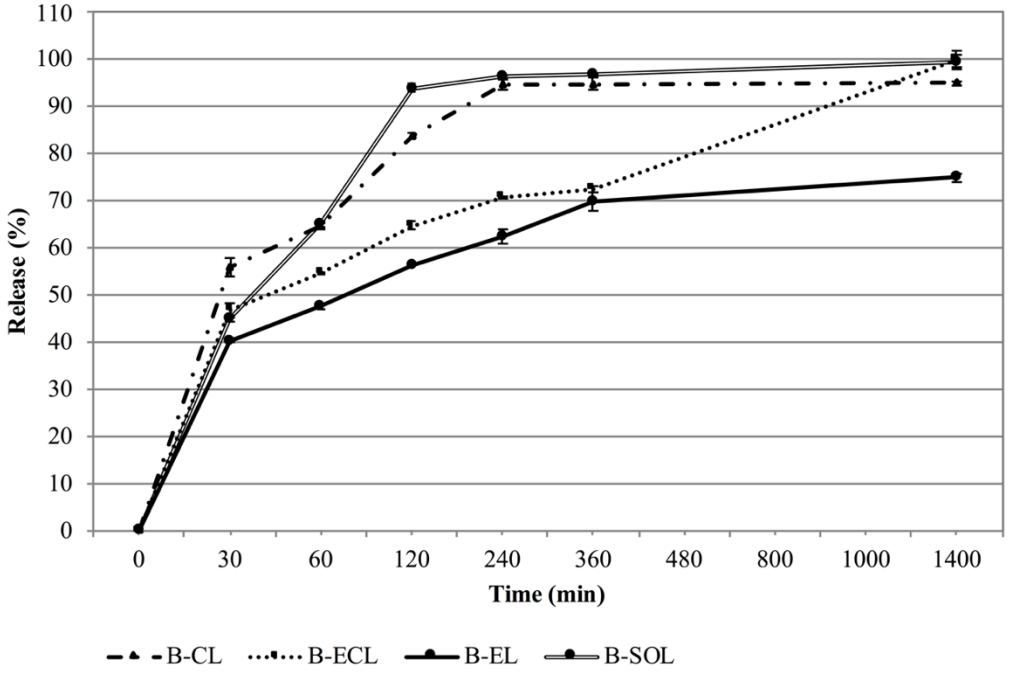

Figure 12. BRB release (%) from B-CL (conventional liposome loaded with BRB), B-ECL (conventional liposome loaded with ESN and BRB), B-EL (BRB loaded escinosome) and B-SOL (BRB aqueous solution). Data are shown as mean ± sd (n=3).

25.6. Hyaluronidase inhibition assay

In the present study, ESN anti-inflammatory, venotonic and anti-oedematous potential activities, once it is formulated in B-EL, were evaluated by the hyaluronidase inhibition assay *(Facino RM, 1995; Girish KS, 2009)*. In fact, different pathological processes related to inflammation, venous insufficiency and oedema present hyaluronidase deficiency. The hyaluronidase inhibition activity of ESN formulated in B-EL (BRB loaded escinosome) was investigated and compared to that of free ESN, as well as the inhibition activity of free BRB and CL (used as control) was evaluated. The assay was carried out using a colorimetric method reported by Murata and coworkers *(Murata T, 2012)*. CL samples did not exhibit any inhibitory effects on hyaluronidase, as estimated, while ESN was found to show inhibitory effects on the enzyme, as previously reported by Facino at al. (*Facino RM, 1995)*. To be specific, IC_{50} of free ESN resulted 197±19 μM, while IC_{50} of ESN loaded in B-EL was 210±18 μM. By contrast, free BRB did not exhibit any inhibitory activity at the concentration used for B-EL. Accordingly, ESN inhibitory effect on hyaluronidase was unaffected by the formulation and the presence of BRB.

25.7. Skin-PAMPA™ in vitro permeation

In order to predict BRB and ESN absorption across the outermost layer of the skin, a simple and fast strategy was applied using the Skin-PAMPA™, a high reproducible fast test to predict trans-cutaneous penetration of compounds. This is a preliminary permeation test where the chemical composition of the synthetic membranes simulates the *stratum corneum*. Piroxicam and progesterone were used as reference with low and high P_e, respectively. BRB loaded in B-ECL showed a better permeability across the artificial membranes, since the P_e was higher when compared with the other formulations (Table 14). The highest P_e of BRB found for B-ECL formulation could be explained by the higher lipophilicity of the vesicle due to the simultaneous presence of ESN and CHOL. Meanwhile, the very similar P_e of BRB for B-CL and BRB loaded escinosome (B-EL) formulations could further support the hypothesis that ESN, in addition to being a vesicle bilayer forming material, could even have a role in allowing the *stratum*

corneum penetration of vesicles, measured in terms of BRB permeated and recovered in the acceptor compartment of the skin-PAMPA™. By contrast, ESN was not detectable in the acceptor compartment, probably because the vesicle structure remained stable during the short tested period (5 h) and ESN could not cross this artificial membrane.

Table 14. Effective Permeability (P_e) of BRB loaded in B-CL (conventional liposome loaded with BRB), B-ECL (conventional liposome loaded with ESN and BRB), B-EL (BRB loaded escinosome) and B-SOL (BRB aqueous solution) and of the standard references (piroxicam and progesterone). Results are shown as mean ± sd (n=3).

Formulation	P_e (10^{-6} cm/s)
B-CL	2.06 ± 0.01
B-ECL	4.30 ± 1.87
B-EL	2.16 ±0.02
B-SOL	1.12 ± 0.03
Piroxicam	0.24 ± 0.10
Progesterone	1.19 ± 0.35

25.8. Histological evaluation of rabbit ear skin and human abdominal skin

The rabbit ear skin was reported to possess a similar thickness of the *stratum corneum* compared with pig ear skin, although the underneath epidermal layers have a slightly different structure; for this reason, it has been proposed as a reliable model for *in vitro* transdermal tests *(Nicoli S, 2007)*. In the present study, the rabbit ear skin tissue was histologically evaluated as a substitute for human abdominal skin. Figure 13 shows representative histological sections of rabbit ear skin (Figure 13a) and human abdominal skin (Figure 13b). In both pictures, the various layers of the epidermis and the dermis can be easily identified. To note that, in some areas, the *stratum corneum* appears detached from the underlying layers, probably due to freezing and sectioning artifacts. The histological structure was very similar in both tissues, with the exception of sweat glands, which were lacking in the rabbit skin. The results suggested that the rabbit ear skin is a suitable model to study both lipophilic and hydrophilic permeants.

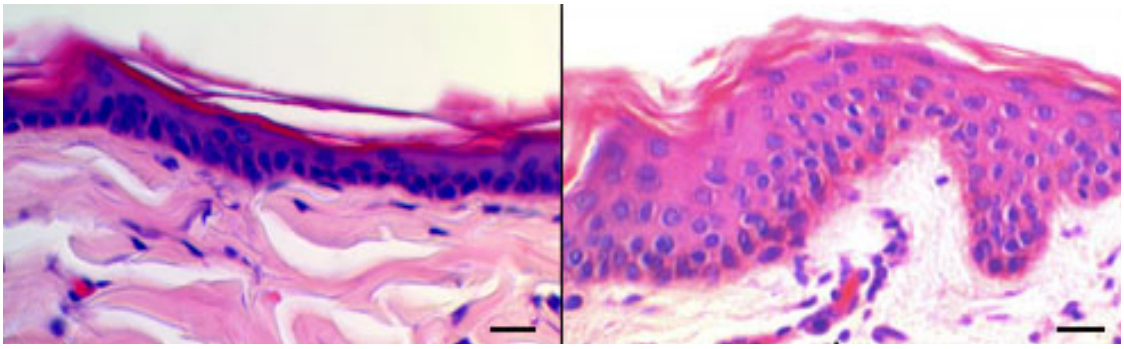

Figure 13. Light microscopic images of (**a**) rabbit ear skin and (**b**) human abdominal skin. In both specimens, the epidermal epithelia show a thin *stratum corneum*. Bars = 50 μm.

25.9. Percutaneous penetration studies and subsequent histological analysis using rabbit ear skin

The diffusion process through the skin primarily depends on the *stratum corneum*, the main and rate-limiting skin barrier. Since this is not a viable layer, its functionality is similar *in vivo* and *in vitro (Lehman PA, 2011)*, thereby the *in vitro* skin permeation model has been largely used over years to predict the human percutaneous absorption, even if it has not yet been validated. In the present study, the rabbit ear skin was used to evaluate the *in vivo* permeation of the developed nanovesicles. The experiment was performed using the vertical diffusion Franz cells in order to compare the permeation ability of the three different vesicles loaded with BRB inside the skin layers and across the skin, as well as to predict BRB absorption. The permeation study was carried out using the finite dose technique, namely applying doses normally used in clinical conditions. In fact, human exposure to chemicals by topical application of drug is usually of few milligrams of drug per square centimeter of skin, 2-5 mg/cm^2 *(Lehman PA, 2011)*. As a first step of our investigation, a conventional histological analysis of the rabbit ear skin samples taken after the permeation studies were carried out (Figure 14). The investigation allowed to exclude the occurrence of major morphological alterations due to the sampling and handling procedures, thus accounting for reliability of the permeation assay.

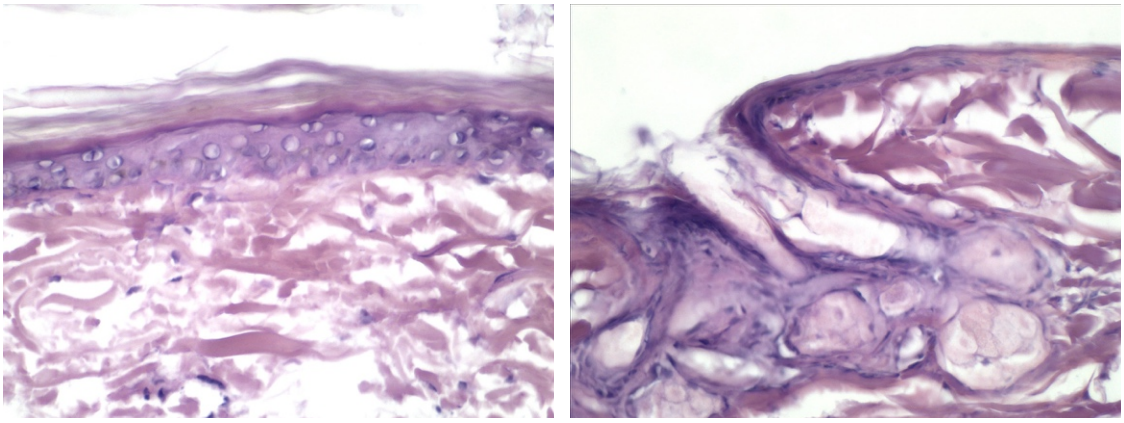

(a) **(b)**

Figure 14. Histological features of rabbit ear skin after the permeation test: (**a**) epidermis (**b**) hair follicle and sebaceous gland. Bars = 50 μm.

Then, sections of rabbit ear skin samples were examined by UV fluorescence microscopy after 6 h (Figure 15) and 24 h (Figure 10) of permeation. Distribution of BRB in the rabbit ear skin samples was easily evidenced by emission of a specific yellow-green fluorescence under UV excitation. Figure 15 provides the comparison between the untreated rabbit ear skin (Figure 15a), the skin treated with B-SOL (Figure 15b) and the three formulations with BRB (Figure 15c-15e) after 6 h of permeation. B-SOL was used as reference of free-BRB permeation. When B-SOL was assayed (Figure 15b), it was evidenced that, after 6 h of permeation test, BRB remained entrapped in the *stratum corneum*, which displayed the highest fluorescence when compared with the other samples (Figure 15c-15e). In fact, the permeation test using B-EL and B-ECL (Figures 15c, 15d) after 6 h showed a weaker florescence of the *stratum corneum* and a more uniform distribution of BRB in the epidermal layers. The 6 h permeation test with B-CL (Figure 15e), on the other hand, displayed a strong florescence of the *stratum corneum*, but also a uniform distribution of BRB from the epidermal layers to the dermal-epidermal junction (DEJ), similarly to B-SOL (Figure 15b).

These findings can be explained by the lower EE% of BRB in B-CL formulation compared to the other formulations (the not entrapped BRB is free to permeate immediately) as well as by the faster BRB release from B-CL than from the other formulations. All these factors result in a greater permeation of BRB loaded in B-CL, in the early hours of the experiment.

After 24 h of permeation test using B-SOL (Figure 16b), BRB florescence was mainly present in the region of DEJ; only a weak fluorescence remained in the

epidermal layers, index of the fast permeation of free-BRB across the skin. By contrast, after the same test period using B-ECL (Figure 16d), BRB still showed the smallest and less uniform permeation.

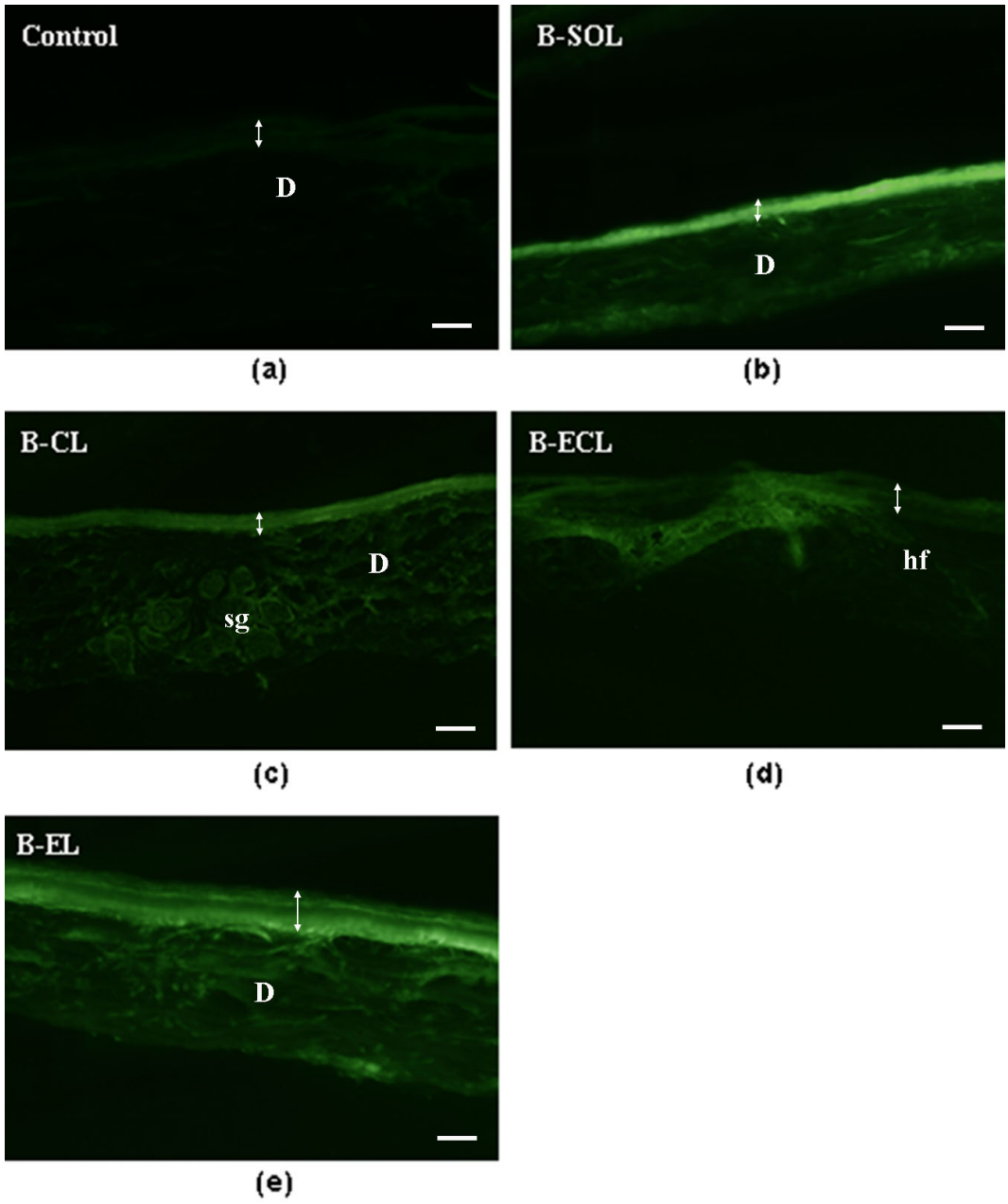

Figure 15. Yellow-green fluorescence images of BRB in sections of rabbit ear skin samples examined after 6 h of permeation test: (**a**) untreated skin (control); (**b**) skin treated with B-SOL (BRB aqueous solution); (**c**) skin treated with B-EL (BRB loaded escinosome); (**d**) skin treated with B-ECL (conventional liposome loaded with ESN and BRB); (**e**) skin treated with B-CL (conventional liposome loaded with BRB). The experiments were performed in triplicate. D, dermis; sg, sebaceous gland; hf, hair follicle. The double arrow indicates the width of the epidermis. Bars = 50 μm.

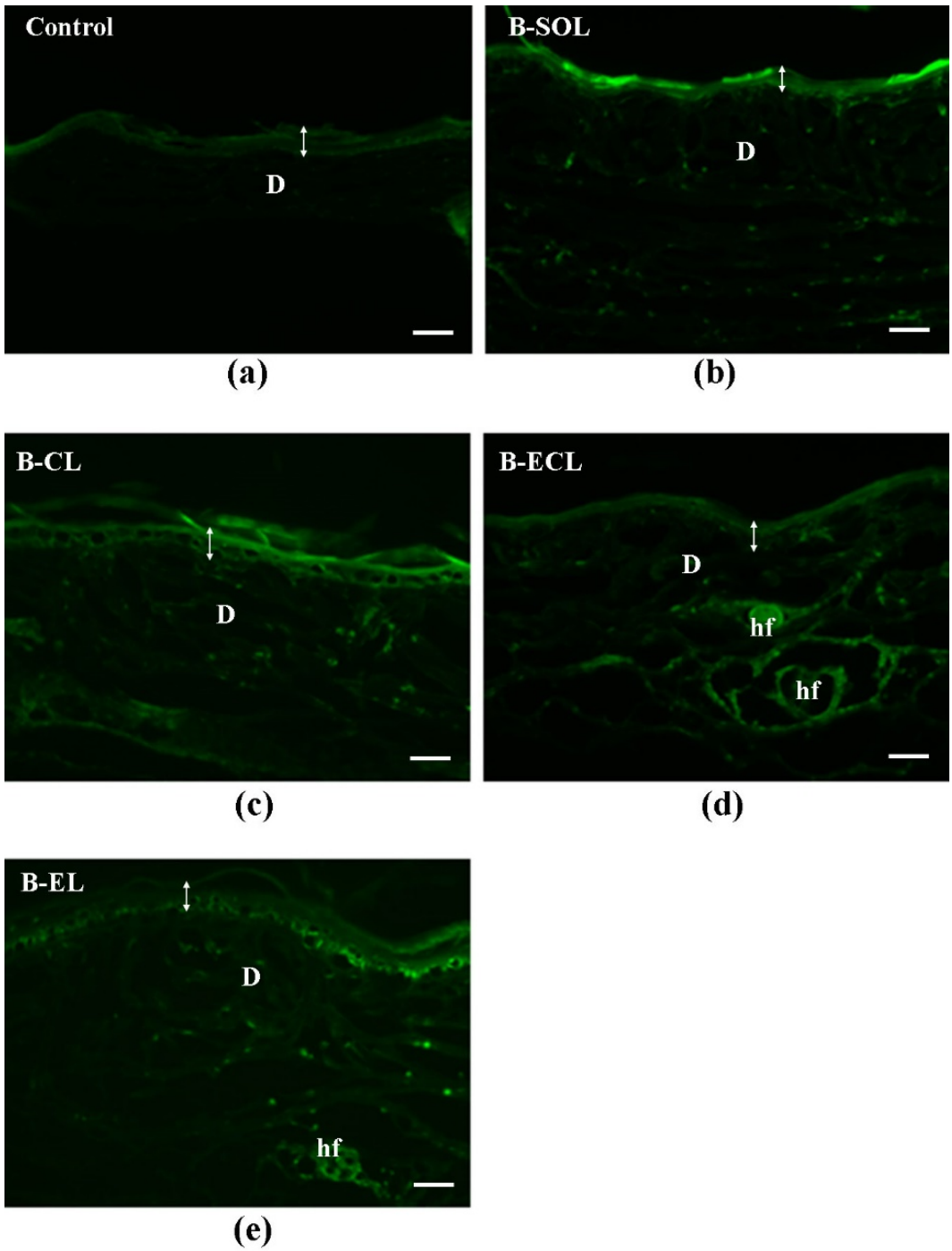

Figure 16. Yellow-green fluorescence images of BRB in sections of rabbit ear skin samples examined after 24 h of permeation test: (**a**) untreated skin (control); (**b**) skin treated with B-SOL (BRB aqueous solution); (**c**) skin treated with B-EL (BRB loaded escinosome); (**d**) skin treated with B-ECL (conventional liposome loaded with ESN and BRB); (**e**) skin treated with B-CL (conventional liposome loaded with BRB). Experiments were performed in triplicate. D, dermis; hf, hair follicle. The double arrow indicates the width of the epidermis. Bars = 50 μm.

This behaviour can be attributed to the lack of deformability of the vesicles (data are shown in Table 12) and consequently their greater retention in the upper layers of the skin. Meanwhile, the 24 h permeation test with B-CL (Figure 16e), showed a behaviour very similar to that of BRB loaded escinosome (B-EL, Figure 10c), whit a uniform distribution of BRB fluorescence in the epidermal layers and a good fluorescence to level of the DEJ. Thereby, despite the initial faster permeation of BRB loaded in B-CL than in B-EL, a comparable fluorescence distribution was found after 24 h, index of a comparable ability in allowing BRB absorption. The advantage related to B-EL formulation is the more controlled permeation of BRB, probably explained by the higher EE% of BRB and the slower release of BRB over time (results are shown in Table 13 and Figure 12, respectively). Moreover, the comparable permeability of B-CL and B-EL can also support the initial hypothesis that ESN is a vesicle bilayer forming material and can simulate CHOL as bilayer component of the vesicles, imparting physical stability, as well as allowing a certain deformability and permeability.

To confirm the results obtained by florescence microscopy, the percutaneous penetration of BRB in the rabbit ear skin was successively evaluated by HPLC quantitative analysis of the solutions/samples in the acceptor/donor compartments of Franz cells, as well as of the skin eluates (Table 15). The following permeation parameters were investigated: the absorbed dose after 24 h of permeation (A_{24}), expressed as percentage of the applied dose absorbed through the skin and recovered in the acceptor compartment; the absorbable dose retained inside the skin after 24 h (S_{24}), expressed as percentage of the applied dose recovered inside the skin; and the total absorbed dose after 24 h (TA_{24}), expressed as the sum of A_{24} and S_{24}. In keeping with the florescence microscopy data, B-SOL (0.13% solution of BRB in water) yielded the highest TA_{24} value (*ca.* 1.5%) after application of 1 ml of sample and more than a half of permeated BRB (TA_{24}) was retained above the DEJ (S_{24}), in the skin (*ca.* 0.9%), as also evidenced in Figure 16b. As expected by fluorescence microscopy, a similar TA_{24} value (*ca.* 1%) was found for B-CL. According to Figure 16e and Table 15, the conventional liposomes accumulated in the *stratum corneum* and also reached the epidermal layers beneath, in fact S_{24} was quite high around 0.8%. However, the percentage of BRB recovered in the receptor compartment was much lesser than that found after the permeation test of B-SOL (Table 15): A_{24} was close to those obtained with the other liposome formulations, B-ECL and BRB loaded escinosome (B-EL). By contrast, TA_{24} values after the 24 h of permeation with B-

EL and B-ECL were much lower (0.51 and 0.57% respectively) than that obtained with B-CL (1.11%), by about a half, because only a little amount of BRB was retained in the skin (S_{24} was *ca.* 0.2%, Table 15). Overall, A_{24} found for liposome loaded with BRB was lower than that found for B-SOL and it can be stated that liposomes allowed a slower permeation of BRB than the aqueous solution.

Table 15. Permeation parameters: A_{24} (Absorbed dose), S_{24} (absorbable dose retained inside the Skin) and TA_{24} (Total Absorbed dose) related to B-SOL (BRB aqueous solution), B-EL (BRB loaded Escinosome), B-ECL (Conventional Liposome loaded with ESN and BRB) and B-CL (Conventional Liposome loaded with BRB). Results are shown as mean ± sd (n=3).

Formulation	**BRB**		
	A_{24} (%)	**S_{24} (%)**	**TA_{24} (%)**
B-SOL	0.60 ± 0.37	0.92 ± 0.17	1.52 ± 0.05
B-EL	0.32 ± 0.01	0.19 ± 0.06	0.51 ± 0.03
B-ECL	0.33 ± 0.03	0.24 ± 0.04	0.57 ± 0.06
B-CL	0.32 ± 0.13	0.79 ± 0.11	1.11 ± 0.04

26. Discussion

Nanoparticle formulations represent a smart approach to increase stability and/or solubility and as a consequence bioavailability of natural products *(Isacchi B, 2011; Isacchi B, 2012; Isacchi B, 2017; Falconieri MC, 2017; Bilia AR, 2018a; Guccione C, 2018)*, but also to enhance permeation and crossing biological barriers including blood brain barrier *(Grossi C, 2017; Guccione C, 2017; Bilia AR, 2019a)*.

Particularly, nanovesicles have great ability to modulate drug penetration through the skin and allow sustained and controlled release of the encapsulated drugs. Their composition, size and charge strongly affect their interaction with the skin and penetrability: therefore, a direct evaluation of the skin penetration enhancement in comparison with conventional drug formulations is helpful for the optimization of efficient nanopharmaceuticals for dermatological purposes. Different *in vitro* approaches have been suggested to investigate the permeation of drugs loaded in nanovectors as alternative to human skin, principally skin from different animals and, more recently, smart simulation systems such as Skin-PAMPA™. These tests can provide a valuable alternative to human skin but in some cases, due to obvious anatomic and physiological differences, they show substantial differences in trans-cutaneous absorption as compared with human skin.

In this study, BRB, a natural quaternary ammonium benzylisoquinoline alkaloid, was chosen as active drug to be loaded in the nanovesicles, due to the numerous biological activities against diverse skin diseases. This alkaloid is hydrophilic in nature (logP = −1.5), and its water solubility is pH- and temperature-dependent. A solution of about 2 mg/ml of BRB was reported to be stable at 25 °C *(Battu SK, 2010)*.

Three different nanovesicles (CL, ECL and escinosomes EL) based on P90G, CHOL and ESN, were developed and optimized. In particular, ESN, a natural mixtures of structurally correlated pentacyclic triterpene saponins *(Abudayeh ZH, 2015)*, largely employed as a vasoprotective anti-inflammatory, anti-edematous and antinociceptive agent, was used at a dose of 5 mg/mL to formulate ECL and EL nanovesicles.

BRB was loaded in the developed nanovesicles and the physical and chemical properties were investigated in terms of AHD, PdI, ζ-potential, deformability, R% and EE%, stability and release kinetics. The results demonstrated that B-EL possesses the best characteristics for skin application, particularly optimal PdI (0.17) and deformability, high negative ζ-potential value, great EE% (*ca.* 67%), high physical and chemical stability and the best BRB release properties (*ca.* 75% after 24 h). At the end of the release study, only 16-18% of ESN was found in the release medium, indicating that ESN was strongly retained in the vesicles and suggesting that ESN could work as a bilayer-forming material. ESN hyaluronidase inhibition activity was unaffected by the formulation and the presence of BRB. Thus, ESN anti-inflammatory, venotonic and anti-oedematous potential activities were preserved, once it was formulated as vesicle component.

The Effective Permeability (P_e) of BRB in solution (B-SOL) or loaded in vesicles, namely B-CL, B-ECL, B-EL was firstly evaluated using the Skin-PAMPA™, a smart, validated test for fast prediction of human skin penetration through an artificial membrane mimicking the human *stratum corneum*. P_e of B-SOL (1.12 x 10-6 cm/s) was very similar to that of progesterone (1.19 x 10-6 cm/s), used as reference standard drug of high permeability. Surprisingly, B-ECL displayed a 4-fold higher P_e value than that calculated for B-SOL, probably explained by the simultaneous presence of ESN and CHOL. B-CL and B-EL displayed similar P_e values, which were twice times the value of B-SOL. These results evidenced that ESN was able to replace CHOL not only structurally but also functionally.

The *in vitro* permeation studies were preceded by the histological comparison between rabbit ear skin and human abdominal skin. Both tissues showed comparable characteristics with respect to the *stratum corneum* and epidermal thickness as well as hair follicular structure and density. The permeation of BRB with the different formulations was then evaluated by the vertical diffusion Franz cells, observing the distribution of BRB fluorescence and performing quantitative analysis. Despite the higher TA_{24} values found for B-CL, it was found that the skin samples treated with B-EL displayed a comparable BRB absorption as compared with those treated with B-CL. B-EL and B-CL displayed similar composition, except for ESN replacing CHOL in B-EL. CHOL in the bilayer structure of liposomes influences the lipid dynamics because of its rigid ring structure, reducing gauche-trans isomerization, rotational and lateral diffusion of lipids, which results in an ordering effect on the liquid crystalline state with a final fluidizing effect in the gel state *(Perez-Cullell N, 2000)*. Probably the rigid ring structure of ESN, which is very similar to that of sterols, could have a similar, significant effect on membrane dynamics, confirming that ESN was not simply encapsulated but it is included within the membrane bilayer of the vesicle, giving physical stability and allowing a certain deformability and permeability. It is noteworthy that these two nanovesicles shared major favourable characteristics for skin delivery purposes, i.e. high deformability, proper size, PdI and ζ-potential. In addition, B-EL was superior to B-CL in terms recovery, encapsulation efficiency and release properties.

Of note, the results of the permeation tests with rabbit ear skin and Skin-PAMPA™ were substantially different. The latter test principally simulated the permeation through the *stratum corneum*, the main barrier of the epidermis owing to the presence of an abundant lipid matrix containing ceramides, CHOL and free fatty acids, constituents that are different from those of the lower epidermal layers. These characteristics can clarify the faster crossing properties of the epidermis shown by BRB loaded in liposomes when compared with aqueous BRB. By contrast, the test with rabbit ear skin indicated a different performance of the aqueous BRB, with improved permeation through the deepest epidermal layers, annexa and dermis, characterized by less lipids and more aqueous tissues. The behaviour of BRB in the Skin-PAMPA™ and in the test with rabbit ear skin showed striking differences with the results reported in the literature, which identify BRB having high hydrophilicity and low dermal permeability *(Torky AS, 2018)*. Indeed, BRB has an amphiphilic structure, ascribable to the hydrophilic

portion of the quaternary ammonium salt and to the lipophilic benzylisoquinoline moiety: these features can extremely influence its penetration through the *stratum corneum*, as well as the underlying epidermal layers. Future studies should be focused on evaluating the concentration role of ESN, when combined with P90G, in the bilayer stability and on better investigating the cohesive interactions occurring between the sugar groups of ESN and the phospholipid headgroups, possibly driven by hydrogen bonds, in particular with the carbonyl and negatively charged phosphate groups of the phospholipid.

HYDROXYPROPYL METHYLCELLULOSE HYDROGEL OF BERBERINE CHLORIDE-LOADED ESCINOSOMES: DERMAL ABSORPTION AND BIOCOMPATIBILITY

27. Results and Discussion

27.1. Nanovesicle preparation and characterization

Nanovesicles, specifically blank liposomes (L) used as reference formulation, escinosomes (EL) and BRB-loaded escinosomes (B-EL), were prepared using the thin layer evaporation method. The main physical parameters of nanovesicles, namely size, PdI and ζ-Potential, were determined by DLS/ELS. EL showed PdI (0.26), small sizes (about 137 nm) and excellent deformable properties. Similarly, EL loaded with BRB (B-EL) also presented high homogeneity (PdI about 0.17), average sizes suitable for dermal application (about 150 nm) and good deformability. The two formulations were stable in terms of electro- static repulsion because ζ-Potential was approximately −41 mV for EL and approximately −35 mV for B-EL. Finally, the EE% of ESN resulted high in both EL and B-EL (*ca.* 95%), whereas EE% of BRB in B-EL was around 67% *(Vanti G, 2019)*.

27.2. Preparation of HPMC-hydrogels

Vesicles cannot be easily administered as such for cutaneous route, because they are liquid with a consequent low residence time on the skin, and a rapid drug leakage. Thereby, incorporation in hydrogel matrices overcomes these drawbacks and provide a convenient dosage form, suitable for the topical application. HPMC was selected because it is a hydrophilic polymer characterized by polar and non-polar groups, widely used as a matrix former in the design of dermal and transdermal delivery systems *(Rincón-Iglesias M, 2019; Arca HC, 2018)*. Carbomer and hydroxyethyl cellulose (HEC) were also tested as gelling agents for escinosomes. Carbomer hydrogels were not homogeneous and clearly the formation of stable aggregates was evidenced. HEC was able to form a homogenous and viscous hydro- gel, but much higher concentrations of polymer were necessary, when compared with HPMC. Therefore, HPMC (3% *w*/*v*) was selected as gelling agent for the escinosome formulations. Gelation occurred quickly by the manual incorporation of HPMC in the aqueous vesicle dispersions, obtaining G-L, G-EL and G-B-EL. The HPMC-hydrogels prepared

with the water dispersion of pure ESN and ESN plus BRB (G-ESN_W, G- BE_W) were also prepared. All the formulated hydrogels were left at 4 °C for two days before the use, in order to remove air bubbles. The resulting hydrogels were viscous and suitable to obtain a homogeneous coverage of the excised skin surface, during the *in vitro* skin absorption test. In addition, pH of the escinosome loaded HPMC-hydrogels was 3.93 ± 0.16 for G-EL and 3.52 ± 0.05 for G-B-EL. These pH values were lower than the range of skin surface pH in normal circumstances (pH 4–6), *(Rippke F, 1999)*, but the developed hydrogels resulted extremely biocompatible, as reported in Section 3.7.

27.3. HPMC-hydrogel viscosity

Viscosity measurements of escinosome HPMC-hydrogels were performed according to the test method reported in Figure 1S, as detailed described in the experimental part, calibrating the viscometer to compensate for the absence of the guard lag and for the smaller container compared to the recommended vessel. Thereby, the new ranges of viscosity measurements (FSR, Full-Scale Range) were calculated for each selected speed, according to the different experimental conditions (Table 16). All viscosity measurements clear-fell within the obtained FSR and were plotted on a graph, which represented an up-down rate ramp of viscosity as a function of the spindle rotational speed (Figure 2S and Figure 17). Both the escinosome HPMC-hydrogels (G-EL and G-B-EL) showed similar viscosity behaviour (Figures 2S-17). The viscosity was determined at different speeds and both G-EL and G-B-EL resulted non-Newtonian fluids, because they have different viscosities at different speeds, as displayed by the graphs (Figures 2S-17). In addition, the hydrogels were found to be time-independent fluids, since the viscosity behaviour did not change as a function of time when measuring at specific speeds: the down rate ramp matched the initial up rate ramp (Figures 2S-17). The shear thinning behaviour of the hydrogels is another important property. Hence, the hydrogels showed a decrease of viscosity when the spindle rotational speed was increased (Figures 2S-17).

Table 16. Viscometer recalibration obtained by calculating the new FSR (Full-Scale Range), namely the new ranges of viscosity measurements, according to the different experimental conditions (50 mL beaker and absence of guard lag) using a 06 spindle.

Rotational speed (rpm)	Standard FSR	New FSR
2.5	400,000	480,808
4	250,000	300,505
5	200,000	240,404
10	100,000	120,202
20	50,000	60,101
50	20,000	24,040
100	10,000	12,020

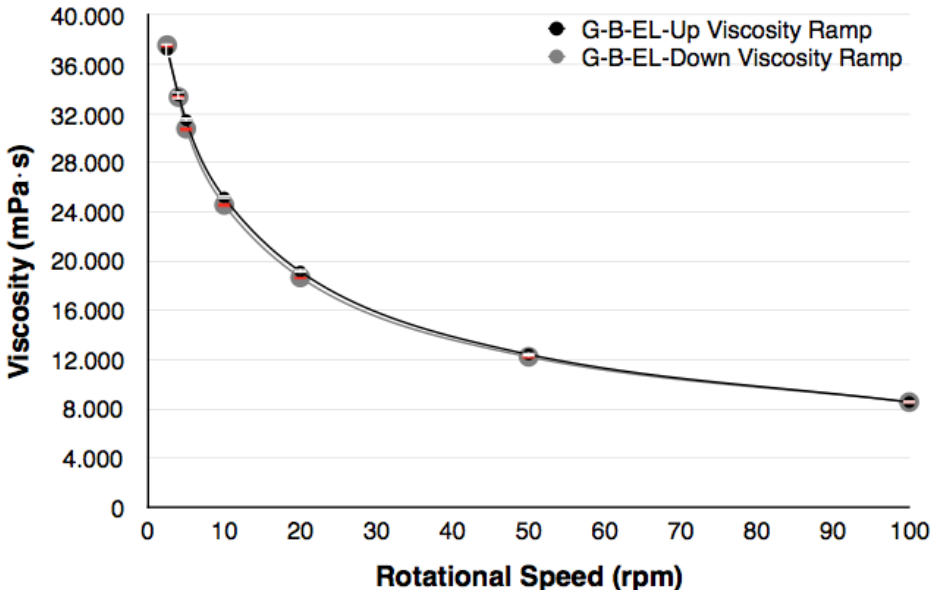

Figure 17. Up-down ramp viscosity of G-B-EL (hydrogel of escinosomes loaded with BRB). Up viscosity ramp is the viscosity curve obtained from the spindle rotational speed increasing from 2.5 to 100 rpm, while down viscosity ramp is the viscosity curve obtained from the spindle rotational speed reduction from 100 to 2.5 rpm. Data are shown as Mean ± SD (n = 3). Solid lines are not related to a fitting model.

27.4. Release of BRB and ESN from HPMC-hydrogels

The release rate of BRB and ESN from escinosomes loaded HPMC-hydrogels (G-B-EL and G-EL) was investigated using the vertical diffusion Franz cells and the cellulose nitrate filters as membranes. Thus, for many years cellulose-based synthetic membranes have been used the release studies, because they are not barriers and they only act as supports, simply separating the formulation from the acceptor medium without limiting the flow rate of drugs *(Ng SF, 2012)*. Since

cellulose nitrate membranes allow high-flux of molecules and minimal diffusional resistance, thanks to the high porosity, they are very useful to study the *in vitro* release. In our investigation, ESN and BRB release from escinosome hydrogels was compared to the ESN and BRB release from hydrogels obtained with ESN and BRB aqueous dispersions (G-BEW and G-ESNW). The study evidenced that the release profile of BRB from G-B-EL and G-BEW was similar, but the amount of released BRB was higher for G-BEW (Figure 18). Similarly, ESN showed a greater release from the hydrogels based on aqueous dispersion (G-ESNW and G-BEW) compared to the escinosome hydrogels (G-B-EL and G-EL), as displayed in Figure 19. It is noteworthy that BRB did not affect ESN release either in hydrogels based on vesicular systems or on aqueous dispersions (Figure 19). Moreover, the low ESN release (about 10% after 24 h) from the escinosome hydrogels confirmed the strong ESN interaction with the vesicular bilayer *(Vanti G, 2019)*, which is maintained also in the hydrogel formulation.

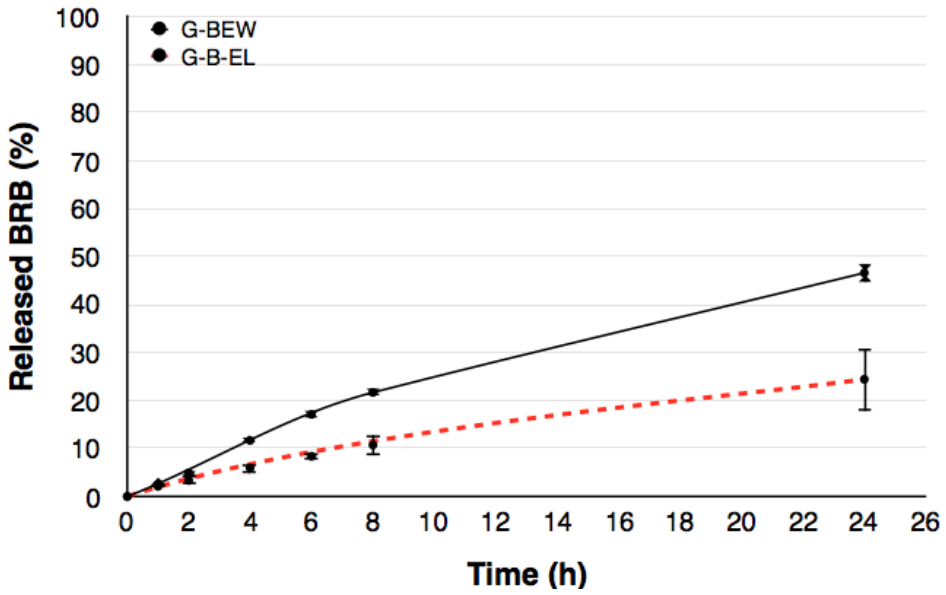

Figure 18. BRB release from G-B-EL (hydrogel of escinosomes loaded with BRB) and G-BEW (hydrogel of ESN plus BRB water dispersion). The release medium was withdrawn and analysed after 1, 2, 4, 6, 8 and 24 h for each sample. Data are shown as Mean ± SD (n = 3).

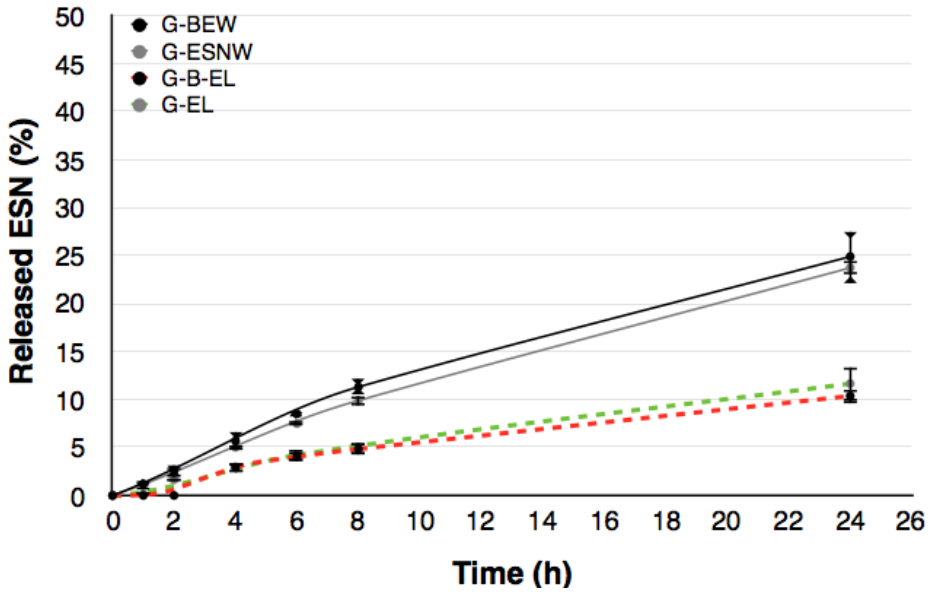

Figure 19. ESN release from escinosome HPMC-hydrogels (G-B-EL and G-EL), and from aqueous dispersion hydrogels (G-BEW and G-ESNW). The release medium was withdrawn and analysed after 1, 2, 4, 6, 8 and 24 h for each sample. Data are shown as Mean ± SD (n=3).

27.5. HPMC-hydrogel stability

Chemical and physical stability of the escinosome loaded HPMC- hydrogels (G-B-EL and G-EL) was monitored after 45 days of storage at 4 °C in the dark. Specifically, the pH of G-B-EL slightly decreased from 3.52 ± 0.05 to 3.15 ± 0.01, whereas the pH of G-EL changed from 3.93 ± 0.16 to 3.38 ± 0.01. However, these pH changes did not affect the formulations characteristics. The viscosity measurements were repeated after 45 days using the same viscosity test method adopted during the physical characterization step of the hydrogels. Both G-B- EL and G-EL demonstrated unchanged viscosity properties: the time- independence was maintained since the up viscosity ramp matched the down viscosity ramp exactly as on day 1 (Figures 3S-20), and the shear thinning behaviour was also maintained since the hydrogels still showed a decrease in viscosity as a consequence of an increase in spindle rotational speed (Figures 3S-20). Moreover, all viscosity measurements determined after 45 days matched those recorded on day 1 (Figures 3S-20).

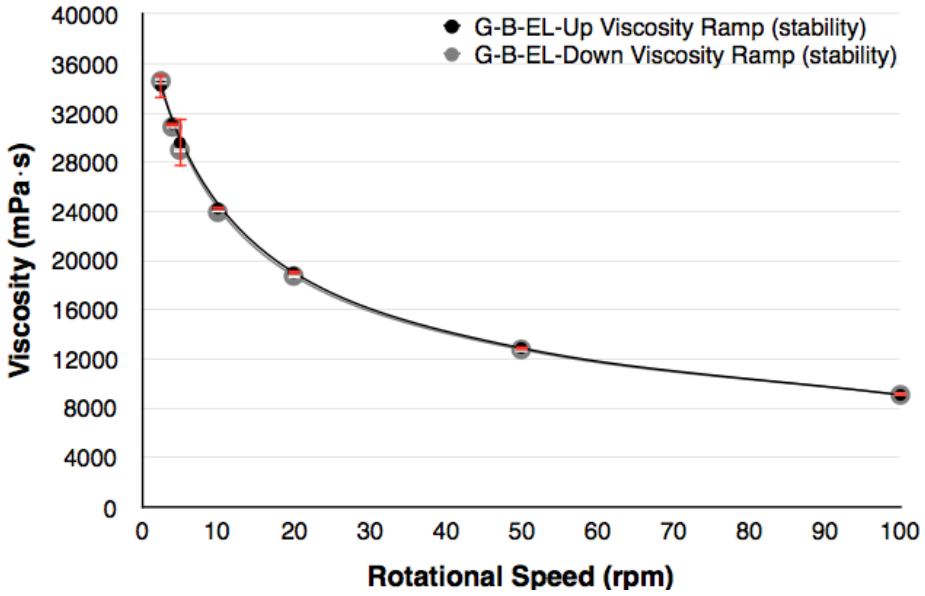

Figures 20. Physical stability of G-B-EL (hydrogel of escinosomes loaded with BRB): up-down ramp viscosity of G-B-EL after 45 days of storage. Up viscosity ramp is the viscosity curve obtained from the spindle rotational speed increasing from 2.5 to 100 rpm, while down viscosity ramp is the viscosity curve obtained from the spindle rotational speed reduction from 100 to 2.5 rpm. Data are shown as Mean ± SD (n = 3).

27.6. In vitro skin absorption studies with nude mouse skin

In the present study, the permeation properties of EL and B-EL were investigated by the vertical diffusion Franz cell system, using a proved skin absorption model with nude mouse skin. Specifically, the absorption by the skin was explored for both BRB and ESN, using the vesicular formulations and the aqueous dispersions, namely EL/B-EL and ESN_W/BE_W respectively. In parallel, the HPMC-hydrogels of each sample were tested by the skin absorption assay (G-EL, G-B-EL, G-ESN_W, G-BE_W), being the final dosage form. The experiments were carried out using the same concentrations of the active molecules in all samples, namely 5 mg/mL for ESN and 1.3 mg/mL for BRB, as reported in the experimental part.

27.7. ESN skin absorption from water dispersion (ESN_W) and escinosomes (EL)

ESN absorbed through the skin and recovered in receptor compartment of Franz cells (A_{24}) reached a maximum value when escinosomes (EL) were tested, resulting approximately a 100% total absorption (TA_{24}), (Table 17). By contrast, ESN in free form (ESN_W) showed a rather lower TA_{24}. ESN was detectable in the receptor compartment only after 24 h of permeation test, due to its low UV–

visible absorption. As a consequence, permeation and flux of ESN through the skin was not calculated. However, the quantitative data of A_{24} and S_{24} demonstrated that EL improved ESN absorption in the skin, probably thanks to the vesicular system *(Vanti G, 2019)*.

Table 17. BRB and ESN skin absorption parameters related to B-EL (BRB-loaded escinosomes) and BE_W (BRB plus ESN water dispersion), EL (escinosomes), and ESN_W (ESN water dispersion) obtained from the *in vitro* test with nude mouse skin, by vertical diffusion Franz cells. Results are shown as Mean ± SD (n=3). A_{24} = absorbed dose; S_{24} = absorbable dose retained inside the skin; TA_{24} = total absorbed dose.

Sample	**BRB**		
	A_{24} (%)	**S_{24} (%)**	**TA_{24} (%)**
B-EL	69.16±11.77	4.30±0.59	73.41±12.59
BE_W	53.75±2.69	5.11±1.89	59.27±5.16
Sample	**ESN**		
	A_{24} (%)	**S_{24} (%)**	**TA_{24} (%)**
EL	76.59±1.82	24.37±1.44	100.96±0.38
B-EL	26.10±5.00	26.97±10.13	36.90±12.74
ESN_W	24.51±4.04	3.53±0.46	26.69±2.61
BE_W	0.90±0.25	6.19±3.41	7.09±3.47

27.8. ESN skin absorption from water dispersion (BE_W) and BRB-loaded escinosomes (B-EL)

ESN skin absorption from BE_W and B-EL had a similar behaviour of those previously reported from ESN_W and EL. In fact, ESN skin absorption from B-EL was higher compared to that of the water dispersion BE_W (Table 17). However, A_{24} and TA_{24} for B-EL and BE_W were found to be lower than those from EL and ESN_W, despite a similar ESN skin retention. It is noteworthy that ESN A_{24} and consequently TA_{24} were affected by the presence of BRB, which seemed to decrease ESN permeation through the skin, in both B-EL and BE_W samples (Table 17). In addition, permeation of ESN over time (Figure 21a) was quantifiable at different time intervals during 24 h, only for sample B-EL. The graph indicated that ESN permeation increased in a linear way after 8 h. Accordingly, ESN flux (μg/cm^{2}h) across the skin became constant after 8 h and it was calculated as the slope of the regression line after reaching the steady state conditions, namely in the time interval 8–24 h (Figure 21b). Therefore, ESN permeability coefficient K_p resulted (3.19 ± 0.72) × 10^{-3} cm/h.

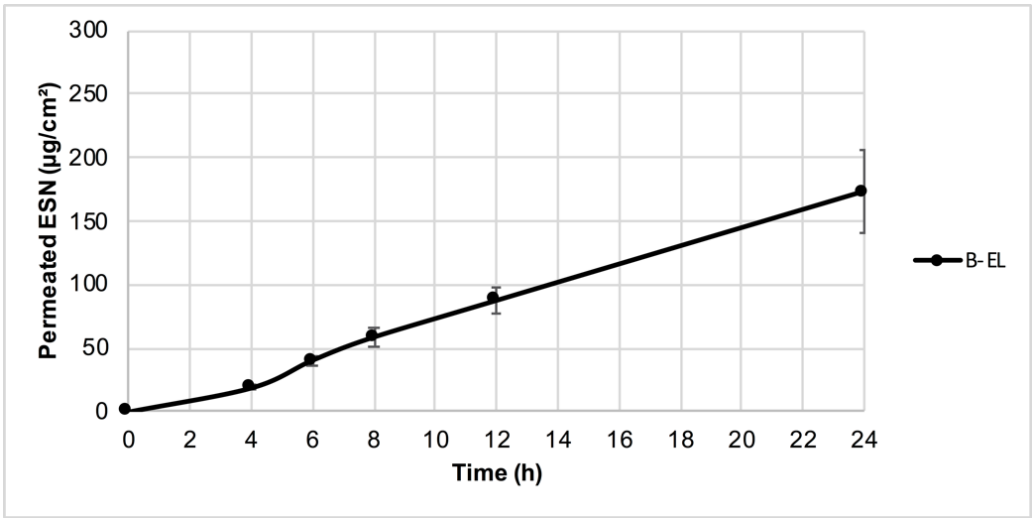

(a)

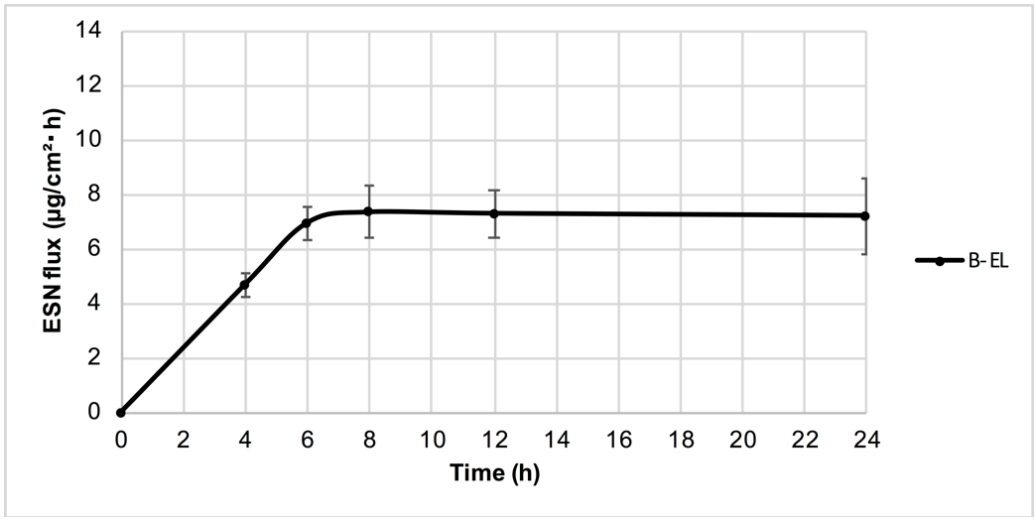

(b)

Figure 21. ESN skin absorption from vesicular formulation. ESN skin absorption, expressed as µg/cm² **(5a)**, and ESN skin flux, expressed as µg/cm²h **(5b)**, through the nude mouse skin treated with B-EL (escinosomes loaded with BRB). The acceptor solution was withdrawn and analysed after 2, 4, 6, 8, 12 and 24 h of absorption test. All results are showed as Mean ± SD (n = 3).

27.9. BRB skin absorption from water dispersion (BE_W) and BRB-loaded escinosomes (B-EL)

Escinosomes increased BRB skin absorption, since A_{24} and TA_{24} were found to be higher than the values obtained with BE_W (Table 17). It was supposed that ESN modified the structure of skin cell membranes, due to the known interaction with membrane cholesterol and phospholipids *(Geisler R, 2019)*. By contrast, the skin retention S_{24} of BRB was comparable for the two samples B-EL and BE_W (Table 17). BRB skin absorption A_{24} did not increase in a linear way for both B-EL

and BEw (Figure 22a); consequently, BRB flux never achieved the steady state conditions (Figure 22b) and it was not possible to calculate flux and K_p values. Therefore, the flux was only plotted as function of time. In conclusion, the escinosomes (EL and B-EL) had the best skin absorption profile and the highest skin absorption rate for both ESN and BRB, when compared with those of ESNw and BEw. The behaviour was probably due to the lipid vesicular structure, as well as with the presence of the saponin which acted as penetration enhancer *(Geisler R, 2019)*. It is noteworthy that viscosity due to the three-dimensional HMPC network is responsible for the lower drug penetration and, at the same time, for the higher residence time on the skin, both for ESN and BRB *(Elnaggar YS, 2014)*.

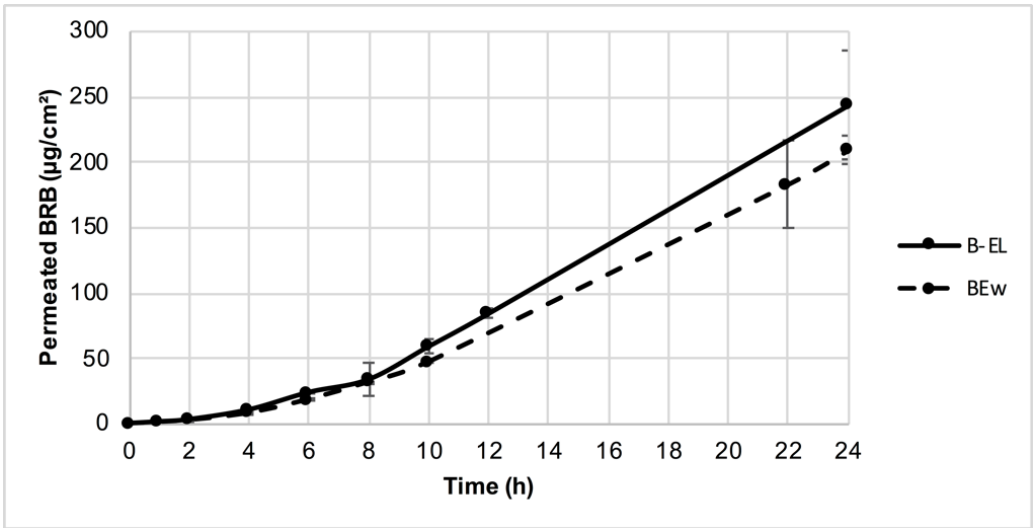

(a)

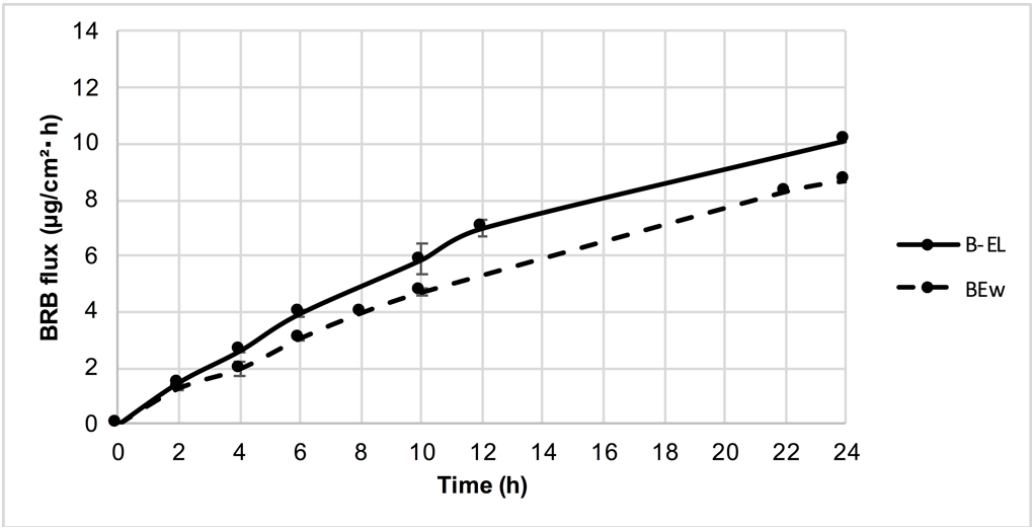

(b)

Figure. 22. BRB skin absorption from vesicular and aqueous formulations. BRB skin absorption, expressed as µg/cm² (Fig. 22a), and BRB skin flux, expressed as µg/cm²h

(Fig. 22b), using the nude mouse skin, which was treated with B-EL (escinosomes loaded with BRB) and BE_W (ESN plus BRB water dispersion). All results are showed as Mean ± SD (n = 3).

27.10. ESN skin absorption from HPMC-hydrogels (G-EL, G-ESN_W, G-B-EL, G-BE_W)

Finally, the hydrogels obtained from escinosomes (G-EL and G-B-EL) and the hydrogels obtained from the water dispersions (G-ESN_W and G-BE_W) were also tested by the Franz cell system. Similarly to the previously described formulations (Section 27.7), TA_{24} found for ESN from gelled escinosomes (G-EL) was higher than TA_{24} value recovered from the gelled aqueous dispersions (G-ESN_W), as shown in Table 18. By contrast, when the gelled dispersion of BRB plus ESN was compared with the escinosomes (B-EL), ESN skin absorption was found to be very similar. Moreover, it is notable that ESN skin absorption from the hydrogel containing BRB-loaded escinosomes (G-B-EL) was not greatly affected by the presence of BRB, in contrast to the behaviour of the hydrogel of BRB plus ESN aqueous dispersion (G-BE_W), as shown in Table 18. ESN concentration was not detectable at the different time intervals during the permeation test, thereby ESN flux and K_P were not calculated.

Table 18. ESN and BRB skin absorption parameters related to G-EL (hydrogel of escinosomes), G-B-EL (hydrogel of BRB-loaded escinosomes), G-ESN_W (hydrogel of ESN water dispersion) and G-BE_W (hydrogel of BRB plus ESN water dispersion), obtained from the *in vitro* test with nude mouse skin, by vertical diffusion Franz cells . Results are shown as Mean ± SD (*n*=3). A_{24} = absorbed dose; S_{24} = absorbable dose retained inside the skin; TA_{24} = total absorbed dose.

Sample	**ESN**		
	A_{24} (%)	**S_{24} (%)**	**TA_{24} (%)**
G-EL	4.67±2.62	0.56±0.35	5.23±2.29
G-B-EL	2.52±0.90	0.39±0.08	2.90±0.79
G-ESN_W	-	0.99±0.16	0.99±0.16
G-BE_W	3.67±0.28	0.82±0.12	4.48±0.41
Sample	**BRB**		
	A_{24} (%)	**S_{24} (%)**	**TA_{24} (%)**
G-B-EL	46.09±13.83	4.13±0.27	50.22±13.67
G-BE_W	41.45±3.24	2.98±0.27	44.43±3.36

27.11. BRB skin absorption from HPMC-hydrogels (G-B-EL, G-BE$_W$)

A_{24} and S_{24} values found for BRB resulted slightly higher for G-B-EL compared to those of G-BE$_W$ (Table 18). Therefore, the vesicular form was found to be superior when compared with the behaviour of the aqueous dispersions, both for ESN and BRB skin absorption. BRB skin absorption over time was quantified for both G-B-EL and G-BE$_W$. BRB skin absorption for G-B-EL did not increase in a linear way (Fig. 23a), BRB flux never achieved the steady state conditions and it was not possible to calculate the exact value. Consequently, the flux was only plotted as function of time (Fig. 23b) and the K_p was not determined. By contrast, G-BE$_W$ showed a linear increase of BRB skin absorption after 10 h of experiment (Fig. 23a). After that point, BRB flux (μg/cm^{2}h) across the skin became constant (Fig. 23b) and BRB K_p resulted 0.33 ± 0.46 cm/h.

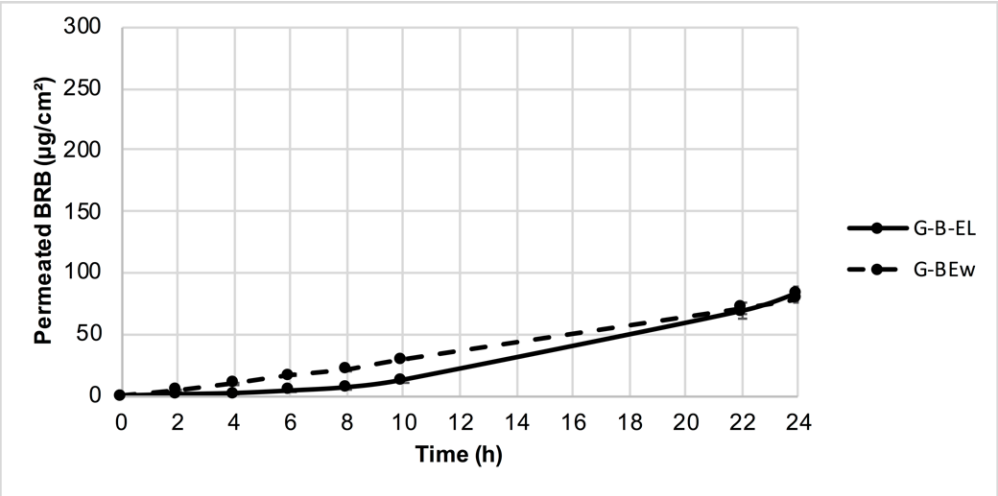

(a)

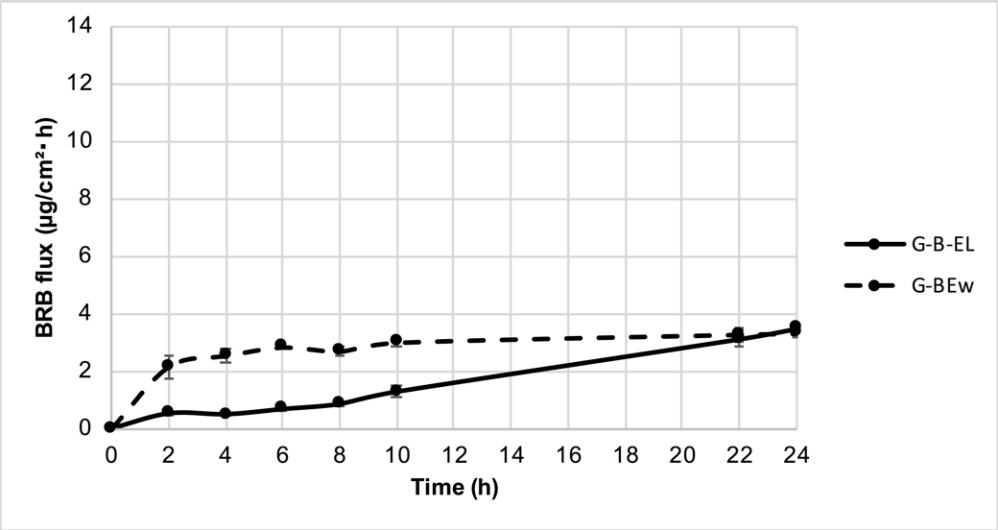

(b)

Figure 23. BRB skin absorption from escinosome HPMC-hydrogel formulations. BRB skin absorption, expressed as μg/cm² (Figure 7a), and BRB skin flux, expressed as μg/cm²h (Figure 7b), using the nude mouse skin, which was treated with G-B-EL (hydrogel of escinosomes loaded with BRB) and G-BEw (hydrogel of ESN plus BRB water dispersion). All results are showed as Mean ± SD (*n*=3).

27.12. In vivo test: acute dermal irritation/corrosion

The safety profile for a dermatological use, of the developed formulations, was assessed by the acute irritation and corrosion test, carried out according to the OECD guidelines. During the experiment, no rats were sacrificed and no erythema or oedema were found (Table 18 and Fig. 24). HPMC-hydrogels obtained from the gelled vesicles (G-EL and G-B-EL) showed no irritant effects on rats after 24 h application. Thus, the formulations can be considered safe for human dermal administration.

Table 18. Appearance of rats belonging to the control group (C) and to the groups treated with: G-L (hydrogel of blank liposome), G-EL (hydrogel of escinosomes) and G-B-EL (hydrogel of BRB-loaded escinosomes). Experiments were completed on 6 animals for each group.

Group	Erythema (normal for"√")	Oedema (normal for"√")	Death/Total animals
C	√	√	0/3
G-L	√	√	0/6
G-EL	√	√	0/6
G-B-EL	√	√	0/6

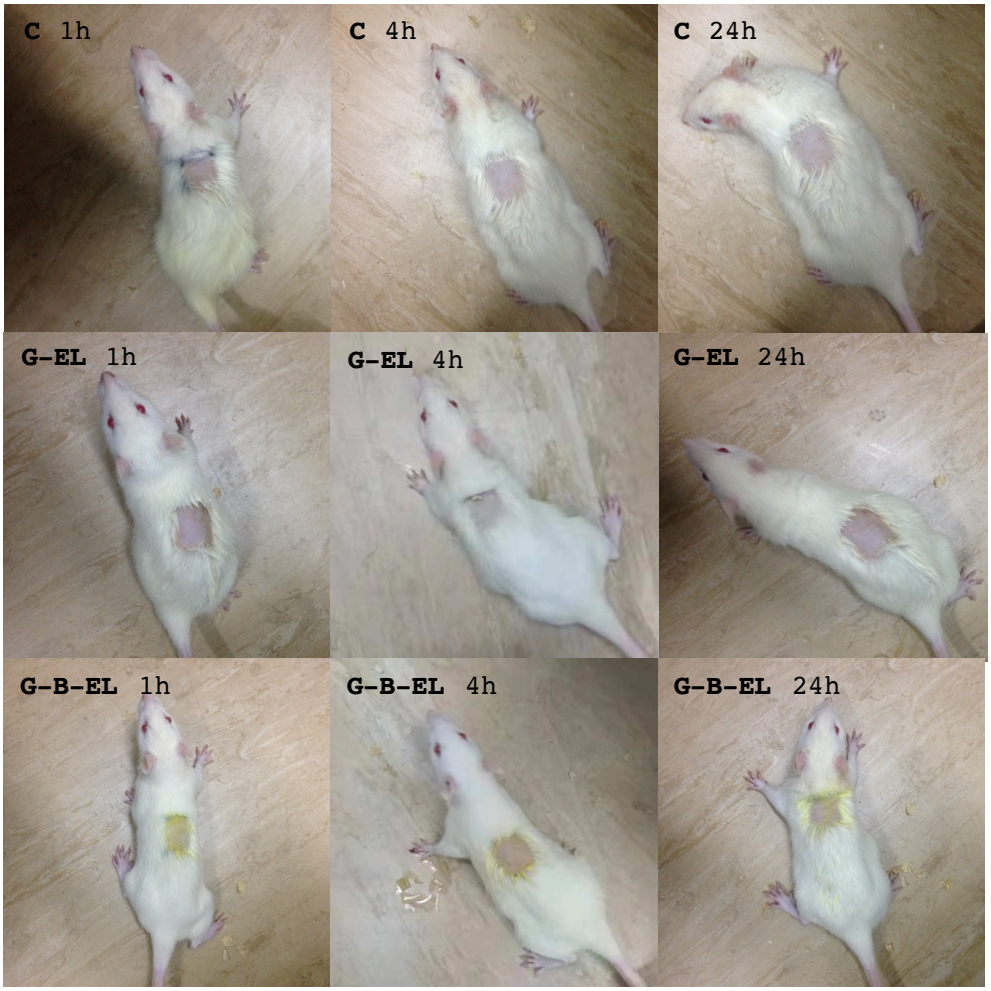

Figure. 24. Acute dermal irritation/corrosion test. Rat skin appearance after 1 h, 4 h and 24 h of observation (from left to right, respectively). First line: rats not treated with escinosome HPMC-hydrogel, C (control group). Second line: rats treated with G-EL (hydrogel of escinosomes). Third line: rats treated with G-B-EL (hydrogel of escinosomes loaded with BRB). Experiments were done on 6 animals for each group.

HYDROXYETHYL CELLULOSE HYDROGEL FOR SKIN DELIVERY OF KHELLIN LOADED IN ASCOSOMES: CHARACTERIZATION, *IN VITRO*/*IN VIVO* PERFORMANCE AND ACUTE TOXICITY

28. Results and Discussion

28.1. Development and characterisation of khellin-loaded vesicles

As a first step of this study, conventional liposomes of P90G (L) and ascosomes based on P90G plus ASC8 (LA8) or P90G plus ASC10 (LA10) were prepared and characterized in terms of size, PdI and ζ-potential. Successively, vesicles loaded with khellin (2 mg/mL, KL, KA8 and KA10 respectively) were developed and characterized also in terms of khellin EE% and R%, obtained by HPLC-DAD analysis. Polydispersity indices were always less than 0.3, indicating great homogeneity of the vesicular systems, while the ζ-potential resulted less than −19 mV, suggesting high stability of the vesicles. Khellin loaded in the ascosomes did not affect so much the physical parameters of the developed vesicles, namely size, PdI, and ζ-potential. In particular, KA8 and KA10 maintained very suitable ζ-potential values and sizes for dermatological applications and deep skin penetration *(Bilia AR, 2017; Bilia AR, 2019b)*. R% of khellin in KL was *ca.* 90%, values obtained for KA8 and KA10 were about 85% and 94%, respectively. Encapsulation efficiency determined by HPLC-DAD was quite high for all the developed vesicles and ranged between 81% and 90%. From the above results, KA10 demonstrated the best values in terms of size, ζ-potential, and EE% (Table 19).

Table 19. Characterization of developed vesicles.

Sample	P90G (mM)	ASC8 (mM)	ASC10 (mM)	Khellin (mM)	Size (nm)	PdI	ζ-potential (mV)	EE%
L	84	-	-	-	269.5±3.5	0.24±0.08	-24.3±0.4	-
KL	84	-	-	7.7	273.5±2.3	0.25±0.03	-19.0±0.6	87.0±2.0
LA8	44	40	-	-	163.1±1.5	0.27±0.02	-26.9±0.6	-
KA8	44	40	-	7.7	143.5±3.3	0.25±0.01	-26.5±0.7	81.1±1.1
LA10	44	-	40	-	128.7±2.0	0.27±0.01	-43.1±1.3	-
KA10	44	-	40	7.7	115.0±0.4	0.26±0.01	-40.1±0.8	90.2±0.1

28.2. In vitro release study of khellin-loaded ascosomes

Release characteristics of khellin (2 mg/mL) from liposomes and from ascosomes were evaluated *in vitro* as reported previously *(Risaliti L, 2020a)* and described in the experimental part. The quantification of the released khellin was evaluated by HPLC-DAD. A similar kinetic was observed for all formulations containing khellin, displaying a prolonged release over time, reaching about 80% release after 8 h, as reported in the supplementary section (Figure 4S).

28.3. Ex vivo skin permeation study of khellin-loaded ascosomes

Skin permeation of khellin was evaluated as reported in the experimental part. Results of the *ex-vivo* skin permeation study indicated that KA10 had the highest permeation capacity of khellin after 24 h of transdermal test (Table 20, Figure 5S). At the end of the test the amount of permeated khellin using KA10 was two-fold higher than KL. Moreover, considering the effective diffusion area of 3.14 cm^2, which was overfilled with 1 mL of vesicles containing 2 mg of khellin, the percentage of permeation for KA10 after 24 h was 42%, for KA8 was 32% and for KL was only 21%, respectively. These results were very interesting, demonstrating that besides the same release properties of the different vesicles loaded with khellin, the *ex vivo* performance of the different vesicles was very different, giving a double permeation of khellin from ASC10 when compared with the release of khellin from KL. The permeability data of the saturated solution were inferior to those of the vesicles (data not shown).

Table 20. Transdermal permeation of khellin from the different vesicles.

Time (h)	KL (μg/cm^2)	KA10 (μg/cm^2)	KA8 (μg/cm^2)
1	3.01±1.54	3.91±1.27	4.75±0.67
2	7.43±1.29	10.83±1.47	12.46±3.59
4	12.53±1.57	18.23±2.33	18.05±1.44
6	18.42±1.97	27.97±2.63	26.77±1.56
8	29.82±2.09	46.55±3.81	45.18±2.78
10	42.85±3.16	72.57±2.24	64.83±2.47
21	53.69±2.75	95.48±3.13	82.08±4.06
24	132.18±9.59	265.23±9.14	206.49±18.03

28.4. Formulation of hydroxyethylcellulose hydrogels and pH characterisation

After the characterization of vesicles, the colloidal systems were subsequently gelled with hydroxyethyl cellulose to obtain a suitable delivery system for dermatological use. The developed blank hydroxyethyl cellulose

hydrogel, namely KL hydrogel, KA8 hydrogel and KA10 hydrogel were characterized in terms pH. Blank hydroxyethyl cellulose hydrogel was obtained using the 3% *w/v* of hydroxyethyl cellulose in PBS. This formulation displayed a pH value of 6.99 ± 0.04, KL hydroxyethyl cellulose hydrogel had a value of 6.89 ± 0.04, KA8 hydroxyethyl cellulose hydrogel a pH of 5.19 ± 0.05 and KA10 hydroxyethyl cellulose hydrogel a pH of 5.03 ± 0.05 (as an average of three measurements). Samples containing ascorbic acid derivatives displayed more acidic pH values due to the ascorbic acid moieties. However, these pH values were suitable for their application on the intact skin but also on lesions. In fact, according to literature, the formulations for damaged skin animals needs pH values between 5.0 and 8.0, while optimal pH for intact skin appears to be between 5.0 and 5.5 *(Tsukada K, 1992; Wilson I, 1979)*.

28.5. Viscosity evaluation of the hydroxyethyl cellulose hydrogel formulations

The ability of the hydrogel formulations to adhere onto the skin is a prerequisite for topical and consequently transdermal delivery, for which is required an essential evaluation of their rheological properties *(Zhang Y, 2018a; Risaliti L, 2018)*. The apparent viscosity of the control (blank hydroxyethyl cellulose hydro- gel, HEC-hydrogel), and of the three vesicles (KL, KA8 and KA10) loaded in the hydrogels was measured at 25 ± 0.5 °C (Figure 1A). The rheograms represent values of shear stress (viscosity) at varying rotational speed.

The obtained data showed how the presence of vesicular systems does not change significantly the viscosity of the hydrogel, both for KL and for KA8 hydroxyethyl cellulose hydrogels, while the hydroxyethyl cellulose hydrogel loaded with KA10 intensely changed the viscosity with respect of the blank hydrogel. By associating the graphs and grouping them according to the conditions in which the data were collected, the viscosity of the four formulations decreased in the following order: KA10 hydrogel, KL hydrogel, KA8 hydrogel and blank hydrogel (Figure 25A).

In addition, for low share speeds the viscosity of KA10 hydrogel was much higher (about a factor of 10) compared to that of KA8 and blank hydrogels, which were instead comparable. By contrast, for high share speeds the viscosity of all samples was comparable.

The three formulations were also tested at 32 ± 0.5 °C to simulate the temperature of human skin (Figure 25B). The viscosity measurements at 32 ± 0.5 °C were lower than those obtained at 25 ± 0.5 °C, but the curve trend was

comparable. KA10 hydroxyethyl cellulose hydrogel was the most vis- cous while the other three tested samples had similar viscosity.

The rheology graphs of blank hydrogel, compared with the hydrogels of KL, KA8 and KA10 at the two tested temperatures (25 ± 0.5 °C and 32 ± 0.5 °C), at time zero and after 35 days of storage, are reported in Figure 26A–D. The viscosity of the formulations decreased when the shear speed increased and *vice versa*. Specifically, at time zero the viscosity of the blank hydrogel, measured at 25 ± 0.5 °C, rapidly decreased when the value of the shear speed increased. By contrast, after 35 days of storage, the viscosity assumed an almost linear trend (Figure 26A).

The KL three graphs showed similar trends to the KA8 and KA10 graphs but with higher values of viscosity (Figure 26B). The analysis of the three KA10 viscosity graphs, evidenced that the increase of the shear speed led to a rapid decrease of the viscosity values. The three graphs differ slightly and their trend was rather similar (Figure 26D). The curves of KA8 samples showed different trend with respect to the KA10 samples, very similar to the blank hydrogel (Figure 26C).

After 35 days of storage, blank hydrogel and KL hydrogel had a viscosity five times lower with respect to the beginning. Furthermore, the viscosity of KA8 hydrogel was four times lower, while the viscosity of KA10 hydrogel was about a half. These data clearly demonstrated that KA10 hydrogel were the most stable formulation.

The rheological analysis indicated that all hydroxyethyl cellulose hydrogels can be described as non-Newtonian fluids with a pseudoplastic shear thinning behaviour according to the Herschel-Bulkley equation *(Tsukada K, 1992; Wilson I, 1979; Dragicevic N, 2019)*. In addition, the upward and downward flow curves were completely overlapped, describing a non-thixotropic behaviour. According to literature, a constant decrease of viscosity indicated a continual loss of polymer entanglement upon increasing shear stress, with shear-thinning behaviour. Shear-thinning is a desirable property of semisolid dosage forms, since they should be "thin" during application and "thick" otherwise. The curves also showed a plastic behaviour of the hydroxyethyl cellulose hydrogels, indicating that the hydroxyethyl cellulose hydrogel network exhibited resistance to an external force *(Tsukada K, 1992; Wilson I, 1979; Dragicevic N, 2019)*. This shear thinning behaviour can be ascribed to the instant arrangement of the hydrogel network structure into layers which can flow in the direction of shear and, as a

consequence, viscosity decreases with the increase of shear rate *(El-Ridy MS, 2018)*. From these data we can assume that KA10 hydrogel is sufficiently viscous, giving a good skin adherence and an easy application. As a consequence, KA10 hydroxyethyl cellulose hydrogel exhibited the best rheological properties for the skin application and, together to the best characteristics of the KA10 vesicles in terms of physical properties, encapsulation and penetration proper- ties through the skin, this formulation was selected among the others for further irritation and acute toxicity *in vivo* studies on rats.

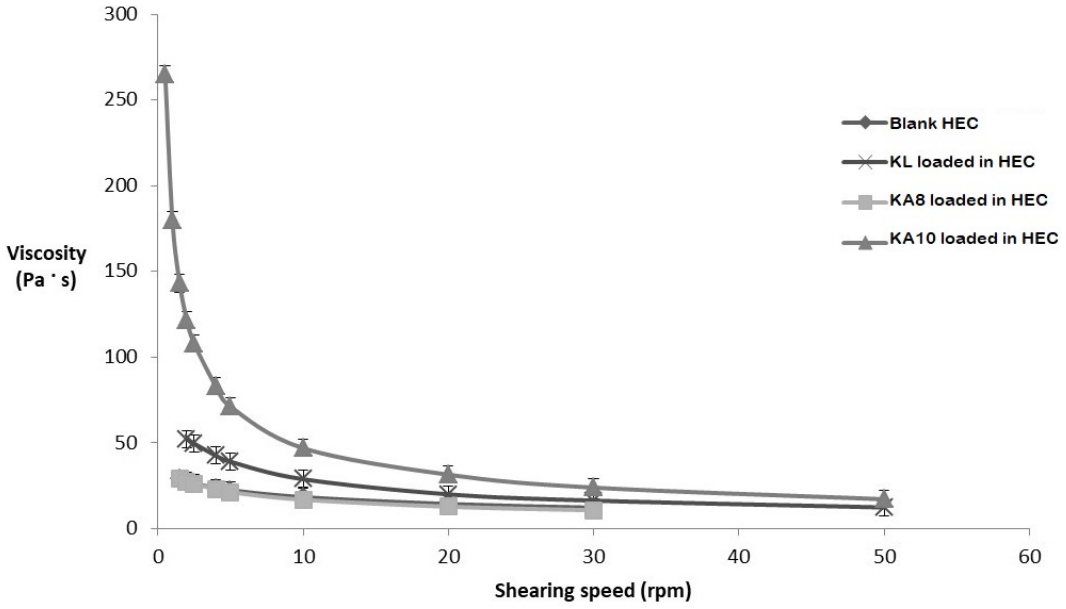

(a)

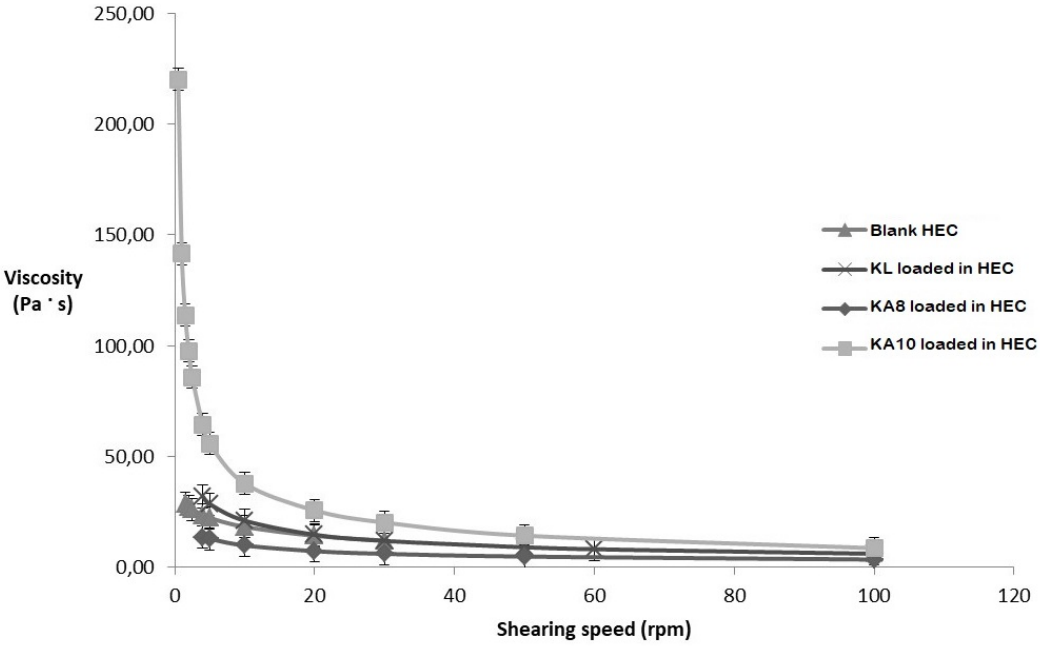

(b)

Figure 25: Rheograms of blank hydroxyethylcellulose (HEC), liposomal khellin (KL) in HEC, khellin loaded in ASC8 (KA8) and formulated in HEC, khellin loaded in ASC10 (KA10) and formulated in HEC, at 25± 0.5°C (A) and at 32± 0.5°C (B)

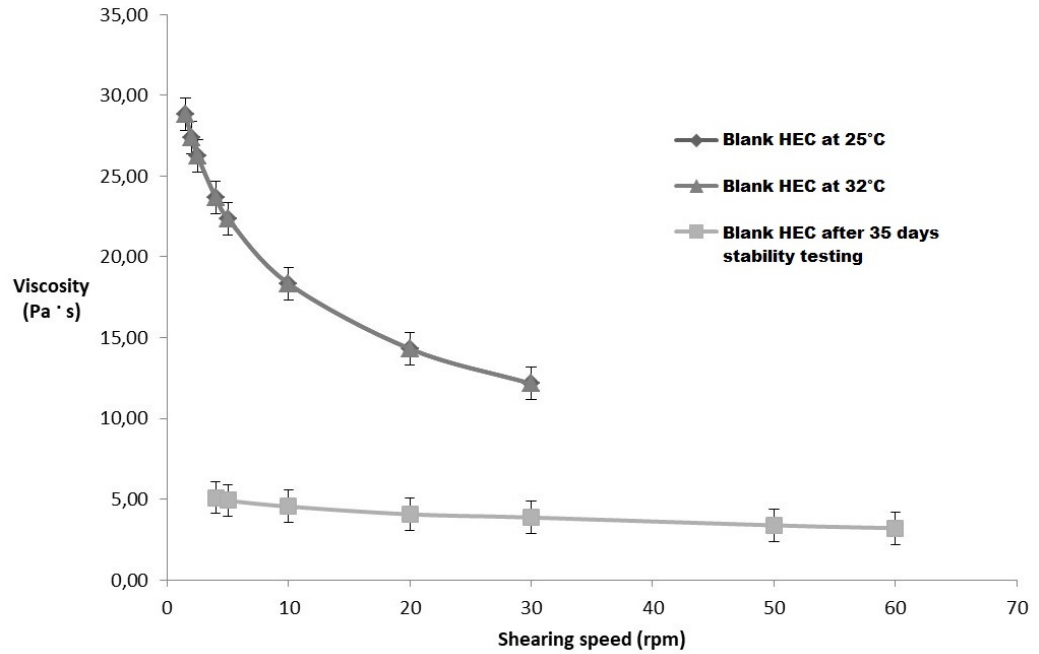

(a)

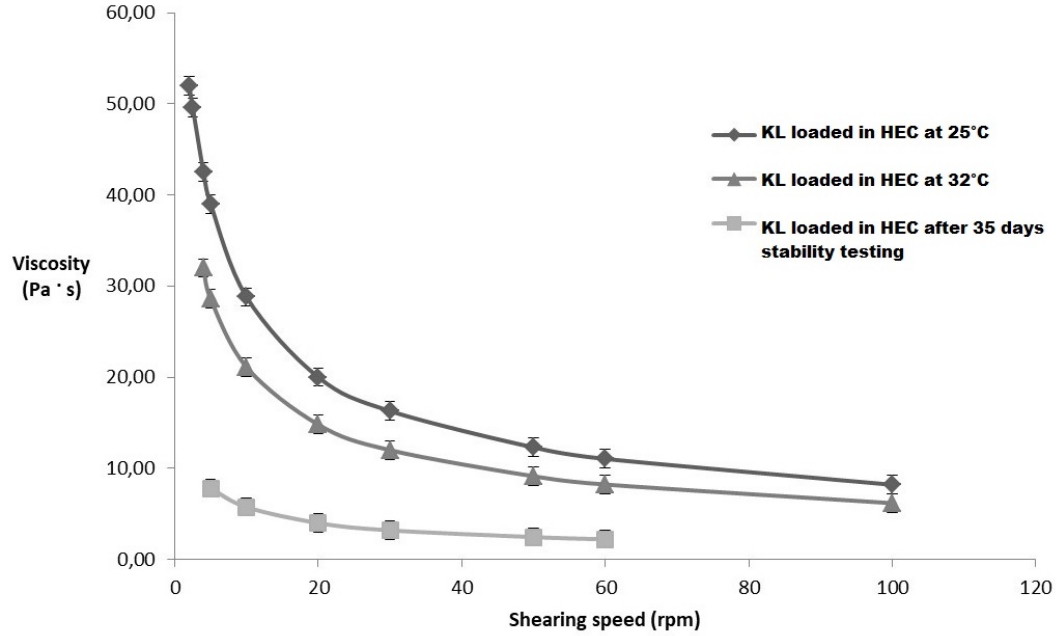
60,00
50,00
40,00
30,00
20,00
10,00
0,00
Viscosity (Pa · s)
0
20
40
60
80
100
120
Shearing speed (rpm)
KL loaded in HEC at 25°C
KL loaded in HEC at 32°C
KL loaded in HEC after 35 days stability testing

(b)

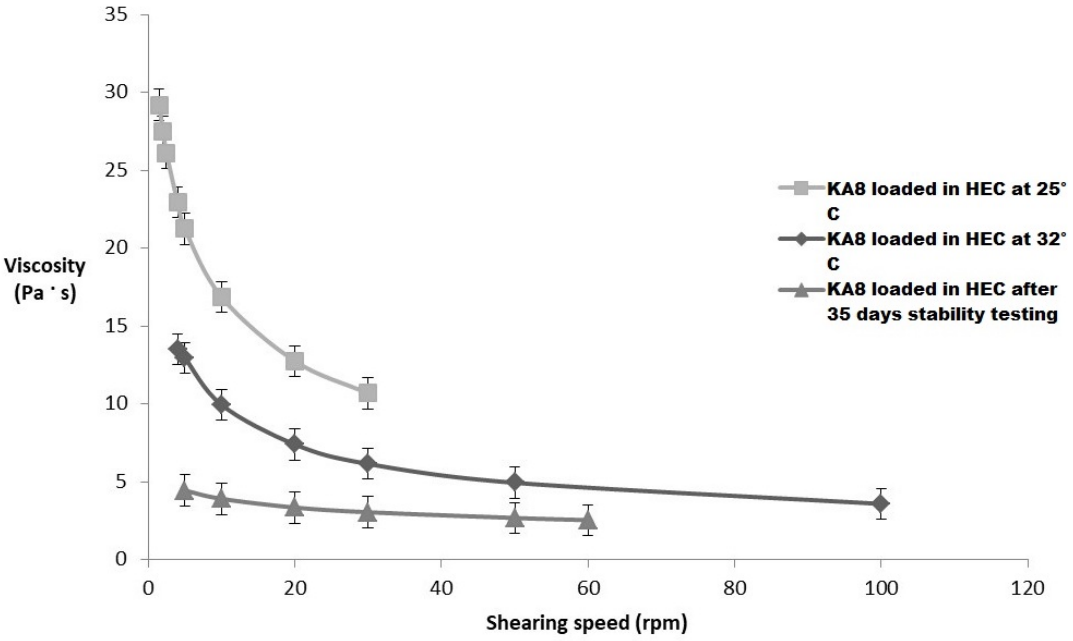
35
30
25
20
15
10
5
0
Viscosity (Pa · s)
0
20
40
60
80
100
120
Shearing speed (rpm)
KA8 loaded in HEC at 25° C
KA8 loaded in HEC at 32° C
KA8 loaded in HEC after 35 days stability testing

(c)

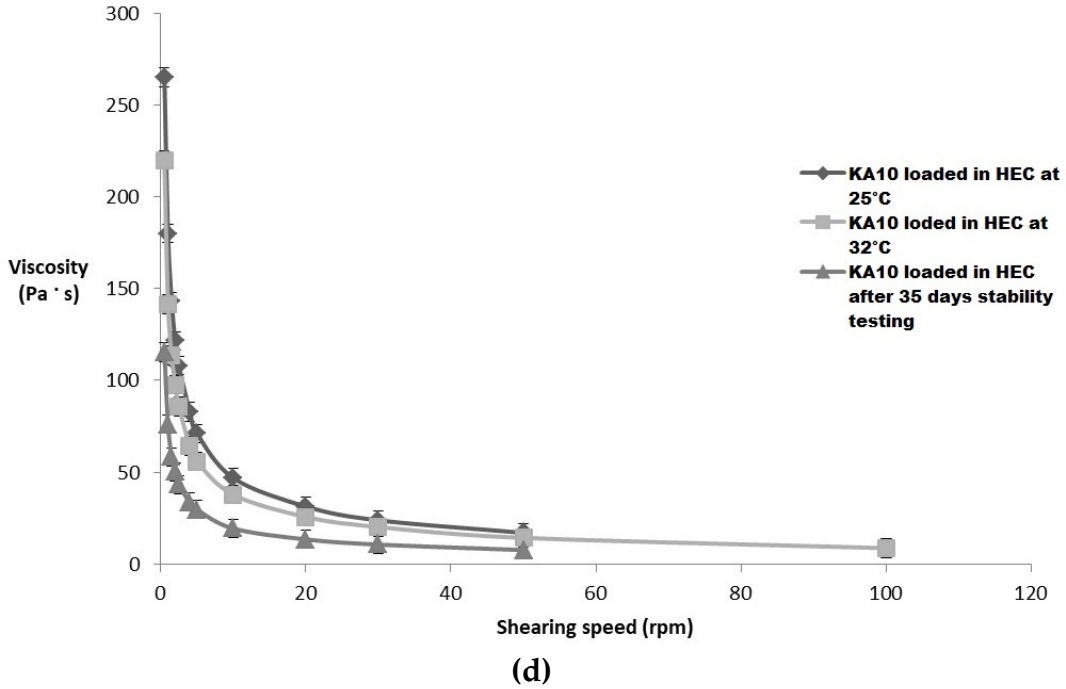

(d)

Figure 26: Rheograms of blank hydroxyethylcellulose (HEC, 2A), liposomal khellin (KL) in HEC (2B), khellin loaded in ASC8 (KA8) and formulated in HEC (2C), khellin loaded in ASC10 (KA10) and formulated in HEC (2D) at 20± 0.5°C (A), at 32± 0.5°C (B) and after 35 days stability testing.

28.6. In vivo irritation test

The following eight groups of rats were investigated: the blank groups (C & DC) to whom the blank hydroxyethyl cellulose hydrogel was administered; the khellin high-dose groups (HK & DHK) to whom high-dose of khellin dispersed in hydroxyethyl cellulose hydrogel was administered; the khellin low-dose groups (LK & DLK) to whom low-dose of khellin dispersed in hydroxyethyl cellulose hydrogel was administered; the ascosomes groups (LKP & DLKP) to whom khellin loaded in ASC10 ascosomes and gelled with hydroxyethyl cellulose hydrogel was administered. Animal behaviour and appearances changes were observed and reported in Table 21.

All the animals of the treated groups had fine mental state, well behaviour, bright hair colour and quick response. Rats' hair in khellin high-dose group (HK, DHK) tarnished after couple days of administration. Obvious resistance was also observed in those two groups, while occasional convulsion was found in HK group. High dose of khellin could cause certain irritation through external administration, however, fur appearance of the high dose groups restored to

normal 7 days after treatment-free withdrawal period. Figure 27 clearly indicated that the irritation of khellin on rats was reversible.

Table 21. Behaviour observation of rats in irritation test.

Group	Skin	Hair	Eye	Behaviour
C	√	√	√	√
DC	√	√	√	√
LKP	√	√	√	√
DLKP	√	√	√	Occasionally scratch
LK	√	√	√	Occasionally scratch
DLK	√	√	√	√
HK	√	Hair tarnish after 3 days	√	Poor compliance with occasional convulsion wit
DHK	√	Hair tarnish2 days after	√	Poor compliance

Normal behaviour is marked as √

[a] Groups were labelled as follows: normal skin control group (C); damaged skin control group (DC); normal skin group treated with hydrogel of khellin-loaded ASC10 ascosomes (LKP); damaged skin group treated with hydrogel of khellin-loaded ASC10 ascosomes (DLKP); normal skin group treated with hydrogel containing low dose khellin (LK); dam- aged skin group treated with hydrogel containing low dose khellin (DLK); normal skin group treated with hydrogel containing high dose khellin (HK) and damaged skin group treated with hydrogel containing low dose khellin (DHK).

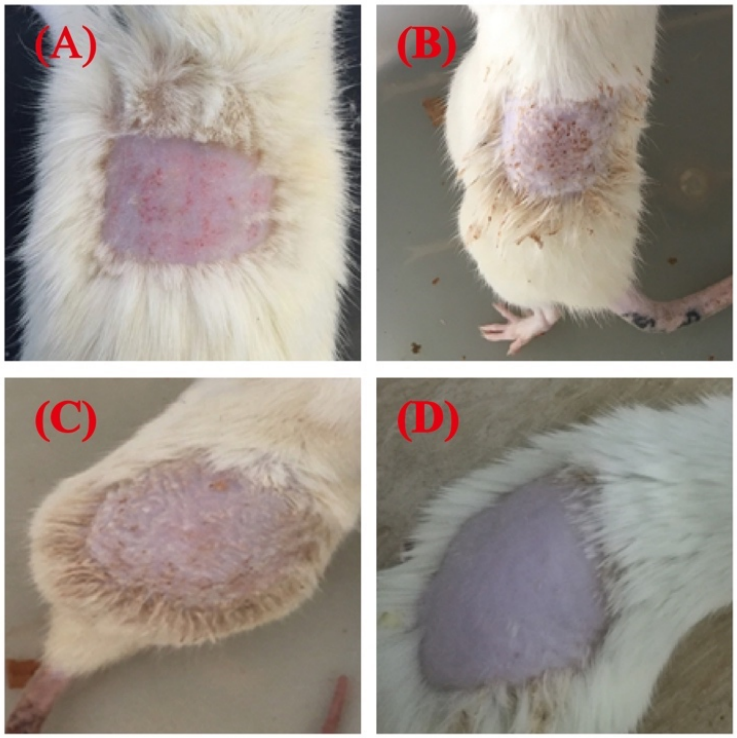

Figure 27: Rats skin appearance on 1st, 4th and 7th day of acute toxicity test. A) DC group Day1; (B) DHK group Day1; (C) DHK group Day4; (D) DHK group at Day7 of withdraw period.

28.7. Acute toxicity study

Khellin is reported to have certain liver toxicity in rats after oral administration, with a LD_{50} of 80 mg/kg of body weight *(Vrzal R, 2013)*. However, no toxicity of khellin after dermatological administration has been reported to the best of our knowledge. In order to check the

possible hepatic damage of khellin for its transdermal preparation in external administration, the acute toxicity test of khellin at high and low-doses using animals with intact skin and damaged skin was carried out, using the same administration method as the irritation test. After 7 days of administration, no death was found in any group. The results of body weight changes were given in Table 22 and Figure 28A. Body weight change is a one of the most direct evidence of drug toxicity. The body weights in all groups were increased during test period, although no significant difference was shown between khellin administered groups and the control group (Figure 28C). Meanwhile, the body weight gain in damaged skin groups and intact skin groups had no statistical difference ($p > 0.05$). Acute weight gain of liver could be attributed to liver injury, which would lead to hepatomegaly or hepatic fibrosis. Liver index from intact skin and damaged skin groups all increased after 7 days. As shown in Figure 28B, Liver index of HK ($p < 0.05$) and DLKP ($p < 0.01$) had statistical difference comparing with that of control group. Certain degree enhancement of liver/body ratio in rats with damaged skin indicated that exposed subcutaneous tissue contacted directly with khellin because of the rather high amount of khellin administered in the case of HK (100 times higher than the clinical dose) and high permeation ability for DLKP (ASC10 vesicles used in damaged skin). The effect of HK group on liver, at a dose 100 times higher than the clinical dose of khellin in DLKP group, was further investigated.

Table 22. Rat body weight, weight gain, liver ratio change (Mean ± SD, n=5).

Group	Initial weight (g)	Body weight after 10 days (g)	Weight gain rate (%)	Hepatic body ratio change
C	194.30±22.63	222.60±43.42	12.03±6.99	3.22±0.09
DC	192.73±3.24	219.50±23.06	11.57±7.98	3.04±0.15
LKP	188.70±7.74	231.60±11.00	17.17±6.64	3.91±0.18
DLKP	190.82±7.13	228.18±16.79	17.37±5.34	4.55±0.79
LK	194.92±8.83	227.28±12.18	14.10±1.30	3.28±0.40
DLK	196.62±2.69	214.50±2.55	8.09±1.16	3.52±0.48
HK	187.12±7.34	199.18±13.41	5.72±7.16	4.15±0.62
DHK	195.44±7.62	217.83±13.05	10.21±7.24	3.73±0.15

[a] Groups were labelled as follows: normal skin control group (C); damaged skin control group (DC); normal skin group treated with hydrogel of khellin-loaded ASC10 ascosomes (LKP); damaged skin group treated with hydrogel of khellin-loaded ASC10 ascosomes (DLKP); normal skin group treated with hydrogel containing low dose khellin (LK); damaged skin group treated with hydrogel containing low dose khellin (DLK); normal skin group treated with hydrogel containing high dose khellin (HK) and damaged skin group treated with hydrogel containing low dose khellin (DHK).

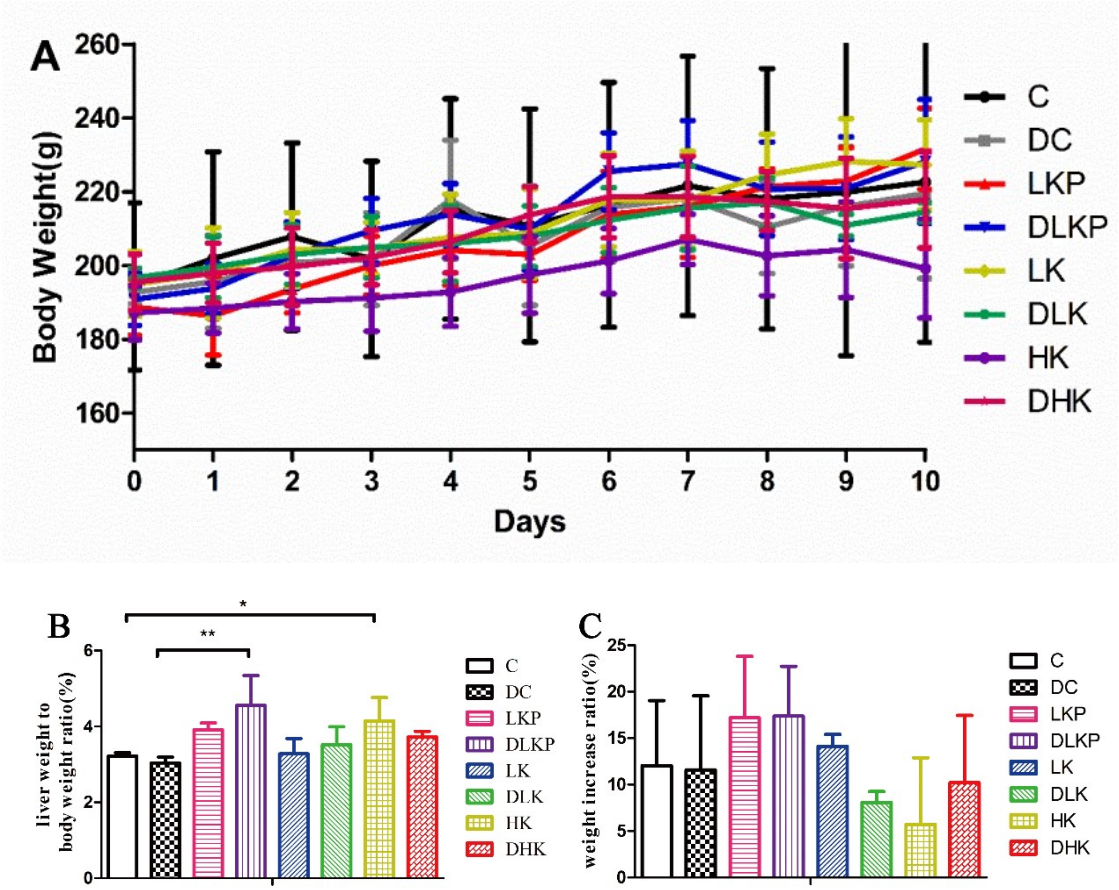

Figure 28: (A) Body weight changes of rats in acute toxicity test (Mean ± SD, n=5); (B) Liver index/liver weight to body weight ratio (Mean ± SD n=5); (C) Rat weight growth rate (Mean ± SD, n=5). * is $p < 0.05$; **is $p < 0.01$; ***is $p < 0.001$.

28.8. Biochemical analysis of plasma and tissues parameters

28.8.1. Evaluation of serum ALT, AST and AKP

ALT and AST are the most significant parameters for liver function and hepatotoxicity. Since ALT are mainly present in the plasma of hepatocytes *(Ozer J, 2008; Mohebbati R, 2018)*, an abnormal increase of ALT amount (more than 200 U/L) can be considered nonspecific, while a value higher than 400 U/L would be

related to hepatocyte membrane damage *(Shu N, 2016; Shivaraj G, 2009)*. From the data shown in Figure 29A, it can be seen that the ALT values remained stable within the normal ranges; therefore, no hepatic toxicity attributable to these enzymatic values was found. However, DLKP formulations administered in the damaged skin animals gave a significantly increase of ALT, when compared with the data found for DC group.

Regarding AST level, generally, levels dozen times of the upper limit (range 0–35 U/L) represent abnormal liver function *(Van Swelm RP, 2014)*. Moreover, the AST values significantly decreased ($p < 0.001$) after administration of

khellin by using ascosomes that demonstrated a protecting activity of 2KA10 hydrogel over the liver enzyme (Figure 29B).

In addition, the increase of AKP also reflected injury on hepatobiliary membrane *(Mohebbati R, 2018; Vijayakumar K, 2018)*. The content of AKP in plasma is usually used as a di- agnostic index of cholestasis, primary biliary cirrhosis and chronic hepatobiliary diseases. There was no significant difference in AKP content among all experimental groups and two control groups (Figure 29C). It's assessed that AKP values were not significantly modified from khellin.

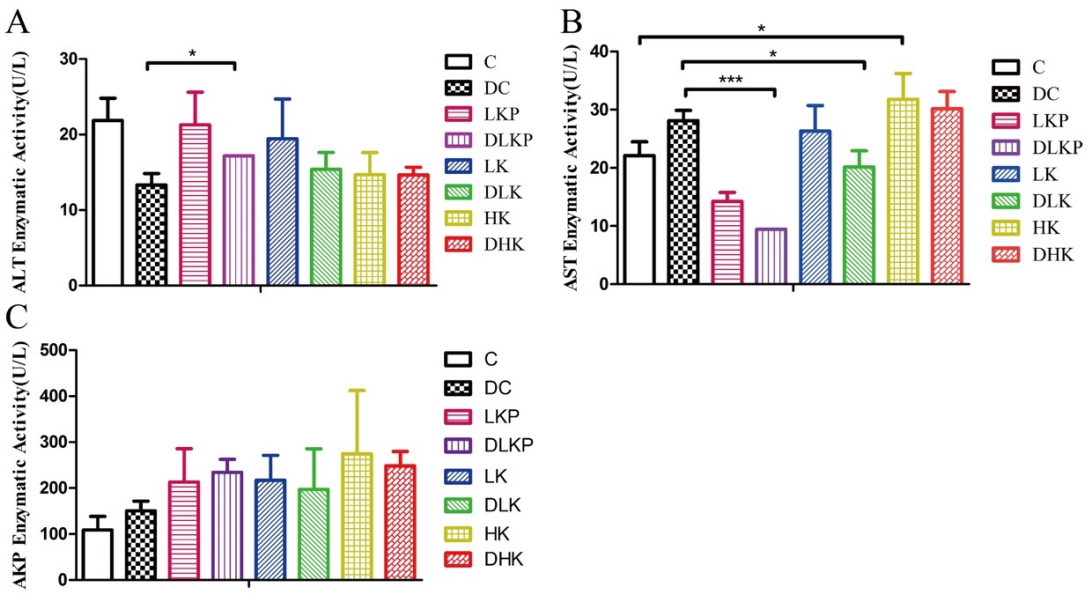

Figure 29: Amount of ALT, AST and AKP in serum (A) amount of ALT in serum; (B) amount of AST in serum; (C) amount of AKP in serum. *is $p < 0.05$; ** is $p < 0.01$; ***is $p < 0.001$.

28.8.2. Evaluation of serum T-CHO, TG, LDL-C and HDL-C

The changes of T-CHO, TG, LDL-C and HDL-C amount in serum were shown in Figure 30. Liver is the regulating organ in lipid metabolism pathway. The amount of lipoproteins in serum had an auxiliary role in the diagnosis of hepatobiliary diseases. The liver injury forms the accretion of abnormal quantities of fats, mainly TG in parenchymal cells. The accumulation of TG can be thought of resulting from an imbalance between the speed of synthesis and release of TG through the parenchymal cells into the systemic circulation. Elevated plasma TG levels might have been partially due to abnormal function of lipoprotein lipase *(Wang YQ, 2018)*. In this study, the TG values of LKP and DLKP groups evidenced a significant ($p < 0.01$) decrease respect to the control group leading to a slight hypolipidemic effect in mice (reduction of 1/3 in values) performed by KA10 hydrogel. The ability to reduce serum TG level might be due to the optimal activity of serum lipoprotein lipase and the antioxidant effect of the loaded ascosomes.

Elevated levels of LDL-C and reduced level of HDL-C demonstrated liver damage as the one produced by CCl4 in the study of Vijayakumar and coworkers *(Vijayakumar K, 2018)*. In this study both levels of LDL-C and HDL-C significantly decreased ($p < 0.01$) especially in DLKP group (enhanced permeation, thus enhanced effect of ASC10 and khellin), however, in both cases, the values were already much lower in control group (0.4 and 4 mM for LDL-C and HDL-C, respectively). For both the values of LDL-C and HDL-C from DLKP group were halved respecting to the control group (Figure 30C and D). Moreover, results described how the total cholesterol content (T-CHO) of each group was decreased in either intact or damaged skin conditions (Figure 30A).

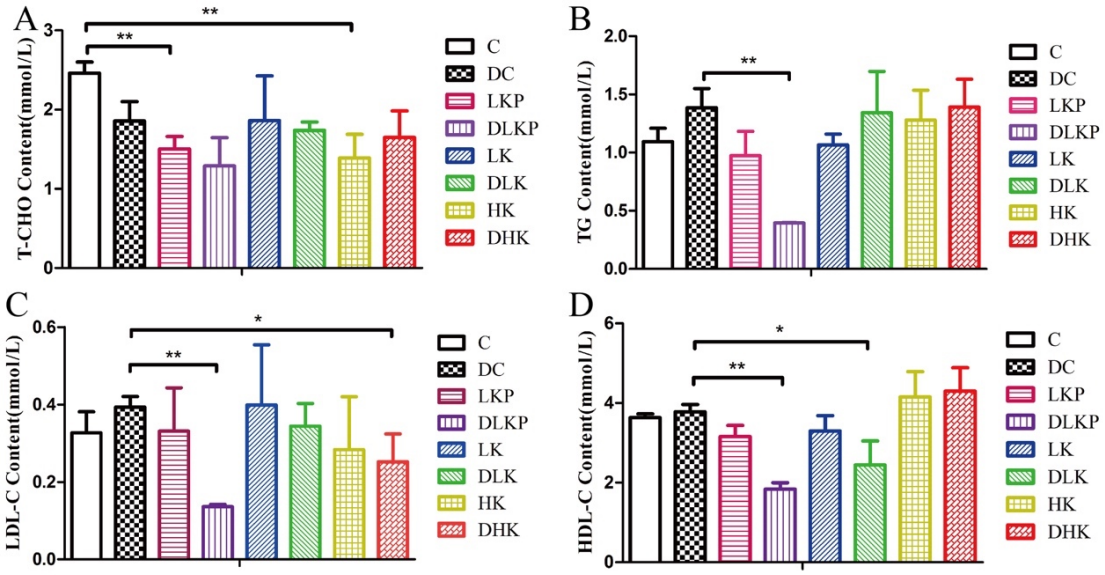

Figure 30: T-CHO, TG, LDL-C and HDL-C in serum (A) T-CHO amount in serum; (B) TG amount in serum; (C) LDL-C amount in serum; (D) HDL-C amount in serum. *is $p < 0.05$; **is $p < 0.01$; *** is $p < 0.001$.

28.9. Oxidative damage index in hepatic tissue

T-SOD, MDA, CAT and GSH-Px content in hepatic tissue was showed in Figure 31. Oxidative stress injury could be found commonly in different processes of liver injury. Inhibition of ROS generation and lipid peroxidation were crucial to hepatoprotective effect *(Zhang C, 2018)*. As metabolism byproducts, mainly composing of oxygen free radicals, peroxides and hydroxyl free radicals, they could be eliminated effectively by redox reaction under normal physiology circumstances. The balance of active oxygen in liver is maintained by enzyme (T-SOD, CAT and GSH-Px) and non-enzyme system (GSH, vitamin E and carotene), *(Samarghandian S, 2017)*. The de- crease of activity of T-SOD would increase the production of oxygen free radicals, thus damaging the structure and function of cell membrane. The change of T-SOD content can indirectly reflect the degree of tissue damage *(Zhang C, 2018; Khattab H, 2015)*. After T-SOD disproportions oxygen free radicals into peroxides, GSH-Px and other enzymes can decompose water and oxygen and complete the scavenging process of active oxygen. Therefore, the changes of GSH-Px activity in blood and liver can reflect the degree of oxidative damage to a certain extent *(Liu YH, 2018; Turna G, 2011)*. CAT can decompose hydroxyl radicals, interact with T-SOD, disproportion oxygen radicals into hydrogen peroxide, and reduce the damage to cells. The

concentration of CAT is an effective index to oxidative damage of hepatotoxicity *(Liu YH, 2018)*. MDA is a kind of lipid peroxide formed by the oxidation of polyunsaturated fatty acids in cell membrane by free radicals. It could destroy cell membrane, increase the permeability and decrease the fluidity of cell membrane, and lead to the injury of tissue and cell. Therefore, the content of MDA can reflect the degree of lipid peroxidation in the body, and indirectly reflect the degree of hepatotoxicity damage *(Liu YH, 2018; Turna G, 2011)*. In the study, there was no significant difference in liver oxidative damage between experimental groups and corresponding controls, in both intact skin and damaged skin groups. The results showed that khellin and its preparation did not affect the scavenging process of oxygen free radicals in liver tissue, and cause no oxidative damage.

It can also be proven from the HE staining slices that the hepatic tis- sue in all groups appeared dark red. Neither inflammation nor necrosis of hepatocytes was found (Figures 32 and 33). Structures of liver lobules, hepatic sinuses were complete and clear, while liver cords were in regular arrangement with radial distribution. Although slight vacuoles were occasionally found in the cytoplasm of hepatocytes in LKP group, HK group and DHK group, which may accused by hepatocyte oedema. It is also indicated that khellin and its preparations have no obvious hepatoxic effect by means of transdermal drug administration.

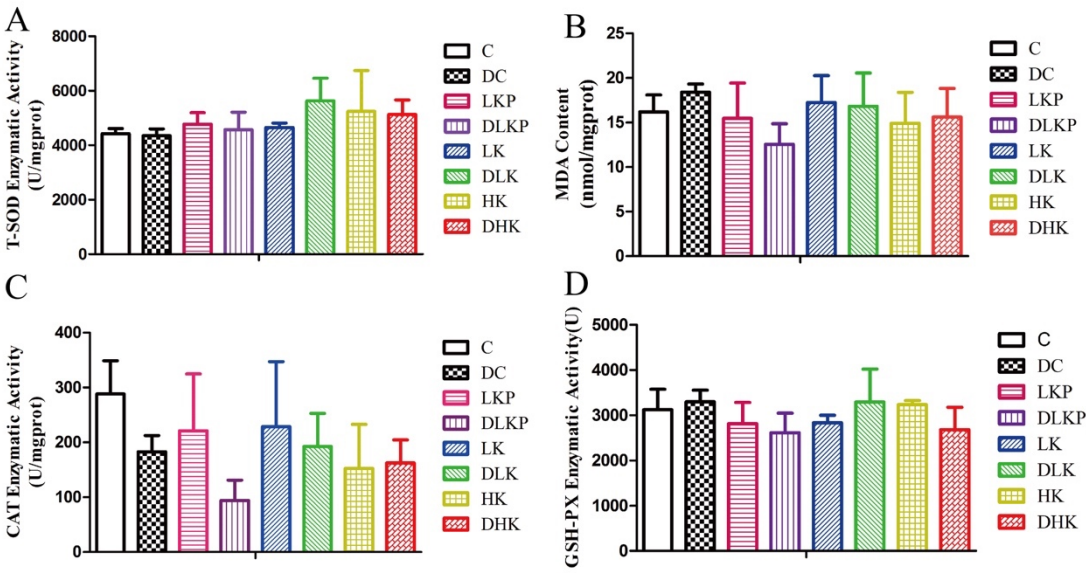

Figure 31: Oxidative damage index in hepatic tissue (A) T-SOD amount in liver; (B) MDA amount in liver; (C) CAT amount in liver; (D) GSH-Px amount in liver. *is $p < 0.05$; **is $p < 0.01$; *** is $p < 0.001$.

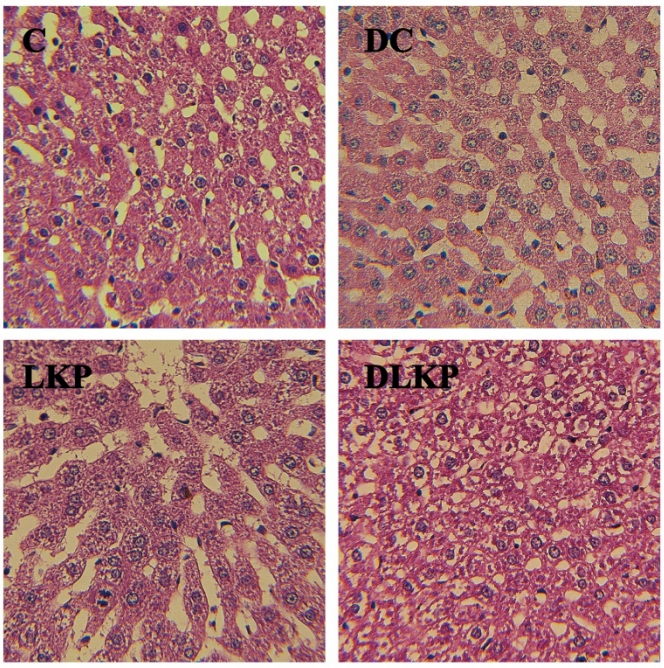

Figure 32: Liver tissues images for C-DC-LKP-DLKP groups (×40).

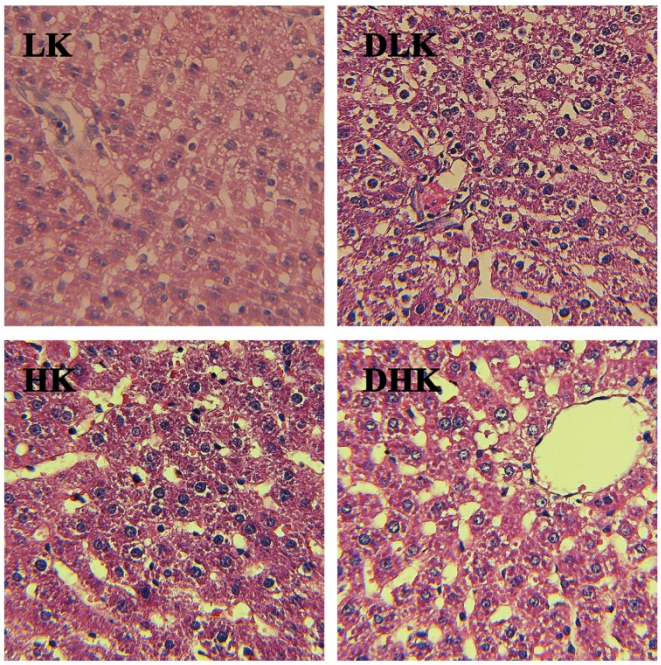

Figure 33: Liver tissues images for LK-DLK-HK-DHK groups (×40).

28.10. Dermal-pathological analysis

It was observed (Figure 34) that the surface layer of dermal tissue was quite complete, while the basal layer, cell layer, granular cell layer and keratinized layer were uniform and clear. The sebaceous glands and hair follicles were clearly visible. Comparing with control groups, less sebaceous glands and hair follicles were found in DC group, LKP group and DLKP group, respectively. Besides, there was no obvious damage in the tissues from LKP and DLKP groups.

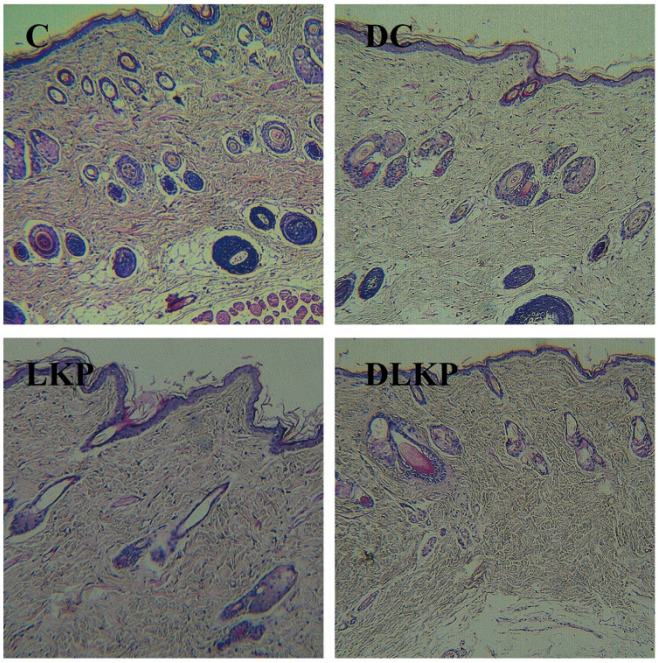

Figure 34: Dermal pathological images for C-DC-LKP-DLKP groups (×10).

GLYCEROSOMES OF *MELISSA OFFICINALIS* L. ESSENTIAL OIL FOR EFFECTIVE ANTI-HSV TYPE 1

29. Results and Discussion

29.1. Chemical analysis of MEO by Gas Chromatography–Mass Spectrometry (GC–MS)

A commercial MEO from Chiron Kentauros was analysed by GC-MS, in order to evaluate the qualitative and quantitative composition (Table 23).

Table 23. *Melissa officinalis* essential oil (MEO) chemical composition obtained by Gas Chromatography–Mass Spectrometry (GC-MS) analysis. Data represent single compound percentages (%).

CONSTITUENTS	%
1-Octen-3-ol	0.30
Methyl heptenone	1.88
Limonene	0.04
cis-Ocimene	0.05
trans-Ocimene	0.37
Linalool	0.51
cis-Rose oxide	0.11
exo-Isocitral	0.49
α-*trans*-Necrodol	0.56
Citronellal	4.31
(E)-Isocitral	1.75
4-*trans*-Caranone	2.62
Citronellol	0.19
Nerol	0.20
Neral	27.31
Geraniol	0.18
Methyl citronellate	0.28
Geranial	36.73
Methyl geranate	0.34
α-Copaene	0.15
β-Bourbonene	0.14
β-Cubebene	0.06
β-Elemene	0.14
β-Caryophyllene	14.85
α-Humulene	0.76
Germacrene D	1.55
α-Muurolene	0.05
γ-Cadinene	0.06
δ-Cadinene	0.14

Caryophyllene oxide	1.09
Total identified constituents	97.21

The obtained results were consistent with the data reported in the literature *(ESCOP, 2013)*. Thirty constituents were unambiguously identified, and they represented 97.21% of total MEO. Two monoterpenes, geranial and neral, and a bicyclic sesquiterpene, β-caryophyllene, were found to be the main constituents of MEO, representing 36.73%, 27.31% and 14.85%, respectively, of the total constituents. Indeed, geranial is also called citral A and it is the trans-isomer, while neral is called citral B and it is the cis-isomer.

29.2. Vesicle preparation and physical characterization

As a first step of our investigation, MEO was formulated in liposomal vesicles using P90G and cholesterol in different ratios in order to optimize the formulation in terms of vesicle average size and homogeneity. However, after adding 5, 10 or 25 mg/mL of MEO, the vesicles were hardly reproducible and poorly stable, with frequent essential oil separation. Therefore, a slightly different approach was adopted to formulate MEO. Glycerosomes, vesicles containing glycerol, were formulated and loaded with MEO. Briefly, the lipid film, composed of P90G and cholesterol, was hydrated in different conditions using a 10% *v/v* glycerol/water solution. MEO (10 mg/mL) was loaded in glycerosomes, optimizing the experimental conditions of preparation, as reported in the experimental section. All the samples were analysed by light scattering techniques in order to select a homogeneous and stable formulation, with nano-sized vesicles. *Melissa officinalis* essential oil-loaded glycerosomes (MEO-GS), obtained with P90G plus cholesterol (60:1) and loaded with 10 mg/mL of MEO, had small dimensions, low Polydispersity Index (PdI) score and good ζ-potential after the hydration process (Table 24), therefore no additional optimization, for example by ultrasonication probe or extrusion, was necessary. In addition, TEM analysis showed the morphological features of MEO-GS, characterized by spherical shape vesicles with several lamellae (Figure 35).

Table 24. Physical parameters of *Melissa officinalis* L. essential oil-loaded glycerosomes (MEO-GS). From left: Size, polydispersity index (PdI) and ζ-potential. Mean±SD (n = 3).

Sample	Size (nm)	PdI	ζ-potential (mV)
MEO-GS*	83.09±5.04	0.20±0.05	-27.85±4.03

* MEO-loaded glycerosomes

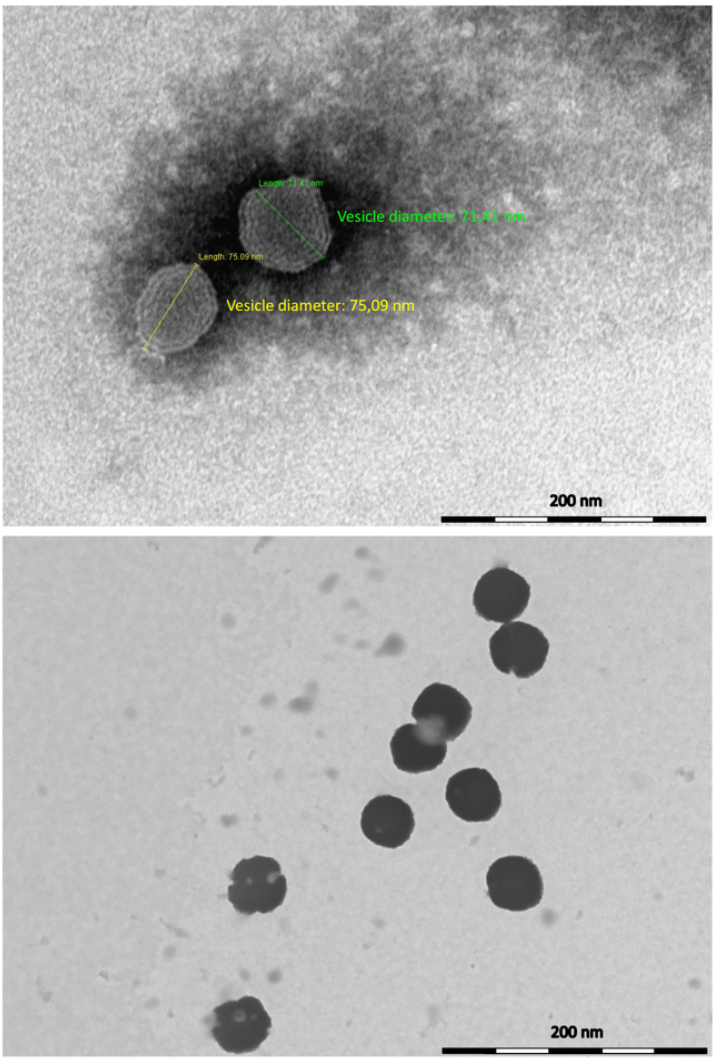

Figure 35. Images of *Melissa officinalis* essential oil-loaded glycerosomes (MEO-GS) obtained by Transmission Electron Microscopic (TEM) analysis.

29.3. Encapsulation efficiency (EE%) and recovery (R) of MEO-GS

Moreover, encapsulation efficiency (EE%) and recovery (R%) of MEO loaded in GS were evaluated by HPLC-DAD and not by GC-MS because of the aqueous medium of vesicles. Due to the complexity of the chemical constituents of MEO,

marker constituents were chosen in order to evaluate the loading of MEO in glycerosomes. Selection of markers was made on the basis of the most representative constituents in terms of percentage, suitability of UV absorbance for an easy detection by DAD and their availability on the market as standard constituents. Accordingly, both β-caryophyllene (about 15%) and citral (about 64%) were selected as markers. In particular, citral is the mixture of the two geometric monoterpene isomers geranial and neral.

MEO recovery (R%) was expressed as percentage of citral and β-caryophyllene recovered after the preparation procedure. Notably, a slight reduction of citral and β-caryophyllene amount occurred during the vesicle preparation, probably due to their high volatility (Table 25). MEO encapsulation efficiency (EE%), in terms of citral and β-caryophyllene encapsulated inside glycerosomes, was quite high for both components, mainly considering the respective R% (Table 25).

Table 25. Chemical parameters of *Melissa officinalis* essential oil-loaded glycerosomes (MEO-GS): recovery (R%) and encapsulation efficiency (EE%) of citral and β-Caryophyllene. Mean ± SD (*n* = 3).

Sample	Citral R%	β-Car R%	Citral EE%	β-Car EE%
MEO-GS*	73.80±3.11	79.01±8.71	51.27±2.76	66.04±8.76

* MEO-loaded glycerosomes

29.4. Deformability

MEO loading inside glycerosomes did not modify the fluidity of the vesicle bilayer, maintaining glycerosome ability to squeeze through skin pores. In fact, deformability of MEO-GS was measured by extrusion process, in order to evaluate the ability of vesicles to penetrate the *stratum corneum* passing through the corneocyte pores without breaking and delivering the essential oil to the lower skin layers. MEO-loaded glycerosomes did not change sizes or homogeneity (Table 26) after the extrusion, proving an excellent deformability. This finding suggested that MEO-GS are able to regain their original form after leaving the corneocyte pores, continuing the penetration process *(Jain S, 2003)*. Therefore, the ratio of phospholipid, cholesterol and glycerol was optimal to give flexibility to the bilayer membrane, allowing MEO-GS to pass through pores smaller than their own diameter.

Table 26. Deformability measurements of different formulations; (Mean ± SD; n = 3).

Sample	Size before extrusion (nm)	Size after extrusion (nm)	PdI before extrusion	PdI after extrusion	Deformability
MEO-GS*	83.92±3.53	82.61±2.56	0.25±0.02	0.23±0.01	1.02±0.01
GS**	80.11±6.92	79.68±4.70	0.39±0.04	0.36±0.03	1.00±0.03

* MEO-loaded glycerosomes; **glycerosomes

29.5. In vitro release

In vitro release profile of MEO from glycerosomes in PBS was investigated using the dialysis bag method and it was compared with the release from a DMSO solution. After 24 h, about 24% of citral, selected as marker constituent of MEO, was released from glycerosomes, whereas 59% *ca.* of citral was released from the DMSO solution. By contrast, β-caryophyllene was never detected. The use of other release mediums, as 20% *v/v* ethanol/PBS solution, 10% *v/v* glycerol/PBS solution, 5% *v/v* DMSO/PBS solution, did not improve β-caryophyllene detection, and PBS was then selected as medium for the release studies. Although the variation of citral percentage within 24 h was comparable between glycerosomes and DMSO solution, with a slow decrease after 7 h probably due to its high volatility, an evident smaller citral release was observed for glycerosomes (Figure 36). Therefore, MEO-GS were able to control and delay MEO release, with a consequent benefit once the formulation will be applied on the skin.

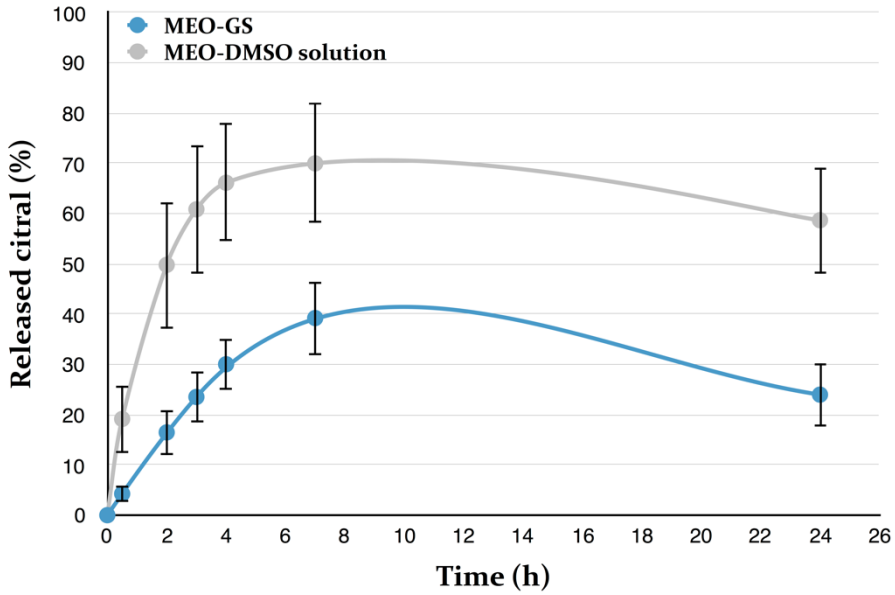

Figure 36. Citral release from *Melissa officinalis* essential oil-loaded glycerosomes (MEO-GS) and MEO-DMSO solution; (Mean± SD; *n*=3).

29.6. Stability studies

The physical and chemical stability of MEO-GS were investigated during storage of the sample for 4 months at 4 °C, protected from light. Every 30 days, size, PdI and ζ-potential were measured by DLS-ELS, whereas R% and EE% of citral and β-caryophyllene were evaluated by HPLC-DAD. Under the same storage conditions, pure MEO chemical stability was also monitored in terms of citral and β-caryophyllene concentrations. MEO-GS showed excellent physical stability, because sizes and PdI remained unchanged during storage (Figure 37A), whereas the ζ-potential constantly, but slightly, become more and more negative (Figure 37B). This variation was not considered a negative effect because high negative values of charge distribution have positive effects on vesicle stability. Stability of stored MEO in terms of the marker constituents' citral and β-caryophyllene was also evaluated.

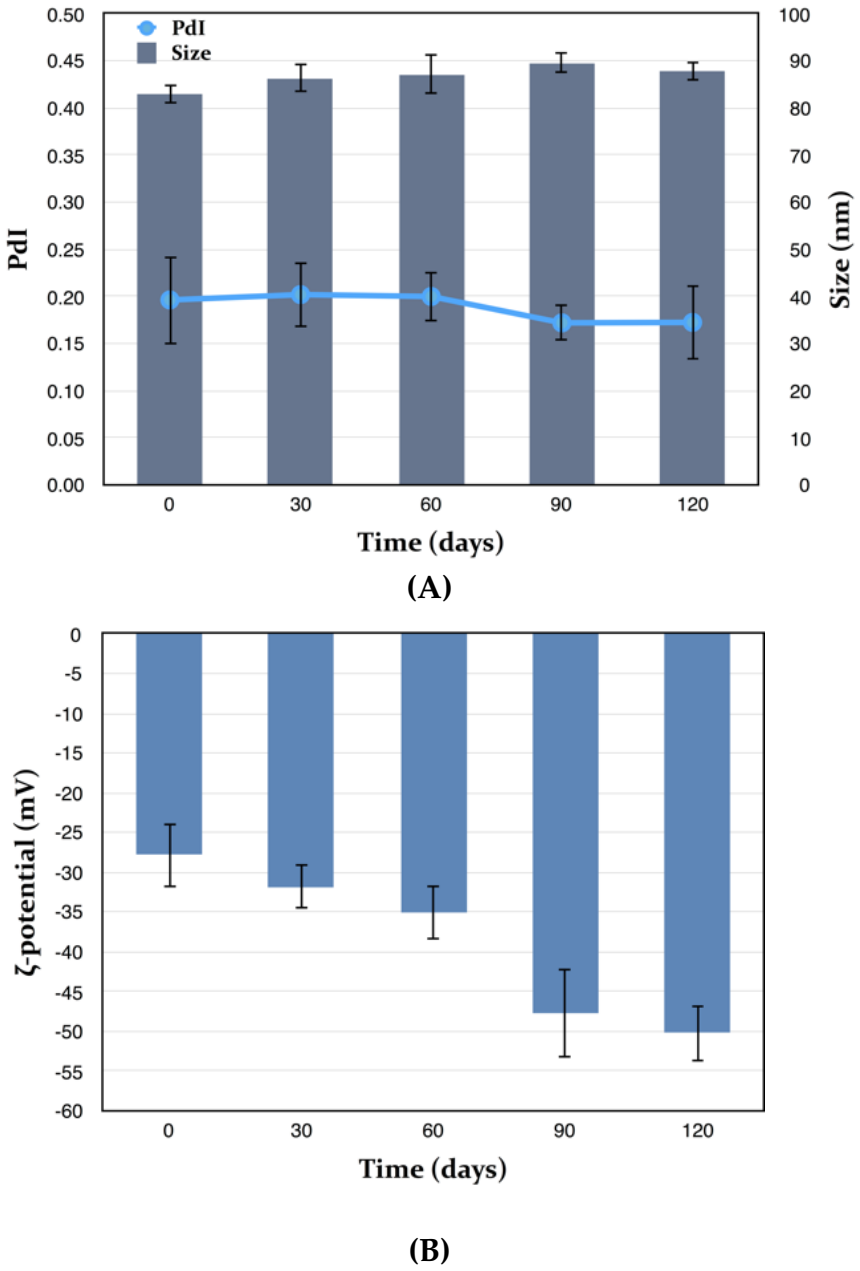

Figure 37. Physical stability of *Melissa officinalis* essential oil-loaded glycerosomes (MEO-GS) during 4 months storage. Size (nm) and PdI [**A**], ζ-potential (mV) [**B**]; (Mean ± SD; *n* = 3).

Pure MEO showed a very low stability of constituents. β-Caryophyllene was detectable in trace amounts after one month of storage. Citral content greatly decreased during storage, and about 59% of citral was lost after 4 months (Figure 38).

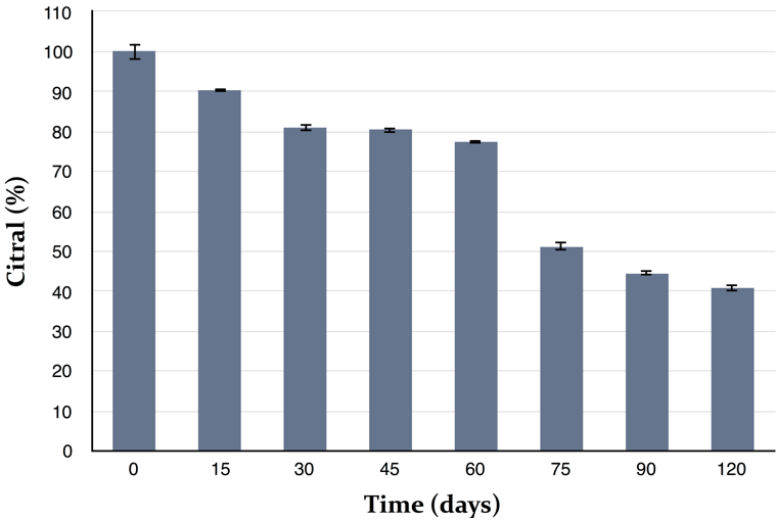

Figure 38. Chemical stability of *Melissa officinalis* essential oil (MEO), in terms of citral concentration, during 4 months storage; (Mean ± SD; *n* = 3).

By contrast, after four months of storage of MEO-GS, citral concentration decreased by approximately 23% in terms of R and by 20% in terms of EE% (Figure 39A). β-Caryophyllene concentration decreased by approximately 35% in terms of R, and by 29% in terms of EE% (Figure 39B). According to the above results, both citral and β-caryophyllene reduction during storage is much less than that observed with the pure MEO, indicating that glycerosomes can better preserve these main MEO constituents from degradation processes or reduce their volatility.

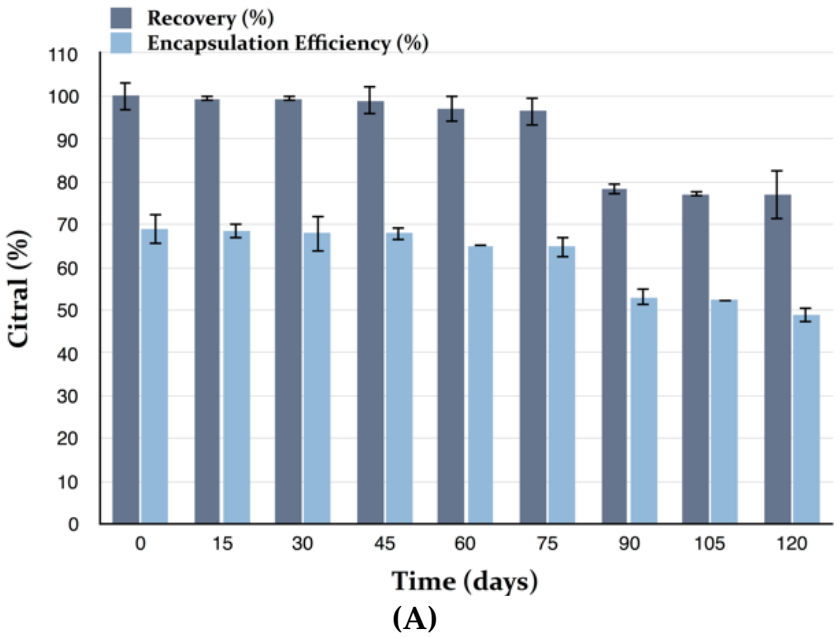

(A)

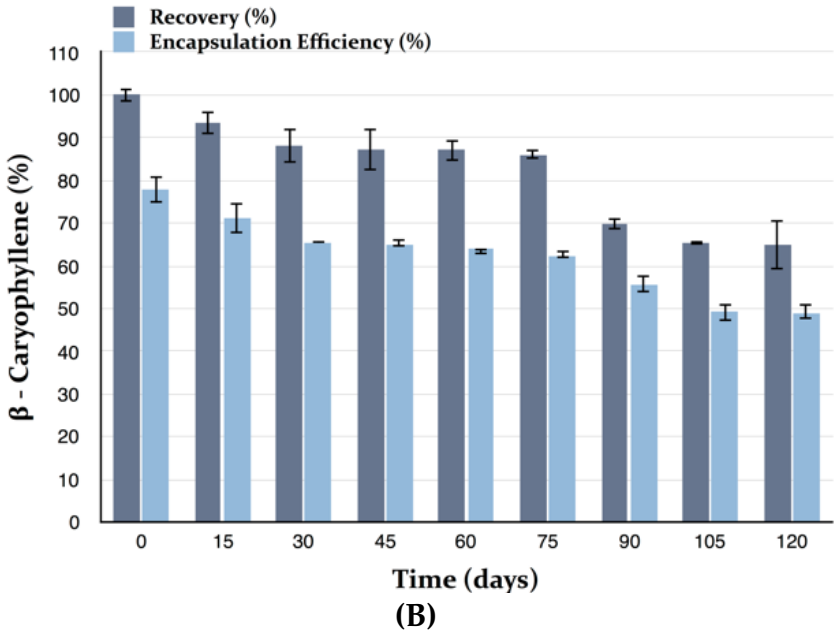

Figure 39. Chemical stability of *Melissa officinalis* essential oil-loaded glycerosomes (MEO-GS) during 4 months storage. Recovery (R%) and Encapsulation Efficiency (EE%) of MEO in terms of citral [**A**] and β-caryophyllene [**B**]; (Mean ± SD; $n = 3$).

29.7. Antiviral assays using luciferase-expressing HSV-1

Antiviral activity of MEO-GS and pure MEO was evaluated by *in vitro* assay on Vero cells. In order to accelerate the screening efforts for novel antivirals, the Department of Pharmacognosy/Pharmacology of the Aristotle University of Thessaloniki (Greece) generated an HSV-1 virus that expresses the firefly luciferase (LUC) gene under the control of the virus TK gene promoter/regulatory elements. This was achieved by substitution of the TK gene coding sequences with those of LUC. The resulting virus (vCLIDA61) expresses luciferase during the infection, with a linear relationship being observed between the amount of virus and the luciferase activity measured. The luciferase activity assays, which are easy, reproducible and very sensitive, can be used to assess virus growth and, by extrapolation, virus inhibition by antivirals, i.e. addition of an antiviral would reduce LUC expression in a dose-dependent manner. Exposure of the LUC-expressing virus (vCLIDA61) to increasing concentrations of MEO prior to and during the early stages of the infection (attachment, absorption and penetration) was found to inhibit LUC expression in a dose-dependent manner, as shown in Figure 40. The antiviral activity of MEO on cells already infected with HSV-1 could not be evaluated, since it was observed that prolonged exposure of cells to MEO produced cytotoxic effects, even at

concentrations as low as 50 μg/mL. It must be noted that such cytotoxic effects were not observed upon short cell exposure (1h) to either MEO or MEO-GS (Figure 41). The antiviral effects of glycerosomes containing MEO (MEO-GS), measured in parallel, were found to be less pronounced, except for high concentration of MEO, such as 500-600 μg/mL.

The results reported in the present study were similar, in terms of magnitude, to those of previous investigations. In particular, MEO inhibitory *in vitro* activity against HSV-1 and HSV-2 was reported on monkey kidney cells using the plaque reduction assay *(Schnitzler P, 2008)*. The IC_{50} values were 4 μg/mL and 0.8 μg/mL for HSV-1 and HSV-2, respectively. The toxic concentration for 50% of cells for HSV-1 was 30 μg/mL *(Schnitzler P, 2008)*. In a further study, MEO was tested on HSV-2 replication in HEp-2 cells. MEO was non-toxic to HEp-2 cells up to a concentration of 100 μg/mL. Strong anti-HVS-2 activity was found in the concentration range between 25 and 50 μg/mL *(Allahverdiyev A, 2004)*. In the literature, there are also a few studies concerning the activity of isolated constituents against HSV-1, namely citral and β-caryophyllene *(Astani A, 2010; Astani A, 2011)*. The maximum non-cytotoxic concentration of citral was 20 μg/mL, while the IC_{50} value was 23 μM, corresponding to about 6 μg/mL *(Astani A, 2010)*. From the literature *(Astani A, 2011)*, β-caryophyllene showed a maximum non-cytotoxic concentration of 10 μg/mL when tested on HSV-1, while the cytotoxic concentration of the drug that reduced viable cell number by 50% was 35 μg/mL. IC_{50} was determined from dose-response curves as 0.25 μg/mL *(Astani A, 2011)*. From the literature it is clear that native essential oils have higher selectivity indices rather than isolated constituents and are preferable for antiviral treatment in patients, however, citral and β-caryophyllene might be the dominant antiviral agents in MEO.

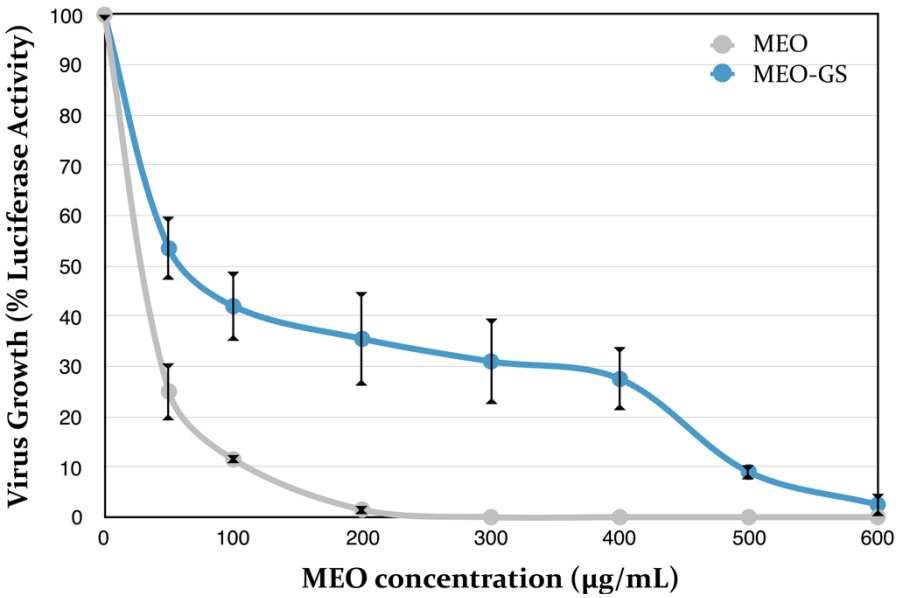

Figure 40. *In vitro* antiviral test. Effects of MEO and *Melissa officinalis* essential oil-loaded glycerosomes (MEO-GS) on the early steps of HSV-1 infection; (Mean ± SD; n = 3).

29.8. Cytotoxicity assays

The potential cytotoxic effects of MEO-GS and MEO were evaluated by performing MTT assays. Specifically, Vero cells were exposed to increasing concentrations of MEO and MEO-GS for exactly 1 hour, to mimic the conditions of exposure during the HSV-1 infection experiments. As shown in Figure 41, the observed cytotoxic effects of these short exposures to MEO and MEO-GS were minimal, even at the highest experimental concentrations (600 µg/mL).

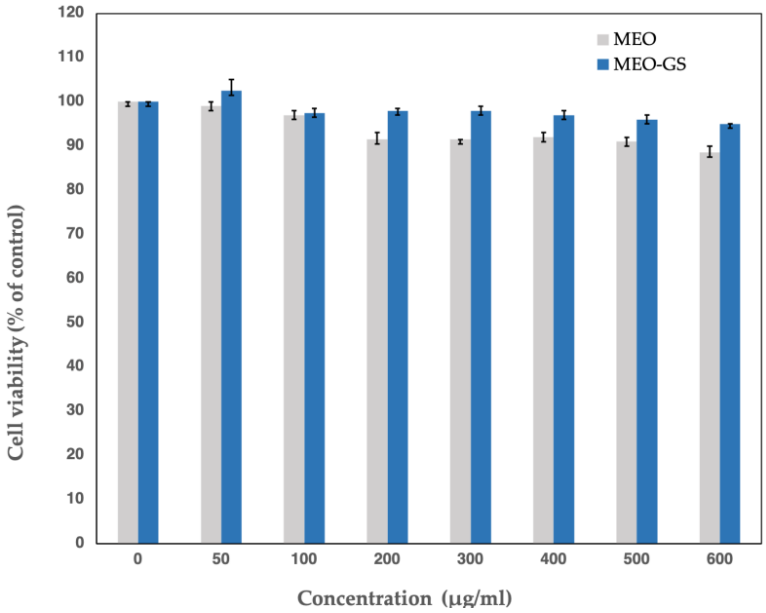

Figure 41. Cytotoxicity assays. Effects of short-term exposure (1h) of Vero cells to *Melissa officinalis* essential oil-loaded glycerosomes (MEO-GS) and pure MEO on their viability; (Mean ± SD; $n = 3$).

NANOVESICLES LOADED WITH *ORIGANUM ONITES* AND *SATUREJA THYMBRA* ESSENTIAL OILS L. AND THEIR ACTIVITY AGAINST FOOD-BORNE PATHOGENS AND SPOILAGE MICROORGANISMS

30. Results and Discussion

30.1. Chemical composition of OOEO and STEO

The yield (*v*/*w*) of the EO obtained from *O. onites* (OOEO) was 3.0%. Overall, thirty-five compounds, representing 100.0% of the OOEO, were identified. In particular, the main components were carvacrol (66.0%), *p*-cymene (7.9%), γ-terpinene (4.9%) and borneol (2.8%). Furthermore, reasonable levels of β-bisabolene (2.3%), myrcene (2.1%), α-terpinene (2.0%) and terpinen-4-ol (1.7%) were also detected, while α-pinene and thymol were found in low percentages (both 1.0%), (Table 27a). Oxygenated monoterpenes (74.1%) comprised the major chemical group of the OOEO, followed by monoterpene hydrocarbons (21.2%) and sesquiterpene hydrocarbons (4.1%), (Table 27b). It is well-known that the OOEO is high rich in carvacrol content (up to 90%), *(Stefanaki A, 2016; Tasdemir K, 2019; Tepe B, 2016; Kokkini S, 2004; Economou G, 2011)*. Vokou and coworkers (1988) investigated the EOs of *O. onites*, originated from different parts of Greece, underlying the high yields of EOs from south-eastern islands (Halki, Symi and Tilos), *(Vokou D, 1988)*. Given that different OOEO chemotypes were reported based on their main volatile constituents *(Tepe B, 2016)*, our studied OOEO revealed a carvacrol chemotype. We should point out that linalool was determined in low amount (0.4%). Previous studies discussed the distinction among the *O. vulgare* ssp. *hirtum* and *O. onites*, mentioning that the EO of the latter species is poor in thymol and/or *p*-cymene, whereas its borneol content ranges more than 2.0% *(Stefanaki A, 2016, Kokkini S, 2004)*. Our findings comply with this distinction since thymol concentration was low (1.0%) and borneol was found in higher level (2.8%).

In the EO of *S. thymbra* (STEO; yield 2.8% *v*/*w*) were identified twenty-nine chemical constituents, representing 99.9% of the total amount (Table 28a). These constituents were grouped into oxygenated monoterpenes (50.0%), monoterpene hydrocarbons (41.9%), sesquiterpene hydrocarbons (7.7%), oxygenated sesquiterpenes (0.2%) and aliphatic alcohols (0.1%) (Table 28b). Precisely, the main compounds were carvacrol (46.0%), γ-terpinene (19.7%), *p*-cymene (7.6%),

β-caryophyllene (7.0%) and α-terpinene (5.1%). Other constituents in lower concentrations were myrcene (2.5%), α-thujene (2.4%), α-pinene (1.6%) and linalool (1.3%). Our results are in accordance with previous studies in EO of *S. thymbra (Skoula M, 2005; Glamočlija J, 2006; Economou G, 2011; Azaz AD, 2005)*.

Comparing the two investigated EOs, carvacrol was the dominant component, while thymol was detected in very low concentrations (< 1.0%) in both samples. We also observed that the high carvacrol (66.0%) content was related to low amount of γ-terpinene (4.9%) in the EO of *O. onites*, whereas the EO of *S. thymbra* demonstrated a relatively lower concentration of carvacrol (46.0%) followed by a high content of γ-terpinene (19.7%). This observation is congruous with a previous study *(Economou G, 2011)* and could be attributed to biosynthetic pathways, considering that γ-terpinene and *p*-cymene are biosynthetic precursors of carvacrol. In addition, the two samples presented similar chemical groups. Both plants were rich in EOs which is directly related to the distinct environmental and geographical conditions of Symi island which belongs to the Dodecanese island complex (SE Aegean region).

Table 27a. Chemical composition (% *v/v*) of *O. onites* essential oil.

No	Compounds	RI[a]	Composition (%)
1	α-thujene	920	0.8
2	α -pinene	928	1.0
3	camphene	941	0.6
4	1-octen-3-ol	970	0.4
5	myrcene	985	2.1
6	α -phellandrene	1000	0.4
7	δ-3-carene	1004	0.2
8	α -terpinene	1010	2.0
9	*p*-cymene	1017	7.9
10	β-phellandrene	1021	0.8
11	(E)-β-ocimene	1040	0.1
12	γ-terpinene	1051	4.9
13	trans-sabinene hydrate	1072	0.3
14	α -terpinolene	1083	0.4
15	linalool	1091	0.4
16	α -campholenal	1120	0.1
17	trans-pinocarveol	1132	0.1
18	borneol	1163	2.8
19	terpinen-4-ol	1171	1.7
20	α -terpineol	1183	0.6
21	carvone	1235	0.1
22	carvacrol methyl ether	1241	0.4

23	linalyl acetate	1250	0.2
24	carvenone	1253	0.2
25	thymol	1285	1.0
26	carvacrol	1300	66.0
27	carvacrol acetate	1366	0.2
28	β-cubebene	1383	0.7
29	β-caryophyllene	1414	0.7
30	aromadendrene	1435	0.2
31	ledene	1495	0.1
32	β-bisabolene	1501	2.3
33	δ-cadinene	1518	0.1
34	spathulenol	1575	0.1
35	caryophyllene oxide	1580	0.1
	Total identification		100.0

[a] RI: Retention Index calculated against C_9-C_{24} *n*-alkanes on the HP 5MS column capillary column

Table 27b. Grouped components (% *v*/*v*) of *O. onites* essential oil.

Classes of EO constituents	**% *v*/*v***
Monoterpene hydrocarbons	21.2
Oxygenated monoterpenes	74.1
Sesquiterpene hydrocarbons	4.1
Oxygenated sesquiterpenes	0.2
Aliphatic alcohols	0.4

Table 28a. Qualitative and quantitative (% *v*/*v*) composition of *S. thymbra* essential oil.

No	**Compounds**	**RI[a]**	**Composition (%)**
1	α-thujene	920	2.4
2	α-pinene	928	1.6
3	camphene	941	0.3
4	β-pinene	970	0.6
5	myrcene	985	2.5
6	3-octanol	987	0.1
7	α-phellandrene	1000	0.6
8	δ-3-carene	1004	0.2
9	α-terpinene	1010	5.1
10	p-cymene	1017	7.6
11	β-phellandrene	1021	0.9
12	(E)-β-ocimene	1040	0.1
13	γ-terpinene	1051	19.7
14	trans-sabinene hydrate	1072	0.3
15	α-terpinolene	1083	0.3
16	linalool	1091	1.3
17	borneol	1163	0.3
18	terpinen-4-ol	1171	0.9
19	thymol methyl ether	1232	0.7

20	carvone	1235	0.1
21	thymol	1285	0.3
22	carvacrol	1300	46.0
23	carvacrol acetate	1366	0.1
24	β-caryophyllene	1414	7.0
25	aromadendrene	1435	0.1
26	α-humulene	1450	0.4
27	ledene	1495	0.1
28	δ-cadinene	1518	0.1
29	caryophyllene oxide	1580	0.2
	Total identification		99.9

[a] RI: Retention Index calculated against C_9-C_{24} *n*-alkanes on the HP 5MS column capillary column

Table 28b. Grouped components (% *v*/*v*) of *S. thymbra* essential oil.

Classes of EO constituents	**%**
Monoterpene hydrocarbons	41.9
Oxygenated monoterpenes	50.0
Sesquiterpene hydrocarbons	7.7
Oxygenated sesquiterpenes	0.2
Aliphatic alcohols	0.1

30.2. Development and optimisation of nanovesicles loaded with OOEO and STEO

EOs of *O. onites* (OOEO) and *S. thymbra* (STEO) were formulated using diverse nanovesicles. Firstly, OOEO was encapsulated in conventional liposomes using PBS as dispersant medium and phosphatidylcholine (P90G) plus cholesterol in different ratios, trying to optimize average diameter and polydispersity of the vesicles. An amount of 10 mg/mL of OOEO was found to be the optimal concentration to obtain stable formulations without OOEO extrusion from the system, but vesicles resulted not homogeneous. Accordingly, other types of vesicles were approached, in particular those obtained by mixing membrane components with a water-soluble, non-volatile organic solvent, such as a polyol. The resulting nanovesicles are physiologically suitable even when administered intravenously into the human body. In particular, both glycerol and propylene glycol are among the most widely used raw materials in food, cosmetic and pharmaceutical industries. Glycerol shows excellent solubility in water, and, due to its GRAS status, it is very safe to use *(Becker LC, 2019)*. Propylene glycol is a colorless, odorless and completely water-soluble solvent very similar to glycerol, also having the GRAS status and high safety *(Fiume MM, 2012)*. Glycerosomes were prepared according to the recent publication by Vanti and coworkers *(Vanti G, 2020a)*. Different experimental conditions were tested, as reported in the

experimental section. Finally, the lipid film was constituted of P90G (600 mg) plus cholesterol (10 mg). It was hydrated using a 5% *v/v* glycerol/water solution and OOEO (10 mg/mL), or STEO (10 mg/mL) or OOEO plus STEO (5 mg/mL plus 5 mg/mL) were added in this step, obtaining *O. onites* essential oil-loaded glycerosomes (OO-GS), *S. thymbra* essential oil-loaded glycerosomes (ST-GS) and *O. onites* plus *S. thymbra* essential oil-loaded glycerosomes (OOST-GS). In parallel, different nanovesicles were prepared hydrating the lipid film with a 1% *v/v* propylene glycol/water solution and obtaining propylene glycol-nanovesicles (PGV) loaded with: *O. onites* essential oil (OO-PGV), *S. thymbra* essential oil (ST-PGV) and *O. onites* plus *S. thymbra* essential oil (OOST-PGV). All the samples were analysed by light scattering techniques and they showed small dimensions, low Polydispersity Index (PdI) and good ζ-potential (Tables 29-30). The higher standard deviation related to the average sizes of OO-GS and OO-PGV indicates a lower repeatability of sample preparation. However, the application of nanovesicles in food products is not limited by their average dimensions and all the developed formulations have suitable physical characteristics as delivery systems of food preservatives.

The combination of mechanic stirrer and ultrasonic bath during the two hydration processes allowed to obtain homogenous and stable formulations, without any further optimization step. Glycerosomes and PG-nanovesicles loaded with OOEO plus STEO were analysed by transmission electron microscope (TEM, Figures 42a and 42b). The obtained micrographs showed vesicles with spherical shape and several lamellae, mainly visible in glycerosomes (Figure 42a), and with dimensions in accordance with those obtained by DLS.

In addition, the encapsulation efficiency (EE) of OOEO and STEO, expressed as percentage of carvacrol, the marker constituent, was evaluated by HPLC-DAD and resulted high in both glycerosomes (between *ca.* 73% and *ca.* 77%) and PG-nanovesicles (between *ca*. 77% and 83%).

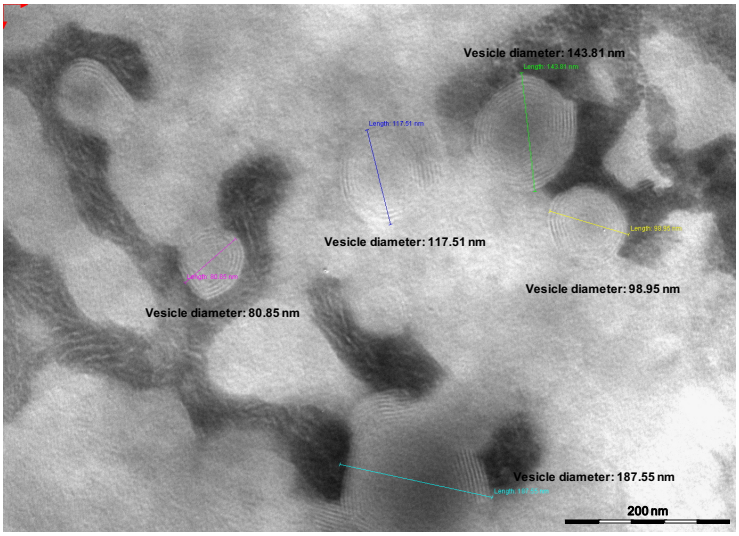

(a)

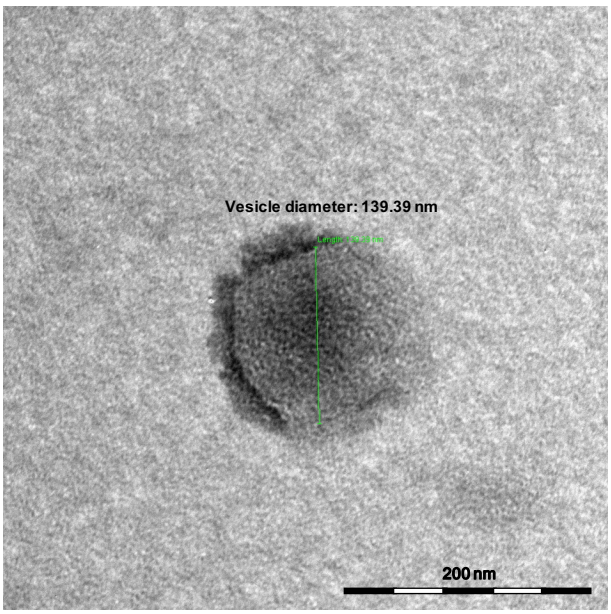

(b)

Figure 42. Pictures of (a) glycerosomes loaded with *O. onites* plus *S. thymbra* essential oils (OOST-GS) and (b) propylene glycol-nanovesicles loaded with O. onites plus S. thymbra essential oils (OOST-PGV), obtained by Transmission Electron Microscope (TEM) analysis.

Table 29. Physical and chemical parameters of glycerosomes loaded with: *O. onites* essential oil (OO-GS), *S. thymbra* essential oil (ST-GS), *O. onites* plus *S. thymbra* essential oils (OOST-GS). From left: Size, polydispersity index (PdI), ζ-potential, recovery (R) and encapsulation efficiency (EE); Mean ± SD (n = 3).

Formulation	Size (nm)	PdI	ζ-potential (mV)	R (%)	EE (%)
OO-GS	148.40±48.34	0.20±0.04	-41.68±5.78	87.02±6.19	72.97±6.46
ST-GS	105.51±13.92	0.22±0.05	-34.03±3.57	91.38±4.77	77.35±7.63
OOST-GS	105.43±15.19	0.17±0.02	-26.50±1.48	89.48±5.93	73.26±6.44

Table 30. Physical and chemical parameters of propylene glycol-nanovesicles loaded with: *O. onites* essential oil (OO-PGV), *S. thymbra* essential oil (ST-PGV), *O. onites* plus *S. thymbra* essential oils (OOST-PG). From left: Size, polydispersity index (PdI), ζ-potential, recovery (R) and encapsulation efficiency (EE); Mean ± SD (n = 3).

Formulation	Size (nm)	PdI	ζ-potential (mV)	R (%)	EE (%)
OO-PGV	138.23±29.17	0.17±0.03	-34.93±8.81	87.92±8.27	83.12±5.16
ST-PGV	73.95±5.71	0.21±0.01	-30.68±6.69	84.64±12.02	79.04±7.34
OOST-PGV	101.09±8.24	0.22±0.06	-28.80±1.15	85.79±9.27	76.73±8.27

30.3. Antibacterial and antifungal activities

Results of the evaluation of antibacterial and antifungal activity of pure and formulated OOEO/STEO are reported in Tables 31 and 32. All tested samples possessed significant antimicrobial effects. The best antimicrobial activities of formulated OOEO/STEO against all tested bacteria and fungi were observed for OO-PGV. The antibacterial minimum inhibitory concentration (MIC) of OO-PGV ranged from 1.00 to 4.00 mg vesicles/mL, while the minimum bactericidal concentrations (MBCs) were within the range of 2.00 to 8.00 mg vesicles/mL. MIC and MBC of essential oils formulated in nanovesicles, reported in Table 31, were calculated taking into account that the amounts of EOs loaded in the nanovesicles were 10 mg EO/g of vesicles. The pure OOEO exhibited stronger antibacterial potential with MICs at 0.0002–0.002 mg/mL and MBCs at 0.0003–0.0025 mg/mL compared to standard antibiotic Streptomycin and formulated OOEO used as reference compounds. The most sensitive bacterial species was *S. aureus*, while *E. coli* was the resistant one among all the tested bacteria. MIC and MFC were reported in Table 32: for OOEO, MICs were in the range 0.0002-0.001 mg/mL against all tested fungi, and MFCs varied within the range of 0.0003-0.0012 mg/mL. Antifungal potential of OOEO was higher than that of formulated OOEO and reference drug Ketoconazole. The most sensitive appeared to be *P. verrucosum*, while both *Candida* species were found to be resistant. In conclusion, the activity of both pure OOEO and STEO was more prominent when compared to the activity of corresponding amounts of formulated EOs. However, this lower antibacterial and antifungal effectiveness of formulated EOs with respect to pure EOs is mainly due to the prolonged release properties of the EOs loaded in the nanovesicles, as described by other studies on *in vitro* activity of essential oils formulated in glycerosomes and liposomes *(Vanti G, 2020a; Valenti D, 2001)*.

Table 31. Antibacterial activity (mg EO/mL medium) of pure and formulated EOs of *O. onites* (OOEO) and *S. thymbra* (STEO).

		B. cereus	*S. aureus*	*L. monocytogenes*	*E. coli*	*P. aeruginosa*	*S. enterica serovar Typhimurium*
Blank-GS	MIC	n.a.	n.a.	n.a.	n.a.	n.a.	n.a.
	MBC	n.a.	n.a.	n.a.	n.a.	n.a.	n.a.
OO-GS	MIC	0.015	0.015	0.010	0.040	0.020	0.010
	MBC	0.020	0.020	0.040	0.080	0.040	0.020
ST-GS	MIC	0.020	0.010	0.020	0.040	0.040	0.020
	MBC	0.040	0.020	0.040	0.080	0.080	0.040
OOST-GS	MIC	0.020	0.015	0.020	0.040	0.020	0.020
	MBC	0.010	0.030	0.040	0.080	0.040	0.040
Blank-PGV	MIC	n.a.	n.a.	n.a.	n.a.	n.a.	n.a.
	MBC	n.a.	n.a.	n.a.	n.a.	n.a.	n.a.
OO-PGV	MIC	0.010	0.010	0.010	0.040	0.020	0.015
	MBC	0.020	0.020	0.020	0.080	0.030	0.040
ST-PGV	MIC	0.015	0.010	0.010	0.040	0.030	0.020
	MBC	0.040	0.020	0.020	0.080	0.040	0.040
OOST-PGV	MIC	0.010	0.020	0.015	0.040	0.020	0.020
	MBC	0.020	0.040	0.020	0.080	0.040	0.040
OOEO	MIC	0.0006	0.0012	0.0020	0.0010	0.0002	0.0005
	MBC	0.0012	0.0025	0.0025	0.0020	0.0003	0.0006
STEO	MIC	0.0003	0.0012	0.0006	0.0010	0.0003	0.0010
	MBC	0.0012	0.0025	0.0012	0.0012	0.0006	0.0012
Streptomycin	MIC	0.10	0.05	0.20	0.20	0.10	0.20
	MBC	0.20	0.10	0.40	0.40	0.20	0.30

MIC=minimum inhibitory concentration; MBC=minimum bactericidal concentration; "n.a."=not activity at tested concentration of of 8 mg formulation/mL medium, corresponding to 0.080 mg EO/mL medium. Blank-GS: Blank-glycerosomes; OO-GS: Glycerosomes loaded with *O. onites* essential oil; ST-GS: Glycerosomes loaded with *S. thymbra* essential oil; OOST-GS: Glycerosomes loaded with *O. onites* plus *S. thymbra* essential oils; Blank-PGV: Blank-propylene glycol-nanovesicles; OO-PGV: Propylene glycol-nanovesicles loaded with *O. onites* essential oil; ST-PGV: Propylene glycol-nanovesicles loaded with *S. thymbra* essential oil; OOST-PGV: Propylene glycol-nanovesicles loaded with *O. onites* plus *S. thymbra* essential oils

Table 32. Antifungal activity (mg EO/mL of medium) of pure and formulated EOs of *O. onites* (OOEO) and *S. thymbra* (STEO).

		A. fumigatus	*A. niger*	*T. viride*	*P. verrucosum*	*C. albicans*	*C. krusei*
Blank-GS	MIC	n.a.	n.a.	n.a.	n.a.	n.a.	n.a.
	MFC	n.a.	n.a.	n.a.	n.a.	n.a.	n.a.
OO-GS	MIC	0.015	0.010	0.010	0.010	n.a.	0.080
	MFC	0.040	0.020	0.020	0.020	n.a.	> 0.080
ST-GS	MIC	0.010	0.020	0.015	0.020	0.040	0.060
	MFC	0.040	0.040	0.030	0.040	0.080	0.080
OOST-GS	MIC	0.020	0.015	0.020	0.015	0.040	0.060
	MFC	0.040	0.030	0.040	0.030	0.080	0.080

Blank-PGV	MIC	n.a.	n.a.	n.a.	n.a.	n.a.	n.a.
	MFC	n.a.	n.a.	n.a.	n.a.	n.a.	n.a.
OO-PGV	MIC	0.010	0.020	0.020	0.020	0.060	0.080
	MFC	0.020	0.040	0.040	0.040	0.080	> 0.080
ST-PGV	MIC	0.005	0.010	0.020	0.005	0.080	0.080
	MFC	0.010	0.040	0.040	0.010	> 0.080	> 0.080
OOST-PGV	MIC	0.020	0.010	0.020	0.015	0.080	0.060
	MFC	0.040	0.020	0.040	0.030	> 0.080	0.080
OOEO	MIC	0.0002	0.0004	0.0003	0.0003	0.0010	0.0006
	MFC	0.0003	0.0006	0.0006	0.0006	0.0012	0.0012
STEO	MIC	0.0004	0.0006	0.0003	0.0003	0.0006	0.0003
	MFC	0.0006	0.0012	0.0006	0.0006	0.0012	0.0006
Ketoconazole	MIC	0.20	0.20	1.00	0.20	0.50	0.50
	MFC	0.50	0.50	1.50	0.50	1.00	1.00

MIC=minimum inhibitory concentration; MFC=minimum fungicidal concentration; "n.a."=not activity at tested concentration of 8 mg formulation/mL medium, corresponding to 0.080 mg EO/mL medium. Blank-GS: Blank-glycerosomes; OO-GS: Glycerosomes loaded with *O. onites* essential oil; ST-GS: Glycerosomes loaded with *S. thymbra* essential oil; OOST-GS: Glycerosomes loaded with *O. onites* plus *S. thymbra* essential oils; Blank-PGV: Blank-propylene glycol-nanovesicles; OO-PGV: Propylene glycol-nanovesicles loaded with *O. onites* essential oil; ST-PGV: Propylene glycol-nanovesicles loaded with *S. thymbra* essential oil; OOST-PGV: Propylene glycol-nanovesicles loaded with *O. onites* plus *S. thymbra* essential oils.

30.4. Cytotoxicity on HaCaT cell line

The cytotoxic effect of pure and formulated OOEO/STEO was assessed on HaCaT cell line (Table 33), a spontaneously transformed aneuploid immortal keratinocyte cell line from adult human skin and very sensible cell line, used as an effective *in vitro* alternative, for an initial orientating screening of safety issues of substances. Blank-GS and Blank-PGV samples showed no toxicity towards HaCaT up to 500 μg/mL, which is indicative of carrier low cytotoxicity. All the investigated samples showed to be weakly cytotoxic towards this cell line. The results showed that OO-GS sample showed the highest cytotoxic effect on the human immortalized keratinocytes, followed by OOST-GS (combination of essential oils loaded in glycerosomes). OO-PGV (propylene glycol-nanovesicles loaded with *O. onites* essential oil) was the only sample with a cytotoxic effect below 500 μg/mL. Although weak cytotoxicity could be acknowledged for some samples, further application of propylene glycol-nanovesicles should be considered when formulating antimicrobial preparations, since this carrier expressed no toxicity to immortalized cell line. These safety data are encouraging for further safety studies to demonstrate the safe use of the developed nanovesicles.

Table 33. Cytotoxic properties of pure and formulated EOs of *O. onites* (OOEO) and *S. thymbra* (STEO) on human immortalized keratinocyte cell line.

Samples	**IC_{50}% (μg/mL) HaCaT cell line**
Blank-GS	>500
OO-GS	311.24±8.22
ST-GS	487.34±4.46
OOST-GS	385.83±1.51
Blank-PGV	>500
OO-PGV	492.14±11.74
ST-PGV	>500
OOST-PGV	>500
OOEO	>500
STEO	>500
$K_2Cr_2O_7$	16.29±1.42

Blank-GS: Blank-glycerosomes; OO-GS: Glycerosomes loaded with *O. onites* essential oil; ST-GS: Glycerosomes loaded with *S. thymbra* essential oil; OOST-GS: Glycerosomes loaded with *O. onites* plus *S. thymbra* essential oils; Blank-PGV: Blank-propylene glycol-nanovesicles; OO-PGV: Propylene glycol-nanovesicles loaded with *O. onites* essential oil; ST-PGV: Propylene glycol-nanovesicles loaded with *S. thymbra* essential oil; OOST-PGV: Propylene glycol-nanovesicles loaded with *O. onites* plus *S. thymbra* essential oils. Different letters mean significant difference between IC_{50} values of samples ($p>0.01$).

DEVELOPMENT OF NANOLIPOSOMES LOADED WITH CARBON DIOXIDE *SERENOA REPENS* (SAW PALMETTO) EXTRACT

31. Results and Discussion

This study represents the first report on the formulation of liposomes loaded with saw palmetto CO_2 extract. Previously, only liposomes loaded with CO_2 extract of cardamom essential oil *(Paul K, 2019)* and CO_2 leaf extract of sea buckthorn, containing mainly flavonoids *(Ghatnur SM, 2012)*, were reported in the literature. Due to the chemical nature of the constituents and the physical characteristics of the extract, which appears as a soft orange jelly insoluble in water, the development of nanoliposomes was selected as the best formulating approach *(Bilia AR, 2017; Bilia AR, 2019a)*. Indeed, liposomes represent, among the nanocarriers, the most useful ones to be applied for topical use because they can penetrate the epidermal barrier to a greater extent compared to other conventional dosage forms, and loaded drugs are generally accumulated in the upper layers of the *stratum corneum* and appendages (hair follicles and sweat ducts), providing a "reservoir" and resulting in a more localized action *(Jung S, 2006; Tabbakhian M, 2006)*.

Nanoliposomes, loaded with 0.1% *w/v* of *Serenoa repens* CO_2 extract, were prepared and analysed by DLS and ELS. Their sizes were 145±5 nm, PdI was 0.27±0.05 and ζ-potential was -36.2±3.1 mV. Interestingly, the nanosized range of the vesicles makes them suitable for topical delivery and in particular for the penetration of the encapsulated extract into the hair follicles *(Bilia AR, 2017; Jung S, 2006; Tabbakhian M, 2006)*. In addition, the low PdI value indicated a narrow range of nanosizes with high homogeneity of the vesicles. The high negative ζ-potential value of the nanovesicles imparted a high stability to the liposomal suspension. The high negative ζ-potential was probably due to free fatty acids, which represent the main constituents of saw palmetto CO_2 extract and can also act as penetration enhancers. Morphological characteristics of the developed nanoliposomes, observed by TEM, (Figure 43) clearly defined nanoliposomes as small and spherical vesicles, with a slight inner lamellar structure and sizes (*ca.* 125 nm) similar to those obtained by DLS analysis.

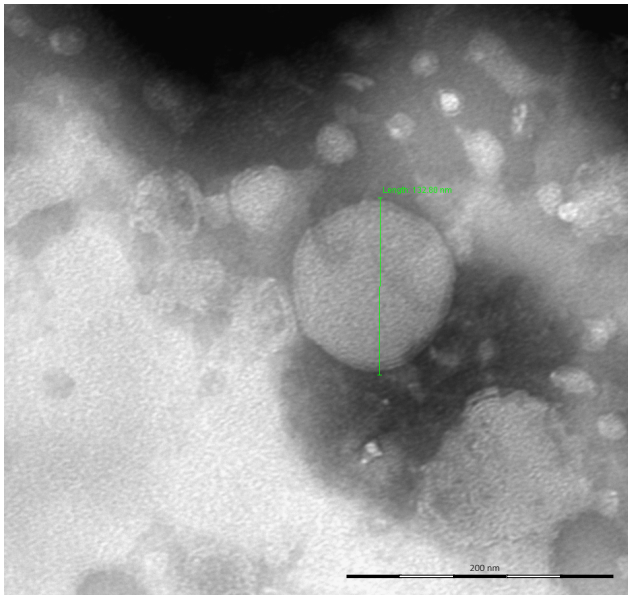

Figure 43. TEM picture of liposomes loaded with saw palmetto CO_2 extract.

CO-DELIVERY OF BERBERINE CHLORIDE AND TARIQUIDAR IN NANOLIPOSOMES ENHANCED INTRACELLULAR BERBERINE CHLORIDE IN A DOXORUBICIN-RESISTANT K562 CELL LINE DUE TO P-gp OVEREXPRESSION

32. Results

32.1. Formulation of nanoliposomes and characterization

Different combinations and gravimetric ratios of P90G or P100H plus Chol were tested (Table 8) in order to select, by DLS analysis, the best formulations to load BRB.

The hydration of the lipid film by using glass beads led to multilamellar vesicles with dimensions ranging from 800 to 1000 nm, which were optimized by ultrasonication, as reported in the experimental part. P90G plus Chol was found to be the best combination for the preparation of suitable nanoliposomes for parenteral administration in terms of size (less than 200 nm) and homogeneity (PdI less than 0.3).

All the nanovesicles based on P90G plus Chol had good PdI (0.20–0.25), but the nanoliposomes having P90G/Chol concentration ratio of 65:30 mg/mL were larger than 200 nm and not suitable for the parenteral administration. The liposomal formulation 66:10 (P90G:Chol) was finally selected on the basis of the physical characteristics and BRB loading ability. Increasing amounts of BRB were loaded in the nanoliposomes to reach a maximum of 0.7 mg/mL using the different P90G/Chol ratios, in order to maximize the optimal size and PdI for the parenteral route, as well as the highest encapsulation of BRB. Table 34 describes the physical and chemical characteristics of the investigated BRB nanovesicles (BRB-L).

Table 34. Physical characterization in terms of Size, PdI and ζ-potential of BRB-L. All results are expressed as mean ± SD (*n* = 3).

P90G/Chol Ratio (mg/mL)	Size (nm)	PdI	R (%)	EE (%)
33:1	138.3 ± 1.3	0.25 ± 0.01	/	/
33:2	154.9 ± 1.2	0.25 ± 0.01	/	31.18 ± 0.80
33:10	154.0 ± 1.6	0.20 ± 0.01	/	61.78 ± 0.40
66:10	127.8 ± 29.6	0.22 ± 0.03	103.41 ± 6.37	63.80 ± 6.41
66:20	162.6 ± 7.3	0.21 ± 0.02	98.92 ± 4.51	42.17 ± 6.49
65:30	230.3 ± 38.6	0.25 ± 0.07	92.36 ± 6.55	76.94 ± 8.04

Nanoliposomes based on P90G/Chol with a concentration ratio of 66:10 (mg/mL) showed highest encapsulation efficiency of BRB (*ca.* 64%). These nanoliposomes had also an optimum ζ-potential value (−20.3 ± 2.5 mV) to protect nanoliposomes from aggregation and precipitation.

These nanoliposomes were selected to load also Pg-p inhibitors, i.e., TAR (TAR-L) and TPGS (TPGS-L), and to formulate BRB plus TAR-loaded nanoliposomes (BRB/TAR-L). TAR concentration was 0.647 mg/mL (1 mM) in both liposomes, whereas BRB concentration was 0.7 mg/mL. The physical characterization (*n* = 3) was carried out by DLS. BRB/TAR-L evidenced sizes of 137.9 ± 11.7 nm, and PdI of 0.25 ± 0.03. In addition, R% and EE% (*n* = 3) of BRB and TAR, determined by HPLC-DAD, were found to be 99.43 ± 2.42% and 57.01 ± 11.1% for BRB, and 85.64 ± 4.24% and 78.76 ± 3.03% for TAR. TAR-L had similar R% and EE%, average sizes of 141.3 ± 0.4 nm and PdI of 0.184 ± 0.004. TPGS-L had an EE% near to 100% and dimensions and PdI values similar to the unloaded nanovesicles.

Finally, the morphological characterization of the nanoliposomes was carried out by TEM. The microscopic analysis highlighted the vesicular and spherical structure of all the developed nanoliposomes, confirming the sizes and the homogeneity of the samples, in agreement to the DLS data. In particular, TEM analysis of BRB-L and BRB/TAR-L, performed before and after the dialysis step, evidenced that both formulations were not affected by this purification process (Figure 44A–D).

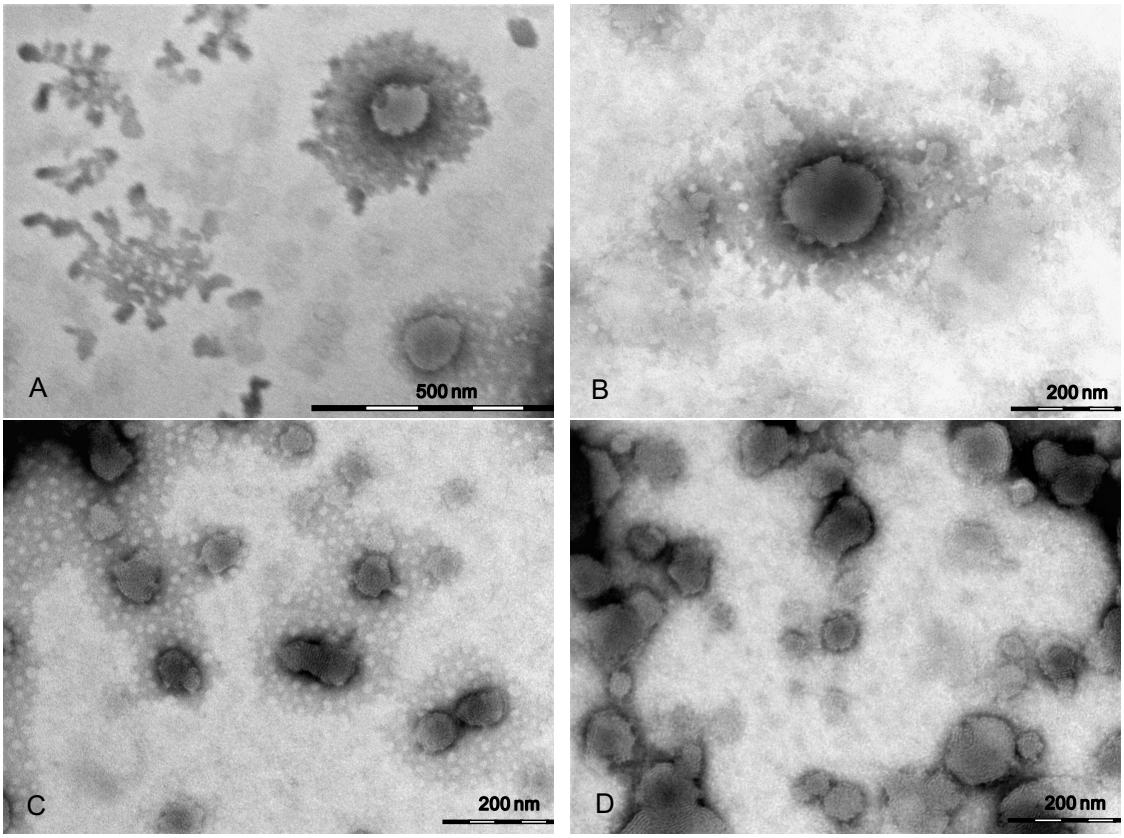

Figure 44. TEM pictures of BRB-L before (**A**) and after dialysis process (**B**), and of BRB/TAR-L before (**C**) and after dialysis process (**D**).

32.2. Stability Studies of Nanoliposomes in Cell Culture Medium

Physical and chemical stability of the dialyzed BRB-L and BRB/TAR-L was evaluated after incubation for 2 h at 37 ± 2 °C in the culture medium (RPMI medium 1640 at 10% FBS). At the end of the incubation time, each sample was analysed by DLS and HPLC-DAD (Table 35). Both nanoliposomes were physically stable ($n = 3$) over time. BRB-L showed a slight increase (less than 4%) for both size and PdI after two hours of incubation. BRB/TAR-L, after two hours of incubation, showed a small deacrease of the hydrodynamic diameter (from 137.6 nm to 135.3 nm), while the PdI reached the value of 0.332 (Table 35).

In parallel, the amounts of BRB and TAR were monitored by HPLC-DAD (Table 35). Being nanoliposomes purified before testing, only EE% was determined after incubation. EE% was decreased a little for either BRB or TAR, in both nanovesicles.

Table 35. Physical and chemical characterization in terms of size, PdI, EE% and R%, of the dialyzed nanoliposomes BRB-L and BRB/TAR-L at time zero (T_0) and after 2 h incubation (T_{2h}). All results are expressed as mean ± SD (n = 3).

Sample	Size (nm)	PdI	BRB R%	BRB EE%	TAR R%	TAR EE%
BRB-L T_0	147.9 ± 3.7	0.219 ± 0.027	99.67 ± 0.41	64.15 ± 3.97	/	/
BRB-L T_{2h}	150.6 ± 1.41	0.231 ± 0.004	/	60.66 ± 4.61	/	/
BRB/TAR-L T_0	137.6 ± 0.6	0.276 ± 0.011	97.46 ± 1.46	73.83 ± 0.30	82.56 ± 0.38	76.44 ± 0.67
BRB/TAR-L T_{2h}	135.3 ± 1.1	0.332 ± 0.022	/	71.36 ± 4.04	/	69.30 ± 5.81

32.3. BRB in vitro release from nanoliposomes

Figure 45 represents the release profiles of BRB from BRB-L and BRB/TAR-L, compared to the release from BRB solution (Sol BRB), obtained using 100 mL of PBS at pH 7.4 as release medium, at a constant temperature of 37 °C, for 2 h, and applying a magnetic stirring of 100 rpm. Before the test, BRB-L and BRB/TAR-L were dialyzed and diluted in the cell culture medium, in order to simulate the experimental conditions of the *in vitro* test. BRB release from both nanoliposomes was rapid. After 15 min, about 50% of BRB was recovered in the PBS external medium for both formulations. However, after 60 min the release became slower and more constant, reaching a BRB release of about 85% for BRB-L and approximately 95% for BRB/TAR-L, after 120 min. Accordingly, TAR did not greatly influence the release of BRB from the nanoliposomes.

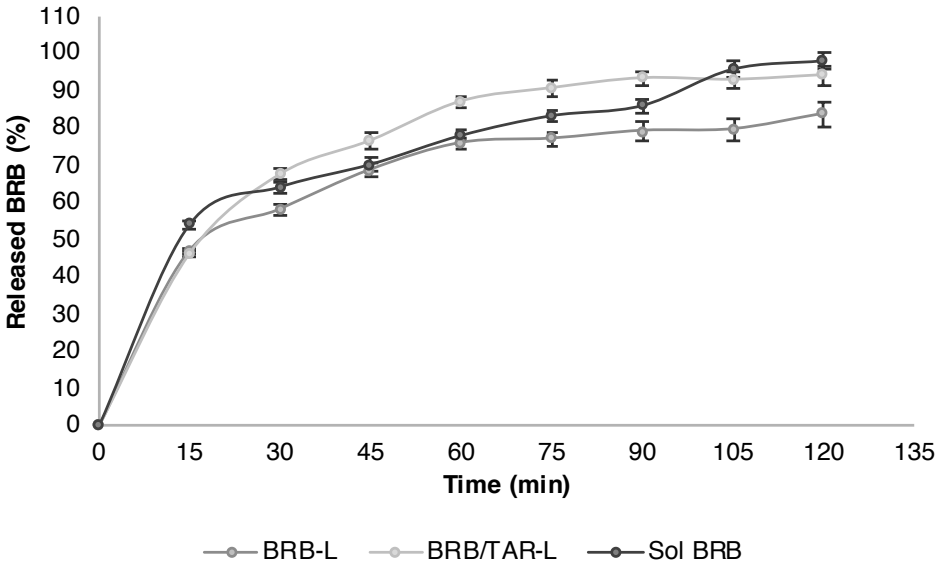

Figure 45. BRB release over time from dialyzed BRB-L and BRB/TAR-L, compared with BRB solution (BRB-SOL).

32.4. Interaction of horseradish peroxidase-loaded nanoliposome with cell membranes of K562 and K562/DOXO cell lines by TEM

The interactions of developed nanoliposomes with cell membranes of K562 and K562/DOXO cell lines was studied by TEM (Figures 46–49 and S1 and S2). Nanoliposomes were loaded with the electron dense enzyme horseradish peroxidase as reported in Section 16.6. DLS analysis of the developed nanoliposomes gave a size of 161.13 ± 19.33 nm and a PdI of 0.287 ± 0.051 (mean ± SD, n = 3). TEM highlighted the morphological interactions of horseradish peroxidase-loaded nanoliposomes with the cells, detecting their localization and structural shape within them.

The horseradish peroxidase-loaded nanoliposomes were incubated with the two cell lines and analyzed by TEM to evaluate their behavior after 15 (Figures 46 and 48) and 120 min (Figures S1 and S2) of exposure and compared with the controls (Figures 47 and 49). After 15 min, the K562 cells (Figure 46) were surrounded by several membrane-bound particles with electron-dense content, consistent with liposomes by their size and shape: these particles adhered to the plasma membrane and sometimes appeared to undergo endocytosis by clathrin-coated pits and vesicles, suggesting the involvement of a mechanism of receptor-mediated endocytosis/phagocytosis.

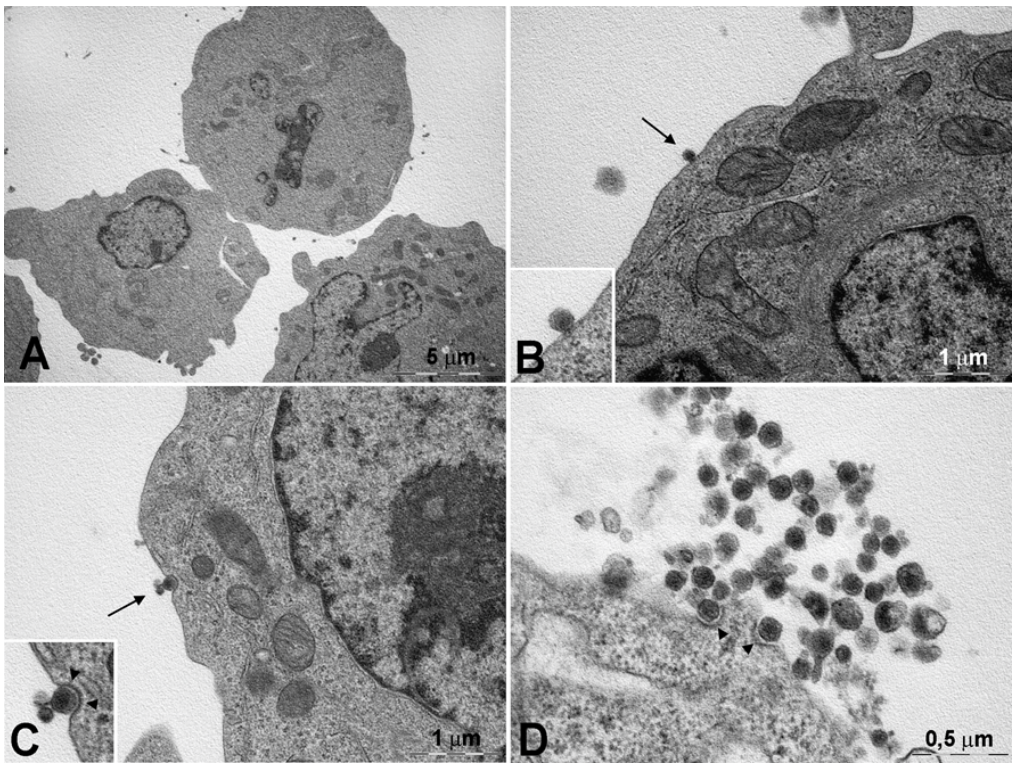

Figure 46. K562 cells after 15-min incubated with peroxidase-containing liposomes. (**A**) Cells still show a normal ultrastructure and one of them (top) appears in mitosis. (**B**) A liposome, in the form of a membrane-bound particle with electron-dense content, is attached to the plasma membrane (arrow and insert); to note that mitochondria show a normal appearance. (**C**) A liposome undergoing internalization by a coated pit (arrow and insert): the typical clathrin coating (arrowheads) is suggestive for a mechanism of receptor-mediated endocytosis. (**D**) A group of liposomes in proximity of a cell's surface: some of them appear in the course of receptor-mediated endocytosis (arrowheads).

After 15 min of incubation, the cells still showed a normal appearance, similar to that of the controls (Figure 47). After 2-h exposure to horseradish peroxidase-loaded nanoliposomes, most cells showed clear-cut signs of necrosis, with cytoplasmic vacuolization, swollen mitochondria with disruption of cristae, dispersed chromatin, multiple ruptures of the plasma membrane and leakage of cytoplasm. Occasional liposome-like electron-dense particles were found close to the plasma membrane remnants and within cytoplasmic vacuoles (Figure S1).

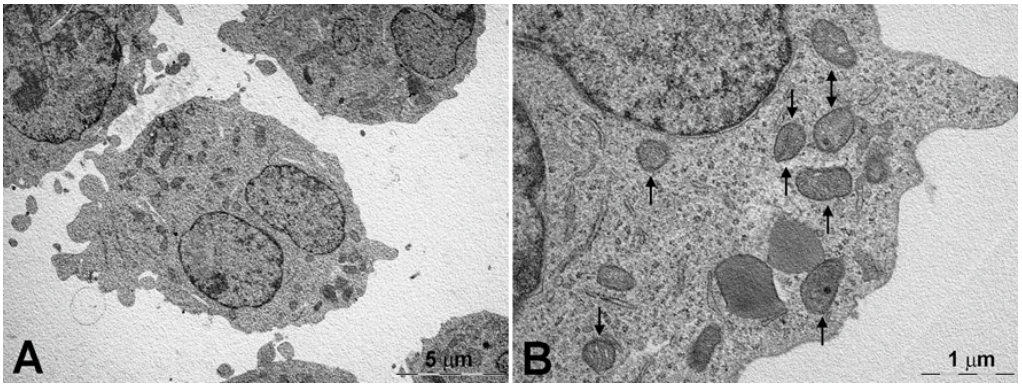

Figure 47. Control K562 cells. (**A**) The cells show a normal ultrastructure. (**B**) Numerous mitochondria (arrows) rich in cristae and with dense inner matrix-as usual in normally functioning organelles-can be seen in the cytoplasm.

The resistant K562/DOXO clone shows the same results at the investigated times (Figures 48, 49 and S2). Therefore, the horseradish peroxidase-loading nanoliposomes, once penetrated into the cell, cause irreversible damage of the cytomembranes, severe mitochondrial dysfunction, leading to cell death.

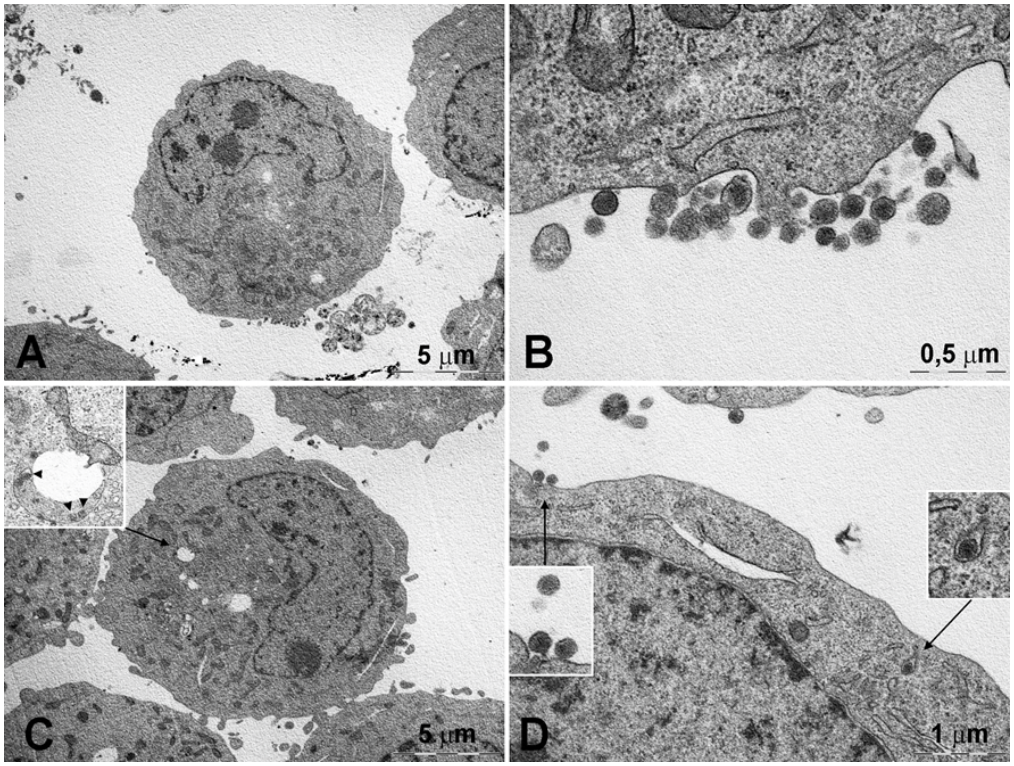

Figure 48. K562/DOXO cells after 15-min incubation with peroxidase-containing liposomes. (**A**) The cells show a normal ultrastructure and one of them (center) shows

a cluster of membrane-bound, electron-dense particles, identified as liposomes, opposed to the plasma membrane. (**B**) Detail of the liposomes shown in (**A**), some of which are attached to the plasma membrane; mitochondria still show a normal appearance. (**C**) Cells showing moderate cytoplasmic vacuolation (see insert) and electron-dense particles corresponding to liposomes (arrowheads). (**D**) Detail of the cell in (**C**).

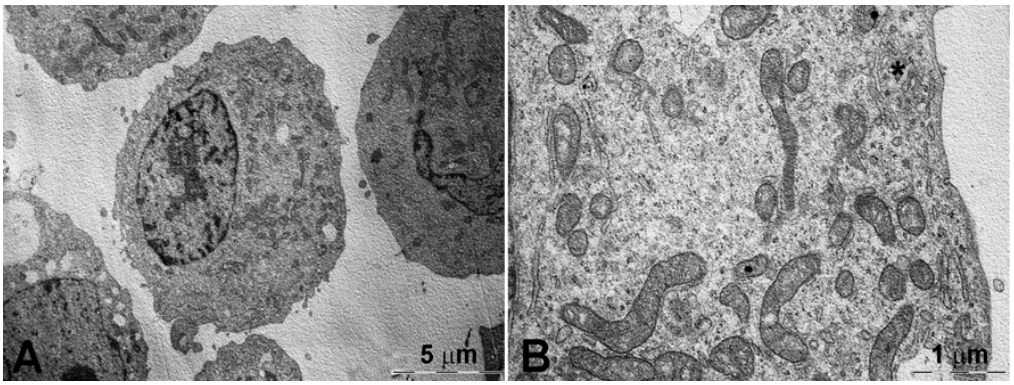

Figure 49. Control K562/DOXO cells. (**A**) Representative images of cells showing normal ultrastructure. (**B**) Rod-shaped mitochondria, with numerous cristae and dense inner matrix, typical features of normally functioning organelles, can be seen.* Golgi apparatus is indicated by the asterisk.

32.5. Cytotoxicity of DOXO in the K562/DOXO cell line incubated with TAR, TAR-L, TPGS and TPGS-L

In order to select the most efficient pump inhibitor, the effect of DOXO, DOXO plus TAR, DOXO plus TPGS, DOXO plus TAR-L, or DOXO plus TPGS-L were studied using K562/DOXO cell line by the apoptosis assay, performed 24 h after the end of the incubation with DOXO, as reported in the experimental part (Figure 50). DOXO cytotoxicity was revealed after 60 min of DOXO incubation with K562/DOXO cells at a concentration of 10 μM.

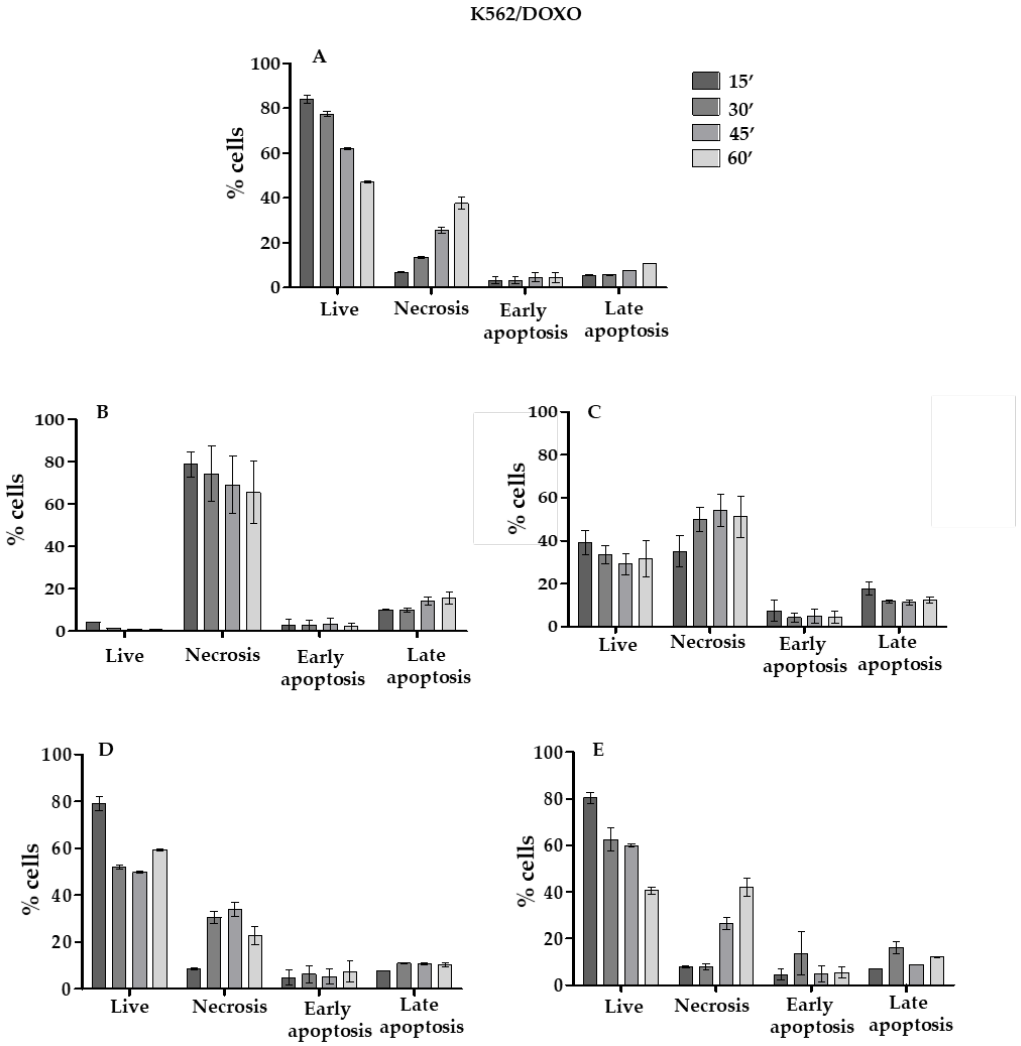

Figure 50. Effects of pump inhibitors (free or liposomal TAR and TPGS) on DOXO cytotoxicity in K562/DOXO cells. In particular, data are reported for DOXO (**A**), DOXO plus TAR (**B**), DOXO plus TAR-L(**C**), DOXO plus TPGS (**D**) and DOXO+TPGS-L (**E**). Cytotoxic effects are expressed as the percentage of live, necrotic, and apoptotic cells detected in the samples incubated with DOXO in the presence and in the absence of the different pump inhibitors free and formulated.

A comparison of the results obtained in K562/DOXO cell line treated with DOXO and TAR solution (Figure 50B) or TAR-L (Figure 50C), highlighted that the necrotic cell percentage in the sample treated with free TAR is very high (approximately 80%) after 15 min treatment, remaining stable even in the other times.

The cell necrosis with TAR-L, in the first 15 min is low (approximately 50% of the free TAR), reaching, after 60 min, the 76% compared to that of free TAR.

As expected, TAR solution enables a better saturation of the P-gp pump rather than the TAR-L. However, interestingly, in the sample treated with the TAR-L, the percentages of both early and late apoptotic cells were higher when compared to sample treated with TAR solution. The TPGS was less active when compared with both free and formulated TAR. Its contribution to the cytotoxicity of DOXO is low with a very similar percentage of necrotic cells at 60 min to that of the sample treated with DOXO in the absence of the inhibitor. For this reason, TAR was selected as pump inhibitor for the co-delivery with BRB in nanoliposomes.

32.6. Uptake studies

BRB, due to its intrinsic fluorescence, was used for the direct measurement of cell uptake, and the functionality of P-gp pump in the absence and in presence of TAR was investigated (Figure 51). The uptake of the BRB-loaded in nanoliposomes was tested by a FACS flow cytometer, using directly the fluorescence of the molecule.

Specifically, K562 and K562/DOXO cell uptake of BRB-loaded in nanoliposomes was compared to a solution of free BRB (Figure 51A). The uptake of BRB in parental K562 cells after 2 h of incubation is not significantly different between the two BRB samples, the free molecule in solution or that encapsulated BRB in nanoliposomes. Therefore, the fluorescence ratios (RF) were comparable, overlapping the signals, with RF = 30.9 or RF = 29.9, when the cells were incubated in the presence, respectively, of the free BRB or BRB-L. K562 cells sensitive to DOXO did not show P-glycoprotein expression, and the use of any specific pump inhibitor is not necessary. On the contrary, K562/DOXO cells, having P-gp overexpression, showed a moderate increase in the accumulation of BRB-L.

Uptake in K562/DOXO cells was also evaluated after 2 h of incubation with BRB, BRB-L, BRB plus TAR as free molecules in solution, BRB-L plus free TAR or BRB plus TAR both encapsulated in nanoliposomes (Figure 51B). The BRB/TAR-L formulation gave a RF = 16, which represents the 76% of the value of the sample treated with BRB and TAR in solution (RF = 21) and is significantly different ($p < 0.05$) from the value of the BRB-L + TAR formulation (RF = 12); this feature makes it optimal for the simultaneous, safe and effective release of BRB and TAR.

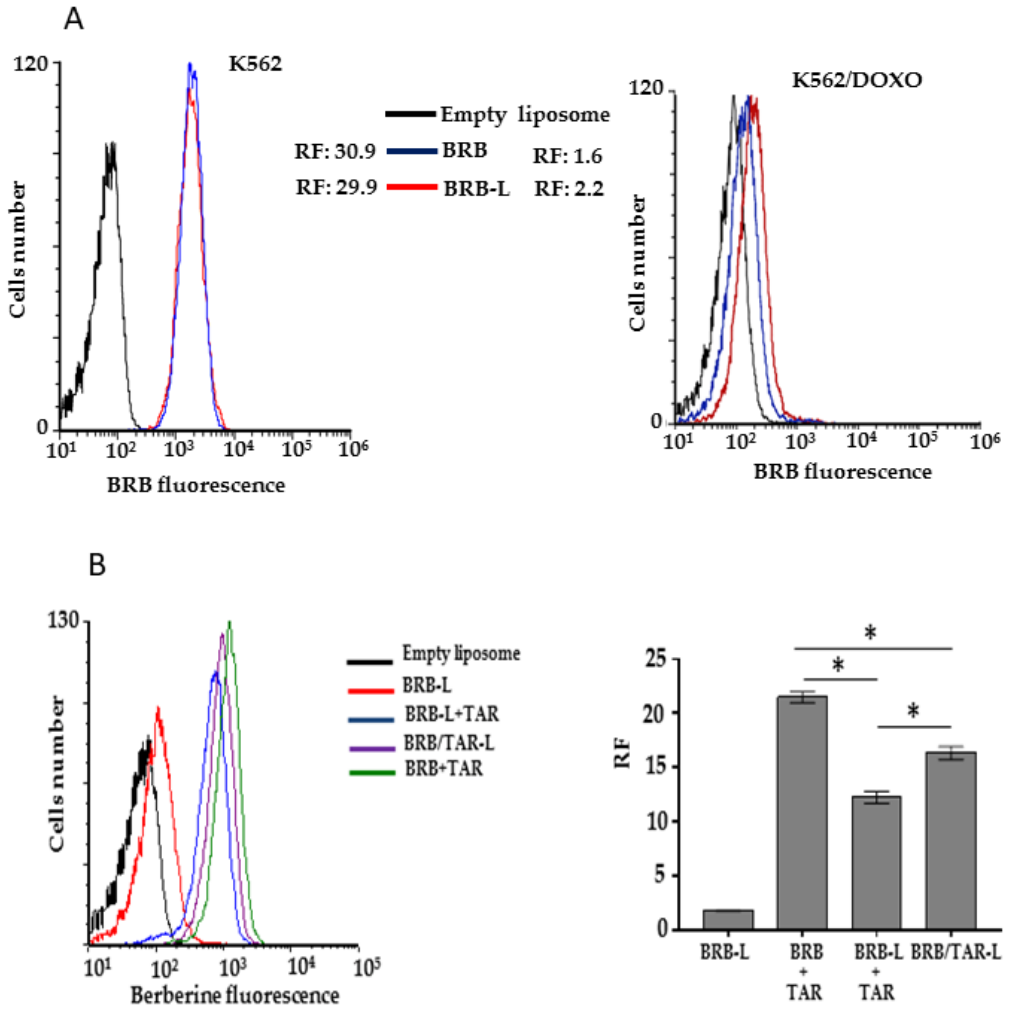

Figure 51. (**A**) uptake of BRB or BRB-L by K562 and K562/DOXO cells, after 2 h-incubation ; (**B**) uptake of BRB/TAR, BRB-L/TAR, or BRB/TAR-L by K562/DOXO cells, after 2 h-incubation. RF = fluorescence ratios of sample treated and the control (empty liposome), * $p < 0.05$.

33. Discussion

In this paper, we investigated the simultaneous delivery of the anticancer drug, BRB, and a P-gp efflux pump modulator, TAR, using nanoliposomes to enhance BRB intracellular concentration. Untargeted liposomes loaded with antineoplastic drugs are the most successful nano-drug delivery systems translated into clinical applications and approved for their marketing, including for the treatment of hematological cancers. These nanocarriers minimize drug degradation and inactivation upon administration, as well as increase the drug's bioavailability and the fraction of drug delivered within the pathological area, thus improving efficacy and/or minimizing drug toxicity. The developed

nanoliposomal formulations encapsulating BRB plus TAR allowed us to increase the concentration of BRB inside the tumor cells, thus improving the potency. Nanoformulations were obtained by lipid hydration using different ratios of P100H or P90G plus Chol. The optimization of nanoliposome composition was carried out by fixing the concentration of P90G and P100H at values, which have been already optimized in previous studies, and solely modulating the content of cholesterol because of its key role in the rigidity of bilayers and as a consequence the loading of BRB. Accordingly to the DLS measurements and BRB EE%, the selected nanocarriers were those based on P90G plus Chol, because P100H, the hydrogenated phosphatidylcholine, combined with Chol did not produced suitable nanoliposomes for parenteral administration.

Nanoliposomes made of P90G/Chol (66:10 mg/mL) had the best of BRB EE%, PDI and ζ-potential values. Furthermore, this formulation was clear and not viscous compared with the formulation having higher P90G/cholesterol concentration ratio (65:20 or 65:30 mg/mL). The same P90G/Chol ratio was maintained to formulate TAR-L, TPGS-L and BRB/TAR-L.

As a first step of the study, the stability of the native and dialyzed nanoliposomes was assessed by TEM analysis because the purified liposomes were used in the tests. Dialysis removal of unencapsulated BRB and TAR from nanoliposomes was revealed as a simple protocol to obtain purified liposomes without any variability of the size and morphology of vesicles and an efficient method to preserve the entrapped drug in the liposomes, as suggested by the HPLC-DAD analyses. In addition the physical and chemical stability of nanoliposomes in the cell culture medium, RPMI medium 1640 with 10% FBS, were performed. Slight variance, less than 4%, for both the hydrodynamic diameter and PdI value were found. Overall, the tested formulations resulted physically and chemically stable under the experimental conditions, which are intended to mimic the *in vitro* studies within the two cell lines. Future studies will be oriented to the stability studies of the nanoformulations after storage in order to evidence the eventual need to lyophilize the nanoliposome in order to extend their shelf life.

Finally, release properties of the dialyzed nanoliposomes were also assessed using the same medium used for stability, i.e., RPMI medium 1640 with 10% FBS, evidencing good biopharmaceutical properties of nanoliposomes.

A key step of the present study was the evaluation of interaction of nanoliposome with cell membranes of K562 and K562/DOXO cell lines by TEM.

The study was carried out using the enzyme horseradish peroxidase as electron dense material giving their localization and structural shape within the cells. TEM analysis evidenced the ability of the developed nanoliposomes to enter in both K562 and K562/DOXO cell lines by receptor-mediated endocytosis. This process was already evidenced after 15 min of incubation, but after 2-h exposure to horseradish peroxidase-loaded nanoliposomes, most cells showed clear-cut signs of necrosis, with cytoplasmic vacuolization, swollen mitochondria with disruption of cristae, dispersed chromatin, multiple ruptures of the plasma membrane and leakage of cytoplasm. These findings suggested that peroxidase loaded in liposomes, likely due to the cytomembrane destabilization, is highly toxic for both cell lines, which are prompted to massive necrosis.

Furthermore, two P-gp inhibitors, TAR and TPGS both the free molecules and loaded in nanoliposomes were tested with DOXO in resistant cells, K562/DOXO, for their effects against overexpression of P-gp. TAR both in the free solution and encapsulated in liposomes was superior in overcoming DOXO resistance with respect to TPGS. In addition, from the cytotoxicity data it was hypothesized that the amount of Pg-p inhibitor available in the first instants of the experiment is greater with the inhibitor in solution, as nanoliposomes modify their release. In particular, it is remarkable to evidence that the toxicity of DOXO when treated with TAR-L is delayed compared to the toxicity observed in the sample treated with DOXO and TAR in solution. Consequently, the advantage of the slower release is a reduction in cell death by necrosis. According to the literature, cell necrosis is a process that heavily damages cells with leakage of the cell content into the surrounding environment and consequent inflammatory processes *in vivo (D'Arcy MS, 2019)*. Thereby, the delayed effect of the nanodelivery system is strongly positive in clinical therapy. Subsequently, the liposomes loaded with both BRB and TAR were optimized (BRB/TAR-L) and this formulation showed a significant increase in BRB uptake by the K562/DOXO cell line.

These results together with the ability of TAR-L to significant resensitization of the resistant variant for DOXO, suggest that the co-delivery of the P-gp inhibitor, TAR, and the cytotoxicity inducer, BRB, looks like a promising approach to overcome the MDR. The optimized co-administration system can also be useful for all antitumoral drugs that are substrates of P-pg with the advantage of being able to reduce the dose of cytotoxic drugs by increasing their efficacy. Finally, the nanoliposomes described in this study have a protective

value both for the molecules transported and for the healthy tissues in an *in vivo* administration. Toxicity of the nanoliposomes based on P90G and Chol is generally trivial, because of their composition. However, intravenously injected liposomes can interact with plasma proteins, can stimulate or suppress the immune system due to their physical and chemical characteristics. Future studies will be oriented to the *in vivo* studies to examine the eventual intrinsic toxicity, the drugs retention and circulation properties of the nanosystems, which results quite interesting, due to an easy synthesis and scale-up by the pharmaceutical industry.

MUCOADHESIVE MICROEMULGEL FOR THE TOPICAL DELIVERY OF CLOBETASOL PROPIONATE IN THE TREATMENT OF MUCUS MEMBRANE PEMPHIGOID OF THE ORAL CAVITY

34. Results and Discussion

34.1. Preparation of CP-ME and pseudo-ternary phase diagram construction

Vitamin E acetate was selected as oily phase, Cremophor RH 40 (polyoxyl 40 hydrogenated castor oil) as surfactant, and glycerol as cosolvent and humectant agent. All components of the microemulsions were chosen for their flavour, as well as for their safety profile. They are in fact compatible with the injured buccal mucosa and they are already used in marketed products for buccal mucosa, such as Buccagel afte, Alovex gel, Tantum verde SOS afte gel. In addition, they are safe by ingestion, since they are suitable for the oral administration.

The pseudo-ternary phase diagram (Figure 52) was constructed by the water titration technique, using different combinations of vitamin E acetate and S_{mix} (Cremophor RH 40/glycerol, 1:1 *w*/*w*). The green area represents the microemulsion existence range, the blue area is the emulsion region, the light blue area is the gel, and the gray area is the turbidity zone. The selected microemulsion, composed of 80% water, 2% vitamin E acetate, 9% glycerol and 9% Cremophor RH 40, was loaded with 0.054% *w*/*w* of CP, by dissolution of the active ingredient in an exact amount of ME.

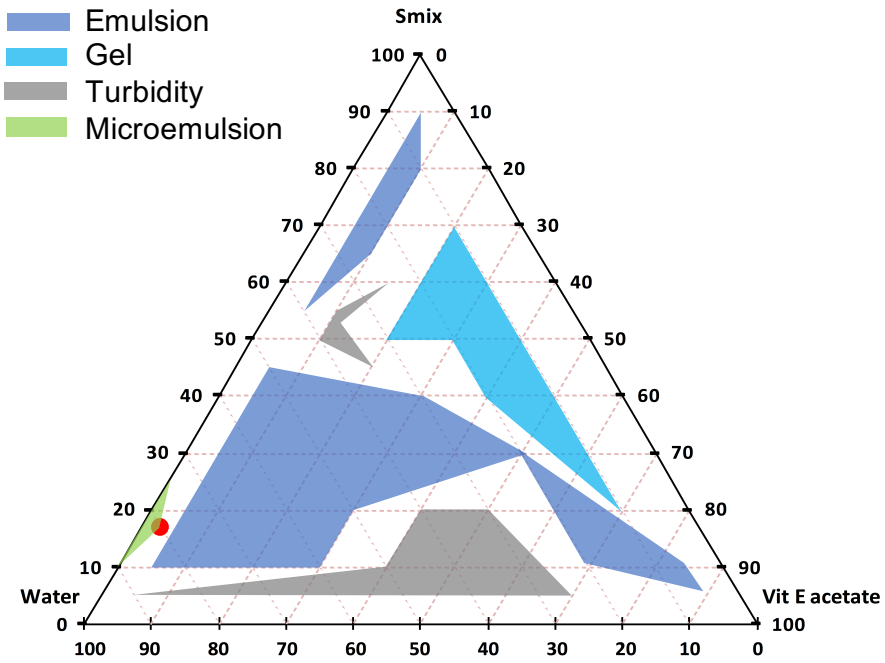

Figure 52. Pseudo-ternary phase diagram. Green area represents the ME existence region, the blue area is the emulsion, the light blue is the gel and the grey area is turbidity.

34.2. Physical and chemical characterization of CP-ME: Size, PdI, Recovery

Developed ME and CP-ME were analysed by DLS. Both formulations were clear with small droplet dimensions and high homogeneity (Table 36). CP loading did not affect the physical parameters of the microemulsion, which presented average globule sizes of approximately 29 nm and PdI about 0.2 (Table 36). Moreover, the addition of 1 g/mL aqueous solution of anhydrous citric acid as pH regulator did not significantly changed Size and PdI of the formulation, as well. A highly concentrated aqueous solution was prepared in order to add a minimum volume as possible.

The micrographs obtained by STEM analysis of the microemulsion showed perfectly and homogeneously distributed small and spherical droplets (Figure 53), confirming light scattering data.

Furthermore, the exact amount of CP recovered in the microemulsion after the preparation procedure, determined as total recovery (R%), was found to be approximately 100%.

Table 36. Physical characterization, in terms of Size and PdI, of ME and CP-ME (clobetasol propionate-loaded microemulsion) . Data are shown as Mean ± SD (n=3).

Sample	Size (nm)	PdI
ME	28.49±2.00	0.202±0.060
CP-ME	29.61±1.60	0.217±0.046
CP-ME + ACA	31.55±0.58	0.262±0.008

ACA= aqueous solution of anhydrous citric acid

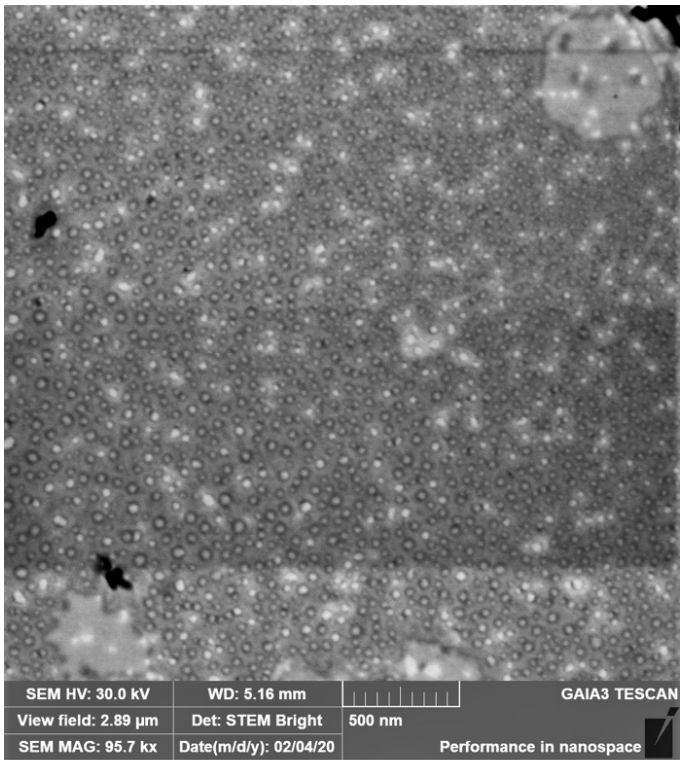

Figure 53. Picture of CP-ME (clobetasol propionate-loaded microemulsion) by STEM.

34.3. Physical and chemical stability of CP-ME

The stability studies on CP-ME were carried out storing the sample at 4 °C and 25 °C, far from the light. CP-ME stored at 4 °C showed higher physical stability in terms of droplet dimensions (Size) and sample homogeneity (PdI), because Size and PdI slightly increased during the 3 months of storage (Figure 54). By contrast, both samples showed high chemical stability, because the CP recovery was constant during all period of storage at 4 °C and 25 °C (Figure 55).

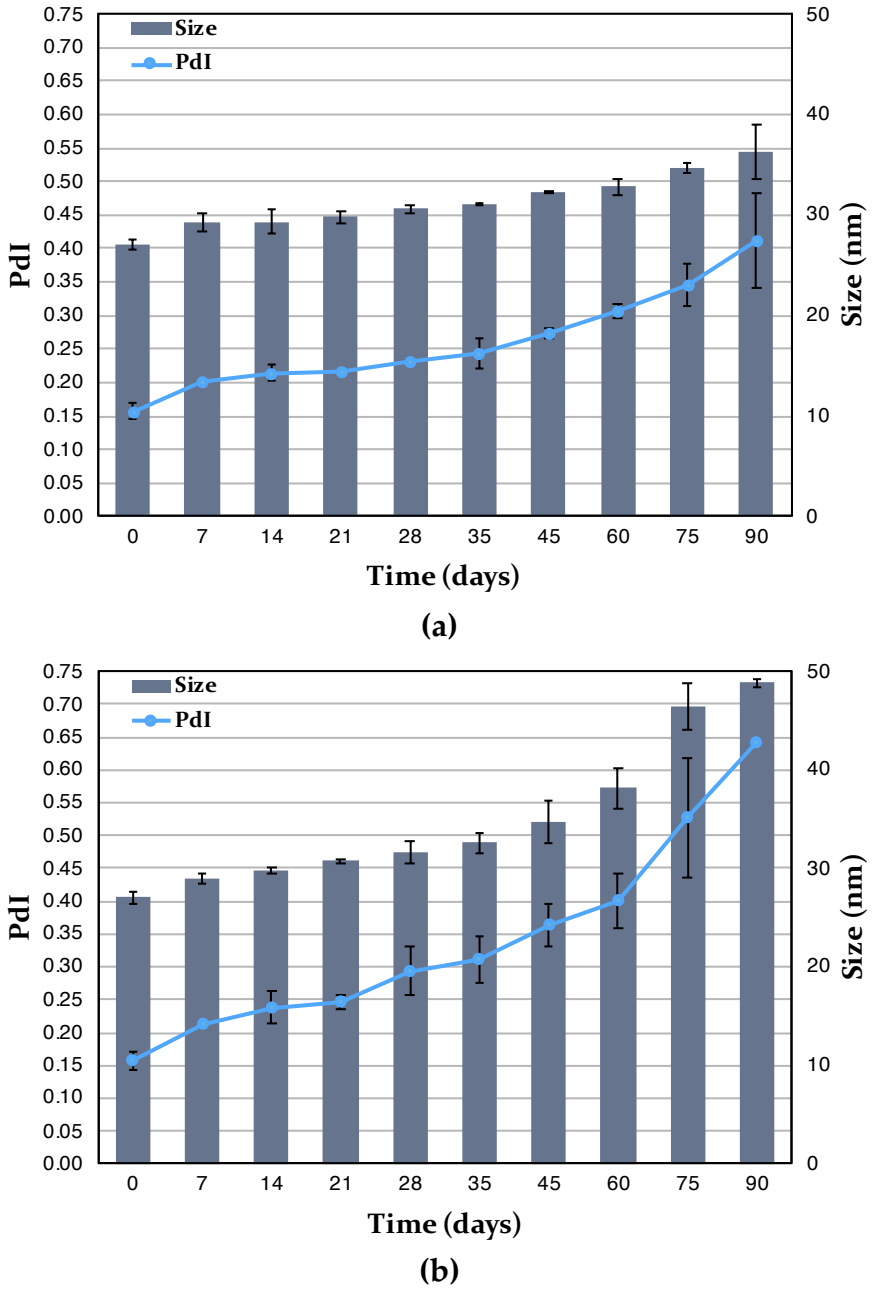

Figure 54. Physical stability, in terms of Size and PdI, of CP-ME (clobetasol propionate-loaded microemulsion), stored at **(a)** 4 °C and **(b)** 25 °C. Mean ± SD (n=3).

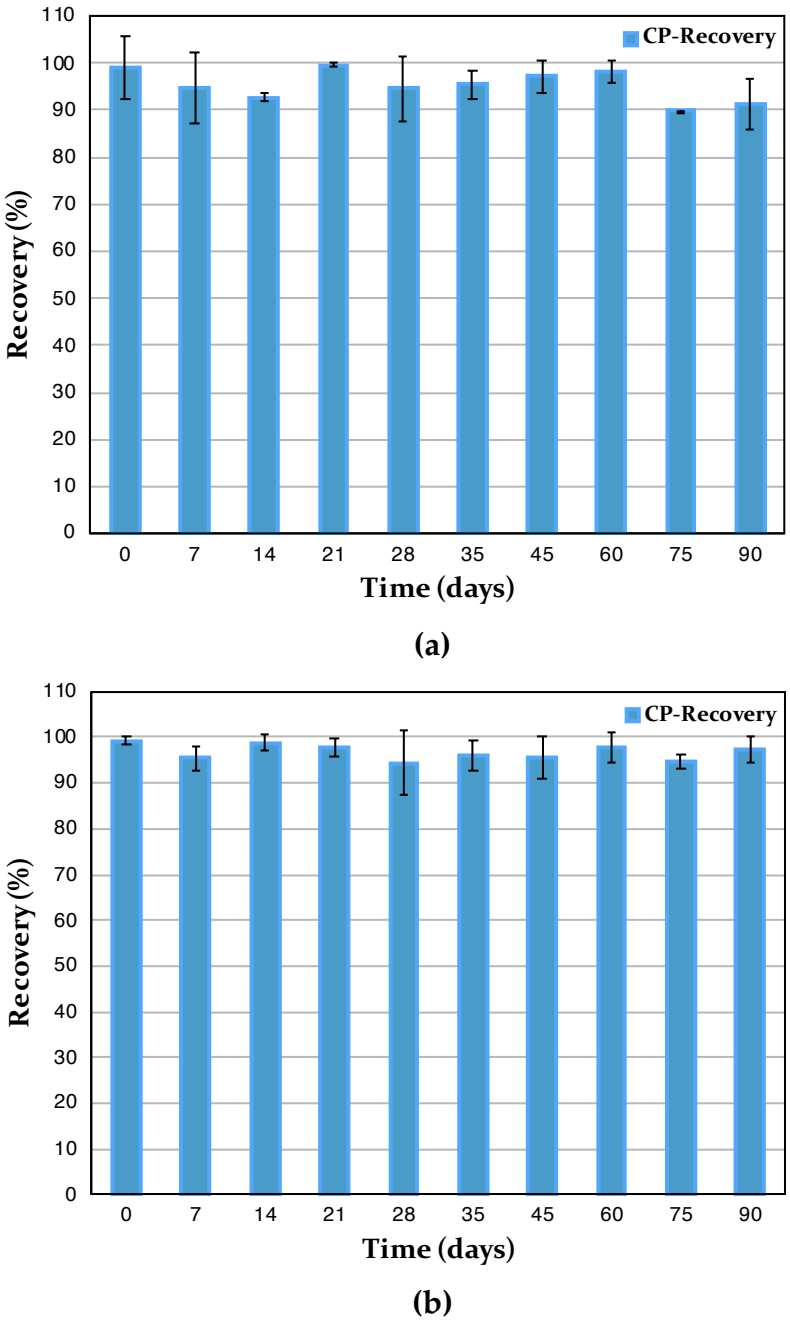

Figure 55. Chemical stability, in terms of total recovery, of CP-ME (clobetasol propionate-loaded microemulsion), stored at **(a)** 4 °C and **(b)** 25 °C. Mean ± SD (n=3).

34.4. Preparation of CP-MEgel

Once the CP-ME was prepared, various gelling agents (sodium carboxymethyl cellulose, CMC; hydroxypropyl methylcellulose, HPMC; carboxymethyl chitosan, CMChit and xanthan gum) were added in different percentages (0.1, 0.5, 1, 2, 3)% *w/w*.

It was observed that the xanthan gum at 0.1% *w/w* concentration was completely dissolved in CP-ME, but the formulation remained liquid. At 0.5%, the formulation was viscous, but opalescent and not homogeneous.

HPMC was tested exclusively at the concentration of 0.1% to which the system became opalescent and not homogeneous. Consequently, HPMC was not used at further concentrations.

By contrast, CMC and CMChit quickly incorporated CP-ME at low concentrations (0.1% and 0.5%), whereas they needed vigorous manual dispersion for the highest concentrations (1%, 2%, 3%). Gradually increasing the gelling agent concentration, the formulation became more viscous, remaining transparent (with CMC) or light yellow (with CMChit) and very homogenous.

CMC is an excipient widely used in many commercial preparations also for buccal application, whereas CMChit is an innovative component. Both CMC and CMChit were selected as the best thickening agents because of their ability to rapidly and uniformly jellifying the system, as well as for their mucoadhesive property, in addition to the biocompatibility, biodegradability, moisture absorption/retention and role in skin regeneration and wound healing.
Subsequently, CMC and CMChit were combined in different percentages in order to obtain an microemulgel with optimal viscosity and mucoadhesion properties.

The tested percentages were (1.5, 2, 2.5, 3, 3.5, 4, 5, 6) % *w/w* for CMC and (0.5, 1, 1.5, 2, 2.5, 3, 3.5, 4, 5, 6)% *w/w* for CMChit. The microemulgels obtained with 1.5% CMC plus 5% CMChit, 4% CMC plus 2% CMChit and 5% CMC plus 2% CMChit were found to be the most promising formulations, since they had the greatest viscosity without aggregates.

34.5. Physical and chemical characterizazion of CP-MEgel

34.5.1. Viscosity measurement

Viscosity of three most promising microemulgels was measured at 25 °C by the rotational viscometer, recalibrated as described by Vanti and coworkers *(Vanti G, 2020b)*. All viscosity measurements clear-fell within the obtained FSR (Full-Scale Range) and were plotted on a graph, which represents the up/down rate ramps of viscosity, as a function of the spindle rotational speed (Figure 56). The three microemulgels showed similar viscosity properties. They were found to be non-Newtonian, since they have different viscosities at different rotational

speeds; time-indipendent, because the viscosity did not change as a function of time when measuring at specific speeds: the down-ramp matched the initial up-ramp; shear thinning, because the viscosity decreased when the spindle rotational speed was increased. However, the microemulgel with 5% CMC plus 2% CMChit showed the greatest viscosity and it was selected as final microemulgel of clobetasol propionate (CP-MEgel). The viscosity of CP-MEgel was also measured at 37 °C, in order to mimic the mouth temperature, and it was observed a decrease in viscosity values (Figure 57).

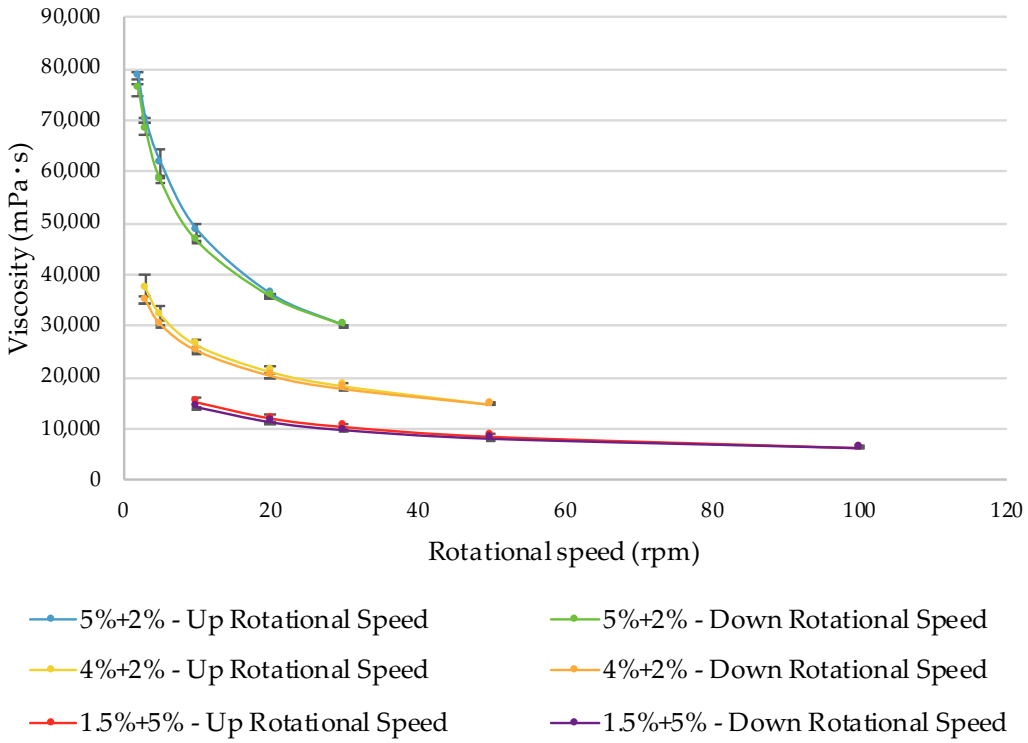

Figure 56. Up and down viscosity ramps of the three microemulgels of clobetasol propionate obtained with: 5% CMC (carboxymethyl cellulose) plus 2% CMChit (carboxymethyl chitosan), 4% CMC plus 2% CMChit, 1.5% CMC plus 5% CMChit. Up viscosity ramp is the viscosity curve obtained from the spindle rotational speed increasing from 2 rpm to 30-50-100 rpm, while down viscosity ramp is the viscosity curve obtained from the spindle rotational speed reduction from 30-50-100 rpm to 2 rpm. Data are shown as Mean ± SD (n=3).

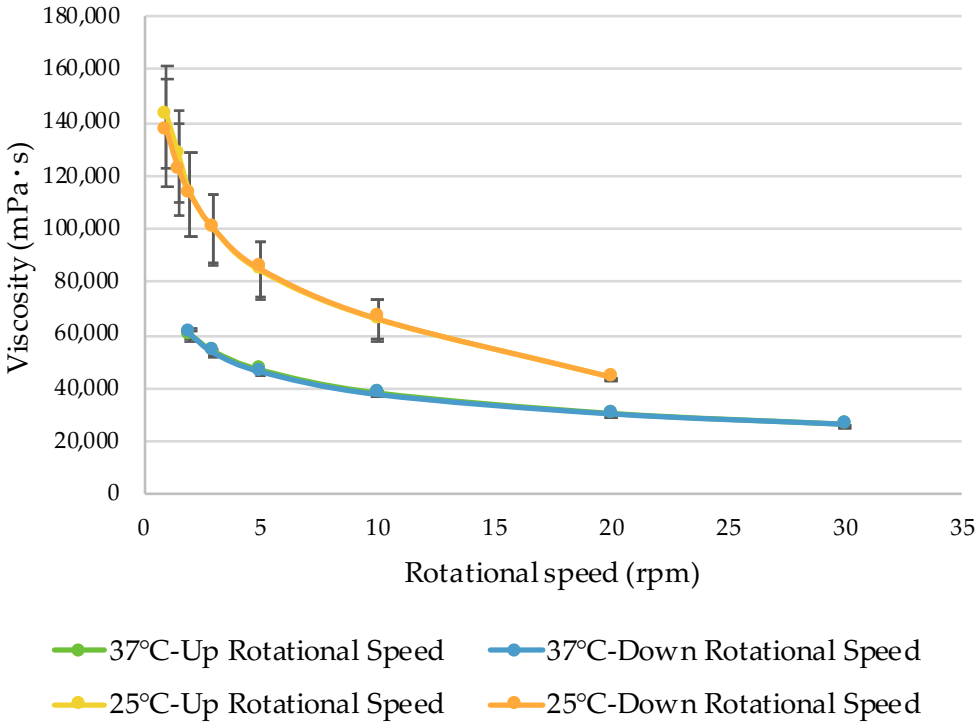

Figure 57. Up and down viscosity ramps CP-MEgel (microemulge of clobetasol propionate), measured at 25 °C and 37 °C. Up viscosity ramp is the viscosity curve obtained from the spindle rotational speed increasing from 1-2 rpm to 20-30 rpm, while down viscosity ramp is the viscosity curve obtained from the spindle rotational speed reduction from 20-30 rpm to 1-2 rpm. Data are shown as Mean ± SD (n=3).

34.5.2. DLS analysis

CBD-MEgel was analyzed by DLS after 20-fold dilution in ultrapure water, and it was observed that dimensions (size) and homogeneity (PdI) of the microemulsion droplets were practically unchanged after the gelation process.

Moreover, the addition of 0.1% *w/w* of 50% benzalkonium chloride aqueous solution to the microemulgel slightly affected average droplet sizes and PdI, which resulted (43.30±1.24) nm and (0.264±0.012), respectively.

34.5.3. STEM analysis

Subsequently, CP-MEgel and CBD-MEgel after 20-fold dilution in ultrapure water were analysed by the Scanning Electron Microscope (SEM) Gaia 3 with a bright-field TEM detector. The obtained findings were in accordance with those derived from DLS analysis. Pictures of both CP-MEgel (a) and CP-MEgel after aqueous dilution (b) showed in fact a lot of spherical droplets with the same sizes

of those of CP-ME, demonstrating that the microemulsion structure remained stable after the gelation with CMC and CMChit (Figure 58).

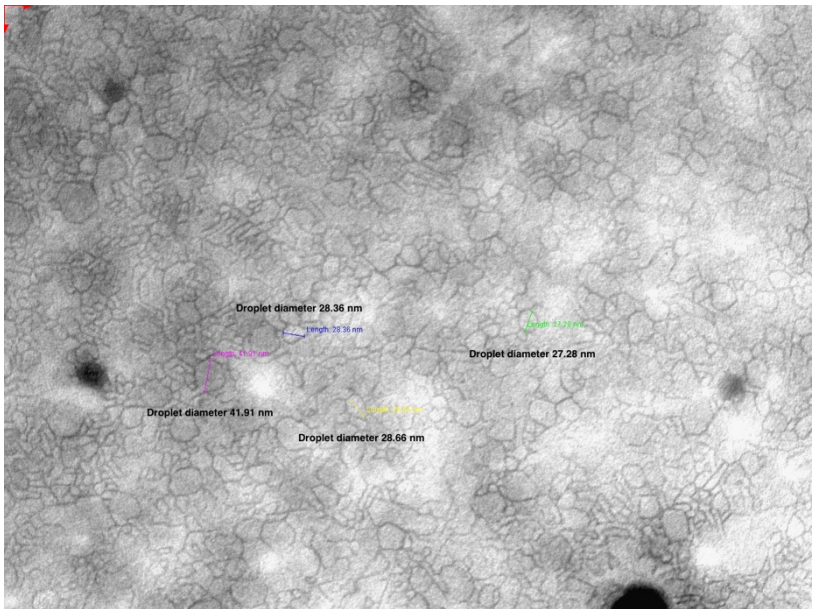

(a)

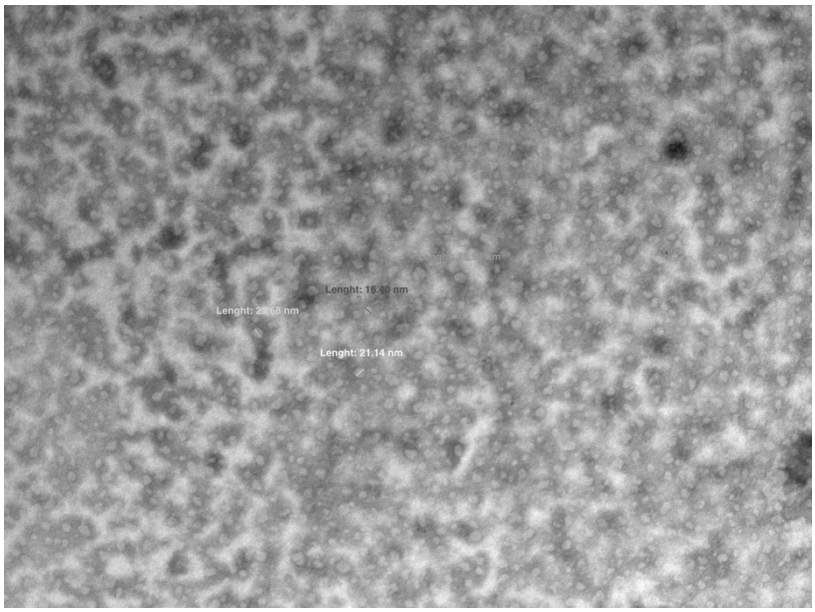

(b)

Figure 58. Pictures of **(a)** CP-MEgel (microemulgel of clobetasol propionate) and **(b)** CP-MEgel after aqueous dispersion, by STEM.

34.5.4. pH determination

The pH of developed CP-MEgel was found to be 9.80±0.10. The addition of 0.5% *w/w* aqueous solution of anhydrous citric acid, during the preparation step

of CP-ME, decreased the pH to 7.36±0.58. The obtained pH was compatible with the mouth mucosa since the physiological pH of saliva is normally around 6-7 *(Satheesh Madhav NV, 2009)*.

34.6. Physical and chemical stability of CP-MEgel

Physical and chemical stability studies were carried out on the formulation stored at room temperature (25 °C), far from the light. After 3 months of storage the amount of CP recovered in the microemulgel was nearly 100%.

Viscosity of CP-MEgel, measured at 25 °C (Figure 59), was found to be a little decreased compared to the viscosity at time zero (T0), whereas viscosity measured at 37 °C (Figure 59) resulted a little increased. Despite these slight variations, the microemulgel was still non-Newtonian and, particularly, time-independent, since the up viscosity ramp matched the down viscosity ramp. It was also shear thinning, because the viscosity decreased as spindle rotational speed increased (Figure 59a and 59b).

Light scattering analysis finally demonstrated a little increase in average droplet sizes (66.16±0.84 nm) and PdI (0.449±0.007) of the gelled microemulsion, without affecting its homogeneity by visual inspection. Overall, CP-MEgel showed a great physical and chemical stability at the analysed storage conditions.

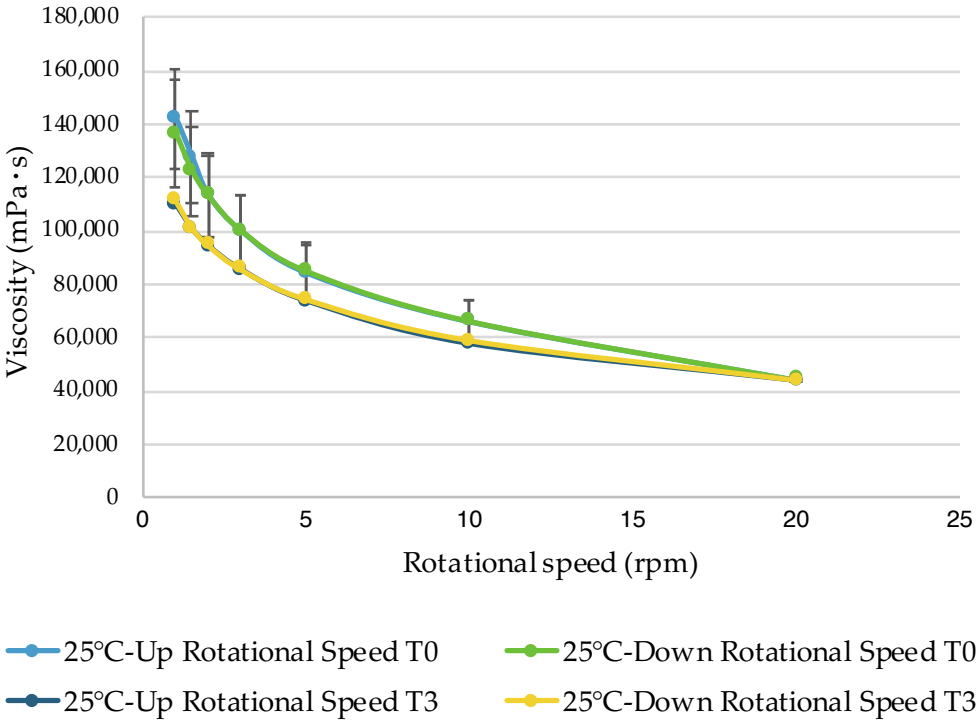
180,000
160,000
140,000
120,000
100,000
80,000
60,000
40,000
20,000
0
Viscosity (mPa·s)
0
5
10
15
20
25
Rotational speed (rpm)
25°C-Up Rotational Speed T0
25°C-Down Rotational Speed T0
25°C-Up Rotational Speed T3
25°C-Down Rotational Speed T3

(a)

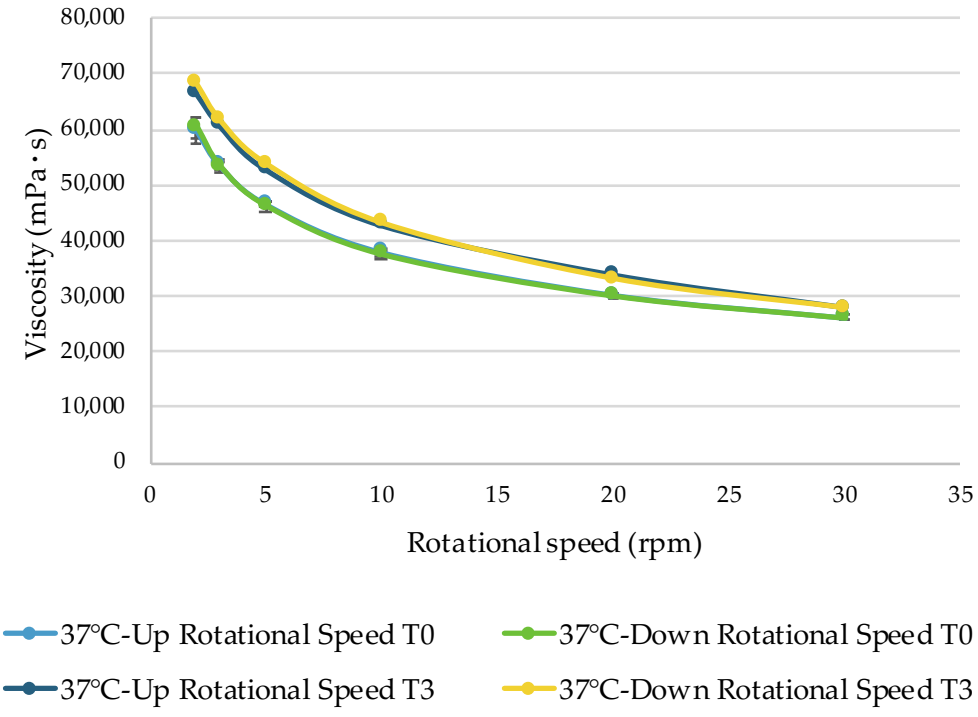
80,000
70,000
60,000
50,000
40,000
30,000
20,000
10,000
0
Viscosity (mPa·s)
0
5
10
15
20
25
30
35
Rotational speed (rpm)
37°C-Up Rotational Speed T0
37°C-Down Rotational Speed T0
37°C-Up Rotational Speed T3
37°C-Down Rotational Speed T3

(b)

Figure 59. Physical stability of CP-MEgel (microemulgel of clobetasol propionate) after 1 month of storage: **(a)** up-down ramp viscosity at 25 °C; **(b)** up-down ramp viscosity at 37 °C. Up viscosity ramp is the viscosity curve obtained from the spindle rotational speed increasing from 0.6-1 rpm to 20-30 rpm, while down viscosity ramp is the viscosity curve obtained from the spindle rotational speed reduction from 20-30 rpm to 0.6-1 rpm. Data are shown as Mean ± SD (n = 3).

34.7. Release study of CP-MEgel by vertical diffusion Franz cells

The passive diffusion of CP from CP-MEgel to the buccal mucosa was investigated measuring the CP release rate from the microemulgel. The experiment was carried out using the Franz cell system and 0.45 μm cellulose nitrate membranes, selected for their high porosity, which allows high-flux of molecules and minimal diffusional resistance. Cellulose-based synthetic membranes are widely used in the release studies for many years, because they do not act as barriers, but like supports, without limiting the flow rate of drugs. Particularly, CP release from CP-MEgel was compared to CP release from CP-gel. The study highlighted that the CP release was low for both gels, probably due to a strong interaction of the active with the polymeric matrix of CMC and CMChit (Figure 60). The two gels also had the same kinetic profile, which follows the zero order model: $R^2 = 0.995$ for CP-MEgel and $R^2 = 0.994$ for CP-gel. However, CP release from the gelled microemulsion (CP-MEgel) was slightly slower (about 0.74% after 7h) compared to the release from CP-gel (about 0.99%). Taking into account the exchange area between the gel and the receptor compartment, separated by the cellulose membrane, it was found that 1.1526±0.1782 μg/cm^2 of CP were release after 7 h from CP-MEgel and 1.7079±0.1225 μg/cm^2 were released from CP-gel.

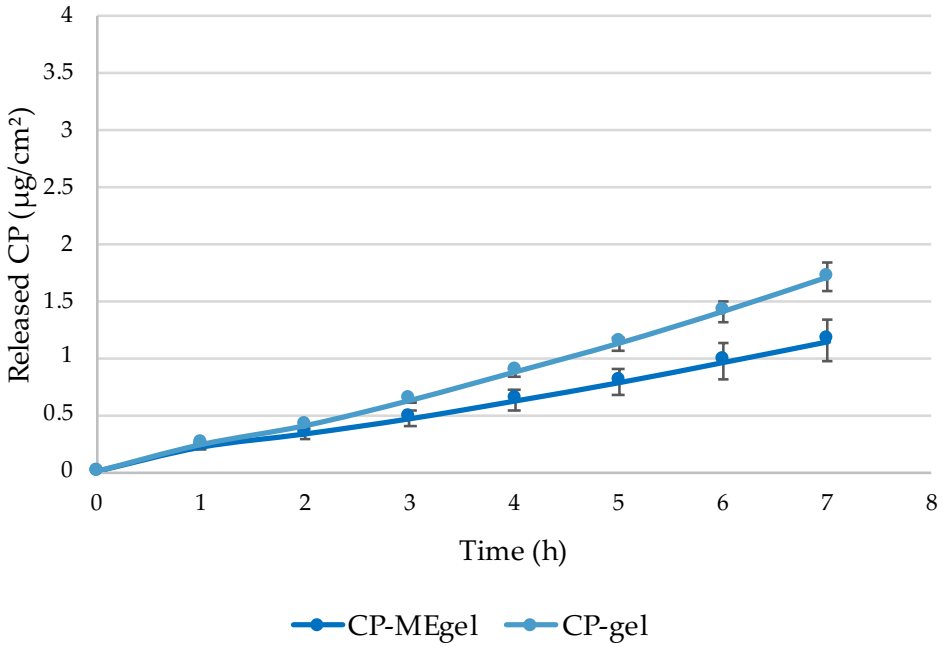

Figure 60. Release of CP from CP-MEgel (microemulgel of clobetasol propionate) and CP-gel (hydrogel of clobetasol propionate aqueous dispersion). Mean±SD (n=3).

34.8. Permeation study of CP through porcine buccal mucosa

The absorption rate of CP through porcine buccal mucosa was explored by the vertical diffusion Franz cells for 7 h, maximum supposed residence time of the formulation on the buccal mucosa upon administration. The investigation was carried out for both CP-MEgel and CP-gel, in order to evaluate the effect of CP loading in the gelled microemulsion in comparison to the conventional CP formulation in a gelled aqueous dispersion. After 7 h of incubation, CP was not recovered in the receptor compartment, but it was quantitatively determined in the mucosa, 0.11±0.02% for CP-MEgel and 0.31±0.05% for CP-gel, compared to the CP amount in the donor compartment. Considering the effective diffusion area of 3.14 cm^2, total CP absorbed and retained in the porcine buccal mucosa (M_7) was 0.1632±0.0158 $\mu g/cm^2$ and 0.4701±0.0659 $\mu g/cm^2$ for CP-MEgel and CP-gel, respectively. Overall, as CP release rate is slower for the microemulgel, the total CP absorbed in the mucosa (M_7) is also lower in comparison to the hydrogel of the aqueous dispersion. This phenomenon can be due to the reservoir system represented by the gelled microemulsion, which delays the passive diffusion of the active ingredient toward the deeper mucosa layers.

DEVELOPMENT AND OPTIMIZATION OF BIOPHARMACEUTICAL PROPERTIES OF A NEW MICROEMULGEL OF CANNABIDIOL FOR LOCALLY-ACTING DERMATOLOGICAL USE

35. Results and Discussion

35.1. Pseudo-ternary phase diagram construction and preparation of CBD-ME

All components of the microemulsion were chosen for their biopharmaceutical properties and their safety profile after cutaneous application. Isopropyl myristate, selected as the oily phase, is an emollient and a well-known skin penetration enhancer, widely used in cosmetics and pharmaceutical preparations. Solutol HS 15 (polyoxyl 15 hydroxystearate) is a potent emulsifying and solubilizing agent, used as non-ionic surfactant, whereas Transcutol P, largely investigated for the skin penetration enhancing property, was chosen as cosolvent. The pseudo-ternary phase diagram (Figure 61) was prepared by the water titration method, using different combinations of isopropyl myristate and S_{mix} (Solutol HS 15/Transcutol P, 20:9 *w*/*w*), as described in the experimental part. Each mixture was titrated slowly taking care for proper stirring of liquid phases to achieve equilibrium. After being equilibrated, the mixtures were assessed visually for transparency and further titrated over the entire phase region. The light grey area of the pseudo-ternary phase diagram (Figure 61) represents the microemulsion existence range, whereas the dark grey area is the emulsion region. Selection of the microemulsion was based on values of PdI (less than 0.4) and mean count rate (higher than 80) measured as kilo counts per seconds (kcps), namely number of photons per second arriving at the detector and index of the scattering intensity of the sample. The selected ME, consisting of 66% water, 5% isopropyl myristate, 20% Solutol HS 15 and 9% Transcutol P, was loaded with 1.03% *w*/*w* of CBD, by dissolving the drug in the lipophilic excipients, as described in the experimental section, in order to obtain a final 1% *w*/*w* concentration in the MEgel.

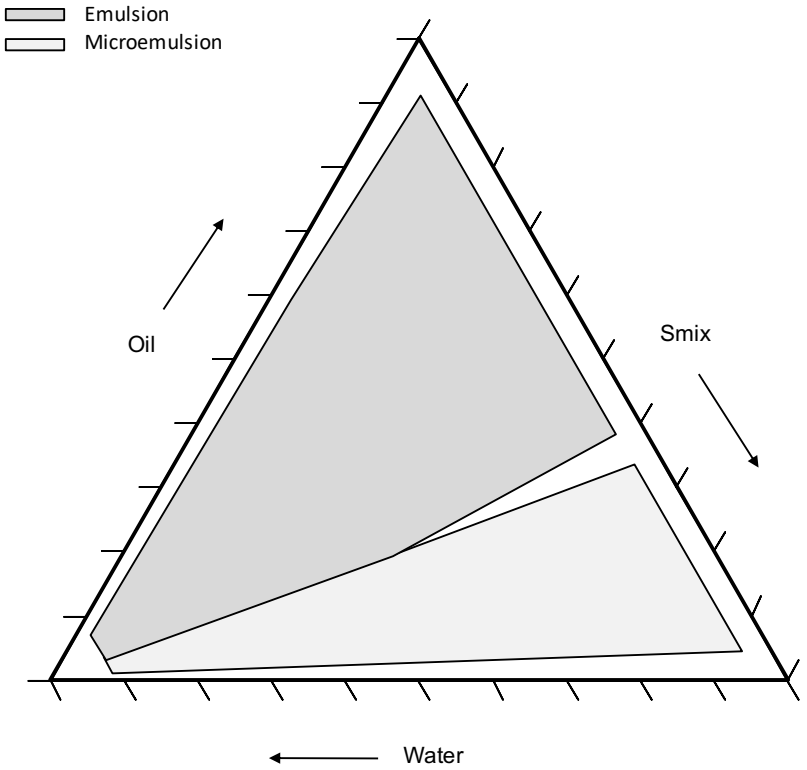

Figure 61. Pseudo-ternary phase diagram. Light grey area represents the ME existence region, while the dark grey area represents the emulsion. Oil = isopropyl myristate, while S_{mix} = Solutol HS 15 plus Transcutol P.

35.2. Formulation of CBD-MEgel

CBD-MEgel was prepared by jellifying the ME by adding various viscosifiers (Carbomer, xanthan gum and Sepigel 305) to CBD-ME, in different percentages (1.5, 2, 2.5)% *w*/*w*.

At the highest tested concentration, the xanthan gum was completely dissolved in the microemulsion, but the formulation was not adequately viscous. 2.5% *w*/*w* Carbomer easily produced a viscous and transparent gel, but small aggregates were slowly formed in the formulation. Instead, Sepigel 305, an excellent rheology modifier, was quickly incorporated in CBD-ME, by vigorous manual stirring, forming a clear, viscous and homogeneous gel. The highest percentage (2.5% *w*/*w*) was optimal to provide a MEgel with good spreadability for cutaneous application. Sepigel 305 is a widely diffused gelling agent, because extremely easy to process, both hot and cold, in addition to be stable in the pH range between 3 and 12. It contains polyacrylamide, C13-14 Isoparaffin and Laureth-7, which confer a great flexibility in use because of their lipodispersible

character. C13-14 Isoparaffin is a good emollient and Laureth-7 helps to improve the texture and feel of skincare products and cosmetics.

35.3. Physical characterization of CBD-ME and CBD-MEgel

35.3.1. Droplet size and PDI measurement

Both empty and CBD-loaded ME appeared clear by visual observation and showed small droplet dimensions with a narrow distribution, meaning of high homogeneity. Empty ME had a PdI of 0.195±0.007, while that loaded with CBD had a PdI of 0.224±0.024. The mean hydrodynamic diameter of the empty formulation was 30.33±0.18 nm, while that loaded with CBD was 34.47±1.62 nm (Table 37). Moreover, the addition of 0.2% *w*/*w* of $PABA_{mix}$ to CBD-ME, as preservative against the microorganism growth, did not change average sizes and homogeneity of the system (Table 1). Overall, both loading CBD and adding $PABA_{mix}$ did not affect the physical parameters of the ME.

CBD-MEgel was also analysed by DLS after 20 folds dilution in water, and it was observed that droplets were homogeneously distributed in the microemulgel as well as in the microemulsion (PdI was about 0.19), even if the droplet dimensions have undergone a little reduction from about *ca.* 34 nm to 25 nm (Table 37). Finally, the warming up to 35 °C (average skin temperature) did not affected the MEgel structure, because the average globule sizes remained around 26 nm (Table 37).

Table 37. Physical characterization, in terms of Size and PdI, of ME, CBD-ME (cannabidiol-loaded microemulsion), CBD-ME + $PABA_{mix}$ (paraben mixture of methyl parahydroxybenzoate plus propyl parahydroxybenzoate) and CBD-MEgel (cannabidiol-loaded microemulgel). Data are shown as Mean ± SD (n=3).

Sample	Size (nm)	PdI
ME	30.33±0.18	0.195±0.007
CBD-ME	34.47±1.62	0.224±0.024
CBD-ME + $PABA_{mix}$	35.80±0.50	0.256±0.015
CBD-MEgel	24.78±0.33	0.192±0.005
CBD-MEgel 35°C	25.59±0.15	0.260±0.014

35.3.2. Scanning and Transmission Electron Microscope analysis

CBD-ME and CBD-MEgel were morphologically analysed by the Scanning Electron Microscope (SEM) Gaia 3 with a bright-field TEM detector. Microscopy observation of the formulations confirmed the previous DLS results. Picture of

CBD-ME clearly shows a large amount of homogeneously distributed dispersed droplets, with spherical shape and small dimensions (Figure 62), which confirmed the formation of the microemulsion.

Micrographs of CP-MEgel (Figure 63b) and CP-MEgel after aqueous dilution (Figure 63c) also displayed spherical droplets with equal or slightly reduced dimensions compared to CBD-ME. Therefore, the microemulsion structure remained stable and very homogeneous after the gelation process with Sepigel 305.

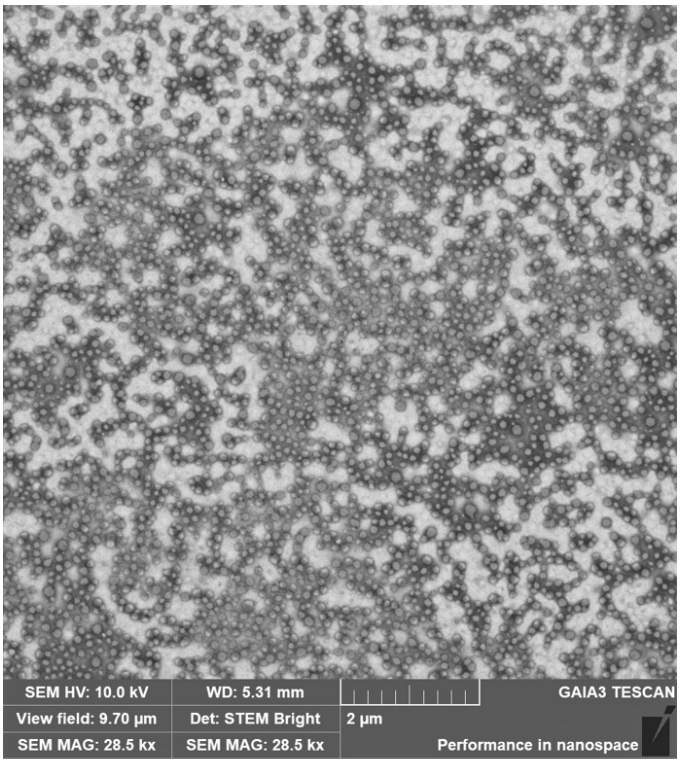

(a)

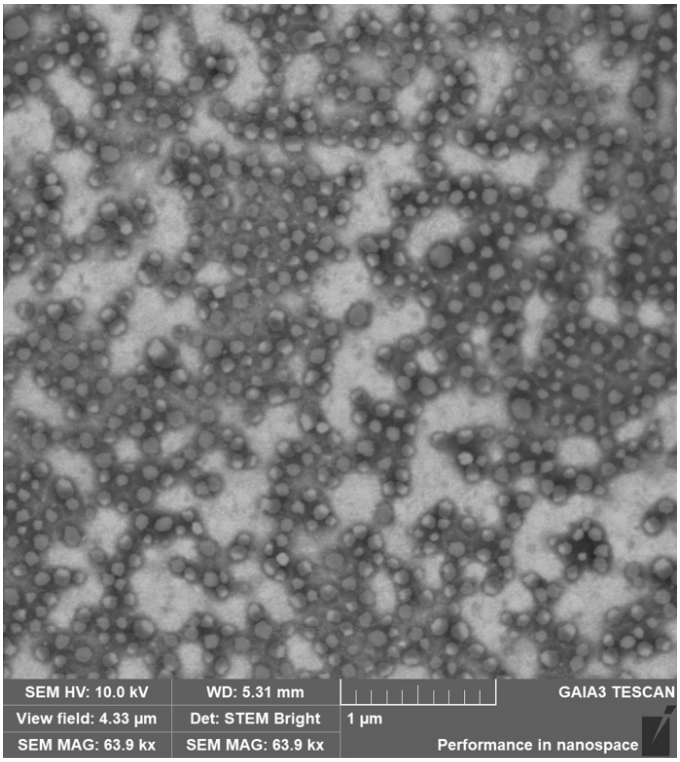

(b)

Figure 62. Pictures of CBD-ME (cannabidiol-loaded microemulsion) obtained by STEM analysis.

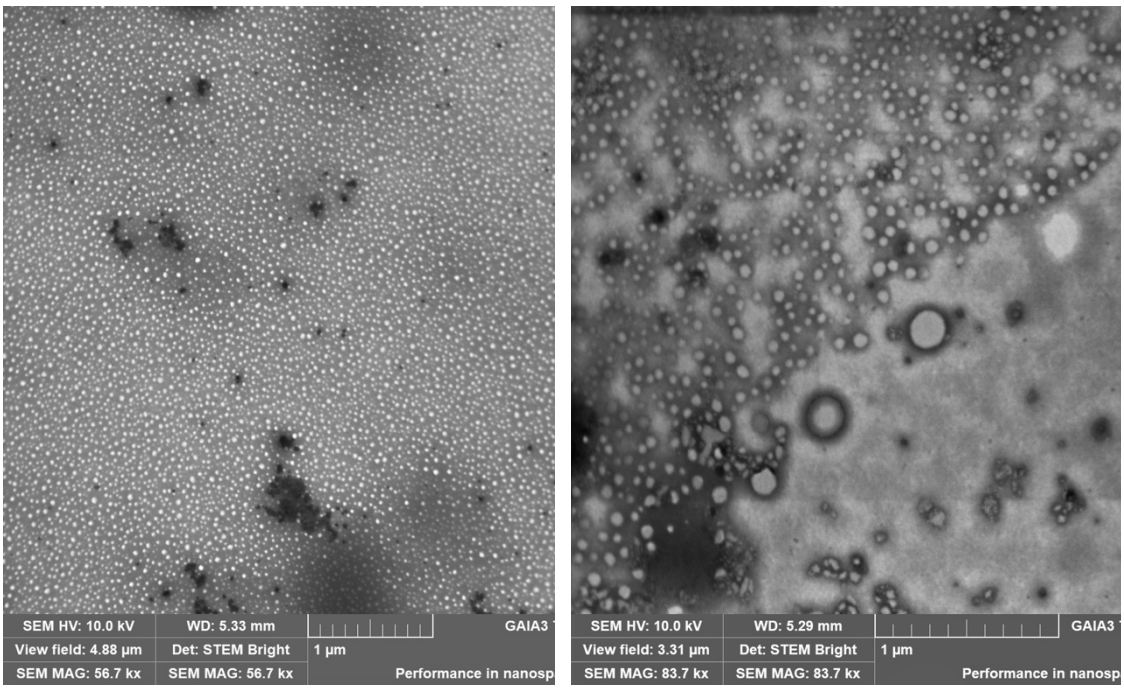

(a)

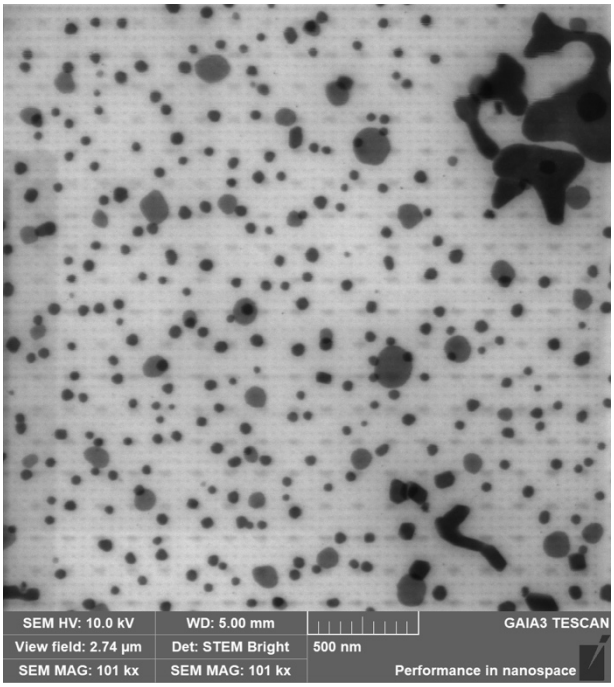

(b)

Figure 63. Pictures of **(a)** CBD-ME-GEL (hydrogel of cannabidiol-microemulsion) and **(b)** CBD-ME-GEL after aqueous dispersion, obtained by STEM analysis.

35.4. Chemical characterization: R% and pH of CBD-ME and CBD-MEgel

CBD R%, determined after the preparation of ME and MEgel, was found to be approximately 100%, indicating that any experimental condition affected the final concentration of the active. In addition, the pH (*ca.* 6.5) of the obtained CBD-ME, CBD-ME plus $PABA_{mix}$ and the correspondent CBD-MEgel was found to be stable after the addition of paraben mixture and viscosifier (Table 38), besides being suitable for dermal applications.

Table 38. pH values of CBD-ME (cannabidiol-loaded microemulsion), CBD-ME + $PABA_{mix}$ (paraben mixture of methyl parahydroxybenzoate plus propyl parahydroxybenzoate) and CBD-MEgel (cannabidiol-loaded microemulgel). Data are shown as Mean ± SD (n=3).

Sample	pH
CBD-ME	6.54±0.15
CBD-ME + $PABA_{mix}$	6.56±0.17
CBD-MEgel	6.56±0.20

35.5. Rheological properties of CBD-MEgel

Viscosity properties of the developed CBD-MEgel were evaluated at 25 °C (storage temperature) and 35 °C (average skin temperature), by the rotational viscometer, recalibrated as described by Vanti and coworkers *(Vanti G, 2020b)*. All viscosity measurements clear-fell within the obtained FSR (Full-Scale Range) and were plotted on a graph (Figure 64), which displays the up and down rate ramps of viscosity, as a function of the spindle rotational speed. CBD-MEgel was found to be non-Newtonian, time-indipendent and shear thinning. The MEgel had, in fact, different viscosities at different rotational speeds and the viscosity did not change as a function of time when measured at specific speeds (the down viscosity ramp matched the up viscosity ramp). In addition, the viscosity decreased when the spindle rotational speed was increased. It is noteworthy that CBD-MEgel viscosity values measured at 35 °C, in order to mimic the cutaneous temperature, matched those obtained at 25 °C. Therefore, the temperature did not influenced the viscosity of the formulation (Figure 64).

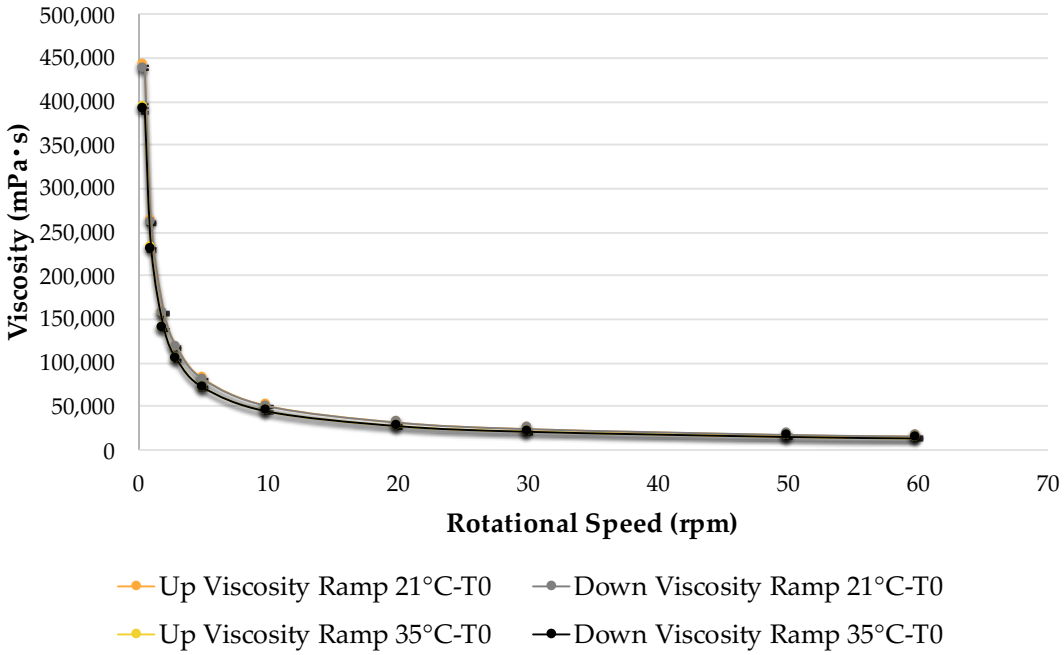

Figure 64. Up and down viscosity ramps of CBD-MEgel (cannabidiol-loaded microemulgel), measured at 25 °C and 35 °C. Up viscosity ramp is the viscosity curve obtained from the spindle rotational speed increasing from 0.5 rpm to 60 rpm, while down viscosity ramp is the viscosity curve obtained from the spindle rotational speed reduction from 60 rpm to 0.5 rpm. Data are shown as Mean ± SD (n=3).

35.6. Acceptor medium selection

From the study (Table 39), it was found that both Tween 20 and Tween 80 were suitable surfactants to enhance the solubility of CBD in the acceptor medium used for release and permeation studies. Specifically, the mixture constituted of 5% *v/v* Tween20/PBS was selected because it allowed a CBD solubility in the acceptor compartment more than 10-fold higher compared to the saturation point of the drug, and providing skin conditions during all the assay (Table 39). Solubility in 5% *v/v* PG/PBS and 5% *v/v* PEG/PBS mixtures were not determined because lower than the limit of detection of CBD.

Table 39. Cannabidiol solubility in different buffer solutions. Mean ± SD (n=3).

Acceptor solution	CBD solubility (mg/mL)
5%Tween20/PBS	16.97±0.91
5%Tween80/PBS	10.83±0.46
5%PG/PBS	n.d.
5%PEG400/PBS	n.d.

PG= propylene glycol, PEG400=polyethylene glycol 400, n.d.=not determined

35.7. In vitro release by vertical diffusion Franz cells

The *in vitro* release test was performed to investigate the release rate of CBD, in order to predict the passive diffusion of the active from the MEgel preparation to the skin, upon dermal administration. The experiment was carried out using the vertical diffusion Franz cells and the cellulose nitrate filters as membranes. Cellulose-based synthetic membranes have high porosity, allowing high-flux of molecules and minimal diffusional resistance, without limiting the flow rate of drugs. Specifically, CBD release from CBD-MEgel was compared to CBD release from CBD-gel. The study evidenced that the CBD release was low for both the formulations, probably due to a strong interaction of the drug with the Sepigel matrix (Figure 65). However, CBD release from the MEgel was slower and smaller (about 3%) compared to the release from CBD-gel (about 7%). The graph shows the different release profiles (Figure 65). The MEgel allowed a more controlled diffusion of CBD from the formulation to the acceptor compartment according to the Higuchi model ($R^2 = 0.9979$) with a consequent prolonged release upon dermal administration, whereas hydrogel of the aqueous dispersion followed a first order kinetic ($R^2 = 0.9998$).

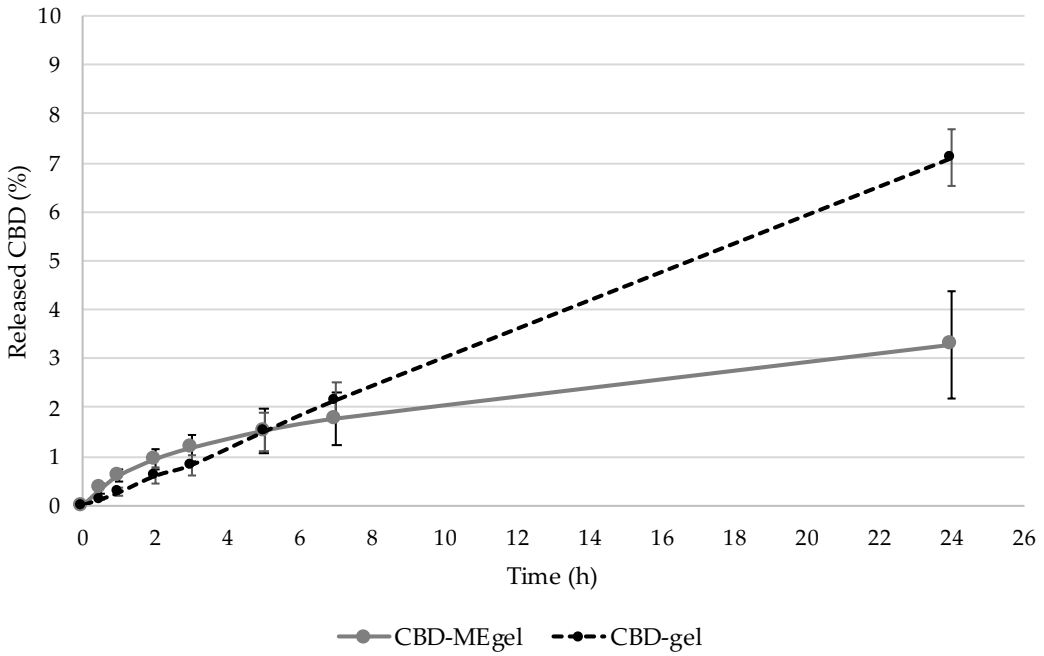

Figure 65. CBD release from CBD-MEgel (CBD-loaded microemulgel) and CBD-gel (hydrogel of CBD aqueous dispersion). The release medium was collected and analysed after 0.5, 1, 3, 5, 7 and 24 h for each sample. Data are shown as Mean ± SD (n = 3).

35.8. Permeation studies through rabbit ear skin and skin accumulation

Permeation studies of CBD through rabbit ear skin were carried out using vertical diffusion Franz cells, in order to predict transdermal CBD absorption upon dermal application. Permeation rate of CBD-MEgel and CBD-gel (with and without the microemulsion, respectively) was compared, in order to evaluate the *in vitro* performance of CBD loading in the MEgel in comparison to a conventional CBD hydrogel. From HPLC-DAD analysis, first CBD signals in the acceptor compartment were observed after 3h for CBD-gel and after 7h for CBD-MEgel (Table 40). After 24 h of incubation, 4.48±1.14 μg/cm^2 had permeated through the rabbit ear skin for CBD-gel and 2.98±1.38 μg/cm^2 were permeated for CBD-MEgel, meaning of a slower permeation related to the MEgel. CBD amount absorbed and retained inside the skin, determined at the end of the assay, was found to be 10.77±4.87 μg/cm^2 and 5.29±1.43 μg/cm^2 for CBD gel and CBD MEgel, respectively (Table 40). Overall, the lower skin permeation of CBD loaded in the MEgel, without significant transdermal absorption, made CBD-MEgel a suitable dermal delivery system for topical application.

Table 40. Transdermal permeation of CBD by CBD-MEgel (cannabidiol-loaded microemulgel) and CBD-gel (hydrogel of cannabidiol aqueous dispersion) through rabbit ear skin. Results are shown as Mean ± SD (*n*=3).

	CBD-MEgel	**CBD-gel**
Time (h)	**A (μg/cm²)**	**A (μg/cm²)**
2	/	/
3	/	1.26±0.48
5	/	1.51±0.52
7	1.06±0.60	1.80±0.49
24	2.98±1.38	4.48±1.14
	S_{24} (μg/cm²)	**S_{24} (μg/cm²)**
	5.29±1.43	10.77±4.87
	TA_{24} (μg/cm²)	**TA_{24} (μg/cm²)**
	7.29±1.64	15.26±3.84

A=absorbed dose; S_{24} =dose retained inside the skin after 24h; TA_{24} = total absorbed dose after 24h

35.9. CBD-ME and CBD-MEgel stability study

35.9.1. Physical and chemical stability of CBD-ME

CBD-ME was stored at 4 °C and 21±2 °C in the dark, in order to monitor the chemical and physical stability. After 3 months of storage, both formulations presented a slight increase in the average droplet dimensions (approximately from 33 nm to 48 nm) and in PdI (Figure 66A). However, CBD-ME was still visually clear and without phase separation or sedimentation phenomena; the formulation was, thus, physically stable. CBD-ME also showed optimal chemical stability, because CBD R% remained around 100% and pH was also constant during all the storage period, at both monitored temperature (4 °C and 25 °C), (Figure 66B).

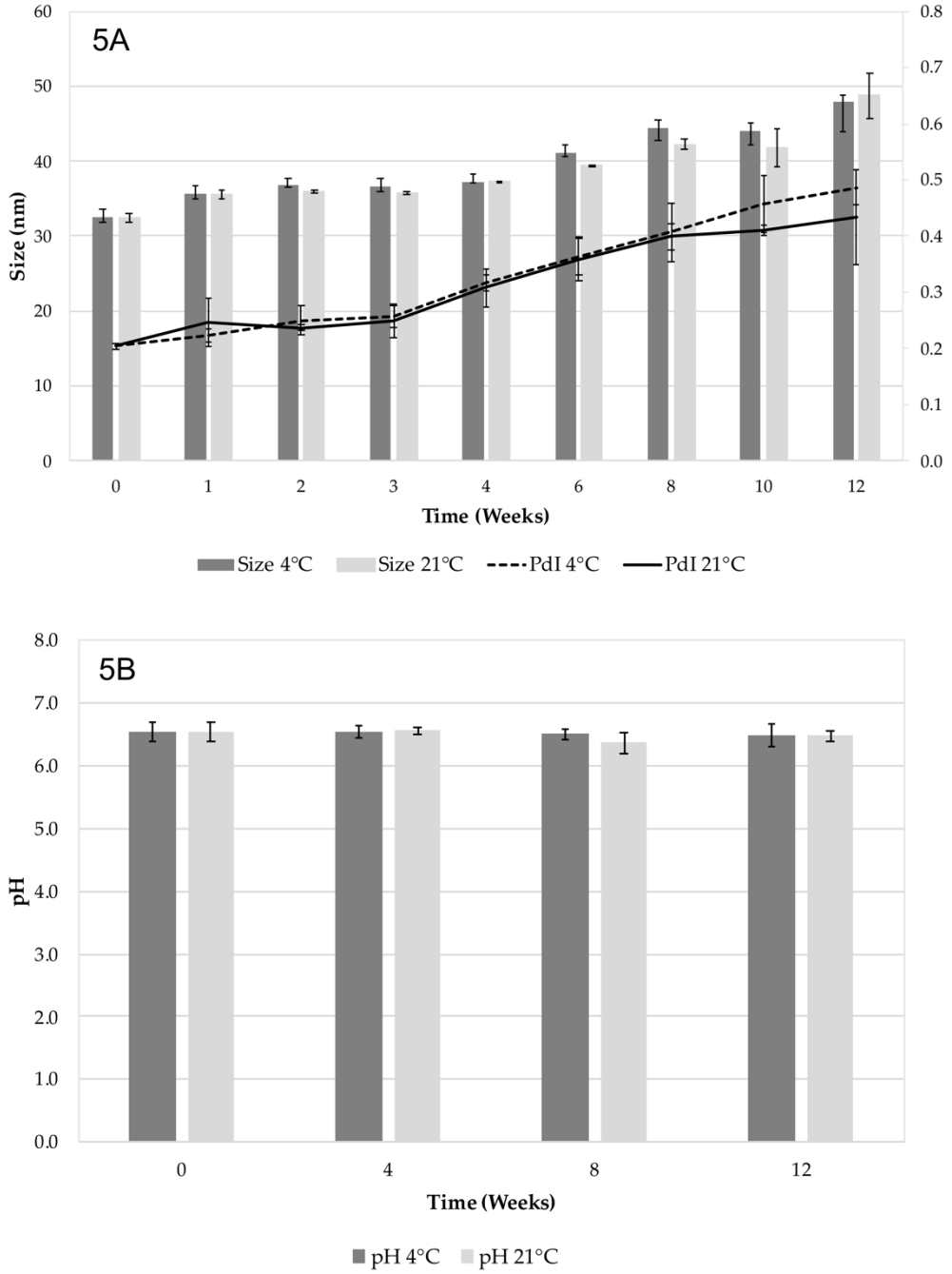

Figure 66. (A) Physical stability, in terms of Size and PdI, of CBD-ME (CBD-loaded microemulsion), stored at 21 °C and 4 °C for 3 months. Results are shown as Mean ± SD (n=3). **(B)** pH stability of CBD-ME (cannabidiol-loaded microemulsion), stored at 21°C and 4°C for 3 months. Results are shown as Mean ± SD (n=3).

35.9.2. Physical and chemical stability of CBD-MEgel

Chemical and physical stability of CBD-MEgel was also evaluated for three months, storing the sample at 21±2 °C, away from the light. Once every month CBD R% and pH were determined and average sizes, PdI and viscosity of the

formulation were also measured. CBD-MEgel presented an optimal chemical stability, because CBD concentration was constant (*ca.* 100%) over time and the pH value always remained around 6 (Table 41).

DLS analysis showed that average droplet sizes were substantially unchanged after 3 months (28.95±0.32 nm) and only a little increase in PdI was observed (0.335±0.001). However, gelation of the ME seemed to stabilize the formulation in terms of dimensions of the dispersed phase, because the increase in diameter observed in the stability study of CBD-ME was not observed for CBD-MEgel. The rheological properties were also unaltered at both the monitored temperatures (21 °C and 35 °C; Figure 67A). CBD-MEgel demonstrated a non-Newtonian behaviour, particularly it appeared as a time-independent and shear thinning fluid, since the up and down viscosity curves were perfectly superimposable and the viscosity decreased as spindle rotational speed increased (Figure 67B). Besides a slight increase of viscosity from the second month, probably due to a little evaporation, overall, the developed CBD-MEgel showed excellent chemical and physical stability at the checked storage conditions.

Table 41. Chemical stability in terms of pH of CBD-MEgel (cannabidiol-loaded microemulgel) stored at 21 °C for 3 months. Mean ± SD (n=3).

Time (months)	pH
0	6.56±0.20
1	6.28±0.24
2	6.38±0.19
3	6.64±0.39

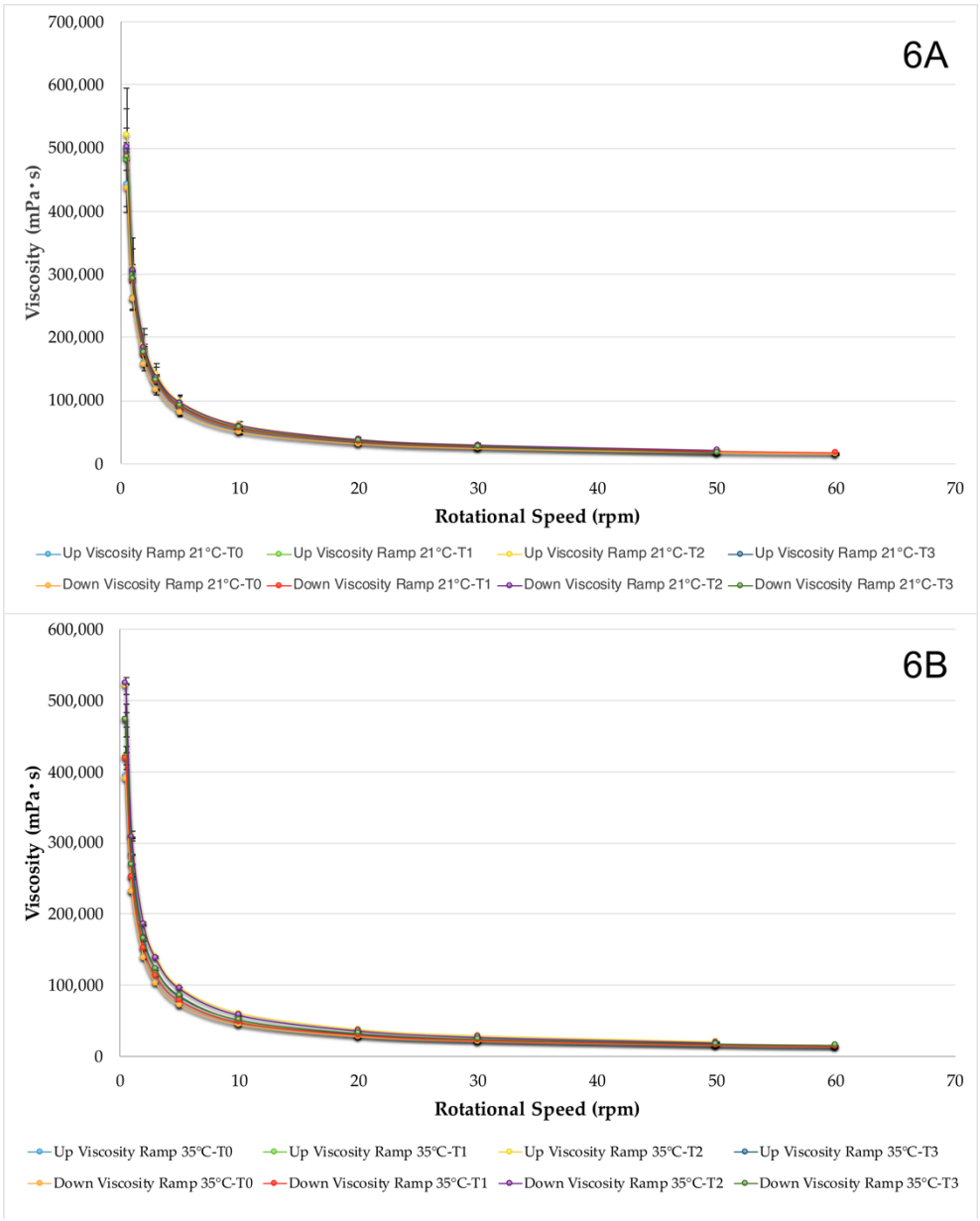

Figure 67. Viscosity stability of CBD-MEgel (cannabidiol-loaded microemulgel) during 3 months of storage, measured at **(A)** 21°C and **(B)** 35°C. Data are shown as Mean ± SD (n = 3).

MICROEMULSION-HYDROGEL COMPOSITE AS A PROMISING VEHICLE FOR DERMAL DELIVERY OF LIPOPHILIC MOLECULES: THE CASE OF KHELLIN

36. Results and discussion

36.1. Formulation of ME and pseudo-ternary phase diagram production

First aim of this study was the formulation of an O/W ME, an isotropic thermodynamically stable nanosized dispersion formed when an oily phase, water, and surfactant/cosurfactant are mixed in appropriate proportions. ME are extraordinary drug delivery systems for topical application because of the vast superficial area due to their nanosized droplets and their composition, that enables the use of penetration enhancers in the same formulation. Selection of components of the ME was based on their peculiar properties: the oily phase was vitamin E acetate, essential for the maintenance of healthy skin, Labrasol® was chosen because a safe surfactant with penetration enhancer activity, and glycerol as cosurfactant, well known for improvement of skin barrier function and mechanical properties, hydration, and acceleration of wound-healing processes.

The ME system was created using "pseudo-ternary phase diagram", where each apex of a triangular phase diagram represents a component, namely the oily phase, water, and the surfactant and cosurfactant mixture, which is jointly taken as a single phase and is located on one apex (Figure 68).

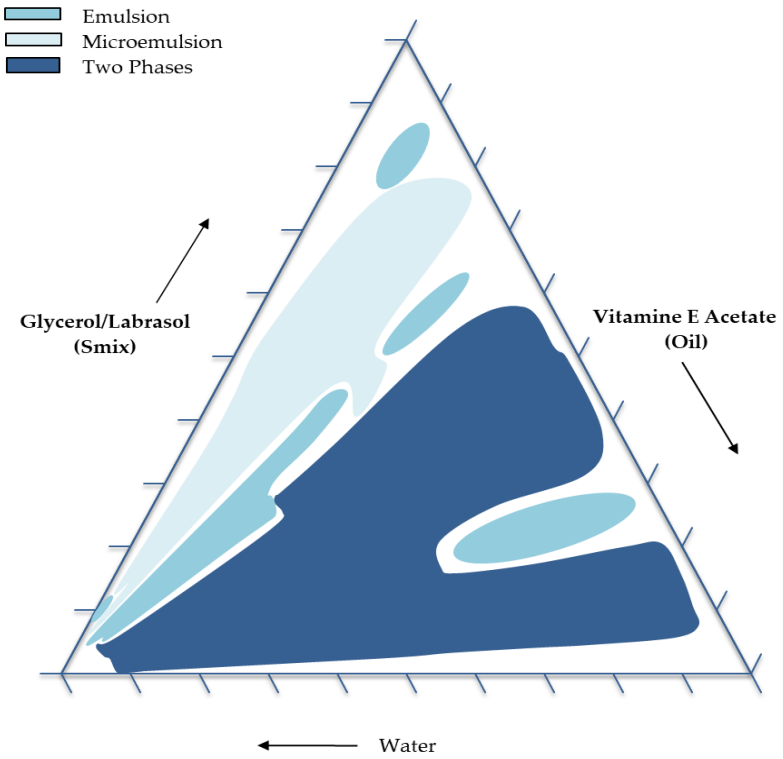

Figure 68. Pseudo-ternary phase diagram.

In order to prepare the ME, vitamin E acetate was firstly solubilised in the surfactant and cosurfactant mixture using a magnetic stirring at 35° C for 5 min and 350 rpm. During titration with water, temperature was maintained at 35±2 °C, at 500 rpm. After titration, the system was left to stabilize under magnetic stirring at 300 rpm for 30 min, at room temperature. The pseudo-ternary diagram was constructed using the titration method. The gravimetric ratio of surfactant/cosolvent (S_{mix} mixture) was kept constant and different gravimetric S_{mix}/oil ratios were evaluated starting from 9:1 to 1:9. The aqueous phase was added to the oil phase (S_{mix}/oil) drop by drop, under magnetic stirring, applying the stirring conditions at 500 rpm and a temperature of 35±2 °C. To verify the effectiveness of the ME formation, visual analysis of the systems was performed during and after titration, evaluating the formation of emulsions, by clouding the system, or of microemulsions, by turning the system from an opalescent to transparent aspect and vice versa. The selected microemulsion was constituted of glycerol (2.25%), Labrasol® (20.25%) vitamin E acetate (2.50%), in addition to water (75.00%).

36.2. Solubility of khellin into ME

After the elaboration of a pseudo-ternary phase diagram, the maximum loading content of khellin into the formulation was evaluated by adding an increasing amount of khellin to the ME under stirring. Khellin is a colourless and odourless solid, with a very low solubility in water, but soluble in organic solvents. It was selected as a representative lipophilic drug. Solubility studies were performed by HPLC-DAD analysis, as reported in the experimental part and resulted 40 mg/100 ml of oily phase, more than the double of its water solubility. The final formulation, after addition of water, was able to incorporate up to 0.1% *w/w* of khellin, without phase separation or precipitation of the molecule.

36.3. ME globules characterisation

Empty and khellin-loaded formulations (K-ME) were physically characterized by dynamic light scattering (DLS) and electrophoretic light scattering (ELS). The analyses confirmed the presence of homogeneous systems with narrow size distribution, low values of polydispersity index (PdI, 0.244±0.005 and 0.247±0.006 respectively), and mean diameter of 17.19±0.20 and 17.34±0.71. The presence of khellin did not affect the physical properties of the system. ζ-potential was also assessed by ELS and it resulted near zero.

36.4. Development of K-ME hydrogel (K-ME-GEL) composite

Due to the low-viscosity of K-ME, they are not suitable formulation for the direct topical application but their rhelogical properties can be adjusted by using an appropriate hydrophylic polymer. CMC and hydroxy-ethyl-cellulose (HEC) were selected as water soluble polymers. The developed K-ME was gelled by adding exactly weighed quantities of two viscosifiers (CMC and HEC) at increasing concentrations, namely from 1 to 6% *w/w*. The formulations were subjected to manual mechanical stirring until complete dispersion of the viscosifiers. CMC dispersed effectively, while HEC was not suitable for the formulations because the obtained dispersion was not homogeneous and as a consequence only CMC was further investigated. Viscosity appears to low for percentages up to 3% and they were too viscous for 5 and 6%. Accordingly the CMC concentration of 4% was apparently the most appropriate, with the formation of a transparent gel. Accordingly, the formulation was also carried out using the ME loaded with 0.1% khellin. Khellin was completely solubilized after

4 h at 35±2 °C under magnetic stirring at 700 rpm. Finally, the CMC in the concentration of 4% *w*/*w* of the total formulation was added and the system was subjected to manual mechanical stirring. Furthermore, after the preparation, the pH measurement of the formulation was carried out. The pH value resulted 6.58±0.20 as a media of four measurements.

36.5. TEM measurements of K-ME and K-ME-GEL

TEM analysis of K-ME revealed droplets were almost spherical with sizes less than 40 nm. Their distribution was uniform, confirming the data obtained by DLS (Figure 69). The TEM of K-ME-GEL (Figure 70) resulted consistent with the homogeneous distribution of nanostructured emulsion, having sizes and PdI comparable to the unformulated K-ME and evidencing that no modification of K-ME occurred after incorporation in the hydrogel.

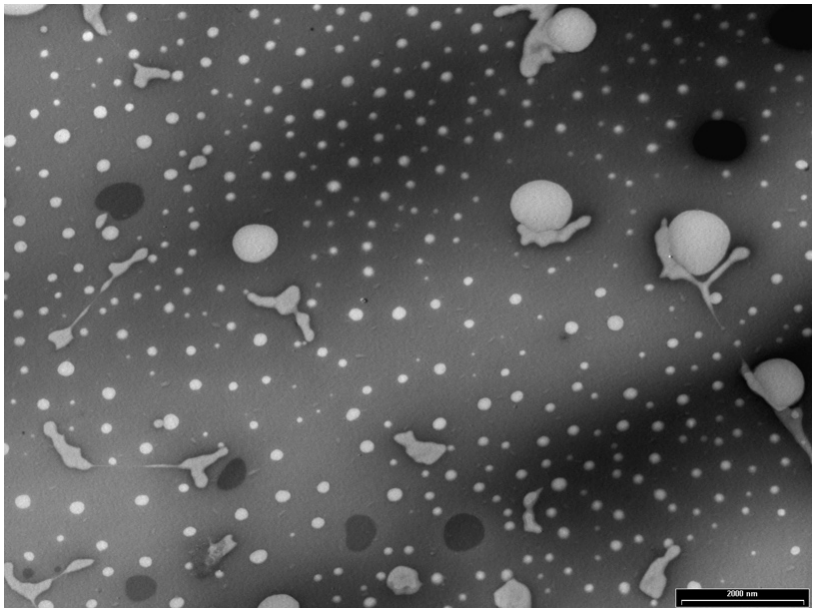

Figure 69. TEM picture of K-ME.

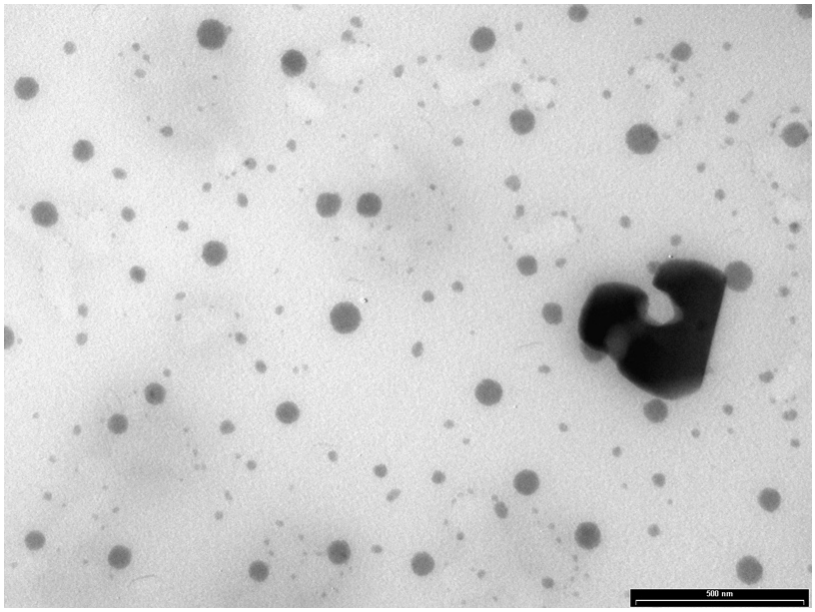

Figure 70. TEM picture of K-ME-GEL.

36.6. K-ME-GEL viscosity measurments

The viscosity of the hydrogel loaded with khellin-ME (K-ME-GEL) was measured at 21±2°C and 35±2°C. Each measurement was made in duplicate and expreseed in mPas·s (mean±sd). The evaluation of viscosity properties of K-ME-GEL was obained as dscribed in the experimental part and results are reported in Figure 71. The curves obtained by increasing and decreasing the rotation of the spindle (up and down) can be superimposed both at 21±2°C and at 35±2°C. The viscosity of optimized K-ME-GEL at 21±2°C was 22,100.0±1555.6 mPas·s, while viscosity of the same formulation at 35±2°C , average temperature of the skin, was decreased to 8,916.5±118.1 mPas·s. As expected from the literature *(Chen H, 2007)*, increasing the temperature from 21±2°C to 35±2°C determined a decreased viscosity of the K-ME-GEL. Hence, K-ME-GEL was suitable for topical application.

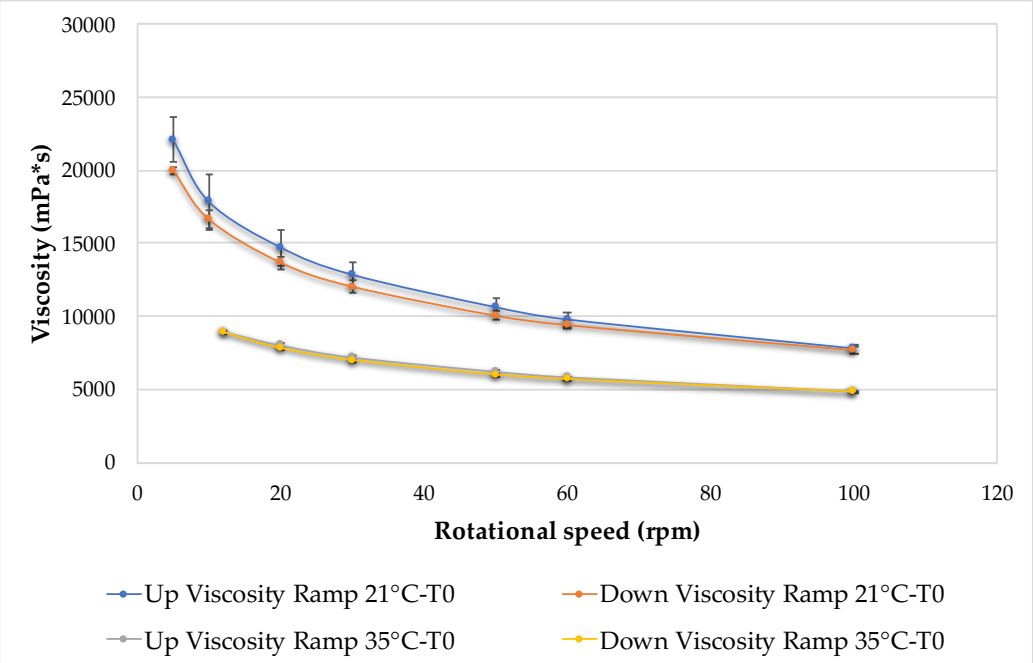

Figure 71: Comparison of viscosity measurements (up and down) of K-ME-GEL at 21±2°C and at 35±2°C. Mean±sd (n=3).

36.7. In vitro khellin release study from K-ME-GEL

To further evaluate the appropriateness of the developed formulation for topical use the release behaviour has been taken into consideration to evaluate if the formulation could guarantee a prolonged release of the khellin. The *in vitro* release study was carried out at the physiological pH (7.4), thus simulating the conditions that the formulation meets after skin absorption (Figure 72). Evaluation of khellin released from the ME-GEL was evaluated by HPLC-DAD at different time points for 24 h. At the end of the test, the percentage of khellin released from the K-ME-GEL reached about 1.56%. The release of khellin is gradual and prolonged, without the burst effect, with a suitable standard deviation as reported in Figure 72.

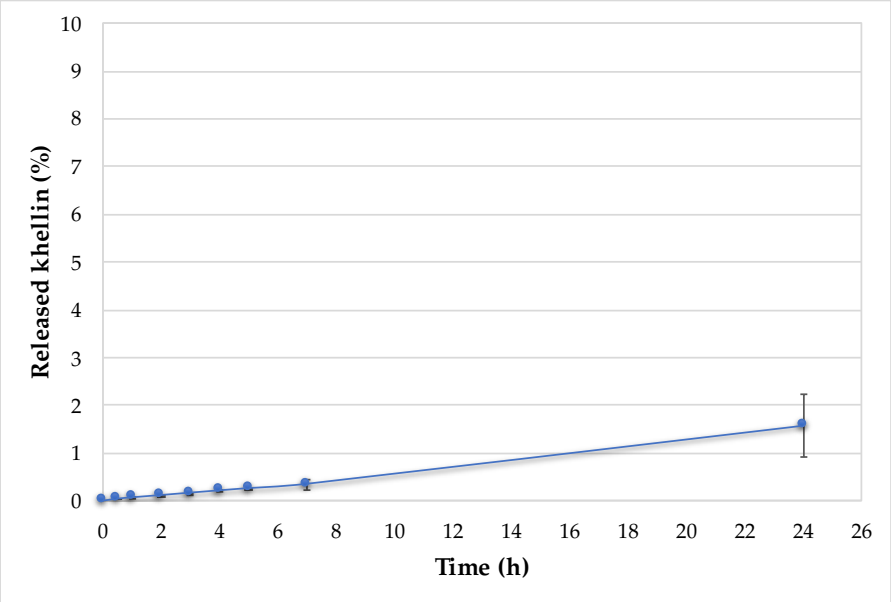

Figure 72. Khellin release from the K-ME-GEL composite. Mean±sd (n=3).

As a second step of this experiment we try to evaluate how khellin release occurs. For the interpretation of the release data, mathematical models were used to predict and recognize the influence of the delivery device laying out parameters on release kinetic formulation. The modeling was performed using model dependent methods, in particular Higuchi, Korsmeyer-Peppas, Hixson and Crowel, and others. The best fitting kinetic model, showing the highest determination coefficient ($R^2 = 0.9943$) was Hixson and Crowel (Table 42). Within this model the predominant mechanism of khellin release is not controlled by diffusion.

Table 42. Kinetic models fitted for K-ME-GEL

Kinetic Model	R^2
Korsmeyer-Peppas	0.6789
Higuchi	0.8525
Hixson Crowell	0.9943

36.8. Stability studies

The viscosity properties, pH and R% of K-ME-GEL were investigated after 4-weeks storage of the formulation at 21±2°C, protected from light. ME-GEL showed excellent physical stability: pH values did not changes during storage, it

was 6.58±0.19 at the beginning of the test and it resulted 6.42±0.34 at the end of the storage period. Viscosity after the storage period did not change and also the rheological properties were the same (Figure 73). Furthermore, recovery did not changed during storage: 93.16±4.39% at time zero and 93.23±2.14% after 4 weeks.

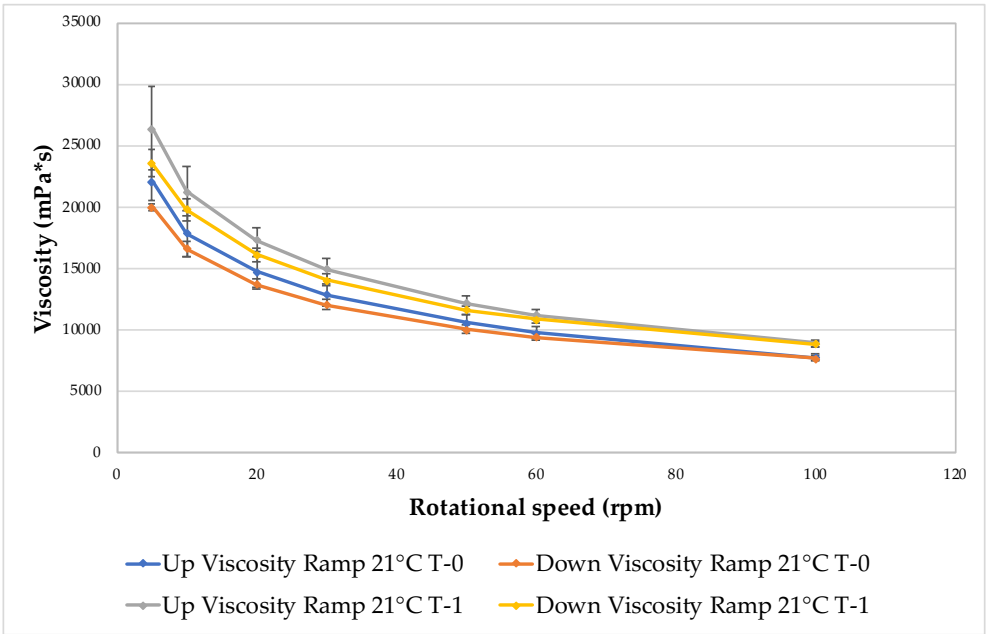

(a)

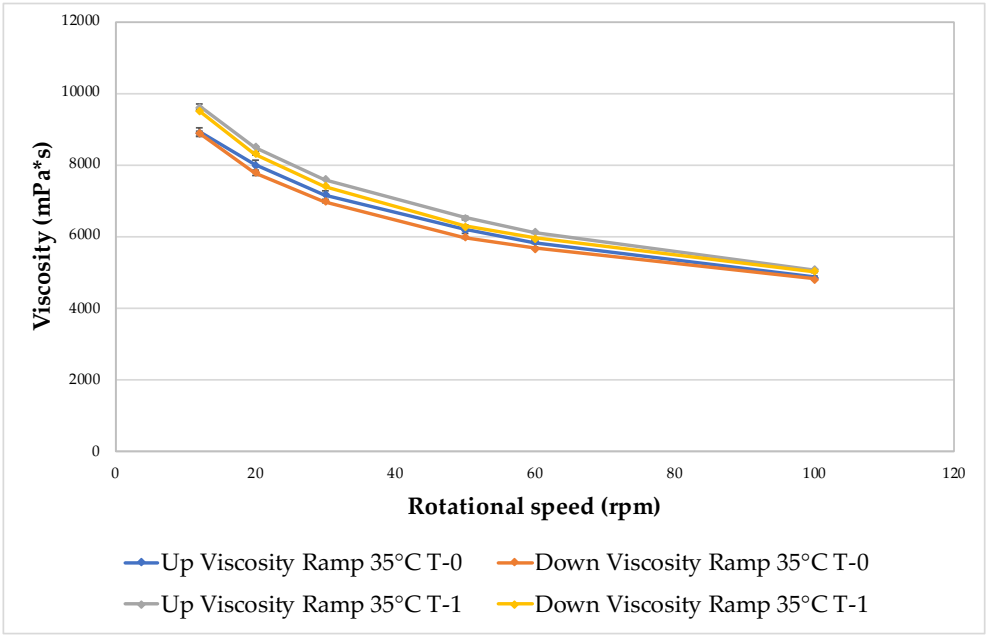

(b)

Figure 73: Comparison of viscosity measurements (up and down) of K-ME-GEL at 21±2°C **(a)** and at 35±2°C **(b)** after 4 weeks storage. Mean±sd (n=3).

FORMULATION OF A PHENOL-RICH EXTRACT FROM UNRIPE OLIVES (*OLEA EUROPAEA* L.) IN MICROEMULSION TO IMPROVE ITS SOLUBILITY AND INTESTINAL PERMEABILITY

37. Results and Discussion

37.1. Phenolic composition and solubility in different vehicles of the phenolic extract

The phenolic composition of the olive extract was characterized using a chromatographic approach already applied in our studies for analyzing the phenolic fraction of olives and derivatives *(Cecchi L, 2018a; Cecchi L, 2018b)*, but avoiding the use of the internal standard. Consequently, the quantitative analysis was carried out using external calibration curves, instead of the internal standard method applied in the above cited papers that required the addition of syringic acid (ISTD) during the preparation of the OE. The presence of a molecule other than those naturally present in the extract would have interfered with and modified the final results of the study. The phenolic composition of the OE is reported in Table 43, while Figure 74 shows the phenolic profile of the OE (Figure 74A) and the chemical structure of the quantified phenolic compounds (Figure 74B).

Table 43. Phenolic composition of the olive extract. Data are expressed as the mean ± SD from three independent determinations.

Compound	extract (mg/kg)		
hydroxytyrosol (mg/kg)	5424.7	±	270.8
tyrosol (mg/kg)	655.2	±	46.4
rutin (mg/kg)	6535.5	±	286.6
luteolin-7-*O*-glucoside (mg/kg)	1696.2	±	613.6
verbascoside (mg/kg)	23786.9	±	628.7
oleuropein (mg/kg)	310187.5	±	2203.1
comselogoside (mg/kg)	7399.8	±	738.2
ligstroside (mg/kg)	31477.1	±	1375.8
Total phenolic compounds (mg/kg)	387162.7	±	4362.8

The concentration of total phenols in the OE is very high (approx. 39% *w*/*w*). In particular, the highest concentrations were for oleuropein (31.0% *w*/*w* of the weight of the extract, representing approx. 80% of the total phenolic content), verbascoside (2.3% *w*/*w*, approx. 6% of the total phenolic content), and ligstroside (3.1% *w*/*w*, approx. 8% of the total phenolic content). To the author's knowledge,

the concentration of phenolic compounds in OE is higher than in other commercial extracts from *Olea europaea* L. As far as the widely used olive leaves extracts, some papers reported variable phenolic contents, usually lower than the values reached with the extraction of unripe dried olives selected for this study: in particular, oleuropein content was found in very low amounts, e.g., 0.077% *w/w* in a paper *(Benincasa C, 2019)*, and ranging from 2.1% to 20.4% in other papers *(Romani A, 2019; Dalla Rosa A, 2019; Amidzic M, 2018; Somerville V, 2019; Xie PJ, 2015a; Wang X, 2019; Xie PJ, 2015b)*, while the total phenolic content ranging 3.4% to 31.6% *(Romani A, 2019; Amidzic M, 2018; Somerville V, 2019; Xie PJ, 2015a; Wang X, 2019; Xie PJ, 2015b)*, and reaching 38.4% only in one paper *(Dalla Rosa A, 2019)*. The typical phytocomplex of olive leaves is different from that of the OE, which shows unique characteristics from both qualitative and quantitative points of view. The yields of the extract on the unripe olives weight (40%) and the concentration of phenols per gram of extract are very high, and thus OE represents a new and interesting nutraceutical ingredient that could be used for the protection of people's well-being and to allow producers the possibility of diversifying their production, and thus new possibilities of income, in a period of the year when olive oil production has not yet commenced. Interestingly, the required amount of OE for the preparation of a microemulsion (see next paragraphs) can be obtained without negatively affecting the olive oil yields in a significantly way.

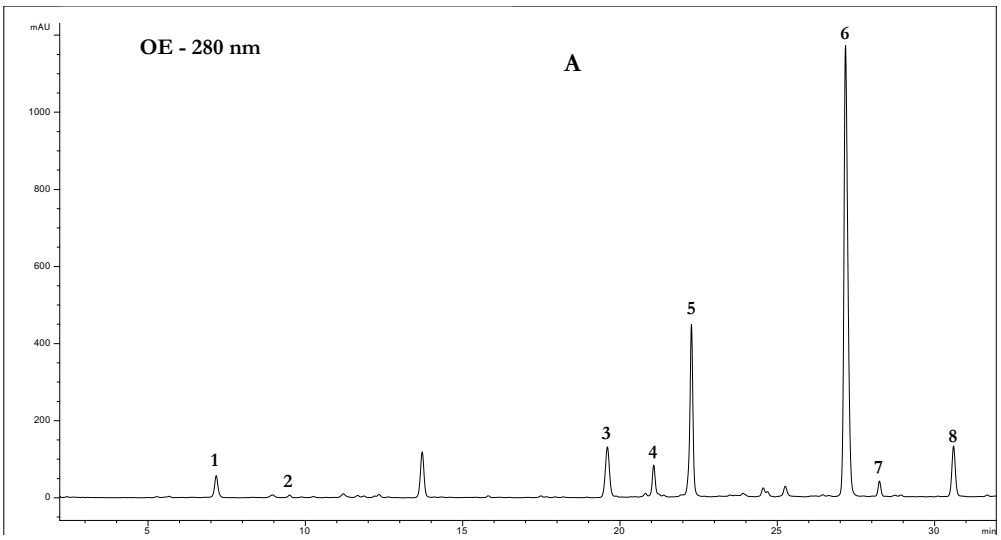

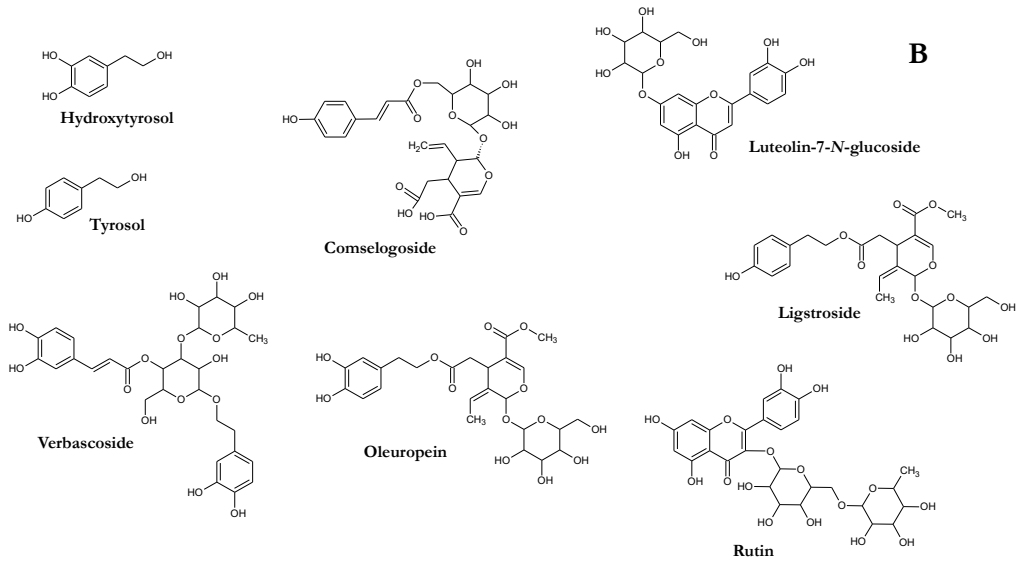

Figure 74. A) Phenolic profile at 280 nm of the olive extract (OE). 1, hydroxytyrosol; 2, tyrosol; 3, rutin; 4, luteolin-7-O-glucoside; 5, verbascoside; 6, oleuropein; 7, Comselogoside; 8, ligstroside. B) The main phenolic compounds detected in the olive extract.

After the chemical characterization, solubility studies of olive extract were performed in water and in different surfactants and lipophilic solvents to select appropriate constituents for ME formulation. Table 44 shows that the vehicles differently affect the solubility of phenolic compounds, if compared with water: Captex 300, Captex 355, Labrafac, Labrafilm 1944, Labrafilm 2125, and Lauroglycol 90 showed a poor solubilization capability, while Transcutol, Labrasol ALF, and Cremophor EL showed the best solubilization capability, higher than water. Transcutol solubilizes a quantity of phenolic compounds that is approximately triple compared to water. These data suggest the possibility to strongly improve the solubility of OE phenolic compounds in comparison with pure water by using an optimized combination of the above vehicles in an ME.

Table 44. Solubility of the main phenolic compounds of the olive extract in different vehicles. Data are expressed as mean ± sd from three independent measurements.

	Verbascoside	**Oleuropein**	**Ligstroside**	**Total phenolic content**
	(mg/mL)	(mg/mL)	(mg/mL)	(mg/mL)
Water	0.243 ± 0.007	3.081 ± 0.007	0.314 ± 0.003	**3.816 ± 0.071**
Capryol 90	0.060 ± 0.009	1.079 ± 0.074	0.115 ± 0.001	**1.292 ± 0.107**
Captex 300	nd	0.058 ± 0.012	0.014 ± 0.001	**0.074 ± 0.013**
Captex 355	nd	0.038 ± 0.005	0.012 ± 0.001	**0.052 ± 0.006**

Labrafac	nd	0.032 ± 0.017	0.007 ± 0.003	**0.039 ± 0.020**
Labrafilm 1944	0.010 ± 0.001	0.411 ± 0.007	0.050 ± 0.003	**0.483 ± 0.002**
Labrafilm 2125	0.010 ± 0.001	0.456 ± 0.007	0.070 ± 0.022	**0.545 ± 0.033**
Labrasol ALF	0.411 ± 0.007	5.331 ± 0.010	0.526 ± 0.011	**6.582 ± 0.057**
Lauroglycol 90	0.018 ± 0.004	0.611 ± 0.001	0.069 ± 0.002	**0.729 ± 0.009**
Transcutol	0.702 ± 0.007	9.036 ± 0.005	0.896 ± 0.025	**11.081 ± 0.046**
Cremophor EL	0.326 ± 0.040	5.269 ± 0.312	0.510 ± 0.047	**6.320 ± 0.419**

37.2. Pseudo-ternary phase diagram

Based on the above results, Capryol 90 was selected as oil phase, and Cremophor EL and Transcutol as surfactant and co-surfactant, respectively. All the selected components have already been used and approved for oral administration purpose. Capryol 90 is propylene glycol monocaprylate and was already selected as oily phase in other studies due to its relative easiness of emulsification *(Borhade V, 2012)*. Capryol 90 has been investigated extensively as the oil phase for the development and optimization of nanoemulsions/microemulsions/SNEDDS/SMEDDS of various poorly soluble drugs both *in vitro* and *in vivo (Shakeel F, 2013)*. Cremophor EL is a complex mixture of hydrophobic and hydrophilic components, with the main components being glycerol polyethylene glycol ricinoleate and glycerol ethoxylates, respectively. It had very good ability to emulsify Capryol 90, as previously reported *(Borhade V, 2012)*. Transcutol is a hydrophilic co-surfactant and increases spontaneity of the ME formation. It improves emulsification of surfactants by penetrating interfacial surfactant monolayer effectively, and it has a superior solubilizing potential performance. Cremophor EL and Transcutol were mixed at different ratios under vigorous stirring to obtain the surfactant mixture (S_{mix}), then the pseudo-ternary phase diagram was constructed by the water titration technique, using different combinations of Capryol 90 and each S_{mix}. Figure 75 shows the obtained pseudo-ternary phase diagram.

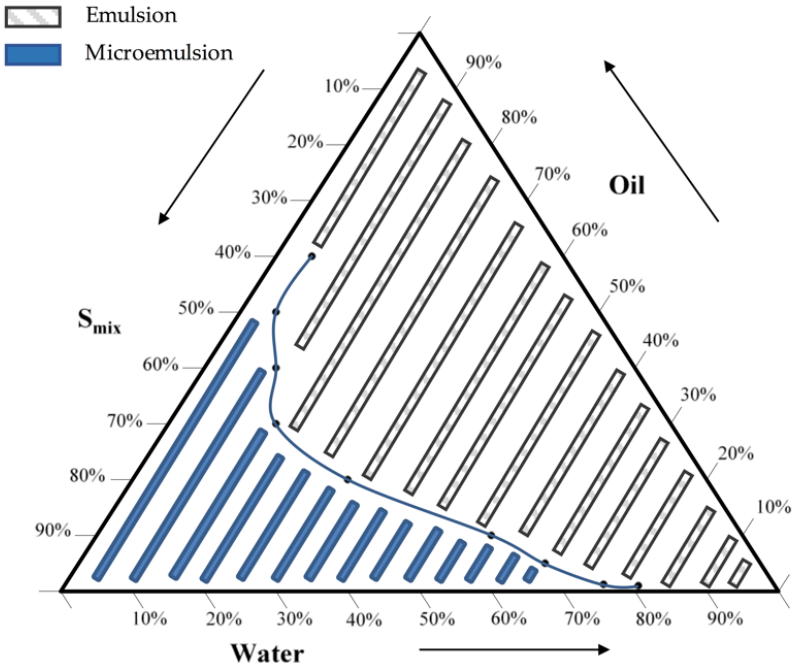

Figure 75. Pseudo-ternary phase diagram. The dark area represents the ME existence range and the grey area means crude emulsion range.

The final microemulsion was constituted by 1% Capryol 90 (oil), 12.7% Cremophor EL (surfactant) and 6.3% Transcutol (co-surfactant), in addition to water (80%).

37.3. Solubility of olive extract into microemulsion

After the elaboration of pseudo-ternary phase diagram, the maximum loading content of OE into the formulation was evaluated adding an increasing amount of extract to the ME under stirring. The formulation was able to incorporate up to 35 mg/mL of OE, corresponding to 13.71 ± 0.01 mg/mL of the identified phenolic molecules, without phase separation or precipitation of the extract. The OE is a hydro-alcoholic extract, partially soluble in water. It contains different phenolic compounds, mainly oleuropein, verbascoside and ligstroside, with different structure and aqueous solubility. The ME increases the solubility of OE more than three times due to the presence of oil phase and tensides, which can realize also a micellar solubilization of the lipophilic compounds.

37.4. Particle size, ζ-potential measurements and in vitro release study

Empty and extract-loaded formulations were physically characterized by Dynamic Light Scattering (DLS) and electrophoretic light scattering (ELS). The analyses confirmed the presence of a homogeneous system with narrow size distribution, low values of polydispersity index (PdI) and mean diameter (Table 45). The presence of the OE did not affect the physical properties of the system. ME showed very small particle size (<100 nm), which could promote the absorption by enterocytes and help avoiding the uptake by the cells of the reticuloendothelial system (RES), *(Win KY, 2005)*.

Then, developed ME represents a successful tool to incorporate OE and to significantly ameliorate its solubility, in that it is able to solubilize 35 mg/mL of OE without destabilization of the system.

Table 45. Physical characterization of ME and olive extract-ME. Results are expressed as means ± standard deviation of at least three experiments.

Sample	size (nm)	PdI	ζ-potential (mV)
ME	13.15 ± 0.19	0.14 ± 0.01	-1.23 ± 0.17
OE-ME	14.03 ± 1.36	0.20 ± 0.08	-1.16 ± 0.48

To further evaluate the appropriateness of the developed formulation for oral use, it is necessary to take into consideration the characteristics of the different environments that it can meet and the possible modifications of the loaded phenolic compounds. ME and hydroalcoholic solution (EtOH-H_2O 70:30) both containing both containing 35 mg/mL of extract were compared and their behaviour has been taken into consideration to evaluated if the formulation could guarantee a prolonged release of the phenolic compounds. A first *in vitro* release study was carried out at the physiological pH (7.4), thus simulating the conditions that the formulation meets after its absorption (Figure 76). After 6 h, the percentage of phenolic compounds released from ME (60.2%) was lower than that obtained with the solution (75.9%). A similar behaviour was obtained in simulated gastric fluid (SGF, Figure 77). By comparing ME and solution, the release of the extract is more gradual and prolonged in the case of ME. It can be noted that already after 2 hour the release of the extract by the solution corresponds to 32.6% of the phenolic compounds, while the formulation releases only the 14.0%.

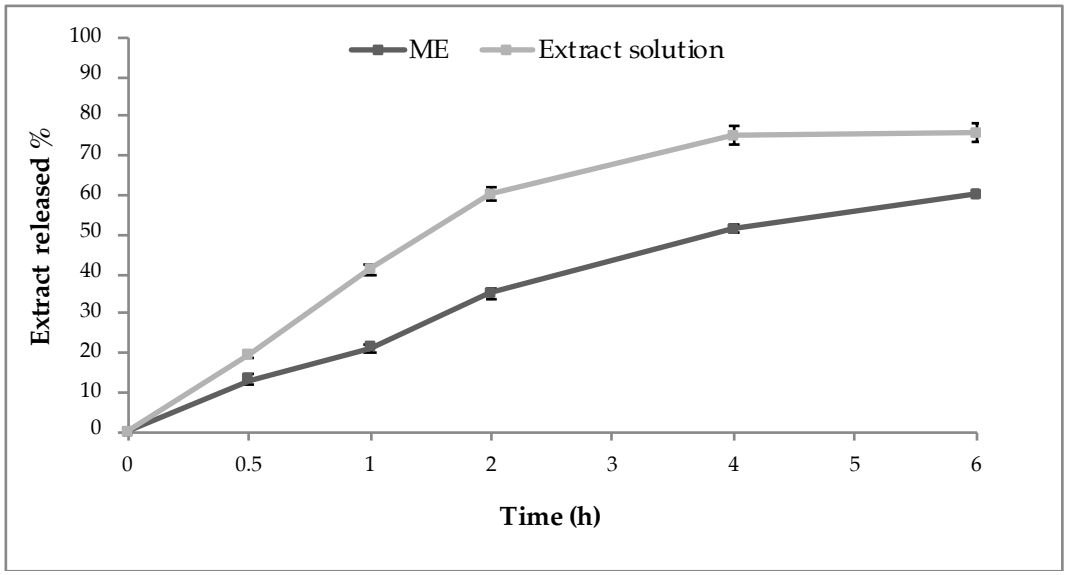

Figure 76. *In vitro* release profile of phenolic compounds from the OE-ME and OE ethanolic solution in Phosphate Buffered Saline (PBS) medium at pH 7.4. Each value is the mean ± SD of three separate determinations.

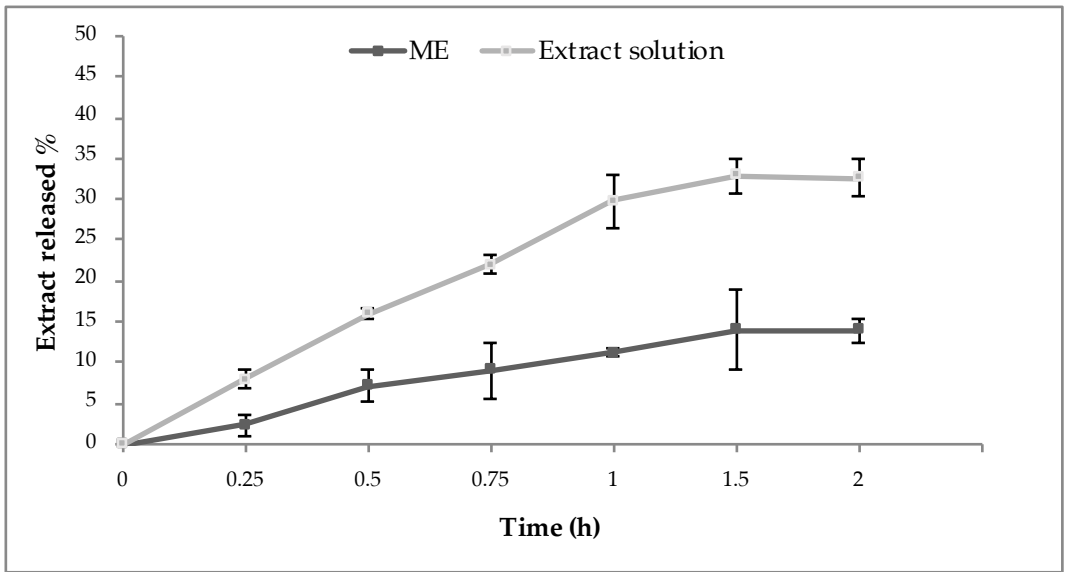

Figure 77. *In vitro* release profile of phenolic compounds from the OE-ME and OE ethanolic solution in Simulated Gastric Fluid (SGF) medium at pH 1.2. Each value is the mean ± SD of three separate determinations.

The last *in vitro* release study was carried out in the SIF at pH 6.8 (Figure 78), in order to simulate the intestinal transit. From the comparison between the two formulations, ME showed a more prolonged release than solution. In this case, the quantities of released phenolic compounds are greater than in the other two cases: after 6 h the percentage reaches 100% with the solution and 78.6% with the

ME. Noteworthy, in this condition the release from the solution was 100% already after 4 h, while the release from the ME is still increasing after 6 h, pointing out the capability of the ME to make the release much more gradual and prolonged then the solution.

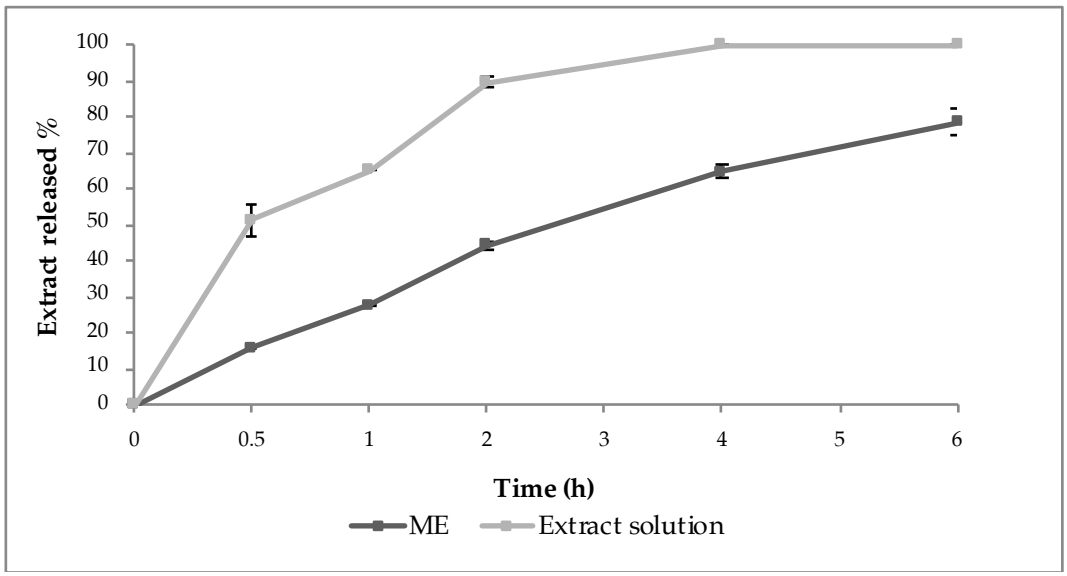

Figure 78. *In vitro* release profile of phenolic compounds from the OE-ME and OE ethanolic solution in Simulated Intestinal Fluid (SIF) medium at pH 6.8. Each value is the mean ± SD of three separate determinations.

ME achieves a gradual release and protects the OE from degradation in the acid environment, because it releases a smaller quantity of phenolic compounds compared to the solution and compared to the amount released in the other two media, i.e. PBS and SIF.

37.5. Chemical and physical stability during storage

In order to estimate the stability of the formulation, the OE-ME was stored in sealed glass containers at 4°C for 3 months. Periodically, chemical and physical stabilities were checked by monitoring transparency, phase separation, colour variation, as well as the changes in particle size, homogeneity, ζ-potential and extract concentration by DLS and HPLC-DAD analyses.

The formulation resulted stable during the whole duration of the test: no phase separation or creaming were observed. Moreover, size, homogeneity and ζ-potential value resulted unchanged after 3 months: size 12.94 ± 0.10 nm, PdI 0.13 ± 0.01, -1.10 ± 0.01 mV. The concentration of phenolic compounds was 13.01 ± 0.32 mg/mL, corresponding to 95% of the starting amount; also the composition

of the phenolic compounds was unchanged, with oleuropein *ca.* 80%, ligstroside *ca.* 8% and verbascoside *ca.* 6%. These findings evidenced the stability during the storage period of the developed formulation and the ability of ME to prevent the degradation of loaded compounds.

37.6. In vitro Parallel Artificial Membrane Permeability Assay (PAMPA)

PAMPA represents a potential approach for rapid assessment of passive-transport permeability. It is performed to estimate passive transcellular permeability. It is a non-cell based permeability model, but is considered robust, reproducible and it results a helpful complement to the cellular permeability model for its speed, low cost and versatility. A combination of PAMPA and Caco-2 permeability model can synergistically provide invaluable permeability/absorption assessment of drug. The assay could be applied not only in the pre-formulation studies of single molecules but it gives information on the behavior of the extracts and recently the authors applied the test to the study of compounds loaded into formulations, i.e. SLN, NLC, nanomicelles and microemulsions *(Perrinjacquet-Moccetti T, 2008; Piazzini V, 2017b; Piazzini V, 2018; Piazzini V, 2019c)*.

The test was carried out in a 96-well, MultiScreen-IP PAMPA (Millipore corporation) filter plate. The ability of compounds to diffuse from a donor compartment into an acceptor compartment was evaluated. The P_e of extract solution (EtOH:PBS 70:30) was $1.44 \pm 0.83 \times 10^{-6}$ cm/s while the P_e of olive extract-ME was $3.74 \pm 0.34 \times 10^{-6}$ cm/s, p=0.0286. The formulation improved the passive permeation of extract across the simulated membrane barrier. The permeability increases due to the increased solubility of the extract and the effect of penetration enhancers of the constituents of ME, in particular of Cremophor EL and Transcutol.

37.7. Transport experiments with Caco-2 cells

In order to complete the *in vitro* characterization of OE-ME, permeation studies were performed using a cell-based model. Caco-2 cells are considered the most predictive *in vitro* model to estimate not only passive intestinal diffusion, as previously described for PAMPA, but also active transport processes, paracellular permeability and active efflux *(Hubatsch I, 2007; Makhey VD, 1998)*.

To find the highest non/low toxic concentrations to be used in the transport experiments, the cytotoxicity of OE-ME was tested. For MTS assay, the cells were

incubated for 2 and 24 h at 37°C with fresh medium containing OE-ME. The results are shown in Figure 79.

OE-ME loaded with 35 mg/mL of extract does not show any sign of cytotoxicity after 2 hours of exposure, being the Caco-2 cellular viability close to 100% for all tested dilutions. After 24 h, the cell viability percentage was still good: for ME diluted 1:100 it was up to 90% compared to untreated cells, confirming that the formulation and the extract do not affect cell viability. The dilution 1:100 was selected for transport experiments, considering that a cell viability > 80% is required for acceptable *in vitro* assay *(Piazzini V, 2018)*. In addition, the Lucifer yellow passage was less than 3%, indicating the integrity of the layer *(Iacomino G, 2013)*.

Caco-2 cells were exposed to OE-ME 1:100 or OE at the same concentration present in the ME formulation (35 mg/mL), for 2 h, in the AP chamber, while the BL was filled with culture medium.

The P_{app} of the OE solution was 16.14 ± 0.05 × 10^{-6} cm/s while the P_{app} of OE-ME was 26.99 ± 0.45 × 10^{-6} cm/s, p=0.0571. By calculating the sum of phenolic compounds concentration in the incubation media of both chambers, we estimate a recovery up to 80%. The permeability coefficient of the ME was significantly higher than that of the unformulated OE.

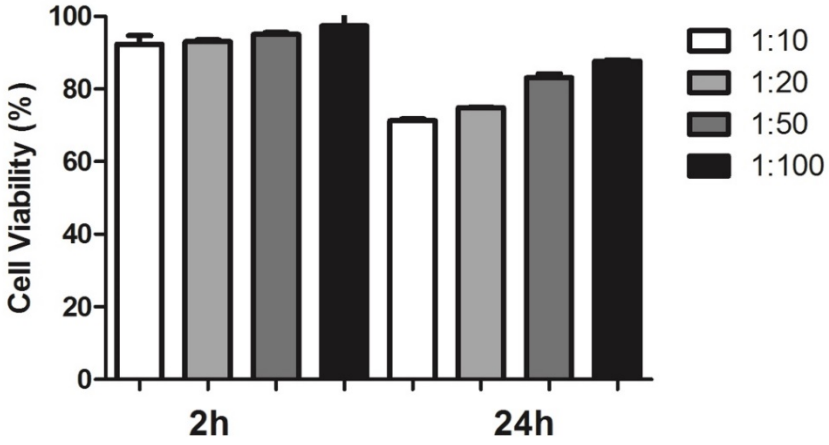

Figure 79. Viability of Caco-2 cells exposed to OE-ME (1:10 to 1:100), for 2 h.

Therefore, the formulation provided enhanced intestinal permeability of OE. This fact is probably due to the presence of surfactant used as stabilizer of the internal phase. As previously reported, the surfactants enhance drug

permeability in many ways such as by increasing transcellular permeability and by inhibiting the efflux transport systems *(Seljak KB, 2014; Bergamante V, 2007)*.

Moreover, non-ionic surfactants also contributed to increase the contact time with the absorption site, and to increase endocytic and transcellular pathways by opening the tight junctions *(Sha X, 2005)*. Much studies have been done to elucidate the P-gp inhibition effect of Cremophor EL as well as other surfactants *(Nerurkar MM, 1996)* and their mechanisms *(Shono Y, 2004)*. It was indicated that Cremophor EL and Transcutol may inhibit the function of P-gp by affecting membrane fluidity *(Yin YM, 2009)*. Cremophor could specifically bind to the hydrophobic domain of the P-gp that may change its secondary and/or tertiary structure and reduce its function *(Nerurkar MM, 1996)*. Furthermore, the small dimensions of droplets of ME characterized by a big surface area increases solubility and absorption.

CONCLUSIONS

Concurrently, natural products, which include a large and diverse group of substances from various natural sources, have assumed an exceptional importance for the prevention and cure of many diseases. This is due to their unique structure and their pleiotropic effects by targeting and modulating multiple pathways. For these reasons, natural products could represent the ideal drugs to a realistic approach of many diseases, especially those with emerging resistance to monofunctional agents, and they are suitable approaches against multifactorial and complex diseases. Since ancient times, natural products found application in the treatment of skin conditions and they are currently largely used in dermatology, both as cosmetic and medicinal preparations, mainly as semi-solid dosage forms, but also as solutions.

By contrast, natural products suffer of many limitations and the majority of constituents are not "drug like". At the same time, there is an increasing interest for nano-drug delivery systems thanks to their potential application in clinic, both for local and systemic administration of drugs. Accordingly, the various nanovectors have been attempted as potential delivery systems for natural products, increasing the stability and solubility of loaded drugs and, thus, making them suitable for the administration. These nanostructures are also able to optimize the biodistribution, with a consequent increased efficacy, as well as to favour the accumulation at target sites, reducing the adverse effects. Furthermore, the selection of biocompatible nanomaterials allows to decrease the formulation toxicity.

This thesis mainly focused on developing innovative formulations for dermal, transdermal or mucosal delivery of natural (escin, berberine chloride, khellin, cannabidiol), semisynthetic (ascorbyl derivates) or synthetic (tariquidar, clobetasol propionate) products or natural extracts (*Serenoa repens* L. CO_2 extract, essential oils of *Melissa officinalis* L., *Origanum onites* L., *Satureja thymbra* L., extract of unripe olives of *Olea europaea* L. species), formulated in conventional liposomes, modified nanovesicles, innovative vesicular systems and oil-in-water microemulsions.

Innovative vesicular systems, modified nanovesicles, conventional liposomes

In the first reported study, the conversion of the bioactive amphiphilic saponin escin (ESN) into a vesicle bilayer-forming component was explore to design innovative nanocarriers composed of phosphatidylcholine plus ESN. Obtained nanovesicles, called escinosomes, were stable and deformable, besides being able to successfully load the quaternary isoquinoline alkaloid berberine chloride (BRB), still preserving the anti-hyaluronidase activity of ESN. Escinosomes also showed favourable skin penetration features for the development of new efficacious dermatological vectors. The presence of two active molecules (ESN and BRB) represents a promising tool with possible synergistic activity between the vesicle bilayer-forming active component and the loaded drug.

Vanti, G., Bani, D., Salvatici, M. C., Bergonzi, M. C., & Bilia, A. R. (2019). Development and Percutaneous Permeation Study of Escinosomes, Escin-Based Nanovesicles Loaded with Berberine Chloride. *Pharmaceutics*, *11*(12), 682.

doi:10.3390/pharmaceutics11120682

Accordingly to these promising findings, escinosomes were formulated in hydrogels of hydroxypropyl methylcellulose (HPMC), a derivative of the natural cellulose, widely used as matrix former for various pharmaceutical dosage forms, as well as dermal/transdermal drug delivery systems, because of its hydrophilicity and ability to make intermolecular and intramolecular interactions thanks to the presence of polar and non-polar groups. The study proved that hydrogels of BRB-loaded escinosomes enhanced ESN and BRB skin absorption when compared to pure substances. HPMC-hydrogels formulations also showed high safety profile by acute dermal irritation and corrosion test and combined the advantages of a modified release and a greater drug permeability across the skin, thanks to the escinosome components, with a higher residence time upon administration, due to the polysaccharide matrix network.

Vanti, G., Wang, M., Bergonzi, M. C., Zhidong, L., & Bilia, A. R. (2020). Hydroxypropyl methylcellulose hydrogel of berberine chloride-loaded escinosomes: dermal absorption and biocompatibility. *International Journal of Biological Macromolecules*, *164*, 232-241.

doi.org/10.1016/j.ijbiomac.2020.07.129

A further study described the formulation of ascosomes, special nanovesicles made of phosphatidylcholine plus alkanoyl-6-O-ascorbic acid esters, namely ascorbyl octanoate (ASC8) and ascorbyl decanoate (ASC10), loaded with the bioactive polyphenol khellin and gelled with hydroxyethyl cellulose (HEC), another semisynthetic derivative of cellulose. This study proved the possible use of HEC as modifier release matrix for the colloidal suspension of ASC10 ascosomes loaded with khellin, which showed increased transdermal permeability of khellin, besides improving skin absorption of derivatized ascorbic acid. ASC10 ascosome hydrogel also demonstrated a good safety profile in rats by the acute dermal irritation/corrosion test. In addition, liver and dermal histological and pathological analyses demonstrated that khellin loaded in ASC10 ascosomes and formulated in HEC-hydrogel had no toxic effects. The combination of nanocarrier and hydrogel provides improved drug targeting, sustained drug release and optimized bioavailability profile, when compared with the administration of the solely nanocarrier or the unformulated drug dispersed in conventional hydrogel, offering innovative and efficient skin-delivery platforms.

Risaliti, L., Yu, X., Vanti, G., Bergonzi, M. C., Wang, M., & Bilia, A. R. (2021). Hydroxyethyl cellulose hydrogel for skin delivery of khellin loaded in ascosomes: Characterization, in vitro/in vivo performance and acute toxicity. *International Journal of Biological Macromolecules*.

doi.org/10.1016/j.ijbiomac.2021.02.206

Modified nanovesicles, such as glycerosomes and propylene glycol-nanovesicles, were investigated in this thesis. Glycerosome are innovative type of vesicles, characterized by high stability and flexibility, with improved permeation through the skin and high *in vitro* biocompatibility toward human keratinocytes *(Manca ML, 2013)*. MEO-loaded glycerosomes (MEO-GS), developed in the present work, represent the first study related to the loading of glycerosomes with an essential oil for antiviral purposes. The investigation proved that loaded-MEO did not modify the fluidity of the vesicle bilayer, maintaining glycerosome ability to squeeze through skin pores. Developed glycerosomes were able to preserve during storage MEO constituents from

degradation processes, as in the case of β-caryophyllene. In addition, the formulation has a strong anti-HSV-1 activity comparable to that of pure MEO, without cytotoxic effects. Developed MEO-GS represent a potential strategic anti-herpetic tool to administer MEO, having numerous advantages over pure MEO, principally the preservation of the essential oil constituents and the extension of MEO release, once the formulation is applied on the skin.

Vanti, G., Ntallis, S. G., Panagiotidis, C. A., Dourdouni, V., Patsoura, C., Bergonzi, M. C., ... & Bilia, A. R. (2020). Glycerosome of Melissa officinalis L. essential oil for effective anti-HSV Type 1. *Molecules*, 25(14), 3111.

doi:10.3390/molecules25143111

This study was designed in order to develop propylene glycol-nanovesicles loaded with EOs from *O. onites* and *S. thymbra* for the first time and to evaluate them as safe and food-grade delivery systems. During the last years, synthetic preservatives are generally used to protect food against microorganisms. However, there is an urgent need to search new antimicrobials because of the increasing resistance against these microorganisms. EOs represent a valid alternative to synthetic preservatives in the food industry, and *Origanum* essential oil has been largely investigated as antimicrobial and antioxidant additive in food products *(Rodriguez-Garcia I, 2016)*. However, in many cases their organoleptic impact in foodstuffs limits their usage. Techniques such as nanoencapsulation can address this problem. In this study, the chemical profiles of the EOs of *O. onites* and *S. thymbra* were identified. Oxygenated monoterpenes comprised the major chemical class in both EOs. In particular, the main components of *O. onites* EO were carvacrol (66.0%), *p*-cymene (7.9%), γ-terpinene (4.9%) and borneol (2.8%). Whereas, the principal compounds of *S. thymbra* EO were carvacrol (46.0%), γ-terpinene (19.7%), *p*-cymene (7.6%), β-caryophyllene (7.0%) and α-terpinene (5.1%). Afterwards, we succeeded to encapsulate the EOs in nanovesicles which presented high homogeneity and optimal encapsulation efficiency either for *O. onites* or *S. thymbra*. Both pure EOs and formulated EOs were evaluated against different food-borne pathogens. The high antimicrobial activity of both EOs could be attributed to their chemical constituents, not only to the high concentration of carvacrol but also to the potential synergy of all the compounds. Our results showed that pure EOs were more active compared to

the corresponding amounts of formulated EOs. We should point out that the lower antibacterial and anti-fungal effectiveness of formulated EOs with respect to pure EOs is assigned mainly to the prolonged release properties of the EOs loaded in the nanovesicles. Cytotoxicity was also tested in HaCaT cells. In conclusion, the present study unveiled that the tested nanovesicles could represent potential biocontrol agents against fungal and bacterial food pathogens with promising GRAS status in mammalian systems, besides being an innovative and completely biodegradable approach for the prolonged and sustained release of the EO, preserving functional properties.

Vanti, G., Tomou, E. M., Stojković D., Ćirić A., Bilia A. R., Skaltsa H. (2021). Nanovesicles loaded with Origanum onites and Satureja thymbra essential oils and their activity against food-borne pathogens and spoilage microorganisms. *Molecules, 26,* 2124.

doi: 10.3390/molecules26082124

Despite the increasing interest in modified and innovative vesicular systems with improved flexibility and permeability, conventional liposomes still represent a promising carrier to formulate and delivery various type of drugs. Indeed, liposomes represent, among the nanocarriers, the most useful ones to be applied for topical use because they can penetrate the epidermal barrier to a greater extent compared to other conventional dosage forms and loaded drugs are generally accumulated in the upper layers of the *stratum corneum* and appendages (hair follicles and sweat ducts), providing a "reservoir" and resulting in a more localized action *(Jung S, 2006; Tabbakhian M, 2006)*. Nanoliposomes based on saw palmetto carbon dioxide (CO_2) extract were selected as the best formulating approach *(Bilia AR, 2017; Bilia AR, 2019a)*, due to the physical characteristics of the extract and the chemical nature of its constituents. Nanoliposomes were developed and characterised in terms of physical and chemical properties, for the topical delivery of the active constituents and the potential usage in hair loss treatment.

Vanti, G., Bergonzi, C., & Bilia, R. (2021). Development of Nanoliposomes Loaded with Carbon Dioxide Serenoa repens (Saw Palmetto) Extract. *Journal of Nanoscience and Nanotechnology*, *21*(5), 2943-2945.

doi.10.1166/jnn.2021.19045

In this work, it was investigated the simultaneous delivery of the anticancer drug, BRB, and the P-gp efflux pump modulator, TAR, using nanoliposomes to enhance BRB intracellular concentration. Untargeted liposomes loaded with antineoplastic drugs are the most successful nano-drug delivery systems translated into clinical applications and approved for their marketing, including the treatment of hematological cancers. Developed nanoliposomes, made of P90G/Chol (66:10 mg/mL), presented sizes around 128 nm and good PdI (*ca.* 0.20) and ζ-potential (*ca.* -20 mV). The formulation had the best BRB EE% (about 64%), in addition to be clear and not viscous, compared to other formulations prepared with higher P90G/cholesterol concentrations.-The stability of native and dialyzed nanoliposomes was assessed by TEM analysis; any variability of size and morphology of the vesicles was observed. In addition, the stability of nanoliposomes in the cell culture medium showed only a slight variance in average sizes, PdI and EE% of BRB. Overall, nanoliposomes resulted physically and chemically stable under the experimental conditions, intended to mimic the *in vitro* studies within the two cell lines. Future studies will be oriented to the stability after storage, in order to evidence the eventual need to lyophilize the nanoliposome to extend their shelf life. Release properties of the dialyzed nanoliposomes were also assessed using the same medium used for the stability, evidencing good biopharmaceutical properties of nanoliposomes. A key step of the present study was the evaluation of the interaction of nanoliposome with cell membranes of K562 and K562/DOXO cell lines by TEM analysis, which evidenced the ability of the developed nanoliposomes to enter in both cell lines by receptor-mediated endocytosis. TAR was selected as pump inhibitor for the co-delivery with BRB in nanoliposomes, since TPGS was less active in overcoming DOXO resistance when compared with both free and formulated TAR. As expected, TAR solution enables a better saturation of the P-gp pump rather than TAR-L, as nanoliposomes modified and delayed its release. However, TAR-L showed a lower cell death by necrosis, which is a positive effect in clinical therapy and it is solely related to the nanodelivery system. Subsequently, liposomes loaded with both BRB and TAR were prepared (BRB/TAR-L). The formulation showed a significant increase in BRB uptake by K562/DOXO cell line, resulting a promising approach to overcome the MDR, also due to easy synthesis and scale-up by the pharmaceutical industry. Future studies will be oriented to *in vivo* administration, in order to examine the eventual intrinsic toxicity and the circulation properties of the nanosystem.

Vanti, G., Coronnello, M., Bani, D., Mannini, A., Bergonzi, M. C., & Bilia, A. R. (2021). Co-Delivery of Berberine Chloride and Tariquidar in Nanoliposomes Enhanced Intracellular Berberine Chloride in a Doxorubicin-Resistant K562 Cell Line Due to P-gp Overexpression. *Pharmaceutics*, *13*(3), 306.

doi.org/10.3390/pharmaceutics13030306

O/W microemulsions

In addition, four research projects aimed to formulate oil-in-water microemulsions loaded with clobetasol propionate, cannabidiol, khellin and unripe olive extract.

An innovative microemulsion loaded with clobetasol propionate (CP-ME) was developed with biocompatible excipients (2% vitamin E acetate, 9% cremophor RH 40, 9% glycerol, 80% water) and it was gelled with carboxymethyl cellulose plus carboxy methyl chitosan, in order to obtain a mucoadhesive microemulgel (CP-MEgel) with longer residence time on the buccal mucosa. Chemical and physical properties, such as average droplet sizes, polydispersity, CP concentration, morphology, pH and viscosity were evaluated for the microemulsion and the correspondent microemulgel, with excellent results. Both systems had small average droplet dimensions (about 30 nm) and high homogeneity (PdI *ca.* 0.22); scanning and transmission electron microscopy analysis showed perfectly distributed spherical droplets. Moreover, the addition of benzalkonium chloride, as preservative against the microorganism growth, did not affect Size and PdI of the microemulgel. pH of CP-MEgel was corrected to *ca.* 7.5 using an aqueous solution of anhydrous citric acid, to obtain a pH compatible with the buccal mucosa. The rheological properties were those of a non-Newtonian fluid with pseudoplastic behaviour, typical of many hydrogels. Lastly, *in vitro* release and permeation studies were performed on cellulose nitrate membranes and porcine buccal mucosa, respectively, in order to predict the *in vivo* absorption of the formulation. CP release rate was low over time and any transmucosal permeation was observed. Hence, the developed microemulgel was found to be suitable for the local delivery of CP with a prolonged release of the active. Mucoadhesive tests are planned before proceeding with the clinical trials on patients affected by MMP.

In parallel, a further study aimed to investigate a new microemulgel based on CBD, developed and characterized for the treatment of cutaneous disorders,

such as atopic dermatitis, thanks to the anti-inflammatory and anti-pruritic properties of CBD. The microemulgel was prepared from a ME constituted of 20% Solutol HS 15, 9% Transcutol P, 5% isopropyl myristate, 66% water and loaded with 1% *w*/*w* CBD. Due to the poor rheological properties of CBD-ME as topical semi-solid dosage form, which influence skin spreadability, adhesion and retention in the application site, CBD-ME was jellified with Sepigel 305®. The obtained CBD-MEgel resulted a pseudoplastic fluid, like most of gels reported in the literature, ideal for topical administration and with excellent skin feel. CBD-MEgel also showed optimal physical and chemical properties: excellent homogeneity of the microemulsion dispersed droplets, as well as high stability in pH, viscosity and CBD content. Permeation studies through rabbit ear skin showed controlled release and absorption properties of CBD formulated in the microemulgel, with good retention in the skin layers. The developed formulation had, thus, suitable rheological and permeability features for a potential use in clinical studies for locally-acting dermatological delivery.

A new micromulsion based on khellin (0.1%), glycerol (2.25%), Labrasol® (20.25%), vitamin E acetate (2.50%), and water (75%) was also developed. The choice of surfactants was based on their dermatological properties, namely Labrasol® (PEG-8 caprylic/capric glycerides) was selected as non-ionic and safe surfactant, with penetration enhancer properties, while glycerol was selected as cosurfactant because it produces stable emulsions with appropriate globule size, but also ensure minimal skin irritancy. Furthermore, vitamin E acetate was chosen because of the numerous healthy effects and the high protection of skin, and khellin for the antioxidant and anti-inflammatory properties. The K-ME-GEL was successfully prepared using CMC 4% as gelling agent to impart a proper viscosity to the preparation as well as to sustain the action of the drug by increasing residence time. The resulting formulation offers convenient supporting matrices with tunable and suitable physical properties for loading lipophilic drugs, and an additional level of control over the spatial and temporal release of the drug. Hence, when lipophilic drugs are directly loaded in the hydrogels they result not stable; giving aggregates formation or uncontrolled burst during release. The formulation had a smooth, creamy and rich texture. It was light, not greasy, characterized by high hydration properties, with fast-absorbing properties.

Lastly, a microemulsion intended for preparation of a suitable oral dosage form, for delivering an olive extract, was investigated for the first time. The olive

extract was obtained in the powder form from Tuscan olives of the Moraiolo cultivar harvested before any stone lignification and immediately lyophilized after freezing them with liquid nitrogen. The extract is characterized by a unique phytocomplex extremely rich of the phenolic compounds ligstroside, verbascoside and particularly oleuropein, making it different from the commercial extracts obtained from olive leaves during the pruning period. The developed microemulsion was suitable in terms of physical and chemical characteristics for oral administration and showed an appropriate chemical and physical stability. The microemulsion had a good solubilizing effect of the Olive Extract and enhanced its intestinal permeability respect to the unformulated extract, both by artificial membranes PAMPA and Caco-2 cells. Specifically, Caco-2 cells confirmed the enhanced passive transcellular diffusion evaluated by PAMPA and also demonstrated a greater permeability due to active transport processes.

Cecchi, L., Piazzini, V., D'Ambrosio, M., Luceri, C., Rocco, F., Innocenti, M., Vanti, G., Mulinacci, N., Bergonzi, M. C. (2020). Formulation of a Phenol-Rich Extract from Unripe Olives (Olea europaea L.) in Microemulsion to Improve Its Solubility and Intestinal Permeability. *Molecules*, *25*(14), 3198.

doi:10.3390/molecules25143198

REFERENCES

Abudayeh, Z. H. M., Al Azzam, K. M., Naddaf, A., Karpiuk, U. V., & Kislichenko, V. S. (2015). Determination of four major saponins in skin and endosperm of seeds of horse chestnut (Aesculus hippocastanum L.) using high performance liquid chromatography with positive confirmation by thin layer chromatography. *Advanced pharmaceutical bulletin*, *5*(4), 587.

Adams, R. P. (2007). *Identification of essential oil components by gas chromatography/mass spectrometry* (Vol. 456). Carol Stream, IL: Allured publishing corporation.

Ali, A., Ahmad, U., Akhtar, J., & Khan, M. M. (2019). Engineered nano scale formulation strategies to augment efficiency of nutraceuticals. *Journal of Functional Foods*, *62*, 103554.

Alipieva, K., Korkina, L., Orhan, I. E., & Georgiev, M. I. (2014). Verbascoside—A review of its occurrence,(bio) synthesis and pharmacological significance. *Biotechnology advances*, *32*(6), 1065-1076.

Allahverdiyev, A., Duran, N., Ozguven, M. E. N. Ş. U. R. E., & Koltas, S. (2004). Antiviral activity of the volatile oils of Melissa officinalis L. against Herpes simplex virus type-2. *Phytomedicine*, *11*(7-8), 657-661.

Amaral, D. M. F., & Bhargava, K. (2015). Essential oil nanoemulsions and food applications. *Adv Food Technol Nutr Sci Open J*, *1*(4), 84-87.

Ametek, B. (2017). More Solutions to Sticky Problems. *Brookfield Engineering Laboratories, Inc*.

Amidžić, M., Marić, P., Fumić, B., Petlevski, R., Bljajić, K., & Končić, M. Z. (2018). Oleuropein-Rich Olive Leaf Extracts May Ameliorate Consequences of Glucose-Induced Oxidative Stress in Hep G2 Cells. *Natural Product Communications*, *13*(6), 1934578X1801300601.

Amiot, M. J., Fleuriet, A., & Macheix, J. J. (1986). Importance and evolution of phenolic compounds in olive during growth and maturation. *Journal of Agricultural and Food Chemistry*, *34*(5), 823-826.

Amiot, M. J., Fleuriet, A., & Macheix, J. J. (1989). Accumulation of oleuropein derivatives during olive maturation. *Phytochemistry*, *28*(1), 67-69.

Arca, H. C., Mosquera-Giraldo, L. I., Bi, V., Xu, D., Taylor, L. S., & Edgar, K. J. (2018). Pharmaceutical applications of cellulose ethers and cellulose ether esters. *Biomacromolecules*, *19*(7), 2351-2376.

Armaka, M., Papanikolaou, E., Sivropoulou, A., & Arsenakis, M. (1999). Antiviral properties of isoborneol, a potent inhibitor of herpes simplex virus type 1. *Antiviral research*, *43*(2), 79-92.

Ashara, K. C., Paun, J. S., Soniwala, M. M., Chavda, J. R., Mendapara, V. P., & Mori, N. M. (2016). Microemulgel: An overwhelming approach to improve therapeutic action of drug moiety. *Saudi Pharmaceutical Journal*, *24*(4), 452-457.

Asprea, M., Leto, I., Bergonzi, M. C., & Bilia, A. R. (2017). Thyme essential oil loaded in nanocochleates: Encapsulation efficiency, in vitro release study and antioxidant activity. *LWT*, *77*, 497-502.

Asprea, M., Tatini, F., Piazzini, V., Rossi, F., Bergonzi, M. C., & Bilia, A. R. (2019). Stable, monodisperse, and highly cell-permeating nanocochleates from natural soy lecithin liposomes. *Pharmaceutics*, *11*(1), 34.

Astani, A., Heidary Navid, M., & Schnitzler, P. (2014). Attachment and Penetration of Acyclovir-resistant Herpes Simplex Virus are Inhibited by Melissa officinalis Extract. *Phytotherapy Research*, *28*(10), 1547-1552.

Astani, A., Reichling, J., & Schnitzler, P. (2010). Comparative study on the antiviral activity of selected monoterpenes derived from essential oils. *Phytotherapy Research: An International Journal Devoted to Pharmacological and Toxicological Evaluation of Natural Product Derivatives*, *24*(5), 673-679.

Astani, A., Reichling, J., & Schnitzler, P. (2011). Screening for antiviral activities of isolated compounds from essential oils. *Evidence-based complementary and alternative medicine*, *2011*.

Astani, A., Reichling, J., & Schnitzler, P. (2012). Melissa officinalis extract inhibits attachment of herpes simplex virus in vitro. *Chemotherapy*, *58*(1), 70-77.

Attia, Y. M., El-Kersh, D. M., Wagdy, H. A., & Elmazar, M. M. (2018). Verbascoside: identification, quantification, and potential sensitization of colorectal Cancer cells to 5-FU by targeting PI3K/AKT pathway. *Scientific reports*, *8*(1), 1-12.

Avdeef, A. (2012). Absorption and drug development: solubility, permeability, and charge state. John Wiley & Sons.

Azaz, A. D., Kürkcüoglu, M., Satil, F., Can Baser, K. H., & Tümen, G. (2005). In vitro antimicrobial activity and chemical composition of some Satureja essential oils. *Flavour and Fragrance Journal*, *20*(6), 587-591.

Bäsler, K., Bergmann, S., Heisig, M., Naegel, A., Zorn-Kruppa, M., & Brandner, J. M. (2016). The role of tight junctions in skin barrier function and dermal absorption. *Journal of Controlled Release*, *242*, 105-118.

Battu, S. K., Repka, M. A., Maddineni, S., Chittiboyina, A. G., Avery, M. A., & Majumdar, S. (2010). Physicochemical characterization of berberine chloride: a perspective in the development of a solution dosage form for oral delivery. *Aaps Pharmscitech*, *11*(3), 1466-1475.

Becker, L. C., Bergfeld, W. F., Belsito, D. V., Hill, R. A., Klaassen, C. D., Liebler, D. C., ... & Heldreth, B. (2019). Safety assessment of glycerin as used in cosmetics. *International journal of toxicology*, *38*(3_suppl), 6S-22S.

Benincasa, C., Santoro, I., Nardi, M., Cassano, A., & Sindona, G. (2019). Eco-friendly extraction and characterisation of nutraceuticals from olive leaves. *Molecules*, *24*(19), 3481.

Benson, H. A., & Watkinson, A. C. (Eds.). (2012). *Topical and transdermal drug delivery: principles and practice*. John Wiley & Sons.

Bergamante, V., Ceschel, G. C., Marazzita, S., Ronchi, C., & Fini, A. (2007). Effect of vehicles on topical application of aloe vera and arnica montana components. *Drug delivery*, *14*(7), 427-432.

Bergonzi, M. C., Hamdouch, R., Mazzacuva, F., Isacchi, B., & Bilia, A. R. (2014). Optimization, characterization and in vitro evaluation of curcumin microemulsions. *LWT-Food Science and Technology*, *59*(1), 148-155.

Bhattacharjee, S. (2016). DLS and zeta potential–what they are and what they are not?. *Journal of controlled release*, *235*, 337-351.

Bhattaram, V. A., Graefe, U., Kohlert, C., Veit, M., & Derendorf, H. (2002). Pharmacokinetics and bioavailability of herbal medicinal products. *Phytomedicine*, *9*, 1-33.

Bilia, A. R., Bergonzi, M. C., Boulos, J. C., & Efferth, T. (2020). Nanocarriers to enhance solubility, bioavailability, and efficacy of artemisinins. *World Journal of Traditional Chinese Medicine*, *6*(1), 26.

Bilia, A. R., Bergonzi, M. C., Guccione, C., Manconi, M., Fadda, A. M., & Sinico, C. (2016). Vesicles and micelles: Two versatile vectors for the delivery of natural products. *Journal of Drug Delivery Science and Technology*, *32*, 241-255.

Bilia, A. R., Bergonzi, M. C., Isacchi, B., Antiga, E., & Caproni, M. (2018a). Curcumin nanoparticles potentiate therapeutic effectiveness of acitrein in moderate-to-severe psoriasis patients and control serum cholesterol levels. *Journal of Pharmacy and Pharmacology*, *70*(7), 919-928.

Bilia, A. R., Bergonzi, M. C., Mazzi, G., & Vincieri, F. F. (2006). Development and stability of semisolid preparations based on a supercritical CO2 Arnica extract. *Journal of pharmaceutical and biomedical analysis*, *41*(2), 449-454.

Bilia, A. R., Guccione, C., Isacchi, B., Righeschi, C., Firenzuoli, F., & Bergonzi, M. C. (2014). Essential oils loaded in nanosystems: a developing strategy for a successful therapeutic approach. *Evidence-Based Complementary and Alternative Medicine*, *2014*.

Bilia, A. R., Nardiello, P., Piazzini, V., Leri, M., Bergonzi, M. C., Bucciantini, M., & Casamenti, F. (2019a). Successful brain delivery of andrographolide loaded in human albumin nanoparticles to TgCRND8 mice, an Alzheimer's Disease mouse model. *Frontiers in pharmacology*, *10*, 910.

Bilia, A. R., Piazzini, V., Asprea, M., Risaliti, L., Vanti, G., & Bergonzi, M. C. (2018b). Plants extracts loaded in nanocarriers: An emergent formulating approach. *Natural Product Communications*, *13*(9), 1934578X1801300914.

Bilia, A. R., Piazzini, V., Guccione, C., Risaliti, L., Asprea, M., Capecchi, G., & Bergonzi, M. C. (2017). Improving on nature: the role of nanomedicine in the development of clinical natural drugs. *Planta medica*, *83*(05), 366-381.

Bilia, A. R., Piazzini, V., Risaliti, L., Vanti, G., Casamonti, M., Wang, M., & Bergonzi, M. C. (2019b). Nanocarriers: a successful tool to increase solubility, stability and optimise bioefficacy of natural constituents. *Current medicinal chemistry*, *26*(24), 4631-4656.

Bonechi, C., Donati, A., Tamasi, G., Pardini, A., Rostom, H., Leone, G., ... & Rossi, C. (2019). Chemical characterization of liposomes containing nutraceutical compounds: Tyrosol, hydroxytyrosol and oleuropein. *Biophysical chemistry*, *246*, 25-34.

Borhade, V., Pathak, S., Sharma, S., & Patravale, V. (2012). Clotrimazole nanoemulsion for malaria chemotherapy. Part I: Preformulation studies, formulation design and physicochemical evaluation. *International journal of pharmaceutics*, *431*(1-2), 138-148.

Bouwstra, J. A., & Honeywell-Nguyen, P. L. (2002). Skin structure and mode of action of vesicles. *Advanced drug delivery reviews*, *54*, S41-S55.

Brown, M. B., Martin, G. P., Jones, S. A., & Akomeah, F. K. (2006). Dermal and transdermal drug delivery systems: current and future prospects. *Drug delivery*, *13*(3), 175-187.

Bulbake, U., Doppalapudi, S., Kommineni, N., & Khan, W. (2017). Liposomal formulations in clinical use: an updated review. *Pharmaceutics*, *9*(2), 12.

Cameron, A., Ewen, M., Auton, M., & Abegunde, D. (2011). The world medicines situation 2011. *Medicines prices, availability and affordability*, *3*.

Carey, B., & Setterfield, J. (2019). Mucous membrane pemphigoid and oral blistering diseases. *Clinical and experimental dermatology*, *44*(7), 732-739.

Carita, A. C., Eloy, J. O., Chorilli, M., Lee, R. J., & Leonardi, G. R. (2018). Recent advances and perspectives in liposomes for cutaneous drug delivery. *Current medicinal chemistry*, *25*(5), 606-635.

Carpi, S., Scoditti, E., Massaro, M., Polini, B., Manera, C., Digiacomo, M., ... & Nieri, P. (2019). The extra-virgin olive oil polyphenols oleocanthal and oleacein counteract inflammation-related gene and mirna expression in adipocytes by attenuating nf-κb activation. *Nutrients*, *11*(12), 2855.

Cecchi, L., Bellumori, M., Cipriani, C., Mocali, A., Innocenti, M., Mulinacci, N., & Giovannelli, L. (2018a). A two-phase olive mill by-product (pâté) as a convenient source of phenolic compounds: Content, stability, and antiaging properties in cultured human fibroblasts. *Journal of Functional Foods*, *40*, 751-759.

Cecchi, L., Guerrini, L., Bellumori, M., Balli, D., Xie, P., Parenti, A., & Mulinacci, N. (2020a). Optimization of the production process of dried unripe olives (Olea europaea L.) as a nutraceutical ingredient naturally rich in phenolic compounds. *LWT*, *129*, 109569.

Cecchi, L., Innocenti, M., Urciuoli, S., Arlorio, M., Paoli, P., & Mulinacci, N. (2019). In depth study of phenolic profile and PTP-1B inhibitory power of cold-pressed grape seed oils of different varieties. *Food chemistry*, *271*, 380-387.

Cecchi, L., Migliorini, M., Cherubini, C., Innocenti, M., & Mulinacci, N. (2015). Whole lyophilized olives as sources of unexpectedly high amounts of secoiridoids: the case of three Tuscan cultivars. *Journal of agricultural and food chemistry*, *63*(4), 1175-1185.

Cecchi, L., Migliorini, M., Zanoni, B., Breschi, C., & Mulinacci, N. (2018b). An effective HPLC-based approach for the evaluation of the content of total phenolic compounds transferred from olives to virgin olive oil during the olive milling process. *Journal of the Science of Food and Agriculture*, *98*(10), 3636-3643.

Cecchi, L., Piazzini, V., D'Ambrosio, M., Luceri, C., Rocco, F., Innocenti, M., ... & Bergonzi, M. C. (2020b). Formulation of a Phenol-Rich Extract from Unripe Olives (Olea europaea L.) in Microemulsion to Improve Its Solubility and Intestinal Permeability. *Molecules*, *25*(14), 3198.

Cevc, G., & Blume, G. (1992). Lipid vesicles penetrate into intact skin owing to the transdermal osmotic gradients and hydration force. *Biochimica et Biophysica Acta (BBA)-Biomembranes*, *1104*(1), 226-232.

Cevc, G., Vierl, U., & Mazgareanu, S. (2008). Functional characterisation of novel analgesic product based on self-regulating drug carriers. *International journal of pharmaceutics*, *360*(1-2), 18-28.

Chacko, I. A., Ghate, V. M., Dsouza, L., & Lewis, S. A. (2020). Lipid vesicles: A versatile drug delivery platform for dermal and transdermal applications. *Colloids and Surfaces B: Biointerfaces*, 111262.

Chatzidaki, M. D., Arik, N., Monteil, J., Papadimitriou, V., Leal-Calderon, F., & Xenakis, A. (2016). Microemulsion versus emulsion as effective carrier of hydroxytyrosol. *Colloids and Surfaces B: Biointerfaces*, *137*, 146-151.

Chen, H., Mou, D., Du, D., Chang, X., Zhu, D., Liu, J., ... & Yang, X. (2007). Hydrogel-thickened microemulsion for topical administration of drug molecule at an extremely low concentration. *International journal of pharmaceutics*, *341*(1-2), 78-84.

Chen, J., Lu, W. L., Gu, W., Lu, S. S., Chen, Z. P., & Cai, B. C. (2013). Skin permeation behavior of elastic liposomes: role of formulation ingredients. *Expert opinion on drug delivery*, *10*(6), 845-856.

Cheng, Y. C., Li, T. S., Su, H. L., Lee, P. C., & Wang, H. M. D. (2020). Transdermal Delivery Systems of Natural Products Applied to Skin Therapy and Care. *Molecules*, *25*(21), 5051.

Clinical and Laboratory Standards Institute. (2009). *Methods for Dilution Antimicrobial Susceptibility Tests for Bacteria that Grow Aerobically, Approved standard* (8th edition); CLSI publication M07-A8; Clinical and Laboratory Standards Institute: Wayne, PA, USA.

Coimbra, M., Isacchi, B., van Bloois, L., Torano, J. S., Ket, A., Wu, X., ... & Schiffelers, R. M. (2011). Improving solubility and chemical stability of natural compounds for medicinal use by incorporation into liposomes. *International journal of pharmaceutics*, *416*(2), 433-442.

D'Arcy, M. S. (2019). Cell death: a review of the major forms of apoptosis, necrosis and autophagy. *Cell biology international*, *43*(6), 582-592.

Dalla Rosa, A., Junges, A., Fernandes, I. A., Cansian, R. L., Corazza, M. L., Franceschi, E., ... & Valduga, E. (2019). High pressure extraction of olive leaves (Olea europaea): Bioactive compounds, bioactivity and kinetic modelling. *Journal of food science and technology*, *56*(8), 3864-3876.

De Almeida Borges, V. R., Ribeiro, A. F., de Souza Anselmo, C., Cabral, L. M., & de Sousa, V. P. (2013). Development of a high performance liquid chromatography method for quantification of isomers β-caryophyllene and α-humulene in copaiba oleoresin using the Box-Behnken design. *Journal of Chromatography B*, *940*, 35-41.

De Bock, M., Hodgkinson, S., Cutfield, W., & Schlothauer, R. C. (2015). *U.S. Patent Application No. 14/426,140*.

De Groot, C., Müsken, M., & Müller-Goymann, C. C. (2018). Novel colloidal microstructures of β-escin and the liposomal components cholesterol and DPPC. *Planta medica*, *84*(16), 1219-1227.

De Matos, S. P., Teixeira, H. F., de Lima, Á. A., Veiga-Junior, V. F., & Koester, L. S. (2019). Essential oils and isolated terpenes in nanosystems designed for topical administration: A review. *Biomolecules*, *9*(4), 138.

De Monte, C., Carradori, S., Granese, A., Di Pierro, G. B., Leonardo, C., & De Nunzio, C. (2014). Modern extraction techniques and their impact on the pharmacological profile of Serenoa repens extracts for the treatment of lower urinary tract symptoms. *BMC urology*, *14*(1), 1-11.

Desmedt, B., Courselle, P., De Beer, J. O., Rogiers, V., Deconinck, E., & De Paepe, K. (2015). In Vitro dermal absorption: Sample application and seal quality in a Franz diffusion cell system. *Skin pharmacology and physiology*, *28*(5), 245-249.

Domínguez-Perles, R., Auñón, D., Ferreres, F., & Gil-Izquierdo, A. (2017). Physiological linkage of gender, bioavailable hydroxytyrosol derivatives, and their metabolites with systemic catecholamine metabolism. *Food & function*, *8*(12), 4570-4581.

Drabova, L., Alvarez-Rivera, G., Suchanova, M., Schusterova, D., Pulkrabova, J., Tomaniova, M., ... & Hajslova, J. (2019). Food fraud in oregano: Pesticide residues as adulteration markers. *Food chemistry*, *276*, 726-734.

Dragicevic, N., & Maibach, H. I. (Eds.). (2017). Percutaneous penetration enhancers drug penetration into/through the skin: Methodology and general considerations. Springer.

Dragicevic, N., Krajisnik, D., Milic, J., Fahr, A., & Maibach, H. (2019). Development of hydrophilic gels containing coenzyme Q10-loaded liposomes: characterization, stability and rheology measurements. *Drug development and industrial pharmacy*, *45*(1), 43-54.

Du, D., Wang-Kan, X., Neuberger, A., van Veen, H. W., Pos, K. M., Piddock, L. J., & Luisi, B. F. (2018). Multidrug efflux pumps: structure, function and regulation. *Nature Reviews Microbiology*, *16*(9), 523-539.

Economou, G., Panagopoulos, G., Tarantilis, P., Kalivas, D., Kotoulas, V., Travlos, I. S., ... & Karamanos, A. (2011). Variability in essential oil content and composition of Origanum hirtum L., Origanum onites L., Coridothymus capitatus (L.) and Satureja thymbra L. populations from the Greek island Ikaria. *Industrial Crops and Products*, *33*(1), 236-241.

El-Ridy, M. S., Yehia, S. A., Mohsen, A. M., El-Awdan, S. A., & Darwish, A. B. (2018). Formulation of Niosomal gel for enhanced transdermal lornoxicam delivery: in-vitro and in-vivo evaluation. *Current drug delivery*, *15*(1), 122-133.

Elnaggar, Y. S., El-Refaie, W. M., El-Massik, M. A., & Abdallah, O. Y. (2014). Lecithin-based nanostructured gels for skin delivery: an update on state of art and recent applications. *Journal of controlled release*, *180*, 10-24.

Euro+Med PlantBase, 2011. http://ww2.bgbm.org/EuroPlusMed/query.asp (Accessed on 24 March 2021).

European Scientific Cooperative on Phytotherapy (ESCOP). (2013). Melissae folium, Melissa officinalis L. leaf. In *ESCOP Monograph.* Thieme Publisher:New York, NY, USA.

Facino, R. M., Carini, M., Stefani, R., Aldini, G., & Saibene, L. (1995). Anti-elastase and anti-hyaluronidase activities of saponins and sapogenins from Hedera helix, Aesculus hippocastanum, and Ruscus aculeatus: factors contributing to their efficacy in the treatment of venous insufficiency. *Archiv der Pharmazie*, *328*(10), 720-724.

Falconieri, M. C., Adamo, M., Monasterolo, C., Bergonzi, M. C., Coronnello, M., & Bilia, A. R. (2017). New dendrimer-based nanoparticles enhance curcumin solubility. *Planta medica*, *83*(05), 420-425.

Fang, J. Y., & Leu, Y. L. (2006). Prodrug strategy for enhancing drug delivery via skin. *Current drug discovery technologies, 3(3),* 211-224.

Fernández-García, R., Lalatsa, A., Statts, L., Bolás-Fernández, F., Ballesteros, M. P., & Serrano, D. R. (2020). Transferosomes as nanocarriers for drugs across the skin: Quality by design from lab to industrial scale. *International journal of pharmaceutics*, *573*, 118817.

Fiume, M. M., Bergfeld, W. F., Belsito, D. V., Hill, R. A., Klaassen, C. D., Liebler, D., ... & Andersen, F. A. (2012). Safety assessment of propylene glycol, tripropylene glycol, and PPGs as used in cosmetics. *International journal of toxicology*, *31*(5_suppl), 245S-260S.

Fluhr, J. W., Darlenski, R., & Surber, C. J. B. J. (2008). Glycerol and the skin: holistic approach to its origin and functions. *British Journal of Dermatology*, *159*(1), 23-34.

Fonseca-Santos, B., & Chorilli, M. (2017). An overview of carboxymethyl derivatives of chitosan: Their use as biomaterials and drug delivery systems. *Materials Science and Engineering: C*, *77*, 1349-1362.

Foster, S. (1996). Goldenseal: Hydrastis canadensis: botanical series# 309. *American Botanical Council*.

Freag, M. S., Torky, A. S., Nasra, M. M., Abdelmonsif, D. A., & Abdallah, O. Y. (2019). Liquid crystalline nanoreservoir releasing a highly skin-penetrating berberine oleate complex for psoriasis management. *Nanomedicine*, *14*(8), 931-954.

Funes, L., Fernández-Arroyo, S., Laporta, O., Pons, A., Roche, E., Segura-Carretero, A., ... & Micol, V. (2009). Correlation between plasma antioxidant capacity and verbascoside levels in rats after oral administration of lemon verbena extract. *Food Chemistry*, *117*(4), 589-598.

Gallelli, L. (2019). Escin: A review of its anti-edematous, anti-inflammatory, and venotonic properties. *Drug design, development and therapy*, *13*, 3425.

Gaonkar, R., Yallappa, S., Dhananjaya, B. L., & Hegde, G. (2016). Development and validation of reverse phase high performance liquid chromatography for citral analysis from essential oils. *Journal of Chromatography B*, *1036*, 50-56.

García-Villalba, R., Larrosa, M., Possemiers, S., Tomás-Barberán, F. A., & Espín, J. C. (2014). Bioavailability of phenolics from an oleuropein-rich olive (Olea europaea) leaf extract and its acute effect on plasma antioxidant status: comparison between pre-and postmenopausal women. *European journal of nutrition*, *53*(4), 1015-1027.

Garro, H. A., Bruna-Haupt, E., Cianchino, V., Malizia, F., Favier, S., Menacho-Márquez, M., ... & Pungitore, C. R. (2020). Verbascoside, synthetic derivatives and other glycosides from Argentinian native plant species as potential antitumoral agents. *Natural product research*, 1-6.

Gavin, A., Pham, J. T., Wang, D., Brownlow, B., & Elbayoumi, T. A. (2015). Layered nanoemulsions as mucoadhesive buccal systems for controlled delivery of oral cancer therapeutics. *International journal of nanomedicine*, *10*, 1569.

Gehring, W., Fluhr, J., & Gloor, M. (1998). Influence of vitamin E acetate on stratum corneum hydration. *Arzneimittel-forschung*, *48*(7), 772-775.

Geisler, R., Dargel, C., & Hellweg, T. (2020). The biosurfactant β-aescin: A review on the physico-chemical properties and its interaction with lipid model membranes and Langmuir monolayers. *Molecules*, *25*(1), 117.

Ghadermazi, R., Hamdipour, S., Sadeghi, K., Ghadermazi, R., & Khosrowshahi Asl, A. (2019). Effect of various additives on the properties of the films and coatings derived from hydroxypropyl methylcellulose—A review. *Food science & nutrition*, *7*(11), 3363-3377.

Ghanbari, R., Anwar, F., Alkharfy, K. M., Gilani, A. H., & Saari, N. (2012). Valuable nutrients and functional bioactives in different parts of olive (Olea europaea L.)—a review. *International journal of molecular sciences*, *13*(3), 3291-3340.

Ghatnur, S. M., Sonale, R. S., Balaraman, M., & Kadimi, U. S. (2012). Engineering liposomes of leaf extract of seabuckthorn (SBT) by supercritical carbon dioxide (SCCO2)-mediated process. *Journal of liposome research*, *22*(3), 215-223.

Gillet, A., Lecomte, F., Hubert, P., Ducat, E., Evrard, B., & Piel, G. (2011). Skin penetration behaviour of liposomes as a function of their composition. *European journal of pharmaceutics and biopharmaceutics*, *79*(1), 43-53.

Giovannelli, L. (2012). Beneficial effects of olive oil phenols on the aging process: Experimental evidence and possible mechanisms of action. *Nutrition and Aging*, *1*(3, 4), 207-223.

Girish, K. S., Kemparaju, K., Nagaraju, S., & Vishwanath, B. S. (2009). Hyaluronidase inhibitors: a biological and therapeutic perspective. *Current medicinal chemistry*, *16*(18), 2261-2288.

Gladstar, R., & Hirsch, P. (Eds.). (2000). *Planting the future: saving our medicinal herbs*. Inner Traditions/Bear & Co.

Glamoclija, J., Sokovic, M., Vukojevic, J., Milenkovic, I., & Van Griensven, L. J. L. D. (2006). Chemical composition and antifungal activities of essential oils of Satureja thymbra L. and Salvia pomifera ssp. calycina (Sm.) Hayek. *Journal of Essential Oil Research: JEOR*, *18*(1), 115.

Godugu, C., Patel, A. R., Doddapaneni, R., Somagoni, J., & Singh, M. (2014). Approaches to improve the oral bioavailability and effects of novel anticancer drugs berberine and betulinic acid. *PloS one*, *9*(3), e89919.

Gowda, S., Desai, P. B., Hull, V. V., Math, A. A. K., Vernekar, S. N., & Kulkarni, S. S. (2009). A review on laboratory liver function tests. *The Pan african medical journal*, *3*.

Grewal, R., Reutzel, M., Dilberger, B., Hein, H., Zotzel, J., Marx, S., ... & Eckert, G. P. (2020). Purified oleocanthal and ligstroside protect against mitochondrial dysfunction in models of early Alzheimer's disease and brain ageing. *Experimental neurology*, *328*, 113248.

Grossi, C., Guccione, C., Isacchi, B., Bergonzi, M. C., Luccarini, I., Casamenti, F., & Bilia, A. R. (2017). Development of blood-brain barrier permeable nanoparticles as potential carriers for salvianolic acid B to CNS. *Planta medica*, *83*(05), 382-391.

Guan, Q., Sun, S., Li, X., Lv, S., Xu, T., Sun, J., ... & Li, Y. (2016). Preparation, in vitro and in vivo evaluation of mPEG-PLGA nanoparticles co-loaded with syringopicroside and hydroxytyrosol. *Journal of materials science: materials in medicine*, *27*(2), 24.

Guccione, C., Bergonzi, M. C., Awada, K. M., Piazzini, V., & Bilia, A. R. (2018). Lipid nanocarriers for oral delivery of Serenoa repens CO2 extract: A study of microemulsion and self-microemulsifying drug delivery systems. *Planta medica*, *84*(09/10), 736-742.

Guccione, C., Oufir, M., Piazzini, V., Eigenmann, D. E., Jähne, E. A., Zabela, V., ... & Bilia, A. R. (2017). Andrographolide-loaded nanoparticles for brain delivery: Formulation, characterisation and in vitro permeability using hCMEC/D3 cell line. *European Journal of Pharmaceutics and Biopharmaceutics*, *119*, 253-263.

Hajimehdipoor, H., Shekarchi, M., Khanavi, M., Adib, N., & Amri, M. (2010). A validated high performance liquid chromatography method for the analysis of thymol and carvacrol in Thymus vulgaris L. volatile oil. *Pharmacognosy magazine*, *6*(23), 154.

Harika, K., Sunitha, K., Kumar, P. P., Maheshwar, K., & Rao, M. Y. (2012). Basic Concepts Of Cellulose Polymers-A Comprehensive Review. *Archives of Pharmacy Practice*, *3*(3), 202.

Hashim, S., Jan, A., Marwat, K. B., & Khan, M. A. (2014). Phytochemistry and medicinal properties of Ammi visnaga (Apiacae). *Pak J Bot*, *46*(3), 861-7.

Hassan, M. A., & Zubair, M. U. (1981). Khellin. In *Analytical Profiles of Drug Substances* (Vol. 9, pp. 371-396). Academic Press.

Hearnden, V., Sankar, V., Hull, K., Juras, D. V., Greenberg, M., Kerr, A. R., ... & Thornhill, M. H. (2012). New developments and opportunities in oral mucosal drug delivery for local and systemic disease. *Advanced drug delivery reviews*, *64*(1), 16-28.

Heuschkel, S., Goebel, A., & Neubert, R. H. (2008). Microemulsions—modern colloidal carrier for dermal and transdermal drug delivery. *Journal of Pharmaceutical Sciences*, *97*(2), 603-631.

Hornedo-Ortega, R., Cerezo, A. B., de Pablos, R. M., Krisa, S., Richard, T., García-Parrilla, M. C., & Troncoso, A. M. (2018). Phenolic compounds characteristic of the mediterranean diet in mitigating microglia-mediated neuroinflammation. *Frontiers in cellular neuroscience*, *12*, 373.

Hou, Q., He, W. J., Wu, Y. S., Hao, H. J., Xie, X. Y., & Fu, X. B. (2020). Berberine: A Traditional Natural Product With Novel Biological Activities. *Alternative Therapies in Health & Medicine*, *26*.

Hu, C. M. J., & Zhang, L. (2012). Nanoparticle-based combination therapy toward overcoming drug resistance in cancer. *Biochemical pharmacology*, *83*(8), 1104-1111.

Hu, D., Wang, H., & Wang, L. (2016). Physical properties and antibacterial activity of quaternized chitosan/carboxymethyl cellulose blend films. *LWT-Food Science and Technology*, *65*, 398-405.

Hubatsch, I., Ragnarsson, E. G., & Artursson, P. (2007). Determination of drug permeability and prediction of drug absorption in Caco-2 monolayers. *Nature protocols*, *2*(9), 2111.

Iacomino, G., Fierro, O., D'Auria, S., Picariello, G., Ferranti, P., Liguori, C., ... & Mamone, G. (2013). Structural analysis and Caco-2 cell permeability of the celiac-toxic A-gliadin peptide 31–55. *Journal of agricultural and food chemistry*, *61*(5), 1088-1096.

Imanshahidi, M., & Hosseinzadeh, H. (2008). Pharmacological and therapeutic effects of Berberis vulgaris and its active constituent, berberine. *Phytotherapy research*, *22*(8), 999-1012.

Iqbal, B., Ali, J., & Baboota, S. (2018). Recent advances and development in epidermal and dermal drug deposition enhancement technology. *International journal of dermatology*, *57*(6), 646-660.

Isacchi, B., Arrigucci, S., Marca, G. L., Bergonzi, M. C., Vannucchi, M. G., Novelli, A., & Bilia, A. R. (2011a). Conventional and long-circulating liposomes of artemisinin: preparation, characterization, and pharmacokinetic profile in mice. *Journal of liposome research*, *21*(3), 237-244.

Isacchi, B., Bergonzi, M. C., Grazioso, M., Righeschi, C., Pietretti, A., Severini, C., & Bilia, A. R. (2012). Artemisinin and artemisinin plus curcumin liposomal formulations: enhanced antimalarial efficacy against Plasmodium berghei-infected mice. *European journal of pharmaceutics and biopharmaceutics*, *80*(3), 528-534.

Isacchi, B., Bergonzi, M. C., Iacopi, R., Ghelardini, C., Galeotti, N., & Bilia, A. R. (2017). Liposomal formulation to increase stability and prolong antineuropathic activity of verbascoside. *Planta medica*, *83*(05), 412-419.

Isacchi, B., Fabbri, V., Galeotti, N., Bergonzi, M. C., Karioti, A., Ghelardini, C., ... & Bilia, A. R. (2011b). Salvianolic acid B and its liposomal formulations: anti-hyperalgesic activity in the treatment of neuropathic pain. *European journal of pharmaceutical sciences*, *44*(4), 552-558.

Ita, K. (2017). Progress in the use of microemulsions for transdermal and dermal drug delivery. *Pharmaceutical development and technology*, *22*(4), 467-475.

Ita, K. B. (2016). Prodrugs for transdermal drug delivery–trends and challenges. *Journal of drug targeting, 24(8),* 671-678.

Jain, H., & Chella, N. (2020). Methods to improve the solubility of therapeutical natural products: a review. *Environmental Chemistry Letters*, 1-11.

Jain, S., Jain, P., Umamaheshwari, R. B., & Jain, N. K. (2003). Transfersomes—a novel vesicular carrier for enhanced transdermal delivery: development, characterization, and performance evaluation. *Drug development and industrial pharmacy*, *29*(9), 1013-1026.

Jaiswal, M., Kumar, A., & Sharma, S. (2016). Nanoemulsions loaded Carbopol® 934 based gel for intranasal delivery of neuroprotective Centella asiatica extract: in–vitro and ex–vivo permeation study. *Journal of Pharmaceutical Investigation*, *46*(1), 79-89.

Jeong, H. W., Hsu, K. C., Lee, J. W., Ham, M., Huh, J. Y., Shin, H. J., ... & Kim, J. B. (2009). Berberine suppresses proinflammatory responses through AMPK activation in macrophages. *American Journal of Physiology-Endocrinology and Metabolism*, *296*(4), E955-E964.

Jung, S., Otberg, N., Thiede, G., Richter, H., Sterry, W., Panzner, S., & Lademann, J. (2006). Innovative liposomes as a transfollicular drug delivery system: penetration into porcine hair follicles. *Journal of Investigative Dermatology*, *126*(8), 1728-1732.

Kanikireddy, V., Varaprasad, K., Jayaramudu, T., Karthikeyan, C., & Sadiku, R. (2020). Carboxymethyl cellulose-based materials for infection control and wound healing: A review. *International Journal of Biological Macromolecules*.

Kansy, M., Senner, F., & Gubernator, K. (1998). Physicochemical high throughput screening: parallel artificial membrane permeation assay in the description of passive absorption processes. *Journal of medicinal chemistry*, *41*(7), 1007-1010.

Karpiński, T. M. (2020). Essential oils of Lamiaceae family plants as antifungals. *Biomolecules*, *10*(1), 103.

Katz, M., & Poulsen, B. J. (1971). Absorption of drugs through the skin. In *Concepts in Biochemical Pharmacology* (pp. 103-174). Springer, Berlin, Heidelberg.

Kerekes, E. B., Vidács, A., Török Jenei, J., Gömöri, C., Takó, M., Chandrasekaran, M., ... & Vágvölgyi, C. (2015). Essential oils against bacterial biofilm formation and quorum sensing of food-borne pathogens and spoilage microorganisms.

Kesarwani, K., & Gupta, R. (2013). Bioavailability enhancers of herbal origin: An overview. *Asian Pacific journal of tropical biomedicine*, 3(4), 253-266.

Khan, I. A., & Smillie, T. (2012). Implementing a "quality by design" approach to assure the safety and integrity of botanical dietary supplements. *Journal of natural products*, 75(9), 1665-1673.

Khattab, H., Fouad, A., Hamza, M., Mohey, M. A., El-Akel, W., Ghoneim, H., ... & Esmat, G. (2015). Relation of ALT and AST levels to the histopathological changes in liver biopsies of patients with chronic hepatitis C genotype 4. *Arab Journal of Gastroenterology*, *16*(2), 50-53.

King, M. (2009). Spoilage and preservation of food. *Food Quality and Standards*, 41-59.

Kogan, A., & Garti, N. (2006). Microemulsions as transdermal drug delivery vehicles. *Advances in colloid and interface science*, *123*, 369-385.

Kokkini, S., & Vokou, D. (1989). Carvacrol-rich plants in Greece. *Flavour and Fragrance Journal*, *4*(1), 1-7.

Kokkini, S., Karousou, R., Hanlidou, E., & Lanaras, T. (2004). Essential oil composition of Greek (Origanum vulgare ssp. hirtum) and Turkish (O. onites) oregano: a tool for their distinction. *Journal of Essential Oil Research*, *16*(4), 334-338.

Korting, H. C., & Schäfer-Korting, M. (2010). Carriers in the topical treatment of skin disease. *Drug delivery*, 435-468.

Kountouri, A. M., Mylona, A., Kaliora, A. C., & Andrikopoulos, N. K. (2007). Bioavailability of the phenolic compounds of the fruits (drupes) of Olea europaea (olives): impact on plasma antioxidant status in humans. *Phytomedicine*, *14*(10), 659-667.

Kováčik, A., Kopečná, M., & Vávrová, K. (2020). Permeation enhancers in transdermal drug delivery: benefits and limitations. *Expert opinion on drug delivery*, *17*(2), 145-155.

Kreilgaard, M. (2002). Influence of microemulsions on cutaneous drug delivery. *Advanced drug delivery reviews*, *54*, S77-S98.

Kumar, A., Chopra, K., Mukherjee, M., Pottabathini, R., & Dhull, D. K. (2015). Current knowledge and pharmacological profile of berberine: an update. *European journal of pharmacology*, *761*, 288-297.

Kyratsous, C. A., Walters, M. S., Panagiotidis, C. A., & Silverstein, S. J. (2009). Complementation of a herpes simplex virus ICP0 null mutant by varicella-zoster virus ORF61p. *Journal of virology*, *83*(20), 10637-10643.

Lagunin, A. A., Dubovskaja, V. I., Rudik, A. V., Pogodin, P. V., Druzhilovskiy, D. S., Gloriozova, T. A., ... & Poroikov, V. V. (2018). CLC-Pred: a freely available web-service for in silico prediction of human cell line cytotoxicity for drug-like compounds. *PloS one*, *13*(1), e0191838.

Lai, F., Sinico, C., De Logu, A., Zaru, M., Müller, R. H., & Fadda, A. M. (2007). SLN as a topical delivery system for Artemisia arborescens essential oil: in vitro antiviral activity and skin permeation study. *International journal of nanomedicine*, *2*(3), 419.

Lane, M. E. (2013). Skin penetration enhancers. *International journal of pharmaceutics*, *447*(1-2), 12-21.

Lawrence, M. J., & Rees, G. D. (2000). Microemulsion-based media as novel drug delivery systems. *Advanced drug delivery reviews*, *45*(1), 89-121.

Lea, T. (2015). Caco-2 cell line. *The impact of food bioactives on health*, 103-111.

Lee, O. H., & Lee, B. Y. (2010). Antioxidant and antimicrobial activities of individual and combined phenolics in Olea europaea leaf extract. *Bioresource technology*, *101*(10), 3751-3754.

Lehman, P. A., Raney, S. G., & Franz, T. J. (2011). Percutaneous absorption in man: in vitro-in vivo correlation. *Skin pharmacology and physiology*, *24*(4), 224-230.

Leto, I., Coronnello, M., Righeschi, C., Bergonzi, M. C., Mini, E., & Bilia, A. R. (2016). Enhanced efficacy of artemisinin loaded in transferrin-conjugated liposomes versus stealth liposomes against HCT-8 colon cancer cells. *ChemMedChem*, *11*(16), 1745-1751.

Leuci, S., Ruoppo, E., Adamo, D., Calabria, E., & Mignogna, M. D. (2019). Oral autoimmune vesicobullous diseases: classification, clinical presentations, molecular mechanisms, diagnostic algorithms, and management. *Periodontology 2000*, *80*(1), 77-88.

Lin, Y., Shen, Q., Katsumi, H., Okada, N., Fujita, T., Jiang, X., & Yamamoto, A. (2007). Effects of Labrasol and other pharmaceutical excipients on the intestinal transport and absorption of rhodamine123, a P-glycoprotein substrate, in rats. *Biological and Pharmaceutical Bulletin*, *30*(7), 1301-1307.

Liu, D., Meng, X., Wu, D., Qiu, Z., & Luo, H. (2019). A natural isoquinoline alkaloid with antitumor activity: studies of the biological activities of berberine. *Frontiers in pharmacology*, *10*, 9.

Liu, Y. H., Huang, Q. H., Wu, X., Wu, J. Z., Liang, J. L., Lin, G. S., ... & Chen, J. N. (2018). Polydatin protects against acetaminophen-induced hepatotoxicity in mice via anti-oxidative and anti-apoptotic activities. *Food & function*, *9*(11), 5891-5902.

Liu, Y. T., Hao, H. P., Xie, H. G., Lai, L., Wang, Q., Liu, C. X., & Wang, G. J. (2010). Extensive intestinal first-pass elimination and predominant hepatic distribution of berberine explain its low plasma levels in rats. *Drug metabolism and disposition*, *38*(10), 1779-1784.

Lombrea, A., Antal, D., Ardelean, F., Avram, S., Pavel, I. Z., Vlaia, L., ... & Danciu, C. (2020). A Recent Insight Regarding the Phytochemistry and Bioactivity of Origanum vulgare L. Essential Oil. *International Journal of Molecular Sciences*, *21*(24), 9653.

Madhav, N. S., Shakya, A. K., Shakya, P., & Singh, K. (2009). Orotransmucosal drug delivery systems: a review. *Journal of controlled release*, *140*(1), 2-11.

Makhey, V. D., Guo, A., Norris, D. A., Hu, P., Yan, J., & Sinko, P. J. (1998). Characterization of the regional intestinal kinetics of drug efflux in rat and human intestine and in Caco-2 cells. *Pharmaceutical research*, *15*(8), 1160-1167.

Manaia, E. B., Abuçafy, M. P., Chiari-Andréo, B. G., Silva, B. L., Junior, J. A. O., & Chiavacci, L. A. (2017). Physicochemical characterization of drug nanocarriers. *International journal of nanomedicine*, *12*, 4991.

Manca, M. L., Zaru, M., Manconi, M., Lai, F., Valenti, D., Sinico, C., & Fadda, A. M. (2013). Glycerosomes: a new tool for effective dermal and transdermal drug delivery. *International journal of pharmaceutics*, *455*(1-2), 66-74.

Manikkath, J., Sumathy, T. K., Manikkath, A., & Mutalik, S. (2018). Delving deeper into dermal and transdermal drug delivery: factors and mechanisms associated with nanocarrier-mediated strategies. *Current pharmaceutical design*, *24*(27), 3210-3222.

Marti, G., Joulia, P., Amiel, A., Fabre, B., David, B., Fabre, N., & Fiorini-Puybaret, C. (2019). Comparison of the phytochemical composition of Serenoa repens extracts by a multiplexed metabolomic approach. *Molecules*, *24*(12), 2208.

Masada, Y. (1976). Analysis of essential oils by gas chromatography and mass spectrometry.

Matos, C., & Lobão, P. (2020). Non-steroidal anti-inflammatory drugs loaded liposomes for topical treatment of inflammatory and degenerative conditions. *Current medicinal chemistry*, *27*(23), 3809-3829.

Matta, M. K., & Panagiotidis, C. A. (2008). High-mobility group protein A1 binds herpes simplex virus gene regulatory sequences and affects their expression. *Archives of virology*, *153*(7), 1251-1262.

Matzneller, P., Kussmann, M., Eberl, S., Maier-Salamon, A., Jäger, W., Bauer, M., ... & Poeppl, W. (2018). Pharmacokinetics of the P-gp inhibitor Tariquidar in rats after intravenous, Oral, and Intraperitoneal administration. *European journal of drug metabolism and pharmacokinetics*, *43*(5), 599-606.

Mazzanti, G., Battinelli, L., Pompeo, C., Serrilli, A. M., Rossi, R., Sauzullo, I., ... & Vullo, V. (2008). Inhibitory activity of Melissa officinalis L. extract on Herpes simplex virus type 2 replication. *Natural product research*, *22*(16), 1433-1440.

McCartney, F., Jannin, V., Chevrier, S., Boulghobra, H., Hristov, D. R., Ritter, N., ... & Brayden, D. J. (2019). Labrasol® is an efficacious intestinal permeation enhancer across rat intestine: ex vivo and in vivo rat studies. *Journal of Controlled Release*, *310*, 115-126.

Mehta, P., Shah, R., Lohidasan, S., & Mahadik, K. R. (2015). Pharmacokinetic profile of phytoconstituent (s) isolated from medicinal plants—a comprehensive review. *Journal of traditional and complementary medicine*, 5(4), 207-227.

Moerman, D. E. (1998). *Native american ethnobotany* (Vol. 879). Portland, OR: Timber press.

Mohammadi, A., Jafari, S. M., Assadpour, E., & Esfanjani, A. F. (2016). Nano-encapsulation of olive leaf phenolic compounds through WPC–pectin complexes and evaluating their release rate. *International journal of biological macromolecules*, *82*, 816-822.

Mohebbati, R., Paseban, M., Beheshti, F., Soukhtanloo, M., Shafei, M. N., Rakhshandeh, H., & Rad, A. K. (2018). The Preventive Effects of Standardized Extract of Zataria multiflora and Carvacrol on Acetaminophen-Induced Hepatotoxicity in Rat:-Zataria multiflora and Carvacrol and Hepatotoxicity. *Journal of pharmacopuncture*, *21*(4), 249.

Morelló, J. R., Vuorela, S., Romero, M. P., Motilva, M. J., & Heinonen, M. (2005). Antioxidant activity of olive pulp and olive oil phenolic compounds of the Arbequina cultivar. *Journal of agricultural and food chemistry*, *53*(6), 2002-2008.

Moreno-Bautista, G., & Tam, K. C. (2011). Evaluation of dialysis membrane process for quantifying the in vitro drug-release from colloidal drug carriers. *Colloids and Surfaces A: Physicochemical and Engineering Aspects*, *389*(1-3), 299-303.

Münch, S., Wohlrab, J., & Neubert, R. H. H. (2017). Dermal and transdermal delivery of pharmaceutically relevant macromolecules. *European Journal of Pharmaceutics and Biopharmaceutics*, *119*, 235-242.

Murata, T., Miyase, T., & Yoshizaki, F. (2012). Hyaluronidase inhibitors from Keiskea japonica. *Chemical and Pharmaceutical Bulletin*, *60*(1), 121-128.

Nachbar, F., & Korting, H. C. (1995). The role of vitamin E in normal and damaged skin. *Journal of Molecular Medicine*, *73*(1), 7-17.

Naeem, S., Viswanathan, G., & Misran, M. B. (2018). Liposomes as colloidal nanovehicles: on the road to success in intravenous drug delivery. *Reviews in Chemical Engineering*, *34*(3), 365-383.

Nastiti, C. M., Ponto, T., Abd, E., Grice, J. E., Benson, H. A., & Roberts, M. S. (2017). Topical nano and microemulsions for skin delivery. *Pharmaceutics*, *9*(4), 37.

National organization for medicines. (2002). *Hellenic Pharmacopoeia* (V ed., Chapter 28.12). Greece, Athens.

Nava, G., Piñón, E., Mendoza, L., Mendoza, N., Quintanar, D., & Ganem, A. (2011). Formulation and in vitro, ex vivo and in vivo evaluation of elastic liposomes for transdermal delivery of ketorolac tromethamine. *Pharmaceutics*, *3*(4), 954-970.

Navarro del Hierro, J., Piazzini, V., Reglero, G., Martin, D., & Bergonzi, M. C. (2020). In Vitro Permeability of Saponins and Sapogenins from Seed Extracts by the Parallel Artificial Membrane Permeability Assay: Effect of in Vitro Gastrointestinal Digestion. *Journal of agricultural and food chemistry*, *68*(5), 1297-1305.

Nerurkar, M. M., Burton, P. S., & Borchardt, R. T. (1996). The use of surfactants to enhance the permeability of peptides through Caco-2 cells by inhibition of an apically polarized efflux system. *Pharmaceutical research*, *13*(4), 528-534.

Ng, S. F., Rouse, J. J., Sanderson, F. D., & Eccleston, G. M. (2012). The relevance of polymeric synthetic membranes in topical formulation assessment and drug diffusion study. *Archives of pharmacal research*, *35*(4), 579-593.

Nicoli, S., & Santi, P. (2007). Suitability of excised rabbit ear skin—Fresh and frozen—For evaluating transdermal permeation of estradiol. *Drug delivery*, *14*(4), 195-199.

Nieto, G. (2017). Biological activities of three essential oils of the Lamiaceae family. *Medicines*, *4*(3), 63.

Nishioka, Y., & Silverstein, S. (1977). Degradation of cellular mRNA during infection by herpes simplex virus. *Proceedings of the National Academy of Sciences*, *74*(6), 2370-2374.

Nolkemper, S., Reichling, J., Stintzing, F. C., Carle, R., & Schnitzler, P. (2006). Antiviral effect of aqueous extracts from species of the Lamiaceae family against Herpes simplex virus type 1 and type 2 in vitro. *Planta medica*, *72*(15), 1378-1382.

Olusanya, T. O., Haj Ahmad, R. R., Ibegbu, D. M., Smith, J. R., & Elkordy, A. A. (2018). Liposomal drug delivery systems and anticancer drugs. *Molecules*, *23*(4), 907.

Omar, S. H. (2010). Oleuropein in olive and its pharmacological effects. *Scientia pharmaceutica*, *78*(2), 133-154.

Organisation for Economic Co-operation and Development (2004), *Guidance Document for the Conduct of Skin Absorption Studies*, OECD Series on Testing and Assessment, No. 28, OECD Publishing, Paris.

Organisation for Economic Co-operation and Development (2015), *Test No. 404: Acute Dermal Irritation/Corrosion*, OECD Guidelines for the Testing of Chemicals, Section 4, OECD Publishing, Paris.

Organisation for Economic Co-operation and Development (2017), *Test No. 402: Acute Dermal Toxicity*, OECD Guidelines for the Testing of Chemicals, Section 4, OECD Publishing, Paris.

Ozer, J., Ratner, M., Shaw, M., Bailey, W., & Schomaker, S. (2008). The current state of serum biomarkers of hepatotoxicity. *Toxicology*, *245*(3), 194-205.

Panagiotidis, C. A., & Silverstein, S. J. (1999). The host-cell architectural protein HMG I (Y) modulates binding of herpes simplex virus type 1 ICP4 to its cognate promoter. *Virology*, *256*(1), 64-74.

Pardi, N., Tuyishime, S., Muramatsu, H., Kariko, K., Mui, B. L., Tam, Y. K., ... & Weissman, D. (2015). Expression kinetics of nucleoside-modified mRNA delivered in lipid nanoparticles to mice by various routes. *Journal of Controlled Release*, *217*, 345-351.

Patel, P., Schmieder, S., & Krishnamurthy, K. (2016). Research techniques made simple: Drug delivery techniques, Part 2: Commonly used techniques to assess topical drug bioavailability. *Journal of Investigative Dermatology*, *136*(5), e43-e49.

Patzelt, A., Mak, W. C., Jung, S., Knorr, F., Meinke, M. C., Richter, H., ... & Lademann, J. (2017). Do nanoparticles have a future in dermal drug delivery?. *Journal of Controlled Release*, *246*, 174-182.

Paudel, K. S., Milewski, M., Swadley, C. L., Brogden, N. K., Ghosh, P., & Stinchcomb, A. L. (2010). Challenges and opportunities in dermal/transdermal delivery. *Therapeutic delivery*, *1*(1), 109-131.

Paul, K., Bhattacharjee, P., Chatterjee, N., & Pal, T. K. (2019). Nanoliposomes of supercritical carbon dioxide extract of small cardamom seeds redresses type 2 diabetes and hypercholesterolemia. *Recent patents on biotechnology*, *13*(4), 284-303.

Perez-Cullell, N., Coderch, L., de la Maza, A., Parra, J. L., & Estelrich, J. (2000). Influence of the fluidity of liposome compositions on percutaneous absorption. *Drug delivery*, *7*(1), 7-13.

Perrinjaquet-Moccetti, T., Busjahn, A., Schmidlin, C., Schmidt, A., Bradl, B., & Aydogan, C. (2008). Food supplementation with an olive (Olea europaea L.) leaf extract reduces blood pressure in borderline hypertensive monozygotic twins. *Phytotherapy Research*, *22*(9), 1239-1242.

Piazzini, V., Cinci, L., D'Ambrosio, M., Luceri, C., Bilia, A. R., & Bergonzi, M. C. (2019a). Solid lipid nanoparticles and chitosan-coated solid lipid nanoparticles as promising tool for silybin delivery: formulation, characterization, and in vitro evaluation. *Current drug delivery*, *16*(2), 142-152.

Piazzini, V., D'Ambrosio, M., Luceri, C., Cinci, L., Landucci, E., Bilia, A. R., & Bergonzi, M. C. (2019b). Formulation of nanomicelles to improve the solubility and the oral absorption of silymarin. *Molecules*, *24*(9), 1688.

Piazzini, V., Lemmi, B., D'Ambrosio, M., Cinci, L., Luceri, C., Bilia, A. R., & Bergonzi, M. C. (2018). Nanostructured lipid carriers as promising delivery systems for plant extracts: The case of silymarin. *Applied Sciences*, *8*(7), 1163.

Piazzini, V., Micheli, L., Luceri, C., D'Ambrosio, M., Cinci, L., Ghelardini, C., ... & Bergonzi, M. C. (2019c). Nanostructured lipid carriers for oral delivery of silymarin: improving its absorption and

in vivo efficacy in type 2 diabetes and metabolic syndrome model. *International journal of pharmaceutics*, *572*, 118838.

Piazzini, V., Monteforte, E., Luceri, C., Bigagli, E., Bilia, A. R., & Bergonzi, M. C. (2017a). Nanoemulsion for improving solubility and permeability of Vitex agnus-castus extract: formulation and in vitro evaluation using PAMPA and Caco-2 approaches. *Drug delivery*, *24*(1), 380-390.

Piazzini, V., Rosseti, C., Bigagli, E., Luceri, C., Bilia, A. R., & Bergonzi, M. C. (2017b). Prediction of permeation and cellular transport of Silybum marianum extract formulated in a nanoemulsion by using PAMPA and Caco-2 cell models. *Planta medica*, *83*(14/15), 1184-1193.

Piazzini, V., Vasarri, M., Degl'Innocenti, D., Guastini, A., Barletta, E., Salvatici, M. C., & Bergonzi, M. C. (2019d). Comparison of chitosan nanoparticles and soluplus micelles to optimize the bioactivity of Posidonia oceanica extract on human neuroblastoma cell migration. *Pharmaceutics*, *11*(12), 655.

Pierre, M. B. R., & Costa, I. D. S. M. (2011). Liposomal systems as drug delivery vehicles for dermal and transdermal applications. Archives of dermatological research, 303(9), 607-621.

Pinnell, S. R., Yang, H., Omar, M., Riviere, N. M., DeBuys, H. V., Walker, L. C., ... & Levine, M. (2001). Topical L-ascorbic acid: percutaneous absorption studies. *Dermatologic surgery*, *27*(2), 137-142.

Pitorre, M., Gondé, H., Haury, C., Messous, M., Poilane, J., Boudaud, D., ... & Bastiat, G. (2017). Recent advances in nanocarrier-loaded gels: Which drug delivery technologies against which diseases?. *Journal of Controlled Release*, *266*, 140-155.

Porter, C. J., Pouton, C. W., Cuine, J. F., & Charman, W. N. (2008). Enhancing intestinal drug solubilisation using lipid-based delivery systems. *Advanced drug delivery reviews*, *60*(6), 673-691.

Porter, C. J., Trevaskis, N. L., & Charman, W. N. (2007). Lipids and lipid-based formulations: optimizing the oral delivery of lipophilic drugs. *Nature reviews Drug discovery*, *6*(3), 231-248.

Puglia C, 2017., Lauro, M. R., Tirendi, G. G., Fassari, G. E., Carbone, C., Bonina, F., & Puglisi, G. (2017). Modern drug delivery strategies applied to natural active compounds. *Expert opinion on drug delivery*, *14(6)*, 755-768.

Pullar, J. M., Carr, A. C., & Vissers, M. (2017). The roles of vitamin C in skin health. *Nutrients*, *9*(8), 866.

Rai, V. K., Mishra, N., Yadav, K. S., & Yadav, N. P. (2018). Nanoemulsion as pharmaceutical carrier for dermal and transdermal drug delivery: formulation development, stability issues, basic considerations and applications. *Journal of controlled release*, *270*, 203-225.

Ramanunny, A. K., Wadhwa, S., Gulati, M., Singh, S. K., Kapoor, B., Dureja, H., ... & Pandey, N. K. (2021). Nanocarriers for treatment of dermatological diseases: Principle, perspective and practices. *European journal of pharmacology*, *890*, 173691.

Refaat, A., Abdelhamed, S., Saiki, I., & Sakurai, H. (2015). Inhibition of p38 mitogen-activated protein kinase potentiates the apoptotic effect of berberine/tumor necrosis factor-related apoptosis-inducing ligand combination therapy. *Oncology letters*, *10*(3), 1907-1911.

Rege, B. D., Kao, J. P., & Polli, J. E. (2002). Effects of nonionic surfactants on membrane transporters in Caco-2 cell monolayers. *European journal of pharmaceutical sciences*, *16*(4-5), 237-246.

Reid, A. M., Juvonen, R., Huuskonen, P., Lehtonen, M., Pasanen, M., & Lall, N. (2019). In Vitro human metabolism and inhibition potency of verbascoside for CYP enzymes. *Molecules*, *24*(11), 2191.

Ricciarelli, R., Maroni, P., Özer, N., Zingg, J. M., & Azzi, A. (1999). Age-dependent increase of collagenase expression can be reduced by α-tocopherol via protein kinase C inhibition. *Free Radical Biology and Medicine*, *27*(7-8), 729-737.

Righeschi, C., Coronnello, M., Mastrantoni, A., Isacchi, B., Bergonzi, M. C., Mini, E., & Bilia, A. R. (2014). Strategy to provide a useful solution to effective delivery of dihydroartemisinin: Development, characterization and in vitro studies of liposomal formulations. *Colloids and Surfaces B: Biointerfaces*, *116*, 121-127.

Rincón-Iglesias, M., Lizundia, E., & Lanceros-Méndez, S. (2019). Water-soluble cellulose derivatives as suitable matrices for multifunctional materials. *Biomacromolecules*, *20*(7), 2786-2795.

Ring, J., Alomar, A., Bieber, T., Deleuran, M., Fink-Wagner, A., Gelmetti, C., ... & Darsow, U. (2012). Guidelines for treatment of atopic eczema (atopic dermatitis) Part II. *Journal of the European Academy of Dermatology and Venereology*, *26*(9), 1176-1193.

Rippke, F., Schreiner, V., & Schwanitz, H. J. (1999). The acidic milieu of the horny layer/new findings on physiology and pathophysiology of the skin ph-value. *Dermatosen in Beruf und Umwelt*, *47*(6), G-230.

Risaliti, L., Ambrosi, M., Calamante, M., Bergonzi, M. C., Nostro, P. L., & Bilia, A. R. (2020a). Preparation and Characterization of Ascosome Vesicles Loaded with Khellin. *Journal of pharmaceutical sciences*, *109*(10), 3114-3124.

Risaliti, L., Kehagia, A., Daoultzi, E., Lazari, D., Bergonzi, M. C., Vergkizi-Nikolakaki, S., ... & Bilia, A. R. (2019). Liposomes loaded with Salvia triloba and Rosmarinus officinalis essential oils: In vitro assessment of antioxidant, antiinflammatory and antibacterial activities. *Journal of Drug Delivery Science and Technology*, *51*, 493-498.

Risaliti, L., Piazzini, V., Di Marzo, M. G., Brunetti, L., Cecchi, R., Lencioni, P., ... & Bergonzi, M. C. (2018). Topical formulations of delta-aminolevulinic acid for the treatment of actinic keratosis: Characterization and efficacy evaluation. *European Journal of Pharmaceutical Sciences*, *115*, 345-351.

Risaliti, L., Pini, G., Ascrizzi, R., Donato, R., Sacco, C., Bergonzi, M. C., ... & Bilia, A. R. (2020b). Artemisia annua essential oil extraction, characterization, and incorporation in nanoliposomes, smart drug delivery systems against Candida species. *Journal of Drug Delivery Science and Technology*, *59*, 101849.

Risaliti, L., Yu, X., Vanti, G., Bergonzi, M. C., Wang, M., & Bilia, A. R. (2021). Hydroxyethyl cellulose hydrogel for skin delivery of khellin loaded in ascosomes: Characterization, in vitro/in vivo performance and acute toxicity. *International Journal of Biological Macromolecules*.

Rodriguez-Garcia, I., Silva-Espinoza, B. A., Ortega-Ramirez, L. A., Leyva, J. M., Siddiqui, M. W., Cruz-Valenzuela, M. R., ... & Ayala-Zavala, J. F. (2016). Oregano essential oil as an antimicrobial and antioxidant additive in food products. *Critical Reviews in Food Science and Nutrition*, *56*(10), 1717-1727.

Romani, A., Ieri, F., Urciuoli, S., Noce, A., Marrone, G., Nediani, C., & Bernini, R. (2019). Health effects of phenolic compounds found in extra-virgin olive oil, by-products, and leaf of Olea europaea L. *Nutrients*, *11*(8), 1776.

Ryan, D., Antolovich, M., Prenzler, P., Robards, K., & Lavee, S. (2002). Biotransformations of phenolic compounds in Olea europaea L. *Scientia Horticulturae*, *92*(2), 147-176.

Ryan, D., Robards, K., & Lavee, S. (1999). Changes in phenolic content of olive during maturation. *International journal of food science & technology*, *34*(3), 265-274.

Sala, M., Diab, R., Elaissari, A., & Fessi, H. (2018). Lipid nanocarriers as skin drug delivery systems: Properties, mechanisms of skin interactions and medical applications. *International journal of pharmaceutics*, *535*(1-2), 1-17.

Samarghandian, S., Azimi-Nezhad, M., Farkhondeh, T., & Samini, F. (2017). Anti-oxidative effects of curcumin on immobilization-induced oxidative stress in rat brain, liver and kidney. *Biomedicine & Pharmacotherapy*, *87*, 223-229.

Sankar, V., Hearnden, V., Hull, K., Juras, D. V., Greenberg, M. S., Kerr, A. R., ... & Thornhill, M. (2011). Local drug delivery for oral mucosal diseases: challenges and opportunities. *Oral diseases*, *17*, 73-84.

Santos, P., Watkinson, A. C., Hadgraft, J., & Lane, M. E. (2008). Application of microemulsions in dermal and transdermal drug delivery. *Skin pharmacology and physiology*, *21*(5), 246-259.

Sattar, M., Sayed, O. M., & Lane, M. E. (2014). Oral transmucosal drug delivery–current status and future prospects. *International journal of pharmaceutics*, *471*(1-2), 498-506.

Schneider, L., Tilles, S., Lio, P., Boguniewicz, M., Beck, L., LeBovidge, J., ... & Wallace, D. (2013). Atopic dermatitis: a practice parameter update 2012. *Journal of Allergy and Clinical Immunology*, *131*(2), 295-299.

Schnitzler, P. (2019). Essential oils for the treatment of herpes simplex virus infections. *Chemotherapy*, *64*(1), 1-7.

Schnitzler, P., Schuhmacher, A., Astani, A., & Reichling, J. (2008). Melissa officinalis oil affects infectivity of enveloped herpesviruses. *Phytomedicine*, *15*(9), 734-740.

Seljak, K. B., Berginc, K., Trontelj, J., Zvonar, A., Kristl, A., & Gašperlin, M. (2014). A self-microemulsifying drug delivery system to overcome intestinal resveratrol toxicity and presystemic metabolism. *Journal of pharmaceutical sciences*, *103*(11), 3491-3500.

Serra, A., Rubió, L., Borràs, X., Macià, A., Romero, M. P., & Motilva, M. J. (2012). Distribution of olive oil phenolic compounds in rat tissues after administration of a phenolic extract from olive cake. *Molecular nutrition & food research*, *56*(3), 486-496.

Sha, X., Yan, G., Wu, Y., Li, J., & Fang, X. (2005). Effect of self-microemulsifying drug delivery systems containing Labrasol on tight junctions in Caco-2 cells. *European journal of pharmaceutical sciences*, *24*(5), 477-486.

Shakeel, F., Haq, N., Alanazi, F. K., & Alsarra, I. A. (2013). Impact of various nonionic surfactants on self-nanoemulsification efficiency of two grades of Capryol (Capryol-90 and Capryol-PGMC). *Journal of Molecular Liquids*, *182*, 57-63.

Shakeel, F., Shafiq, S., Haq, N., Alanazi, F. K., & Alsarra, I. A. (2012). Nanoemulsions as potential vehicles for transdermal and dermal delivery of hydrophobic compounds: an overview. *Expert opinion on drug delivery*, *9*(8), 953-974.

Shariatinia, Z. (2018). Carboxymethyl chitosan: Properties and biomedical applications. *International journal of biological macromolecules*, *120*, 1406-1419.

Sharma, G., Thakur, K., Raza, K., Singh, B., & Katare, O. P. (2017). Nanostructured lipid carriers: a new paradigm in topical delivery for dermal and transdermal applications. *Critical Reviews™ in Therapeutic Drug Carrier Systems*, *34*(4).

Sheriff, T., Lin, M. J., Dubin, D., & Khorasani, H. (2020). The potential role of cannabinoids in dermatology. *Journal of Dermatological Treatment*, *31*(8), 839-845.

Shono, Y., Nishihara, H., Matsuda, Y., Furukawa, S., Okada, N., Fujita, T., & Yamamoto, A. (2004). Modulation of intestinal P-glycoprotein function by cremophor EL and other surfactants by an in vitro diffusion chamber method using the isolated rat intestinal membranes. *Journal of pharmaceutical sciences*, *93*(4), 877-885.

Shu, N., Hu, M., Ling, Z., Liu, P., Wang, F., Xu, P., ... & Liu, L. (2016). The enhanced atorvastatin hepatotoxicity in diabetic rats was partly attributed to the upregulated hepatic Cyp3a and SLCO1B1. *Scientific reports*, *6*(1), 1-13.

Shukla, T., Upmanyu, N., Agrawal, M., Saraf, S., Saraf, S., & Alexander, A. (2018). Biomedical applications of microemulsion through dermal and transdermal route. *Biomedicine & Pharmacotherapy*, *108*, 1477-1494.

Singh, I. P., & Mahajan, S. (2013). Berberine and its derivatives: a patent review (2009–2012). *Expert opinion on therapeutic patents*, *23*(2), 215-231.

Sinico, C., Caddeo, C., Valenti, D., Fadda, A. M., Bilia, A. R., & Vincieri, F. F. (2008). Liposomes as carriers for verbascoside: stability and skin permeation studies. *Journal of liposome research*, *18*(1), 83-90.

Sinkó, B., Garrigues, T. M., Balogh, G. T., Nagy, Z. K., Tsinman, O., Avdeef, A., & Takács-Novák, K. (2012). Skin–PAMPA: A new method for fast prediction of skin penetration. *European Journal of Pharmaceutical Sciences*, *45*(5), 698-707.

Sirtori, C. R. (2001). Aescin: pharmacology, pharmacokinetics and therapeutic profile. *Pharmacological Research*, *44*(3), 183-193.

Skoula, M., & Grayer, R. J. (2005). Volatile oils of Coridothymus capitatus, Satureja thymbra, Satureja spinosa and Thymbra calostachya (Lamiaceae) from Crete. *Flavour and fragrance journal*, *20*(6), 573-576.

Solecki, R. S. (1975). Shanidar IV, a Neanderthal flower burial in northern Iraq. *Science*, *190*(4217), 880-881.

Somerville, V., Moore, R., & Braakhuis, A. (2019). The effect of olive leaf extract on upper respiratory illness in high school athletes: a randomised control trial. *Nutrients*, *11*(2), 358.

Souto, E. B., Baldim, I., Oliveira, W. P., Rao, R., Yadav, N., Gama, F. M., & Mahant, S. (2020). SLN and NLC for topical, dermal, and transdermal drug delivery. *Expert opinion on drug delivery*, *17*(3), 357-377.

Spinozzi, S., Colliva, C., Camborata, C., Roberti, M., Ianni, C., Neri, F., ... & Roda, A. (2014). Berberine and its metabolites: relationship between physicochemical properties and plasma levels after administration to human subjects. *Journal of Natural Products*, *77*(4), 766-772.

Sreij, R., Dargel, C., Moleiro, L. H., Monroy, F., & Hellweg, T. (2017). Aescin incorporation and nanodomain formation in dmpc model membranes. *Langmuir*, *33*(43), 12351-12361.

Srivastava, M., Kohli, K., & Ali, M. (2016). Formulation development of novel in situ nanoemulgel (NEG) of ketoprofen for the treatment of periodontitis. *Drug delivery*, *23*(1), 154-166.

Stefanaki, A., Cook, C. M., Lanaras, T., & Kokkini, S. (2016). The Oregano plants of Chios Island (Greece): Essential oils of Origanum onites L. growing wild in different habitats. *Industrial Crops and Products*, *82*, 107-113.

Stojković, D., Drakulić, D., Gašić, U., Zengin, G., Stevanović, M., Rajčević, N., & Soković, M. (2020). Ononis spinosa L., an edible and medicinal plant: UHPLC-LTQ-Orbitrap/MS chemical profiling and biological activities of the herbal extract. *Food & function*, *11*(8), 7138-7151.

Sun, S., Zhang, X., Xu, M., Zhang, F., Tian, F., Cui, J., ... & Zou, Y. (2019). Berberine downregulates CDC6 and inhibits proliferation via targeting JAK-STAT3 signaling in keratinocytes. *Cell death & disease*, *10*(4), 1-16.

Tabbakhian, M., Tavakoli, N., Jaafari, M. R., & Daneshamouz, S. (2006). Enhancement of follicular delivery of finasteride by liposomes and niosomes: 1. In vitro permeation and in vivo deposition studies using hamster flank and ear models. *International journal of pharmaceutics*, *323*(1-2), 1-10.

Takahashi, Y., Kondo, H., Yasuda, T., Watanabe, T., Kobayashi, S. I., & Yokohama, S. (2002). Common solubilizers to estimate the Caco-2 transport of poorly water-soluble drugs. *International journal of pharmaceutics*, *246*(1-2), 85-94.

Tan, S., Zou, C., Zhang, W., Yin, M., Gao, X., & Tang, Q. (2017). Recent developments in d-α-tocopheryl polyethylene glycol-succinate-based nanomedicine for cancer therapy. *Drug delivery*, *24*(1), 1831-1842.

Tasdemir, D., Kaiser, M., Demirci, B., Demirci, F., & Baser, K. (2019). Antiprotozoal activity of turkish Origanum onites essential oil and its components. *Molecules*, *24*(23), 4421.

Teodori, E., Braconi, L., Bua, S., Lapucci, A., Bartolucci, G., Manetti, D., ... & Coronnello, M. (2020). Dual P-Glycoprotein and CA XII Inhibitors: A New Strategy to Reverse the P-gp Mediated Multidrug Resistance (MDR) in Cancer Cells. *Molecules*, *25*(7), 1748.

Tepe, B., & Cilkiz, M. (2016). A pharmacological and phytochemical overview on Satureja. *Pharmaceutical biology*, *54*(3), 375-412.

Tepe, B., Cakir, A., & Sihoglu Tepe, A. (2016). Medicinal uses, phytochemistry, and pharmacology of Origanum onites (L.): A Review. *Chemistry & Biodiversity*, *13*(5), 504-520.

Torky, A. S., Freag, M. S., Nasra, M. M., & Abdallah, O. Y. (2018). Novel skin penetrating berberine oleate complex capitalizing on hydrophobic ion pairing approach. *International journal of pharmaceutics*, *549*(1-2), 76-86.

Trapani, S., Breschi, C., Cecchi, L., Guerrini, L., Mulinacci, N., Parenti, A., ... & Zanoni, B. (2017). Indirect indices of oxidative damage to phenolic compounds for the implementation of olive paste malaxation optimization charts. *Journal of Food Engineering*, *207*, 24-34.

Tsukada, K. (1992). The pH changes of pressure ulcers related headling process of wound. *Wounds*, *4*, 16-20.

Turna, G., Kilic, N., Yildirim, Z., & Sari, S. (2011). Effects of Thymus sipyleus and taurine on hepatic MDA, GSH, AOPP levels and SOD activity in Ehrlich Acide solid tumor model generated mice.

United States Pharmacopeial Convention Inc. (2002). *United States Pharmacopeia and National Formulary* (25th edition*)*. Rockville, MD, USA.

Valenti, D., De Logu, A., Loy, G., Sinico, C., Bonsignore, L., Cottiglia, F., ... & Fadda, A. M. (2001). Liposome-incorporated Santolina insularis essential oil: preparation, characterization and in vitro antiviral activity. *Journal of liposome research*, *11*(1), 73-90.

Van Den Dool, H., & Kratz, P. D. (1963). A generalization of the retention index system including linear temperature programmed gas-liquid partition chromatography (No. RESEARCH).

Van Hoogevest, P. (2017). Review–an update on the use of oral phospholipid excipients. *European Journal of Pharmaceutical Sciences*, *108*, 1-12.

Van Swelm, R. P., Kramers, C., Masereeuw, R., & Russel, F. G. (2014). Application of urine proteomics for biomarker discovery in drug-induced liver injury. *Critical reviews in toxicology*, *44*(10), 823-841.

Vanti, G., Bani, D., Salvatici, M. C., Bergonzi, M. C., & Bilia, A. R. (2019). Development and percutaneous permeation study of escinosomes, escin-based nanovesicles loaded with berberine chloride. *Pharmaceutics*, *11*(12), 682.

Vanti, G., Coronnello, M., Bani, D., Mannini, A., Bergonzi, M. C., & Bilia, A. R. (2021). Co-Delivery of Berberine Chloride and Tariquidar in Nanoliposomes Enhanced Intracellular Berberine Chloride in a Doxorubicin-Resistant K562 Cell Line Due to P-gp Overexpression. *Pharmaceutics*, *13*(3), 306.

Vanti, G., Ntallis, S. G., Panagiotidis, C. A., Dourdouni, V., Patsoura, C., Bergonzi, M. C., ... & Bilia, A. R. (2020a). Glycerosome of Melissa officinalis L. essential oil for effective anti-HSV Type 1. *Molecules*, *25*(14), 3111.

Vanti, G., Wang, M., Bergonzi, M. C., Zhidong, L., & Bilia, A. R. (2020b). Hydroxypropyl methylcellulose hydrogel of berberine chloride-loaded escinosomes: dermal absorption and biocompatibility. *International Journal of Biological Macromolecules*, *164*, 232-241.

Vergis, J., Gokulakrishnan, P., Agarwal, R. K., & Kumar, A. (2015). Essential oils as natural food antimicrobial agents: a review. *Critical reviews in food science and nutrition*, *55*(10), 1320-1323.

Vijayakumar, K., Rengarajan, R. L., Radhakrishnan, R., & Anand, A. V. (2018). Hypolipidemic effect of Psidium guajava leaf extract against hepatotoxicity in rats. *Pharmacognosy magazine*, *14*(53), 4.

Vincken, J. P., Heng, L., de Groot, A., & Gruppen, H. (2007). Saponins, classification and occurrence in the plant kingdom. *Phytochemistry*, *68*(3), 275-297.

Vokou, D., Kokkini, S., & Bessiere, J. M. (1988). Origanum onites (Lamiaceae) in Greece: distribution, volatile oil yield, and composition. *Economic Botany*, *42*(3), 407-412.

Vrzal, R., Frauenstein, K., Proksch, P., Abel, J., Dvorak, Z., & Haarmann-Stemmann, T. (2013). Khellin and visnagin differentially modulate AHR signaling and downstream CYP1A activity in human liver cells. *PLoS One*, *8*(9), e74917.

Wang, X., Huang, L., Zhang, C., Xie, P., Deng, Y., & Liu, L. (2019). Preparation and physicochemical properties of olive leaf extract. *Chem. Ind. For. Prod*, *39*, 83-90.

Wang, Y. Q., Wei, J. G., Tu, M. J., Gu, J. G., & Zhang, W. (2018). Fucoidan alleviates acetaminophen-induced hepatotoxicity via oxidative stress inhibition and Nrf2 translocation. *International journal of molecular sciences*, *19*(12), 4050.

Wei, S., Daliri, E. B. M., Chelliah, R., Park, B. J., Lim, J. S., Baek, M. A., ... & Oh, D. H. (2019). Development of a multiplex real-time PCR for simultaneous detection of Bacillus cereus, Listeria monocytogenes, and Staphylococcus aureus in food samples. *Journal of Food Safety*, *39*(1), e12558.

Whitley, R., & Baines, J. (2018). Clinical management of herpes simplex virus infections: past, present, and future. *F1000Research*, *7*.

Williamson, E. M. (2001). Synergy and other interactions in phytomedicines. *Phytomedicine*, *8*(5), 401-409.

Wilson, I. A. I., IAI, W., RD, Q., & PJ, B. (1979). The pH of varicose ulcer surfaces and its relationship to healing.

Win, K. Y., & Feng, S. S. (2005). Effects of particle size and surface coating on cellular uptake of polymeric nanoparticles for oral delivery of anticancer drugs. *Biomaterials*, *26*(15), 2713-2722.

Wollenberg, A., Barbarot, S., Bieber, T., Christen-Zaech, S., Deleuran, M., Fink-Wagner, A., ... & Ring, J. (2018). Consensus-based European guidelines for treatment of atopic eczema (atopic dermatitis) in adults and children: part I. *Journal of the European Academy of Dermatology and Venereology*, *32*(5), 657-682.

Wollenberg, A., Barbarot, S., Bieber, T., Christen-Zaech, S., Deleuran, M., Fink-Wagner, A., ... & Ring, J. (2018). Consensus-based European guidelines for treatment of atopic eczema (atopic dermatitis) in adults and children: part II. *Journal of the European Academy of Dermatology and Venereology*, *32*(5), 657-682.

World Health Organization. (2007). *WHO Monographs on Selected Medicinal Plants* (Vol. 3). Geneva, Switzerland: WHO Press.

Wu, Q., Yang, Z., Nie, Y., Shi, Y., & Fan, D. (2014). Multi-drug resistance in cancer chemotherapeutics: mechanisms and lab approaches. *Cancer letters*, *347*(2), 159-166.

Xie, P. J., Huang, L. X., Zhang, C. H., You, F., & Zhang, Y. L. (2015a). Reduced pressure extraction of oleuropein from olive leaves (Olea europaea L.) with ultrasound assistance. *Food and Bioproducts processing*, *93*, 29-38.

Xie, P. J., Huang, L. X., Zhang, C. H., You, F., Wang, C. Z., & Zhou, H. (2015b). Reduced-pressure boiling extraction of oleuropein coupled with ultrasonication from olive leaves (Olea europaea L.). *Advances in Materials Science and Engineering*.

Yang, X., & Liu, K. (2016). P-gp inhibition-based strategies for modulating pharmacokinetics of anticancer drugs: an update. *Current drug metabolism*, *17*(8), 806-826.

Ye, M., Fu, S., Pi, R., & He, F. (2009). Neuropharmacological and pharmacokinetic properties of berberine: a review of recent research. *Journal of Pharmacy and Pharmacology*, *61*(7), 831-837.

Yin, Y. M., Cui, F. D., Mu, C. F., Choi, M. K., Kim, J. S., Chung, S. J., ... & Kim, D. D. (2009). Docetaxel microemulsion for enhanced oral bioavailability: preparation and in vitro and in vivo evaluation. *Journal of Controlled Release*, *140*(2), 86-94.

Yuan, J. J., Qin, F. G., Tu, J. L., & Li, B. (2017). Preparation, characterization, and antioxidant activity evaluation of liposomes containing water-soluble hydroxytyrosol from olive. *Molecules*, *22*(6), 870.

Zanoni, B. (2014). Which processing markers are recommended for measuring and monitoring the transformation pathways of main components of olive oil?. *Italian Journal of Food Science*, *26*(1).

Zhang, C., Wang, N., Xu, Y., Tan, H. Y., Li, S., & Feng, Y. (2018). Molecular mechanisms involved in oxidative stress-associated liver injury induced by Chinese herbal medicine: An experimental evidence-based literature review and network pharmacology study. *International journal of molecular sciences*, *19*(9), 2745.

Zhang, H., Xu, H., Ashby Jr, C. R., Assaraf, Y. G., Chen, Z. S., & Liu, H. M. (2021). Chemical molecular-based approach to overcome multidrug resistance in cancer by targeting P-glycoprotein (P-gp). *Medicinal Research Reviews*, *41*(1), 525-555.

Zhang, K., Zhang, Y., Li, Z., Li, N., & Feng, N. (2017). Essential oil-mediated glycerosomes increase transdermal paeoniflorin delivery: Optimization, characterization, and evaluation in vitro and in vivo. *International journal of nanomedicine*, *12*, 3521.

Zhang, Y. T., Yu, Y. Q., Yan, X. X., Wang, W. J., Tian, X. T., Wang, L., ... & Pan, G. Y. (2019). Different structures of berberine and five other protoberberine alkaloids that affect P-glycoprotein-mediated efflux capacity. *Acta Pharmacologica Sinica*, *40*(1), 133-142.

Zhang, Y., Ng, W., Hu, J., Mussa, S. S., Ge, Y., & Xu, H. (2018a). Formulation and in vitro stability evaluation of ethosomal carbomer hydrogel for transdermal vaccine delivery. *Colloids and Surfaces B: Biointerfaces*, *163*, 184-191.

Zhang, Y., Yuan, Y., Wu, H., Xie, Z., Wu, Y., Song, X., ... & Wang, L. (2018b). Effect of verbascoside on apoptosis and metastasis in human oral squamous cell carcinoma. *International journal of cancer*, *143*(4), 980-991.

Zhou, Y., Hartemink, A. E., Shi, Z., Liang, Z., & Lu, Y. (2019). Land use and climate change effects on soil organic carbon in North and Northeast China. *Science of the Total Environment*, *647*, 1230-1238.

Zhu, H. L., Gao, Y. H., Yang, J. Q., Li, J. B., & Gao, J. (2018). Serenoa repens extracts promote hair regeneration and repair of hair loss mouse models by activating TGF-β and mitochondrial signaling pathway. *Eur. Rev. Med. Pharmacol. Sci*, *22*, 4000-4008.

Zhu, W., Guo, C., Yu, A., Gao, Y., Cao, F., & Zhai, G. (2009). Microemulsion-based hydrogel formulation of penciclovir for topical delivery. *International journal of pharmaceutics*, *378*(1-2), 152-158.

Zinzi, L., Capparelli, E., Cantore, M., Contino, M., Leopoldo, M., & Colabufo, N. A. (2014). Small and innovative molecules as new strategy to revert MDR. *Frontiers in oncology*, *4*, 2.